In situ analysis of grass cell wall polysaccharides

By

Jie Xue

Submitted in accordance with the requirements for the degree of Doctor of Philosophy

The University of Leeds

Faculty of Biological Sciences

November 2013

The candidate confirms that all the work submitted in this thesis is her own. The candidate confirms that appropriate credit has been given within the thesis where reference has been made to the work of others.

Some of the work presented in Chapters 3 and 5 appear in the following publication:

Jie Xue, Maurice Bosch, and J. Paul Knox, 2013. Heterogeneity and glycan masking of cell wall microstructures in the stems of *Miscanthus* x *giganteus*, and its parents *M. sinensis* and *M. sacchariflorus*. Plos ONE 8, e82114.

“Happy is the man who is living by his hobby”

George Bernard Shaw, 1856-1950

Acknowledgements

Firstly I am very grateful to my supervisor, **Professor Paul Knox**, gave me a chance here for my PhD study, and also for all his help, instructions, guidance and patience for my study. The knowledgeable man (responsible for my interest in cell walls) taught me how to do an excellent cell wall research, how to produce a good scientific work and how to be a responsible scientist.

Susan Marcus, the most kind woman in the Knox lab, for being taking very good care of me during these past three years, and also for her excellent lab techniques.

I would also like to thank **Dr Kieran Lee** for his help with the exciting scientific ideas and also his experimental help.

I am also grateful to my secondary supervisor, **Professor Jurgen Denecke**, for his help with the experiment techniques and scientific suggestions.

My current and former Knox Cell Wall Lab members: **Dr Tom Benians, Thomas Torode, Valérie Cornuault, Mercedes Hernández Gómez, Craig Deakin** and **Professor Carem Gledes Vargas-Rechia** for giving me the passionate friendship in our office and lab.

Martin Fuller, for his expertise in teaching me how to produce high quality resin embedded sections of grasses.

Lance Penketh, for his kind help on using the plant growth facilities in University of Leeds greenhouse.

I acknowledge the financial support from the **University of Leeds** and the **China Scholarship Council** over the past three years of my PhD.

Finally, I would like to give my special thanks to my **parents**, my dearest father and mother who always stand by me, and give me spiritual support and so many encouragements during my study in Leeds University.

Abstract

Plant cell walls are important resources of biomass and renewable energy. *Miscanthus* species are fast growing grasses that had been suggested to be potential bioenergy crops. *Miscanthus* x *giganteus* (*M.* x *giganteus*) grows faster and taller than its parents - *M. sacchariflorus* and *M. sinensis.* Wheat is the major food crop for human beings. *Brachypodium distachyon* is considered to be a model plant as it has a small genome size and rapid life cycle. In this study, cell wall polysaccharides in stems of the five grass species at different growth stages have been determined using an indirect immunofluorescence method with sets of specific monoclonal antibodies. Heteroxylan and mixed-linkage-glucan (MLG) epitopes are abundant in all grass species, but with different distributions in parenchyma regions and the detection levels of both polymers change during growth development. For *M.* x *giganteus*, pectic homogalacturonan (HG) epitopes were restricted to intercellular spaces of parenchyma and the high methylesterified LM20 HG epitope was strongly abundant in pith parenchyma cell walls. Some cell wall probes cannot access their target polymers because of masking by other polysaccharides. For all grass species in certain cell wall regions, the xyloglucan epitope is masked by heteroxylan, the pectic-galactan epitope is masked both by heteroxylan and MLG, and the LM2 AGP epitope is masked by pectin. These findings indicate the heterogeneity of polysaccharide distributions and molecular architectures in grasses, and this might be linked to grass anatomical and growth differences and may also be related to distinct cell wall functions between grass species. In summary, this fundamental knowledge of cell wall polysaccharide architectures in these important grass species will help us understand grass growth mechanisms, and may also be beneficial for the development of potential strategies for the efficient deconstruction of grass biomass that may make contribution to the biofuel industry.

Contents

List of Figures

List of Tables

List of Abbreviations

AG	Arabinogalactan
AGPs	Arabinogalactan-proteins
Ara*f*	Arabino- furanosyl
AraT	Arabinosyltransferase
bm	Base of internode
BSA	Bovine serum albumin
CAD	Cinnamyl alcohol dehydrogenase
Calc	Calcofluor White
CAZy	Carbohydrate-active enzyme
CBMs	Carbohydrate-binding modules
CCR	Cinnamoyl-CoA reductase
CESA proteins	Cellulose synthase proteins
COMT	Caffeic acid O-methyltransferase
CSL	Cellulose synthase-like
DMSO	Dimethyl sulphoxide
DP	Degree of polymerisation
dRG-II	Borate-cross-linked RG-II dimer complex
ELISA	Enzyme linked immunoabsorbent assay
ER	Endoplasmic reticulum
FITC	Fluorescein isothiocyanate
FUTs	Fucosyltransferases
G	Guaiacyl
GalA	α-1-4-D-galacturonic acid
Gal*p*	Galacto-pyranosyl
GAX	Glucuronoarabinoxylans
Glc*p*A	Glucopyranosyluronic acid

GPI	Glycosylphosphatidylinositol
GTs	Glycosyltransferases
H	ρ-hydroxyphenyl
HG	Homogalacturonan
HRGPs	Hydroxyproline-rich glycoproteins
HRP	Horseradish peroxidase
Hyp	Hydroxyproline
IDA	Immunodot blot assay
Int2	Second internode
Int4	Fourth internode
Int5	Fifth internode
mid	Middle of internode
MLG	Mixed linkage-(1,3-1,4)-β-D-glucans
P4H	Prolyl-4-hydroxylase
PBS	Phosphate buffered saline
Pec	Pectinex
PL	Pectate lyase
Pro	Proline
PRPs	Proline-rich glycoproteins
RG-II	Rhamnogalacturonan-II
RG-I	Rhamnogalacturonan-I
Rha*p*	Rhamno-pyranosyl
S	Syringyl
SDS	Sodium dodecyl sulphate
SDS-PAGE	SDS-polyacrylamide gel electrophoresis
XGA	Xylogalacturonan
XyG	Xyloglucan
βGlcY	β-glucosyl Yariv reagent

Chapter 1

Introduction

1.1 Importance of grasses

Grasses are among the most important plants worldwide and include several major crops such as wheat, rice and maize. The grass family are of particular interest to humans as they can be used as food and energy. Grass cell walls are major sources of dietary fibre that provide potential health benefits to humans (Harris and Smith 2006). The majority of domestic animals are raised mainly on grasses (Kellogg 2001). Furthermore, grasses have been used for renewable energy due to their fast growth and accumulation of biomass (Vogel 2008). Additionally, grasses play an important part of the urban and suburban landscape in the world (Kellogg 2001). The grasses family includes about 10,000 species classified into 600-700 genera and covers approximately 20% of the earth's land surface (Clayton and Renvoize 1986, Shantz 1954, Watson and Dallwitz 1988). Wheat, *Brachypodium distachyon* and *Miscanthus* species are all in the grass family. Wheat is one of the major crops for humans. *Brachypodium distachyon* is considered to be a model plant owing to its small genome size and rapid life cycle (Kellogg 2001, Vogel 2008). Certain C4 grasses such as switch grass, sorghum and *Miscanthus* species with fast growth and high capacity for biomass accumulation are potential targets to develop as bioenergy crops because the sugars locked in the polysaccharides of the grass cell wall can be converted into liquid fuel (e.g. ethanol) or the entire cell walls can be burned to produce heat or electricity (Ragauskas et al. 2006, Vogel 2008). However, the structurally complex and tightly compacted nature of cell walls make them not amenable to facile enzymatic deconstruction to release sugars (Ragauskas et al. 2006, Robbins et al. 2012). Cell wall recalcitrance is a major hurdle in the optimization of cell wall biomass and therefore understanding cell wall microstructures and cell wall heterogeneity is an important step in their exploitation (Ragauskas et al. 2006, Robbins et al. 2012, Vogel 2008). To date, little is known of cell wall heterogeneity in grass organs such as stems and leaves, especially in the three target grasses - wheat, *Brachypodium distachyon* and *Miscanthus* species.

1.2 Importance of plant cell walls

Plant cell walls present one of the major resources of renewable biomass on Earth (Ragauskas et al. 2006, Somerville et al. 2010). Plant cell walls are important cellular components that perform a number of essential functions during plant growth and development. Cell walls are of great importance to cell morphology, tissue and organ enlargement and differentiation (Keegstra 2010). Plant cell walls often play essential roles in intercellular communications and plant-microbe interactions, such as defence responses against potential pathogens (Keegstra 2010, Vorwerk et al. 2004). In reality, all differentiated cells contain distinct walls resulting in a spectrum of specialized cell walls with both primary and secondary walls as two extremes (Keegstra 2010). The primary cell wall accommodates the cell as it grows, while the secondary cell wall is developed inside the primary wall in certain cell types after the cell has stopped growing. Primary cell walls can expand to allow the cell to grow and divide and its mechanical properties prevent cell bursting, whereas the secondary cell walls give compressive strength to certain cell types (Cosgrove 2005).

1.3 Plant cell wall polysaccharides

Cell walls are complex fibrous composites constructed from a range of polysaccharides, proteins and phenolics. The major component found in all plant cell walls is cellulose. In addition to cellulose, plant cell walls contain a number of polysaccharides that are grouped into two general categories: the non-cellulosic polysaccharides and the pectic polysaccharides (Table1.1). Hemicelluloses are major non-cellulosic polysaccharides include heteroxylans, xyloglucans (XyGs), mixed linkage-(1,3-1,4)-β-D-glucans (MLGs) and heteromannans (Harris and Smith 2006, Scheller and Ulvskov 2010). Pectic polysaccharides include homogalacturonan (HG), rhamnogalacturonan I (RG-I), rhamnogalacturonan II (RG-II) and xylogalacturonan (XGA) (Harholt et al. 2010, Mohnen 2008). Plant

cell walls also contain many proteins and glycoproteins that include several enzymes and structural proteins (Rose and Lee 2010). Cell wall proteins are typically glycoproteins which have polypeptide backbones and carbohydrate side chains (Carpita 1996, McNeil et al. 1984, Vogel 2008). Plant cell walls also contain phenolics polymers such as lignin which is usually found in the thickened secondary walls (Donaldson 2001).

Table 1.1: The main polysaccharides of plant cell walls. The main polysaccharide groups are cellulose, hemicelluloses and pectic polysaccharides.

Polysaccharide group:	Contents:
Cellulose	
Hemicellulose	Heteroxylan
	Xyloglucan (XyG)
	Mixed-linkage glucan (MLG)
	Heteromannan
Pectin	Homogalacturonan (HG)
	Rhamnogalacturonan I (RG-I)
	Rhamnogalacturonan II (RG-II)
	Xylogalacturonan (XGA)

1.3.1 Cellulose

Cellulose is the most abundant biopolymer on Earth because all land plants have cellulose in their cell walls (Lerouxel et al. 2006, Saxena and Brown 2005, Taylor 2008). Cellulose is also found in bacteria, fungi, algae and even in animals (O'Sullivan 1997). Cellulose consists of linear unbranched chains of β-1,4-D-linked-glucose residues that interact with each other via hydrogen bonds and Van der Waals forces (Somerville 2006). Cellulose chains gather together to form crystalline microfibrils about 3nm in diameter, chemically stable and resistant to enzymatic attack (Ochoa-Villarreal et al. 2012). Native cellulose chains found in primary cell walls have a degree of polymerisation (DP) of 8,000 residues (Brown 2004), while this is much higher at around 15,000 residues in secondary cell walls (Brett 2000). In plants, cellulose microfibrils are thought to be composed of 36 individual chains that can give plants high mechanical strength (Somerville 2006) (Figure 1.1). This strength is important in cell walls, where the microfibrils are meshed into a carbohydrate matrix, giving rigidity to plant cells (Somerville 2006). During synthesis of the plant thickened secondary wall, microfibrils often are found further associated into macrofibrils or bundles (Delmer and Amor 1995). The dry weight of cellulose in dicotyledons such as *Arabidopsis thaliana* is about 33% of stem walls, while the monocotyledon grass species have approximately 20-40% of dry weight of cellulose of stem walls (Smole et al. 2005).

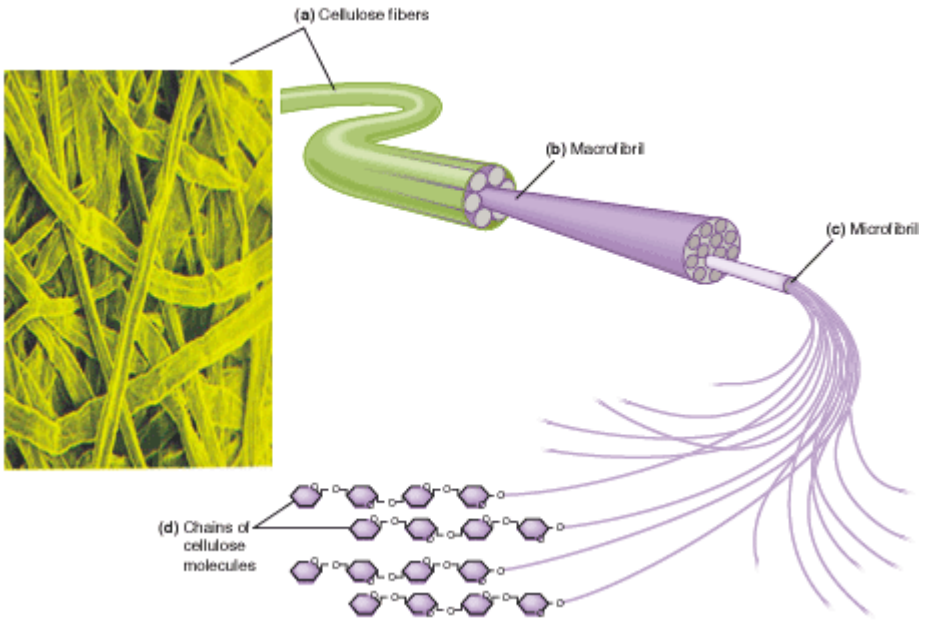

Figure 1.1: Schematic representation of the structure of cellulose. (a) Cellulose fibres from ponderosa pine. (b) Each cellulose fibre is composed of macrofibrils. (c) Each macrofibril is composed of bundles of microfibrils. (d) Microfibrils are composed of cellulose chains (Taken from the Jones and Bartlett online learning website: http://nutrition.jbpub.com/resources/chemistryreview9.cfm).

Cellulose synthesis is a complex process in which glucose residues are assembled at the surface of the plasma membrane by cellulose synthase proteins (Delmer and Amor 1995, Murray et al. 2001, Paredez et al. 2006, Taylor 2008). Cellulose synthase is described as asymmetrical rosettes of six globular complexes about 25-30nm in diameter. Each of the six subunits of a rosette may synthesis six β-1,4-glucan chains which co-crystallize into a cellulose, the 36-glucan chain microfibril (Herth 1983, Kimura et al. 1999) (Figure 1.2). The cellulose synthase proteins in higher plants are known as the CESA proteins. Recent studies of CESA gene expression in *Arabidopsis thaliana* embryos and barley revealed that there are two groups of CESA proteins. The group I CESA proteins including the CESA1, 2, 3, 5, 6, and 9, they are involved in primary cell wall synthesis (Beeckman et al.

2002, Burton et al. 2004, Harpaz-Saad et al. 2012, Persson et al. 2007). While the CESA 4, 7 and 8 are mostly expressed in secondary cell wall tissues such as stems and are designated as Group II (Hamann et al. 2004, Handakumbura et al. 2013, Taylor et al. 2000). For example, the CESA4 promoter:GUS expression studies on maize (*Zea mays*) had been revealed that the *CESA4* gene was mostly or only expressed in the vascular tissues (Holland et al. 2000). After the polymerization or as part of the synthesis process, the deposition of cellulose is then oriented by an interaction between cellulose synthase proteins and microtubules (Somerville 2006). It is generally acknowledged that the energy of the polymerization provides the motive force that moves the cellulose synthase complex through the plasma membrane although the mechanism is not yet completely known (Baskin 2001, Somerville 2006).

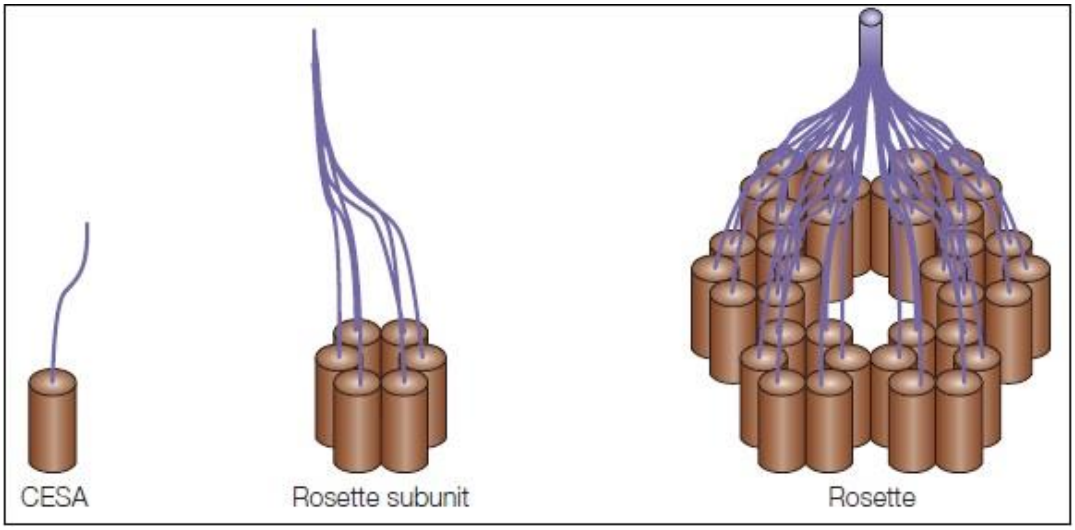

Figure 1.2: Synthesis model of a cellulose microfibril. Each CESA protein can synthesize a single 1,4-β-D-glucan chain. 36 of such chains can make up a cellulose microfibril. (Taken from (Cosgrove 2005)).

In primary cell walls, cellulose microfibrils are important in determining the orientation of cell expansion because of their physical properties, and are thought to be cross linked by non-cellulosic polysaccharides which provide the tensile strength of the wall. After a period of expansion, a secondary wall may accumulate inside the primary wall and provides the mechanical properties of vascular and fibre cells that allow plants to stand upright (Taylor 2008).

1.3.2 Hemicelluloses

Hemicelluloses are a group of branched polysaccharides in plant cell walls that have β-1-4-linked backbones with an equatorial configuration (Scheller and Ulvskov 2010) that include heteroxylans, XyGs, mixed-linkage glucans (MLGs) and heteromannans. These types of non-cellulosic polysaccharides are present in the cell walls of all terrestrial plants, except for MLGs, which are restricted to the Poaceae and a few other groups (Scheller and Ulvskov 2010, Sørensen et al. 2008, Vogel 2008).

1.3.2.1 Heteroxylan

Xylans are a diverse group of polysaccharides with the common backbone of β-1-4-linked xylose residues (Scheller and Ulvskov 2010). Xylans that contain α-1-6-linked arabinose residues attached to the backbone are known as arabinoxylans (Figure 1.10). The α-L-arabinofuranosyl units are attached primarily at the O-3 positions along the β-1-4-D-xylan backbone in grasses rather than the O-2 position in dicotyledons (Darvill et al. 1980b, Zablackis et al. 1995). Glucuronoarabinoxylans (GAXs) also have α-D-glucuronic acids attached to the O-2 position (Scheller and Ulvskov 2010). The presence of phenolics such as ferulic acid esters attached to heteroxylan polymers can form ferulated xylans that can function in cell wall polymer cross-linking and contribute to cell wall recalcitrance (Harris et al. 1997). The O-2 linked xylose residues with substituents

of feruloyl-arabinofuranosyl side chains is common in grasses (Wende and Fry 1997). Xylans/GAXs are the major non-cellulosic polysaccharides in commelinid monocotyledons walls, constituting 20-40% of the primary wall and 40-50% of the secondary wall (Ebringerova et al. 2005, Ishii 1997, McNeil et al. 1984).

Xylan is biosynthesized in Golgi membranes by different enzymes. Xylan synthesis consists of the xylose backbone synthesis, reducing end oligosaccharide synthesis and side chains synthesis (Scheller and Ulvskov 2010). Intensive genetic researches on *Arabidopsis thaliana* has revealed numerous genes involved in xylan biosynthesis (Pauly et al. 2013), and at least five glycosyltransferases (GTs-they are enzymes that are responsible for the biosynthesis of glycosidic bonds from different sugars, there are about 90 families of GTs in the carbohydrate-active enzyme (CAZy) database according to their sequence similarity (Cantarel et al. 2009)) activities may be involved in the biosynthetic process (Faik 2010). Recent studies of the *Arabidopsis thaliana* mutants *irx9, irx10* and *irx14* showed a drastic reduction in xylan chain length which indicated that *Arabidopsis thaliana* members of the GT43 and GT47 families are responsible for the synthesis of the xylan backbone (Brown et al. 2007, Chiniquy et al. 2013, Faik 2010, Lee et al. 2007a, Peña et al. 2007, Wu et al. 2010a, Wu et al. 2009). Observations of the *irx7*, *irx8* and *parvus* of xylan-deficient mutants revealed that they all involved in synthesizing the reducing end oligosaccharide, but the number of GTs needed to make the oligosaccharide is unknown. The *irx7* and *irx8* belong to the GT47 family, and the *parvus* which located in the endoplasmic reticulum (ER) acts as an α-xylosyltransferase transferring the reducing end xylose to a primer (Lee et al. 2007b, Peña et al. 2007, Scheller and Ulvskov 2010). The cell wall polysaccharide is generally synthesized by transfer to the non-reducing end of the growing chain (Scheller et al. 1999). However, xylans may be synthesized in the other direction, that is, from the reducing end (York and O'Neill 2008). Recent xylan studies on wheat and pea revealed that the side chains of xylans are formed by

α-arabinofuranosyl-transferases and α-glucuronsyl-transferases (Baydoun et al. 1989, Porchia et al. 2002, Zeng et al. 2008). The GT61 members are involved in transferring the feruloyl-arabinofuranosyl side chains of xylan in rice and wheat endosperm cell walls (Anders et al. 2012, Mitchell et al. 2007).

Xylans may have a role in the cross-linking of cellulose microfibrils and may thereby regulate cell expansion and strengthen the cell wall (Carpita 1996). Analysis of the xylan-deficient *Arabidopsis thaliana* mutant study suggested that xylans play an important role in strengthening secondary walls (Lee et al. 2007b). A recent study using RNAi to knock down multiple xylanase genes revealed that xylan played significant roles in reducing the *Magnaporthe oryzae* infection of the wheat and barley (Nguyen et al. 2011). In grass cell walls, the diverse chemical structures of heteroxylans make them easy to be modified in response to the functional requirements of the grass cells during growth and development (Fincher 2009). The feruloylation of GAX occurs only in commelinid monocots which differ from dicotyledonous crops, and this linkage is particularly abundant in grasses that cross-linked to lignin (Harris and Trethewey 2010, Ralph et al. 1995). Grasses with decreased feruloylation of GAX in their cell walls may have a lower energy requirement for separation of lignin from polysaccharides during biomass processing (Molinari et al. 2013). Furthermore, xylans can be used as food sweeteners for humans (Ebringerova et al. 2005, Vinkx and Delcour 1996). In addition, in industrial applications xylans can cross-link to form films or gels with good bioaffinities and physical properties (Sarossy et al. 2012).

1.3.2.2 Xyloglucan

Xyloglucan (XyG) has a β-1-4-glucan backbone heavily substituted with α-1-6-xylosyl residues and is found in all vascular plants (Ochoa-Villarreal et al. 2012). XyG is also found in some mosses, lycophytes, and liverworts (Peña et al. 2008). XyG structure is described by a 4 letter code (Figure 1.11). The letter "G" is

the code for one glucose sugar of the backbone, “X” refers to one glucose sugar with its xylosyl side chain, “L” denotes one glucose sugar with its xylosyl and galactosyl side chains, and the letter “F” refers to glucose with its xylosyl, galactosyl and fucosyl side chains. The major division among vascular plant families is related to whether the XXXG or XXGG structure of XyG is predominant (Vincken et al. 1997). The less substituted XXXG structure predominates in cell walls of commelinidae monocotyledons, which are also distinguished by the low content (1-5%) of XyG in the primary walls, typically 15% less compared with dicotyledons (Scheller and Ulvskov 2010, Vincken et al. 1997). Fucosylated (F chain) XyG has been found in *Festuca arundinacea* and rice recently, the transient fucosylation of grass XyG may have implications for the assignment of function to the grass glycosyltrasferases (GTs) of GT37 family (Peña et al. 2008, Scheller and Ulvskov 2010).

The XyG is synthesized by glycosyltransferases (GTs) located in the Golgi membranes. They work together to produce a XyG precursor molecule which is transported to the wall (Scheller and Ulvskov 2010). The first identified fucosyltransferase was purified from *Arabidopsis thaliana* (Perrin et al. 1999). The fucose-deficient *Arabidopsis thaliana* mutant - *mur3* has been shown to encode a XyG-β-1-2-galactosyltransferase which is highly specific for the third galactose in the repeating XXXG unit of XyG (Madson et al. 2003). The GT47 family subgroup A contains 10 members in *Arabidopsis* and only *mur3* has this specific activity confirmed *in vitro* (Li et al. 2004). The α-1-6-xylosyltransferases (GT34 family) are used to transfer xylose residues in XyG. The *XXT1*, *XXT2* and *XXT5* genes have been shown to be involved in the synthesis of XyG in *Arabidopsis* α-1-6-xylosyltransferases (Cavalier and Keegstra 2006, Faik et al. 2002, Zabotina et al. 2008, Zabotina et al. 2012). The backbone of the XyG is synthesized by members of cellulose synthase-like (CSL) proteins which belong to the CSLC family (Scheller and Ulvskov 2010). The *CSCL4* gene from this family has been

reported to encode a β-1,4-glucan synthase in nasturtium (*Tropaeolum majus*) (Cocuron et al. 2007). Acetylation of XyG is on the galactose residues (mostly on O-6) and this acetylation is carried out in the Golgi by acetyl-CoA transferases (Kiefer et al. 1989, Pauly et al. 2000). Recent studies on *Arabidopsis thaliana* using a forward genetic screen revealed that the AXY4 and AXY4L are XyG specific acetyl transferases (Gille et al. 2011, Zabotina 2012).

XyG is thought to be cross-linked with cellulose microfibrils, forming a strong but extensible XyG-cellulose network and act as a tether in plant cell walls and plays a key role in the loosening and tightening of cellulose microfibrils (Cosgrove 2000, Pauly et al. 2013, Somerville et al. 2004). XyG binds to cellulose by two mechanisms. They can be trapped in the cellulose microfbril during the crystallization just after their synthesis, and they could also bind to cellulose by hydrogen bonds (Hayashi et al. 1987, Scheller and Ulvskov 2010). Additionally, XyG can also be covalently linked to pectin (Popper and Fry 2008). Recent studies on pea and *Arabidopsis thaliana mur2*, *xxt1* and *xxt2* mutant revealed that the biosynthesis and/or metabolism of XyG are plant organ-specific, and the XyG metabolism plays essential role in the cell wall growth and development (Cavalier et al. 2008, Pauly et al. 2001, Vanzin et al. 2002). For example, Cavalier et al reported that the *Arabidopsis thaliana xxt1* and *xxt2* double mutant had aberrant root hairs and lacked detectable XyG, and the reduction of XyG in these mutants resulted in significant changes in the plant mechanical properties (Cavalier et al. 2008). XyG also plays an important role as a source of signal molecules, especially for the XXFG products of XyG which was demonstrated to counteract auxin-induced cell expansion (McDougall 1988, McDougall and Fry 1989, York et al. 1984). In industry, XyG can be used as food resources and the XyG derived from Tamarind seed has been used as a carrier for specific drug delivery systems (Mishra and Malhotra 2009, Rolando and Valente 2007, Sumathi and Ray 2002).

1.3.2.3 MLGs

MLGs consist of β-1-3-D-linked and β-1-4-D-linked glucosyl residues (Figure 1.9). They normally have regions of two to five β-1-4-D-linked glucosyl residues separated by β-1-3-D-linked glucosyl residues neither at random nor with predictable regularity, although 5-20 β-1-4-D-linkages of glucosyl residues are also found (Burton and Fincher 2009, Carpita 1996, Meikle et al. 1994). However, the ratio of β-1-3-D-linkage and β-1-4-D-linkage are quite variable in different plants. In cereals, the ratio of β-1-3-D-linkage glucosyl residues and β-1-4-D-linkage glucosyl residues is 2.2-2.6:1 (Burton and Fincher 2009, Fincher and Stone 2004). MLGs are found in all Poales but have not been found in dicotyledons (Smith and Harris 1999). They have recently been found to be present in *Equisetum*, liverworts and algae (Fry et al. 2008, Popper and Fry 2003, Popper et al. 2011, Sørensen et al. 2008). Most recently, MLGs have been found in the cell walls of a barley leaf scald pathogen, *Rhynchosporium secalis* (Pettolino et al. 2009).

It is commonly believed that the MLGs are synthesized in the Golgi membranes and recent research advances include the characterization of cellulose synthase like (*CSL*) gene families which are unique to the grasses and the demonstration that members of the *CSLF* and *CSLH* gene families are responsible for the making of MLGs (Burton et al. 2008, Carpita and McCann 2010, Doblin et al. 2009). The two types of protein can both produce the MLG alone, but the *CSLH* gene is expressed lower than the *CSLF* gene (Doblin et al. 2009). It has been reported that down-regulation of the *CSLF6* gene expression using the RNA interference results in decreased MLGs in wheat endosperm (Nemeth et al. 2010). Taketa et al also reported that the *CSLF6* gene played a unique role in controlling the biosynthesis of MLGs in barley (Taketa et al. 2012). A recent study has shown that the over-expression of specific *HvCsIF* cellulose synthase like genes in transgenic barley could increase the cell wall levels of MLGs (Burton et al. 2011). Although the CSLF and CSLH isoforms are localized in the Golgi which is consistent with

the biosynthesis of MLGs in the Golgi, the MLGs has not been detected in the Golgi (Wilson et al. 2006). Owing to this, Wilson et al and Scheller et al suggested that the MLG epitope is completely masked in Golgi vesicles either by acetylation or that the synthesis takes place in the plasma membrane (Scheller and Ulvskov 2010, Wilson et al. 2006). The MLG biosynthesis is elusive, more research work need to be explored in future studies (Scheller and Ulvskov 2010).

MLGs are thought to be linked to cell elongation in barley coleoptiles and the amount is very growth-stage dependent, the content of MLGs rapidly decreased after the coleoptile growth (Gibeaut et al. 2005), which indicates their important role in the plant development. Another evidence for its role in cell elongation include MLG present abundantly in rapidly growing maize coleoptile cell walls (Carpita and McCann 2010). MLG is also present abundantly in mature stems of rice where it may have a structural role (Vega-Sánchez et al. 2013, Vega-Sánchez et al. 2012). The cereal endosperm such as wheat and barley additionally contains MLGs revealed their seed storage role for cereals (Philippe et al. 2006, Scheller and Ulvskov 2010, Wilson et al. 2006). MLGs are also beneficial constituents of human diets as they can reduce the risk of hypercholesterolemia and other diseases (Brennan and Cleary 2005, Burton et al. 2011).

1.3.2.4 Heteromannan

Mannans have a backbone of β-1-4-D-mannose residues (Figure1.3). Heteromannans are grouped into four distinct classes: mannan, glucomannan, galactomannan, and galactoglucomannan (Scheller and Ulvskov 2010). Mannans with β-1-6-linked glucose substitution of the backbone are known as glucomannans. Mannans with α-D-galactopyranosyl substitution side chain are known as galactomannan. Galactoglucomannan has a main chain of β-1-4-D-mannopyransoyl residues and β-1-4-linked glucopyransosyl units, with α-D-galactopyranosyl units linked as a single side chain to the mannosyl residues in

the main chain (Willför et al. 2008). Mannans and glucomannans are often acetylated (Scheller and Ulvskov 2010). The levels of heteromannans in monocotyledons is generally low, compared with a very abundant amount in secondary cell walls of gymnosperms, and some early land plants such as mosses and lycophytes (Ebringerova et al. 2005, Moller et al. 2007). In wood, mannans are the most abundant β-glycans; in *Arabidopsis*, mannans are localized abundantly to the thickened secondary cell walls of xylem and fibre cells as well as the thickened epidermal walls of both stems and leaves, whereas in the cells lacking secondary walls such as leaves, very little mannan is present (Handford et al. 2003, Maeda et al. 2000, Zablackis et al. 1995). In addition, mannans in tobacco have been reported to be masked by pectin (Marcus et al. 2010) and this will be discussed later in this study.

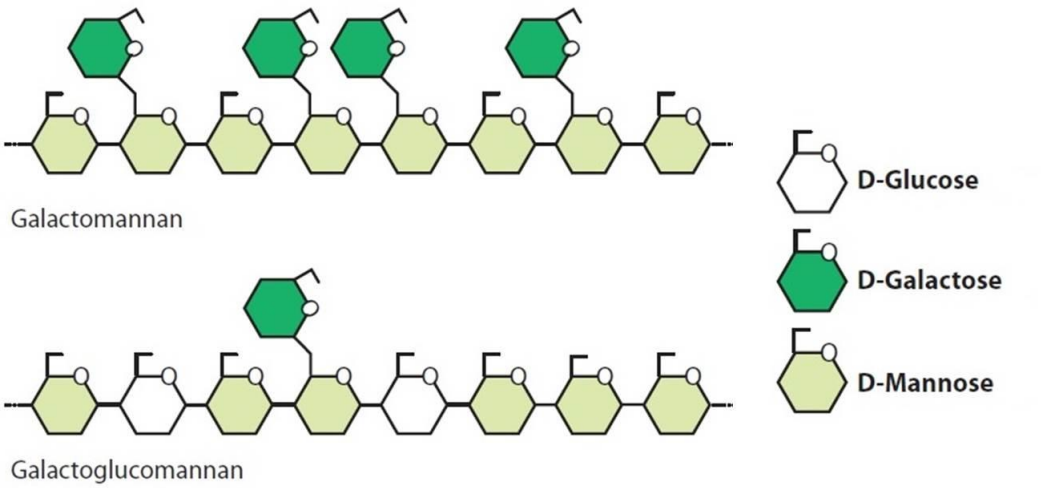

Figure 1.3: Schematic illustration of heteromannan. (Taken from (Scheller and Ulvskov 2010)).

Mannan is synthesized in the Golgi membrane by cellulose synthase-like A (CSLA) gene family proteins. The CSLA family encode glucomannan synthase enzymes that polymerize the β-1-4-D-mannose residue backbones (Liepman et al. 2005, Liepman et al. 2007, Suzuki et al. 2006), and an α-1-6-galactomannan galactosyltransferase which belongs to the GT34 family adds galactopyranosyl residue side chains to the backbone (Edwards et al. 1999). Latest study revealed that the MSR protein (GT65 family) plays an important role in the galactomannan synthesis (Wang et al. 2013). Goubet et al reported that over expression of the *CSLA2*, *CSLA7* and *CSLA9* genes could increase the glucomannan content in *Arabidopsis thaliana* stems, which indicates the CSLA family encodes the glucomannan synthases (Goubet et al. 2009). Recent studies of *Arabidopsis* CLSD5 expressed in tobacco revealed that CLSD proteins are also glucomannan synthases (Yin et al. 2011).

Being hemicelluloses, heteromannan polysaccharides are proposed to cross-link cellulose microfibrils which give plants mechanical structure - but details of this are not clear. Glucomannans are abundant in the endosperm and seeds of legumes, and may be involved in the functions of seed storage (Scheller and Ulvskov 2010), but their amounts are variable in all cell walls. The cell walls of legume seeds are rich in galactomannan as well as the vacuoles of endosperm cells, which also revealed the mannans served as storage polysaccharides (Buckeridge et al. 2000). Besides, these mannan-containing seeds are generally very hard and resistant to mechanical damage (Buckeridge et al. 2000). The *Arabidopsis* cslA7 mutant has been shown phenotypic abnormalities, including pollen tube growth defects and lethal embryo development (Goubet et al. 2003). In contrast, following studies on the deletion of the glucomannan synthase genes expressed in *Arabidopsis thaliana* stems revealed that the mutant plants lacking detectable glucomannan but with no obvious phenotype (Goubet et al. 2009). Mannans also play important roles in wall signalling in *Zinnia elegans* and tissue differentiation (Beňová-Kákošová et al.

2006, del Carmen et al. 2012). In the food industry, mannans are used as a stabilizer and gelling agent (Buckeridge 2010).

1.3.3 Pectic polysaccharides

Pectic polysaccharides are a large family of complex and diverse polymers currently divided into three major polymers but can be part of the same supramolecules within cell walls. These are homogalacturonan (HG), rhamnogalacturonan-I (RG-I) and rhamnogalacturonan-II (RG-II) (Caffall and Mohnen 2009, Harholt et al. 2010, Mohnen 2008). The three major pectic polysaccharides are thought to occur in all primary cell walls of land plants (Willats et al. 2001a). Pectic polymers are generally proposed to be present at lower levels in grass and other commelinid cell walls (2-10% of polymers) (Ridley et al. 2001), compared to the abundant amount in cell walls of dicotyledons and non-commelinid monocotyledon species (non-grasses) (30-35% of polymers), and is also enriched in some fruits, such as citrus and apple (Atmodjo et al. 2013).

Pectin is synthesized in the Golgi and transported to the wall in membrane vesicles (Driouich et al. 2012, Mohnen 2008). At least 67 different glycosyltransferases (GTs), methyltransferases and acetyltransferases are required to the biosynthesis process of the pectin, owning to the complexity of pectin structures (Harholt et al. 2010, Mohnen 2008, Mollet et al. 2013).

Pectin has numerous and distinct functions in plants (Atmodjo et al. 2013). Interactions between pectin and the cellulose-hemicellulose network can give the plant cell wall strong but flexible properties (Caffall and Mohnen 2009, Willats et al. 2001a). Pectic polysaccharides can promote cell-cell adhesion (Bar-Peled et al. 2012, Caffall and Mohnen 2009, Ogawa et al. 2009), and have influence on secondary wall formation in fibers and woody tissues (Hongo et al. 2012, Roach et al. 2011, Siedlecka et al. 2008, Singh et al. 2009). Pectins are important for

plant growth, development, and defense responses by providing oligosaccharide signalling molecules (Ridley et al. 2001, Savatin et al. 2011). Pectins can also affect wall rheology and support *Arabidopsis thaliana* seed and root growth (Harholt et al. 2010, Macquet et al. 2007, Young et al. 2008). Commercially, pectin is well known as a gelling agent and stabilizer in food industries and is widely used in jams and fruit juice production (Imeson 1997, Rolin and De Vries 1990, Willats et al. 2006). It also has positive effects on human health such as lowering cholesterol levels by interfering with cholesterol absorption and by increasing cholesterol turnover (Kelley and Tsai 1978), and decreasing the occurrence of diabetes and cancer (Glinsky and Raz 2009, Jackson et al. 2007, Kelley and Tsai 1978, Yapo and Koffi 2008).

1.3.3.1 Homogalacturonan

Homogalacturonan (HG) is the most abundant pectin polymer, about 60% of pectins in plant cell walls is HG (Ridley et al. 2001). HG is made up of a linear chain of α-1-4-D-galacturonic acid (GalA) residues, and is often referred to as the 'smooth' region as there are no branching side chains (Figure1.4). Some of the carboxyl groups are methyl-esterified at C-6 and GalA residues can be acetyl-esterified at O-2 and/or O-3 positions depending on plant species. In highly methyl-esterified HG more than 50% of the GalA are esterified with methyl groups in the long HG linear units, while the low methyl-esterified HG contains less than 50% esterified GalA (Ochoa-Villarreal et al. 2012). The unmethyl-esterified HG may ionically interact with Ca^{2+} and form a stable gel with other pectin polymers. When there are more than 10 of the unmethyl-esterified-GalA residues the chain can interact with Ca^{2+}, this formed the egg box complex which can induce gelling approximately in 70% of the pectin in plant cell walls (Jarvis and Apperley 1995).

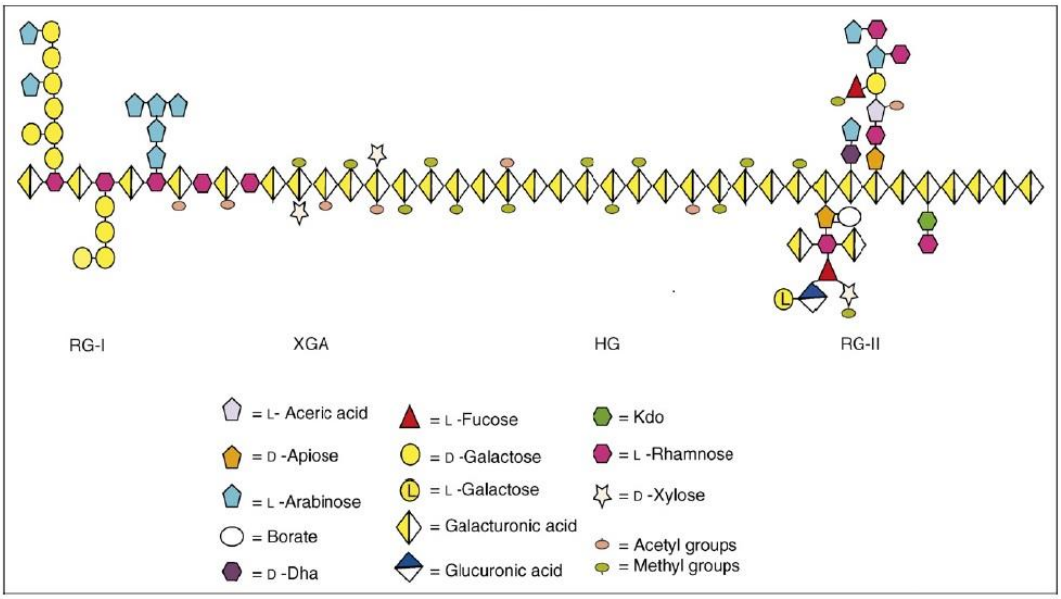

Figure 1.4: Schematic structure of the pectic supramolecule. This structure showing the four pectic polysaccharides: homogalacturonan (HG), rhamnogalacturonan I (RG-I), rhamnogalacturonan II (RG-II) and xylogalacturonan (XGA) linked to each other. (Taken from (Mohnen 2008)).

The GalA residues are added by α-1,4-GalA transferase (HG:α-1,4-GlaAT) to the non-reducing end of the growing HG chain (Scheller et al. 1999). The GAUT1 enzyme has been identified as a HG:α-1,4-GlaAT, it was expressed in human HEK293 cells (kidney cells) and able to synthesis poly-α-1,4-GlaA *in vitro* (Mohnen 2008). The GAUT1 related proteins belong to the *Arabidopsis* GT8 family (Coutinho et al. 2003, Sterling et al. 2006). It is interesting that the *Arabidopsis thaliana* enriched membrane fraction that contained GAUT1 also contained GAUT7. The GAUT7 has no activity when expressed heterologously, but the GAUT1-GAUT7 proteins interact with each other and form a complex to the transfer (Atmodjo et al. 2011, Mohnen 2008). It has been reported that using the HG deficient *qua1* mutant in *Arabidopsis thaliana* could decrease the activity of the HG:α-1,4-GlaAT, and revealed that the GAUT8/QUASIMODO 1 (QUA1) was involved in the HG biosynthesis (Bouton et al. 2002, Leboeuf et al. 2005, Mouille

et al. 2007, Orfila et al. 2005), although the QUA1 may also cause the decreased xylan synthase activity also suggesting a connection to xylan synthesis (Orfila et al. 2005). Recent mutant studies of *Arabidopsis thaliana* also suggested that the function of tumorous shoot development2 (TSD2) and QUA3 as methyltransferase, plays an important role in cell adhesion and plant development (Krupková et al. 2007, Miao et al. 2011).

HG cross-linked with the other cell wall polymers gives the plant mechanical support (Caffall and Mohnen 2009). The GalA oligosaccharides are well known to be part of a signalling cascade that senses plant cell wall pectin degradation upon pathogen attack (Kohorn et al. 2009, Ridley et al. 2001). Recent studies on the transgenic expression of EPG (endo-polygalacturonase) in apple, tomato, soybean hypocotyl and *Arabidopsis thaliana* revealed that the HG-Ca^{2+}complexes played an important role on the cell wall strengthening, and may affect wall expansibility (Atkinson et al. 2002, Capodicasa et al. 2004, Ezaki et al. 2005).

1.3.3.2 Rhamnogalacturonan-I

Rhamnogalacturonan-I (RG-I) represents 20-35% of pectin (Mohnen 2008). It contains a backbone of the repeating disaccharides GalA and rhamnose. The backbone may be acetylated at C2 and/or C3 by α-L-rhamnose residues (Figure 1.4). RG-I is known as the 'hairy' region, due to many branching side chains (Carpita and Gibeaut 1993). RG-I side chains are the sites of feruloylation with both β-1,4-D-galactan and α-1,5-L-arabinan chains in a small group of plants that includes sugar beet (Øbro et al. 2004, Ralet et al. 2005). These two predominant side chains whether linear or branched are linked to approximately half of the rhamnose residues of the RG-I backbone, but the core of the side chains usually does not exceed 50 GalA residues (Eda and Kato 1980).

The pectic arabinosyltransferase (AraT) activity was firstly reported in 1972 by Odzuck et al (Odzuck and Kauss 1972). Recent study has been reported that a

Golgi-localized α-1,5-arabinan:β-1,3-arabinopyranose AraT can transfer a single arabinopyranose residue onto the non-reducing end of the α-1,5-arabinooligosaccharide acceptors (Ishii et al. 2005b, Nunan and Scheller 2003). Ishii et al identified that the arabinopyranosetransferase can transfer a single arabinopyranosyl residue onto the β-1,4-D-galactooligosaccharides in an α-configuration, and the β-1,4-galactan:α-1,4-AraT complex can prevent the further galactosylation of the galactooligosaccharides (Ishii et al. 2004, Ishii et al. 2005a). A recent study on rice revealed that a UDP-arabinopyranose mutase (UAM) can catalyse the reversible formation of the UDP-arabinopyranose to UDP-arabinofuranose (Konishi et al. 2007). An arabinan:α-1,5-arabinosyltransferase (ARAD1, GT47 family, subgroup B) has been identified through *Arabidopsis thaliana* T-DNA insert mutant ARABINAN DEFICIENT1 analysis (Harholt et al. 2006). The knockout mutant of ARAD1/2 stem cell walls reduced 54% of arabinan compared with the wild type *Arabidopsis* (Harholt et al. 2006, Harholt et al. 2012). Recent study reported that *Arabidopsis thaliana* knockout mutants in the corresponding genes of GALACTAN SYNTHASE1 (GALS1), GALS2 and GALS3 (GT92 family) had a decreased β-1,4-galactan content, and overexpression of GALS1 resulted in plants with 50% higher β-1,4-galactan content suggesting GT92 enzyme as β-1,4-galactan synthase (Liwanag et al. 2012).

The RG-I functions as a linkage with the other cell wall polymers such as XyG in wall fractions of tomato, maize, barley and *Arabidopsis* (Keegstra et al. 1973, Popper and Fry 2005, Wilder and Albersheim 1973), giving the plant flexible structure (Caffall and Mohnen 2009). The RG-I and XyG may be linked already in the Golgi although the nature of this linkage is unknown (Popper and Fry 2008), as whether XyG is synthesized onto an RG-I side chain or by transglycosylation reaction (Scheller and Ulvskov 2010). Keegstra et al suggested that XyG is synthesized onto an RG-I galactan side chain (Keegstra et al. 1973). The RG-I side

chains are developmental and tissue-specific differentially regulated in the types of sugars attached to the RG-I backbone, which suggests its various functional specialization although not well studied yet (Ochoa-Villarreal et al. 2012). For example, the rhamnose residues can range from 20-80% of pectin from different plants and extraction methods (O'Neill et al. 1990). It has been reported that the galactan and arabinan side chains of RG-I were not located in the same regions of HG domains and they were spatially regulated in relation to the cell walls of tomato pit fields (Orfila and Knox 2000, Orfila et al. 2001), RG-I arabinan and the HG-calcium complexes could also affect stomatal function of broad bean (*Vicia faba*) (Franks et al. 2001). Besides, the galactan and arabinan are highly mobile polymers among the pectin components, and this mobility can be affected by the hydration of the cell wall (Tang et al. 1999). Recent study using RG-I antibodies-that are LM5, LM6, INRA-RU1 and INRA-RU2 antibodies (Jones et al. 1997, Ralet et al. 2010, Willats et al. 1998) showed that in tobacco seed endosperm the features of the RG-I polymer display spatial heterogeneity at the level of the tissue and the level of single cell walls (Lee et al. 2013). Arsovski et al reported that the arabinan in seeds may have a storage function but also have a more direct role in seed germination (Arsovski et al. 2009).

1.3.3.3 Rhamnogalacturonan-II

Rhamnogalacturonan-II (RG-II) is the most complex and branched polysaccharide in plant cell walls, and it is a minor pectic component of plant cell walls ranges from 0.5 to 8% in monocotyledons and dicotyledons, and less than 0.1% in commelinid monocotyledons primary cell walls (Matsunaga et al. 2004). RG-II is made up of 7 to 9 α-1,4-D-galacturonic acid (GalA) residues backbone (a HG backbone) with 4 complex side chains consisting of 12 different monosaccharides (Jensen et al. 2008, Willats et al. 2006, Willats et al. 2001a, Zandleven et al. 2006) (Figure1.4). The RG-II polymers can be self-associated with borate and form a borate-cross-linked RG-II dimer complex (dRG-II) which was first demonstrated

in sugar-beet, and the RG-II polymers contain about 95% of this complex which makes the structure of the RG-II highly conserved among vascular plants (Ishii and Matsunaga 2001, Matsunaga et al. 2004, O'Neill et al. 2004).

RG-II with its complex structure must require a large number of GTs for its biosynthesis, however, its biosynthesis has not been much studied (Harholt et al. 2010, Mohnen 2008). A group of *Arabidopsis* α-1,3-D-xylosyltransferase RGXT (RGXT1, RGXT2 and RGXT3, GT77 family) proteins has been found involving in the RG-II biosynthesis, which can transfer xylose from UDP-α-D-Xyl onto fucose in an α-1,3 linkage as this glycosidic linkage is only present in the RG-II structure (Egelund et al. 2008, Egelund et al. 2006, Petersen et al. 2009). Iwai et al suggested that the NpGUT1 (glucuronosyltransferase1, GT47 family) protein could transfer the GlcA onto the L-fucose in the RG-II side chainA (Iwai et al. 2002). The *Nicotinan plumbaginfolia* NpGUT1 mutant caused defects in the GlcA of the RG-II, and largely reduced the formation of the dRG-II (Iwai et al. 2002). However, later studies showed that the NpGUT1 is not directly involved in the RG-II synthesis (Wu et al. 2009, Harholt et al. 2010). The NpGUT1 and *IRX*10/*IRX*10L (GT47 family) are identified as orthologs by Wu et al (Wu et al. 2009). The orthologous genes of *Arabidopsis thaliana IRX*10 and *IRX*10L are strongly suggested to be involved in the xylan biosynthesis, and the related *irx*10 and *irx*10L *Arabidopsis thaliana* mutants showed no change in the RG-II structure (Wu et al. 2009). It has been reported that the *Arabidopsis thaliana* mutant male gametophyte defective 4 (MGP4) plays important roles in pollen tube and root growth by acting as a xylosyltransferase involved in the biosynthesis of pectic RG-II (Liu et al. 2011).

The dRG-II complex of RG-II covalently cross-linked among the pectic polymers such as HG, RG-I and RG-II backbone forms the network of the plant cell walls, giving strength, flexibility and functionality to the plant cells (Ochoa-Villarreal et al. 2012). It has been reported that boron played an important role in plant

reproduction, nitrogen fixation, and plant cell wall strengthening as symptoms of slowed root growth, degeneration of new growth, meristematic regions and reproductive organ were showed in boron deficiency *Arabidopsis* plants (Blevins and Lukaszewski 1998). Recent studies also revealed that borate is directly involved in the reversible dimerization of the RG-II polymers, and plays key role in the meristematic and reproductive systems of *Nicotiana tabacum* and *Nicotiana plumbaginifolia* (Bar-Peled et al. 2012, Caffall and Mohnen 2009, Iwai et al. 2002, Iwai et al. 2006).

1.3.3.4 Xylogalacturonan

Xylogalacturonan (XGA) contains a backbone of the chain of GalA residues, with a single xylose residue attached to the O-3 position of the chain (Figure 1.4). XGA is especially abundant in the reproductive tissues of cell walls of dicotyledons, and also present in the other tissues such as *Arabidopsis* leaves and stems (Zandleven et al. 2007).

The XGA xylosyltransferase XGD1 (GT47 family, subgroup C) protein expressed in *Nicotiana benthamiana* (*N. benthamiana*) had been reported to transfer xylose residues onto oligogalacturonides. The xylogalacturonan deficient1 (*xgd1*) *Arabidopsis thaliana* mutant showed reduced levels of pectic XGA, compared with the wild type leaves. This XGD1 protein is localized in the Golgi vesicle by exhibited expression of a fluorescent fusion protein in *N. benthamiana* (Jensen et al. 2008). However, the XGD1 *Arabidopsis thaliana* mutant showed no difference from the wild type upon immunolabeling using the LM8 antibody (Willats et al. 2004), which is specific for highly substituted XGA, suggesting that other yet-to-be-identified β-1,3-XylTs also exist (Jensen et al. 2008). To date, the function of pectic XGA is not well known.

1.4 Arabinogalactan-proteins (AGPs)

1.4.1 Structure

Arabinogalactan-proteins (AGPs) are a diverse group of cell surface proteoglycans widely distributed in the plant kingdom (Majewska-Sawka and Nothnagel 2000, Nothnagel 1997, Showalter 1993, Tan et al. 2012). AGPs belong to the hydroxyproline-rich glycoprotein families (HRGPs), along with the proline (Pro)-rich glycoproteins (PRPs) and the extensins, and they are rich in hydroxyproline-(Hyp, hydroxylated proline) and are highly glycosylated (Nothnagel 1997, Showalter 1993). The AGPs can bind to synthetic compounds known as Yariv reagents, in particular the β-glucosyl Yariv reagent, which is extremely useful in their detection and precipitation (Ellis et al. 2010, Yariv et al. 1967). A recent study has shown that the β-Galactosyl Yariv reagent need at least five residues of β-1,3-galactan chains for precipitation (Kitazawa et al. 2013).

The key structural features of AGPs are their carbohydrate and their protein. Classical mature AGPs also have a glycosylphosphatidylinositol (GPI) membrane anchor (Majewska-Sawka and Nothnagel 2000, Showalter 1993, Showalter 2001). The carbohydrate is usually in the form of the type II arabinogalactan (AG) side chains, which are O-glycosidically linked to the Hyp residues on the protein backbone (Ellis et al. 2010, Showalter 2001). The carbohydrate fraction of the AGPs constitutes the majority of the molecular mass (90-98%, w/w) (Nothnagel 1997). The AG fractions have a backbone of β-1,3-D-linked galactosyl (Gal) residues (that is 1,3-β-D-galactan), substituted at C/O-6 by the β-1,6-D-galactan side chains carrying large numbers of terminal arabinosyl (Ara), rhamnosyl (Rha) and galactosyl residues, and large amounts of glucuronic acid (GlcA) (especially in gum arabic), giving rise to a chain of neutral or negative charge (Ellis et al. 2010). Most AGPs have protein backbones of approximately 100 amino acid residues, while the AG fractions have 10-13 amino acids of protein backbones (Schultz et al.

2002). The protein backbone of AGPs constitutes 1-10% (w/w) of the molecular mass, and is rich in Hyp/Pro, Ala, Ser and Thr (Ellis et al. 2010). Most AGPs identified in plants have the GPI anchor addition signal which is responsible for the anchoring of the AGPs to the cell membrane (Chatterjee and Mayor 2001).

The tertiary structures of AGPs have been proposed as two models: the "wattle blossom" model (Fincher et al. 1983), based on their biophysical properties, and the "twisted hairy rope" model, mainly on their chemical properties (Qi et al. 1991) (Figure 1.5). The major difference between the two types of models is their secondary structure of the glycan side chains. The glycan side chains of the "wattle blossom" model has a thin ellipsoid shape (Fincher et al. 1983), while the glycan side chains of the "twisted hairy rope" model are parallel with the protein core, giving a rod-like appearance (Qi et al. 1991). Mahendran et al suggested that the AGP fraction of gum arabic was consistent with the "wattle blossom" model (Mahendran et al. 2008), whereas another AGP fraction, the AG peptide F1 fraction from gum arabic, was difficult to fit either of the two models (Sanchez et al. 2008). These studies suggested that the tertiary structures of the AGPs are various, and further work needs to be done to clarify the AGP structure (Ellis et al. 2010).

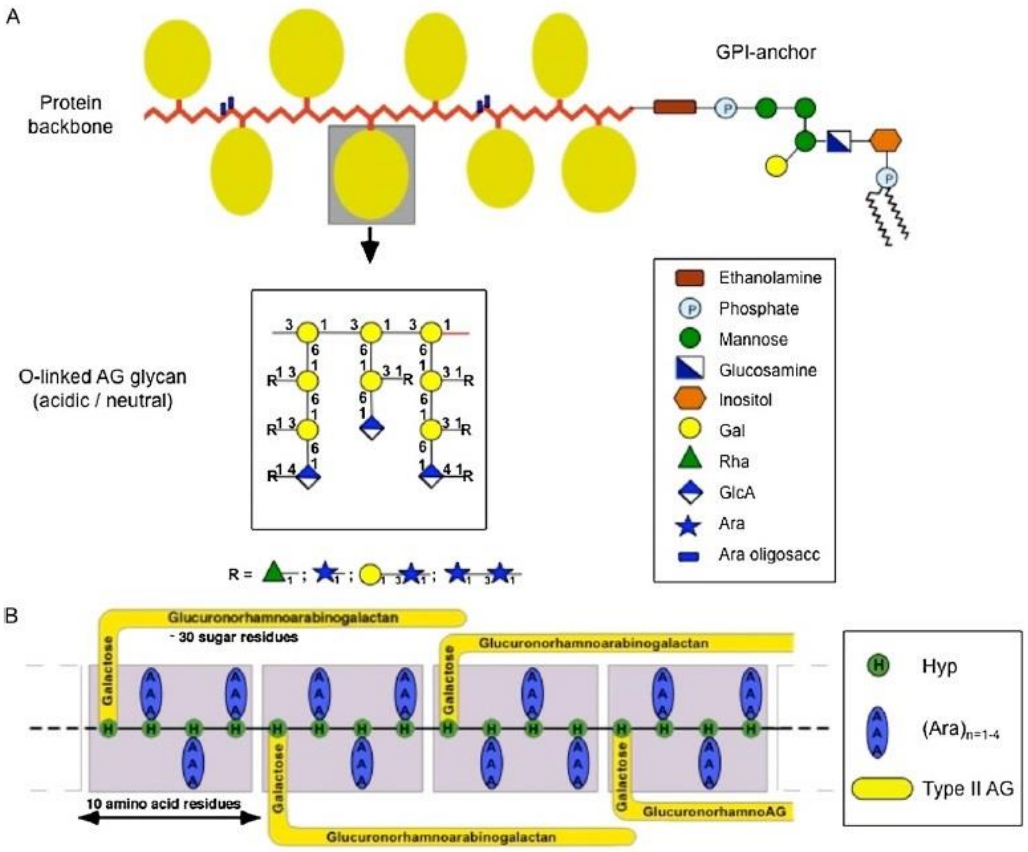

Figure 1.5: Schematic structure of AGPs. **(A):** The "wattle blossom" model of an AGP attached to a GPI membrane anchor. Most Hyp residues of the AGP backbone bear an AG chain. Each AG chain may have 15 or more repeats of the β-1,3-linked Gal residues. The GPI anchor has an ethanol amine-phosphate (P) between the anchor and the C terminus of the protein backbone, and this is common for all GPI anchors. **(B):** The "twisted hairy rope" AGP model. This glucuronorhamnoarabinogalactan (GAGP) has a galactan backbone with GlcA, Rha, and Ara side chains. (Taken from (Ellis et al. 2010)).

1.4.2 Classification

AGPs are divided into "classical" and "nonclassical" forms depending on their core protein (Du et al. 1996, Mau et al. 1995). Classical AGP core proteins generally consists of at least three distinct domains, an N-terminal signal sequence, a region rich in Pro/Hyp, and a hydrophobic C-terminal domain for the addition of a GPI

anchor (Gao et al. 1999, Park et al. 2003). On the other hand, the nonclassical AGPs that have been studied do not have this GPI anchor attachment region (Majewska-Sawka and Nothnagel 2000, Youl et al. 1998). For example, the AG-peptides belong to the classical AGPs (Schultz et al. 2002), while the fascilin-like AGPs (FLAs) are a group of nonclassical AGPs. The FLAs differ from the classical AGPs because they contain conserved fasciclin domains within the mature peptide (Faik et al. 2006).

1.4.3 Biosynthesis

The biosynthesis of AGPs is complex and not well known due to their complex structure. Early studies on carrot and French bean suggested that the core protein might have proline residues modified to hydroxyproline (Bolwell et al. 1985, Chrispeels 1984). Later *Arabidopsis* genome sequencing studies suggested that this process was carried out by the prolyl-4-hydroxylase (P4H) enzyme (P4H-1, P4H-2) (Hieta and Myllyharju 2002, Tiainen et al. 2005). Recent studies reported that the P4H enzymes are located in both the Golgi and the endoplasmic reticulum (ER) (Yuasa et al. 2005). The biosynthesis of carbohydrate glycan side chains required the GT31 glycosyltransferase (GalT) proteins which possess the β-1,3-GalT activity (Ellis et al. 2010). The initial enzyme O-galactosyltransferase adds the first Gal residue to a Hyp residue in the AGP protein backbone, this process is predominantly located in the ER (Oka et al. 2010). After that, several different GalTs will be required to construct the complex glycan side chains (Oka et al. 2010). Recent studies suggested that the AtFUT4 and AtFUT6 enzymes (GT37 family) acted as fucosyltransferases (FUTs) that are specific for AGP glycosylation (Wu et al. 2010b). The location of the AtFUT6 was in the Golgi apparatus supporting that much of the AG side chains occurs in the Golgi (Wu et al. 2010b). Lalanne et al suggested that the *SETH1* and *SETH2* genes are involved in the biosynthesis of the GPI anchor pathway (Lalanne et al. 2004). Tan et al suggested

that the possible biosynthesis mechanisms for ARABINOXYLAN PECTIN ARABINOGALACTAN PROTEIN1(APAP1) - a proteoglycan covalently attached with AG, arabinoxylan and pectin domains might be that after the transportation of pectin and arabinoxylan glycans onto AGP in the Golgi or to GPI-anchored AGP on the plasma membrane, cell wall deposition was formed by the subsequent cleavage of the GPI anchor (Tan et al. 2013). To date, much more work will be required to understand the AGP biosynthesis.

1.4.4 Function

The function of AGPs is various due to their heterogeneous nature. AGPs may act as a type of cross-linker in cell walls, connecting some pectins and non-cellulosic polysaccharide with at least one AGP, providing a network between wall structural proteins and wall polysaccharides (Tan et al. 2013). AGPs have been implicated in many processes in plant growth and development, such as cell expansion, cell division and plant reproductive development (Seifert and Roberts 2007). For example, transgenic cucumber plants expressing CsAGP1 which encode a classical AGP in cucumber have been shown a taller stature and earlier flowering than the wild type plants, suggesting that the CsAGP1 is involved in the stem elongation (Park et al. 2003). Yang and colleagues reported that AGPs had important roles in *Arabidopsis thaliana* growth and development, as the T-DNA knockout mutant have a delayed and smaller growth (Yang et al. 2007). Coimbra et al found that the AGPs are important for the pollen grain development of *Arabidopsis thaliana* (Coimbra et al. 2009). Lamport et al suggested that classical AGPs may act as pectin plasticizers (Lamport et al. 2006). In the moss *Physcomitrella patens* AGPs play essential role in cell expansion specifically in the extension of apical tip-growing cells (Lee et al. 2005b). AGPs also play important role in plant pathogen infection resistance and salt tolerance (Gaspar et al. 2004, Lamport et al. 2006).

1.5 Lignin

1.5.1 Structure

Lignin is the complex phenolic heteropolymer mainly produced by the oxidative coupling of three hydroxycinnamyl alcohol monomers: ρ-coumaryl alcohol, conifer alcohol, and sinapyl alcohol (Boerjan et al. 2003). These monolignols produce ρ-hydroxyphenyl (H), guaiacyl (G) and syringyl (S) phenylpropanoid units when incorporated into the lignin polymer. Dicotyledons angiosperm plants (hardwood) have lignins consisting of more G and S units, and little amount of H units, while gymnosperm plants (softwood) contain lignins mostly of G units with low levels of H units. By contrast, monocotyledons contain lignins with more H units than dicotyledons, and they also have G and S units (Baucher et al. 1998). Lignification is the process by which these different units are linked together through radical coupling reactions (Boerjan et al. 2003, Sarkanen and Ludwig 1971), and it is also called lignin deposition when carried out in the plant cell walls. Lignin deposition appears at the final xylem cell differentiation stages and mainly takes place during the secondary cell wall thickening (Donaldson 2001).

1.5.2 Biosynthesis

The biosynthesis of lignin is complex and remains unclear, although some targeting enzymes such as caffeic acid O-methyltransferase (COMT), cinnamoyl-CoA reductase (CCR) and cinnamyl alcohol dehydrogenase (CAD) involved in the biosynthesis process have been characterized (Boerjan et al. 2003, Halpin et al. 1994, Piquemal et al. 1998, Tsai et al. 1998). Generally, the lignin monolignols are biosynthesized via the phenylpropanoid pathway leading to lignin precursors, all these steps are carried out within the plant cell (Bonawitz and Chapple 2010). After that, these lignin precursors are eventually polymerized in the apoplastic space by peroxidases and laccases, which requires that monolignols be transported across

the plasma membrane by an ATP hydrolysis - dependent transport process (Alejandro et al. 2012, Miao and Liu 2010). Herrero et al reported that the *Arabidopsis* peroxidase 72 (AtPrx72) played an important role in lignification (Herrero et al. 2013). The laccase T-DNA insertion of *Arabidopsis thaliana* mutants - *lac4* and *lac7* mutants had 20-40% lower of lignin content than the wild types, which indicates they are contribute to the lignin deposition (Berthet et al. 2011). Recent studies on *Arabidopsis thaliana* mutant and yeast suggested that the AtABCG29 is a monolignol (ρ-coumaryl alcohol) transporter involved in the lignin biosynthesis (Alejandro et al. 2012).

1.5.3 Function

Lignin is important for the structural integrity of cells with secondary cell walls, and plays crucial role in the stiffness and strength of stems (Chabannes et al. 2001, Jones et al. 2001). Lignin may form chemical bonds with the non-cellulosic polysaccharide in the wall and gradually eliminates water, forming a hydrophobic environment (Boerjan et al. 2003). Additionally, lignin waterproofs the cell wall, making the water and solutes transportation through the vascular system, and protecting plants against pathogens (Boerjan et al. 2003, Sarkanen and Ludwig 1971).

1.6 Plant taxonomy & distinctive cell wall biochemistry of grasses

1.6.1 Taxonomy of plants

The plant kingdom can be divided into algae, bryophyta, ferns, lycophyta and spermatophyte (Figure1.6). Based on the presence of vascular tissue, land plants are divided into nonvascular plants and vascular plants. Nonvascular plants include bryophyta and they do not have true leaves, stems or roots. Vascular plants have vascular tissue with true leaves, stems and roots, but they may or may not

produce seeds (Goldberg 1988). Ferns, horsetails and club mosses are the major seedless vascular plants which reproduce by spores. The vascular plants which reproduce by seeds are divided into two groups: gymnosperms and angiosperms. Gymnosperms have "naked" seeds that are usually protected by cones and include spruce, pines, cedars and firs (Schmidt and Jøker 2001). Angiosperms are flowering plants and the seeds are produced and protected within their fruits. Angiosperms are subdivided into monocotyledons and dicotyledons based on the number of cotyledons or seed leaves in the embryo of the plant (Dahlgren 1980). Monocotyledons have a single seed leaf and leaves with parallel venation, and their vascular tissue scattered in bundles throughout the stem (Ye 2002). Monocotyledons can also be divided into commelinidae and non-commelinidae groups and this is important in terms of cell walls as commelinid monocotyledons have a distinctive cell wall biochemistry (Vogel 2008) that will be discussed later in the following section. The three target plants - *Miscanthus* species, wheat and *B. distachyon* are all in the Poaceae family, which is a family of the commelinidae. In contrast, dicotyledons have two seed leaves. The leaves exhibit net-veined venation and their vascular tissue is scattered in a ring in the stem (Rudall 1992). Monocotyledons are usually herbaceous, but dicotyledons often have secondary growth and produce wood (von Konrat et al. 2008).

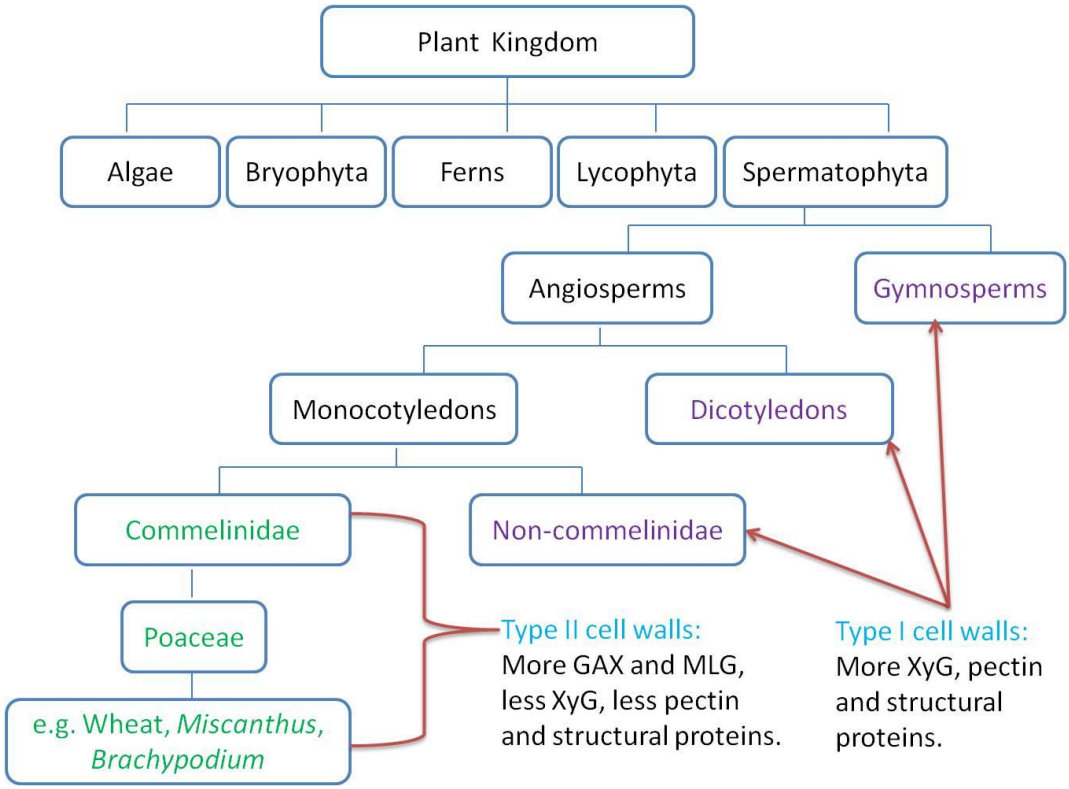

Figure 1.6: Broad taxonomic overview of plants. Wheat, *Miscanthus* species and *B. distachyon* of the Poaceae family are the focus of this project. These species have type II cell walls which have MLGs and more GAXs but less XyG, pectin and structural proteins compared with type I cell walls.

1.6.2 Plant cell wall biochemistry

The primary cell walls of plants are classified into two major groups, type I walls and type II walls (Figure 1.7), based on the chemical structures of components, the cell wall architecture and their biosynthetic processes (Carpita 1996, Carpita and Gibeaut 1993) although recent studies proposed a type III cell wall of some ferns and a lycopod that has distinct feature of being rich in mannans with low pectins (Leroux et al. 2013, Silva et al. 2011). In spermatophytes, mannans and glucomannans are generally much less abundant than xylan, XyG and MLG polysaccharides (Scheller and Ulvskov 2010). Generally type I cell walls, found in dicotyledons, non-commelinidae monocotyledons and gymnosperms, consisting of

cellulose microfibrils encased in a network of XyG, pectin and structural proteins with low levels of heteroxylans and this mostly in secondary cell walls. Type II cell walls, found only in the commelinidae monocotyledons (e.g. Poaceae family) are composed of cellulose microfibrils encased in heteroxylans, and low levels of XyG, pectin and structural proteins (Carpita 1996, Carpita and Gibeaut 1993, Vogel 2008). Previous studies reported that the Poaceae has distinct cell walls and was the only family with MLGs in walls (Vogel 2008), but recent studies has been reported that MLG was also abundantly found in *Equisetum arvense* (Burton and Fincher 2009, Sørensen et al. 2008). In grasses, xylans have the general structure of all xylans but with some unique features such as the highly substituted GAXs which makes up 35% of vegetative tissues cell walls (Ebringerova et al. 2005). In grasses arabinoxylan is the major cell wall polysaccharide, while in nongramineous species this polysaccharide is lower (Darvill et al. 1980a). In barley aleurone and barley malts the highly substituted GAXs contain O-2 and doubly branched O-2, O-3-linked arabinosyl units in addition to the abundant O-3-linked units in wheat and barley (Bacic and Stone 1981, Vietor et al. 1994). In some ryegrasses the acetyl content account for almost 10% of the dry mass of the cell wall (Gordon et al. 1985). The highly substituted GAX has been reported to be associated with the maximum growth rate of maize coleoptiles (Carpita and Whittern 1986). Another unique structural feature of grass xylans is the ferulated arabinoxylan - the feruloyl groups attached on the C-5 position of arabinan residues that contribute to cell wall recalcitrance (Bacic et al. 1988, Harris et al. 1997, Marcia 2009, Wende and Fry 1997, Yu et al. 2005).

In summary, grass cell walls differ dramatically from dicotyledon cell walls in terms of the major structural polysaccharides present and the linkage of polysaccharides (Vogel 2008). However, the distribution and functions of cell wall polysaccharides of three grasses - *Miscanthus* species, wheat, *Brachypodium distachyon* are not well known and as such form the focus of this project.

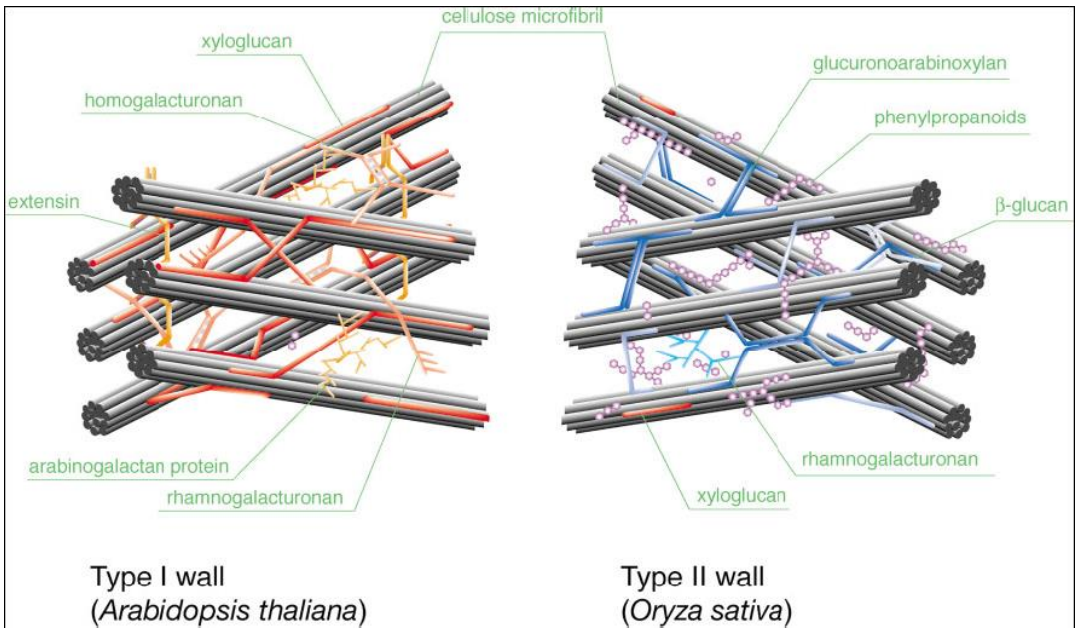

Figure 1.7: Structural models of type I and type II walls, represented by *Arabidopsis* and rice, respectively. (Taken from (Buchanan et al. 2000)).

1.7 Plant species studied in this thesis

1.7.1 *Miscanthus* species

Miscanthus species are grasses which are native to tropical and subtropical regions of southern Asia and Africa. *Miscanthus* is first described by Andersson in 1885 (Scally et al. 2001). *Miscanthus* (*Miscanthus* x *giganteus* GREEF et DEU) was first brought to Europe from Japan in 1935 by Aksel Olsen (Greef and Deuter 1993), and extensive field trials for horticultural have been carried out throughout Europe since 1983 and then widely studied for combustion to produce heat and electricity (Anderson et al. 2011, Lewandowski et al. 2000).

Miscanthus is in the Poaceae family, Panicoideae subfamily and Andropogoneae tribe (Amalraj and Balasundaram 2006, Barkwoeth et al. 2007), the

Andropogoneae tribe also includes economically important grasses in the *Saccharum*, *Sorghum* and *Zea* genera (Barkwoeth et al. 2007). Due to the C4 photosynthetic pathway and high carbon dioxide fixation rate, *Miscanthus* species can grow very rapidly, producing high biomass yields with low-input requirements (Le Ngoc Huyen et al. 2010, Lewandowski et al. 2000, Lewandowski et al. 2003, Purdy et al. 2013).

Miscanthus sinensis (*M. sinensis*) (2n=38) is native to eastern Asia and can grow to 0.8-2 m tall. It is widely used in Japan for forage and thatching. Whilst *Miscanthus sacchariflorus* (*M. sacchariflorus*) (4n=76) is native to temperate Asia, it can grow to 0.9-2.5 m in height. *M. sacchariflorus* is widely used in China in the cellulose industry and in Europe for gardens (Anderson et al. 2011, Clifton-Brown et al. 2008).

Miscanthus x *giganteus* (*M.* x *giganteus*) (3n=57) is the sterile hybrid between *M. sinensis* and *M. sacchariflorus*. It grows faster and higher than its parents (up to 4m in height), producing high annual biomass yields of 20-26 tons dry weight per hectare (Kaack et al. 2003, Yoshida et al. 2008). Spring harvested biomass generally contains between 70-90% cell wall (Hodgson et al. 2010a, Hodgson et al. 2010b). It has been used as biofuel by burning or fermentation to produce heat and electricity since 1983 in Europe. It has been reported that the contribution of *M. sinensis* to the genome of *M.* x *giganteus* is thought to provide adaptation to cooler climates, whereas *M. sacchariorus* provides genetic resources for warmer regions because it is more adapted to a warmer climate (Jørgensen 1997, Lewandowski et al. 2000). As a sterile hybrid, *M.* x *giganteus* does not from seeds and has to be propagated from the rhizome cuttings. In the USA, growing 11.8 million hectares of *M.* x *giganteus* would be required to produce 35 billion gallons of ethanol per year, while it would require much more hectares of corn or switchgrass to produce the same volume of ethanol (Heaton et al. 2008). It has been reported that *M. sinensis* has greater tolerance to a lower temperature in terms of winter survival,

compared with *M.* x *giganteu*s (Clifton-Brown and Lewandowski 2000). However, *M.* x *giganteus* has higher levels of photosynthesis compared with other C4 grasses (such as *zea mays* and switchgrass) under cool conditions (Dohleman and Long 2009, Dohleman et al. 2009, Naidu et al. 2003, Wang et al. 2008). In 2013, Purdy et al reported that *M.* x *giganteus* has a superior tolerance to chilling shock than other two genotypes of *Miscanthus* species, *M. sacchariflorus* and *M. sinensis* (Purdy et al. 2013).

It has been reported that the major compositions of studied *Miscanthus* genotypes were glucan, xylan and lignin (Zhang et al. 2012b). However, the different *Miscanthus* genotypes showed significant diversity in compositions, such as the glucan levels ranging from 27.7% to 48.6% (Zhang et al. 2012b). The *M.* x *giganteus* and *M. sacchariflorus* were much more similar form the composition aspect, compared with *M. sinensis* (Hodgson et al. 2011). *M.* x *giganteus* and *M. sacchariflorus* genotypes contain higher cellulose and lignin but lower hemicelluloses than *M. sinensis* (Hodgson et al. 2011). *M.* x *giganteus* has been described to have much greater concentrations of cellulose and lignin and less hemicellulose compared to its parents *M. sinensis* and *M. sacchariflorus* (Allison et al. 2011).

Owing to its high cellulose content and high biomass yields, *Miscanthus* species has been described as good candidate energy resource for the production of high levels of fermentable glucose into ethanol and this process requires the hydrolysis of cellulose into glucose using polysaccharide-active enzymes and then subsequently fermented into ethanol by yeast or bacteria (Carroll and Somerville 2009, Himmel et al. 2007, Rubin 2008, Sun and Cheng 2002). *Miscanthus* species can be used in the paper industry, pharmaceutical industry and for water and soil conservation (Heaton et al. 2004, Lewandowski et al. 2003). The anatomy and chemistry of stems of various *Miscanthus* genotypes has been reported in 2003 (Kaack et al. 2003). However, the major polysaccharides and their linkages in the

Miscanthus cell walls and their functions during growth have not been reported. Furthermore, nothing is known of the *in situ* location of polysaccharides in *Miscanthus* species of their developmental dynamics and this is the focus of this study.

1.7.2 Wheat

Wheat (*Triticum aestivum* cv. Cadenza) is one of the major crops of the world and it is the major source of energy and dietary fibre that provides numerous health benefits beyond simply providing calories (Harris and Smith 2006, Topping 2007). Recent cell wall studies carried out mainly on the wheat grain endosperms and wheat straw. The cell walls of wheat grain endosperm specifically consists of very high levels of arabinoxylan and MLG, low levels of mannan and cellulose (Saulnier et al. 2012, Suliman et al. 2012). It has been reported that the increase of water soluble arabinoxylan may improve the bread making quality of wheat flour (Saulnier et al. 2012). By contrast, the wheat straw (wheat stems, leaves, and traces of other organs mixture) is mainly composed of higher levels of cellulose, lower levels of non-cellulosic polysaccharide and lignin (Holopainen-Mantila et al. 2013). American farmers produced more than 100 million tons of wheat straw biomass in 1999, and the highest hydrolysis yields were obtained from samples that contain high level of cellulose and low amounts of xylan (Hamman et al. 2005, Holopainen-Mantila et al. 2013). The stem of wheat is an important organ of its nutrition storage and transportation. The cellulose content of stem is an important factor affecting the mechanical strength of wheat stem, and it is also closely related to the wheat yield (Wang et al. 2006). However, *in situ* analysis of the major polysaccharides of wheat stem cell walls during growth development has not been reported in detail.

1.7.3 *Brachypodium distachyon*

Brachypodium distachyon (Poaceae family) is a new model plant for grasses. As a temperate grass, diploid ecotypes of *B. distachyon* (2n=10) have five easily distinguishable chromosomes that display high levels of chiasma formation at the stage of the cell meiosis (Christiansen et al. 2005, Draper et al. 2001, Hasterok et al. 2004, Shi et al. 1993). The genome of the diploid *B. distachyon*-BD21 has been sequenced in 2010 and has a high degree of synteny with other grass genomes ((Rancour et al. 2012), International *Brachypodiumn* Initiative, 2010). The *B. distachyon* nuclear genome is similar in size from that of *Arabidopsis thaliana* which is an important dicotyledon model, making it the simplest genome described in grasses to date. *B. distachyon* is a self-fertile, inbreeding annual with a short life cycle of less than 4 months. These features, coupled with its fast growth, small stature (approximately 20cm at maturity) and undemanding growth requirements should make it a good genetic model plant and amenable to high-throughput genetics and mutant screens (Vogel and Bragg 2009, Vogel et al. 2006). Selected *B. distachyon* ecotypes displayed resistance or disease symptoms when infected by wheat/barley yellow stripe rusts (*Puccinia striformis*) and rice blast, making it also a model system to study the dynamic host/pathogen interactions (Parker et al. 2008, Vogel et al. 2006, Vogel et al. 2006b). Despite its small stature, *B. distachyon* has large seeds that should prove useful for studies on grain filling (Draper et al. 2001).

The improvement of *B. distachyon* as a model is of great value in the areas of plant cell wall biology and biomass research (Bevan et al. 2010, Gomez et al. 2008). It is suggested that the non-cellulosic monosaccharide component of *B. distachyon* is closely related to that of the important agricultural grasses (barley, wheat, *Miscanthus* and *Arabidopsis*), but significantly different from *Arabidopsis* (Gomez et al. 2008). When compared with some C3 grasses (such as winter wheat (*Triticum aestivum* L.); oats (*Avenasativa* L.); reed canarygrass (*Phalaris arundinacea* L.)

and bromegrass (*Bromus inermis Leyss.*)), *B. distachyon* mature stem cell walls have a relative increase of glucose and decrease of lignin (Rancour et al. 2012). The key variation in cell wall composition relied more on the plant organ (leaves, sheaths, stems and roots) rather than developmental stage of the plant (seedling, vegetative-to-reproductive transition and mature seed fill stages) (Rancour et al. 2012). Opanowicz et al reported that the *B. distachyon* grain endosperm has thick cell walls, compared with cereals (Opanowicz et al. 2011). Specifically, *B. distachyon* endosperm contains high cell wall polysaccharide content of 52% (w/w) in comparison with 2-7% (w/w) in other cereals (Guillon et al. 2011). Using FT-IR imaging, Opanowicz et al observed that the cell walls contain similar amounts of MLG and arabinoxylan to that of barley and oats (Opanowicz et al. 2011). The endosperm cell walls contain 40% (w/w) of MLG and made it the main polysaccharides suggesting MLG played an important role as storage compound (Guillon et al. 2011). However, the ratio of ferulic acid to arabinoxylan was higher in both the *B. distachyon* grain and seedlings than in the other cereals (Christensen et al. 2010, Guillon et al. 2011). Using a HPAEC-PAD (High performance anion exchange chromatography - pulsed amperometric detection) method, Christensen et al found that cell walls of *B. distachyon* seedlings contain 50-65% xylose (both from xylans and xyloglucan), less than 5% pectic monosaccharoides rhamnose and galacturonic acid together and MLGs (Christensen et al. 2010). For the *B. distachyon* cell wall biosynthesis study, Valdivia et al reported that the *Brachypodium SWNs* proteins - secondary wall NACs (NACs contain proteins of NAM-no apical meristem, ATAF1/2 protein, and CUC2-CUP SHAPED COTYLEDON 2 protein (Olsen et al. 2005)) may act as switches that turn on the secondary cell wall synthesis and cell death (Valdivia et al. 2013).

Vascular tissue anatomy (Figure1.8) and three-stage development of *B. distachyon* stem has been shown by Matos et al (Matos 2012). The first appearance of stem tissue occurred 18-22 days after germination (the stem elongation stage), the

developmental inflorescence stage occurred 25-30 days after germination, and the senescence stage happened 39-45 days after germination. The first internode increased significantly both in length and width before inflorescence emergence, but not after. Cellulose deposition only accumulated before the inflorescence emergence stage. Lignification increased during all of the stem internode development. The size and number of vascular bundles remained stable after the stem elongation, while the cell walls of the vascular bundle continued to thicken throughout all the plant development, suggesting that the cell wall biosynthesis carried out until plant senescence (Matos 2012).

Although much more cell wall studies have been carried out on *B. distachyon*, most of them focused on the grain and young seedlings. To date, detailed research of polysaccharide compositions and *in situ* analysis of *B. distachyon* stem cell walls have not yet been reported. As illustrated above, *B. distachyon* has been identified as a good genetic model plant, but whether it could also be a good cell wall modification model is not known, and this is what this project focuses on.

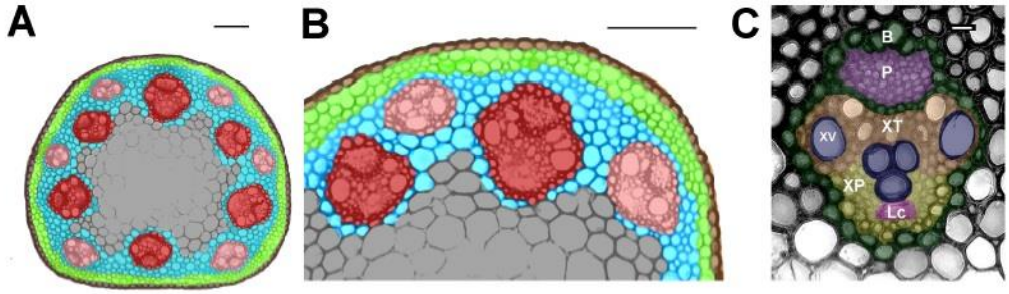

Figure 1.8: Anatomy of *B. distachyon* stem. (A): Cross section of the whole stem of *B. distachyon*, bar = 0.1 mm and (B): Higher magnification image of the first internode of *B. distachyon*, bar = 0.01mm. Brown, epidermis; lime green, chlorenchyma and sclerenchyma cells; cyran, interfascular region with sclerenchyma fibers; gray, pith; pink, outer vascular bundles; red, inner vascular bundles. (C): Vascular bundle, bar = 0.01mm.Green, (B)-bundle sheath; dark purple, (P)-phloem; blue, (XV)-xylem vessels; orange, (XT)-xylem tracheids; magenta, (Lc)-lacuna; yellow, (XP) -xylem parenchyma cells. (Taken form (Matos 2012)).

1.8 Biofuel and biomass degradation

Worldwide consumption of fossil fuels and the impacts of the global climate change have led to much more intensive research efforts in the development of alternative energy (Chundawat et al. 2011, Himmel et al. 2007). The alternative sources usually rely on biofuels, a sustainable and renewable energy resource that can provide ethanol (Han et al. 2011). Non-food plant biomass, such as switchgrass, poplar and *Miscanthus* has been used for deconstruction of their celluloses and non-cellulosic polysaccharide to sugars and upgraded to fuels (Chundawat et al. 2011). Conversion of plant cell walls into bioethanol can be processed into three steps. Firstly, a variety of physical, thermal, and chemical (such as acid and alkali) pretreatments have been carried out to improve the accessibility of the enzymes to the cellulosic biomass (Jordan et al. 2012). An efficient pre-treatment would increase the monosaccharide yields of native biomass hydrolysed with cellulases, xylanases and other enzymes form 20% up to 80% (Jordan et al. 2012). For example, the peroxide pretreatment of wheat straw or NaOH pretreatment of *Miscanthus* can both effectively increase the lignin solubilisation and cellulose availability (Han et al. 2011, Martel and Gould 1990). Secondly, some enzymes are required to release the major fermentable monosaccharides. For example, endocellulases and exocellulases are used to deconstruct cellulose; endoxylanases, β-xylosidases, acetylxylanesterases, and ferulic acid esterases are useful for the catalytic deconstruction of non-cellulosic polysaccharide (Jordan et al. 2012). Finally, these harvested sugars need further fermentation by micro-organisms (Jordan et al. 2012). Recent studies also used carbohydrate-binding modules (CBMs) alongside xylan-directed monoclonal antibodies - CBM2b-12 and CBM15 to study the recognition and degradation of xylan polymers in tobacco cell walls (Hervé et al. 2009, Hervé et al. 2010). However, this conversion process is challenging due to the recalcitrance of the plant cell wall - which has heterogeneous and complex structural wall constituents (Han et al. 2011, Jordan et al. 2012).

Owing to this, to know a clearer knowledge of the plant cell wall architecture will be of great value for the biomass degradation.

1.9 Cell wall probes

How the various polysaccharides present in plant cell walls are assembled and interlinked into their functional composites and changes through growth and development have not been reported in detail. Molecular probes such as monoclonal antibodies and carbohydrate-binding modules (CBMs), targeted to specific cell wall polysaccharides, are specific and sensitive tools that can be used in conjunction with fluorescence imaging to monitor heterogeneities in cell wall composition and organization at the cellular and sub-cellular levels (Freshour et al. 2003, Knox 1997, McCartney et al. 2005, Meikle et al. 1994, Verhertbruggen et al. 2009a). For example, monoclonal antibodies and molecular probes have been used to analyse plant cell wall components such as non-cellulosic polysaccharide and pectin (Marcus et al. 2008, Marcus et al. 2010, Moller et al. 2008). The monoclonal antibody BG1 was generated to detect the MLG in wheat grain (Meikle et al. 1994) (Figure1.9). The monoclonal antibodies LM10 and LM11 were developed to analyse xylan/arabinoxylan, both epitopes were abundant in cell walls of xylem and phloem fibers in tobacco stems, while in wheat grain the LM10 antibody only labelled the outer aleurone cell wall layer, the LM11 antibody labelled all aleurone cell walls (McCartney et al. 2005) (Figure1.10), and the LM12 antibody was developed to analyse the ferulated heteroxylan (Pedersen et al. 2012). The monoclonal antibody LM15, which binds to the XXXG structural motif of XyGs, has been developed for the immunofluorescence analysis of xyloglucan, this LM15 epitope labelled seed cotyledon parenchyma cell walls of both *tamarind* and *nasturtium*, and strongly binds to epidermal and parenchyma cell walls of pea stem (Marcus et al. 2008) (Figure1.11). The LM21 and LM22 monoclonal antibodies have been produced to detect heteromannans in stems of *Arabidopsis thaliana*, pea

and tobacco (Marcus et al. 2010). The LM18, LM19 and LM20 monoclonal antibodies were developed to detect unmethylesterified HG, low methylesterified HG and high methylesterified HG in tobacco stems, respectively (Verhertbruggen et al. 2009a). The LM5 antibody was used to detect (1-4)-β-D-galactan side chains of RG-I in tomato cell walls (Jones et al. 1997), and the LM6, LM13 probes were produced to detect arabinan side chains of RG-1 in lemon fruit and *Arabidopsis thaliana* (Moller et al. 2008, Verhertbruggen et al. 2009a, Willats et al. 1998). In addition, the LM2, MAC207 and the LM14 monoclonal antibodies have been developed to recognize AGPs in rice, carrot and *Arabidopsis thaliana* (Moller et al. 2008, Smallwood et al. 1996). These monoclonal antibodies were produced by immunising rodents with neoglycoproteins consisting of an oligosaccharide derived from the cell wall polysaccharide of interest coupled to BSA (Bovine serum albumin) protein to act as an immunogen (Marcus et al. 2008, McCartney et al. 2005). For carbohydrate-binding modules - CBMs that are derived from the non-catalytic subunits of cell wall degrading enzymes, and they predominantly bind to cell wall celluloses and non-cellulosic polysaccharide (Blake et al. 2006, Boraston et al. 2002, Hervé et al. 2009, Hervé et al. 2010, McCartney et al. 2006, Montanier et al. 2009). For example, the CBM3a has been produced to detect crystalline cellulose in stem cell walls of tobacco and bound strongly to all parenchyma cell walls (Blake et al. 2006), and the xylan-binding CBMs - CBM15, CBM35 were produced to recognize xylans in xylem secondary cell walls in tobacco, pea and flax stems (McCartney et al. 2006).

It has been reported that the XyG epitope is restricted to certain cell types of tobacco stem sections. Following enzymatic removal of HG from equivalent sections, the LM15 epitope was unmasked revealing distinct patterns of epitope occurrence across these stem sections and a diversity of occurrences in relation to the cell wall microstructure of a range of cell types (Marcus et al. 2008). It is also reported that using two novel mannan - directed monoclonal antibodies, LM21 and

LM22, the molecular recognition of mannans can be extensively masked by pectic HG and this masked-mannan was found to be a feature of pit field cell walls in stems of *Arabidopsis thaliana*, pea and tobacco (Marcus et al. 2008, Marcus et al. 2010). Recent studies revealed that the CBM3a cellulose, LM25 XyG epitope (Pedersen et al. 2012), LM19 HG epitope, LM5 galactan and LM6 arabinan epitopes were unmasked in certain endosperm cell walls of tobacco seeds where mannans were abundant after mannanase treatment (Lee et al. 2013, Lee et al. 2012). Davies et al also reported that the LM15 XyG epitope and the LM21 heteromannan epitope are masked by pectic HG in certain regions of syncytial cell walls of *Arabidopsis thaliana* root sections (Davies et al. 2012). These enzymatic and chemical deconstruction of cell walls could further our understanding of cell wall structure heterogeneity and cell wall micro-environments and may provide insights into the functions of specific polysaccharides and corresponding enzymes (Marcus et al. 2010). To date, nothing is known about polysaccharide masking in the three target grass cell walls used in this project and this is also the focus of this study.

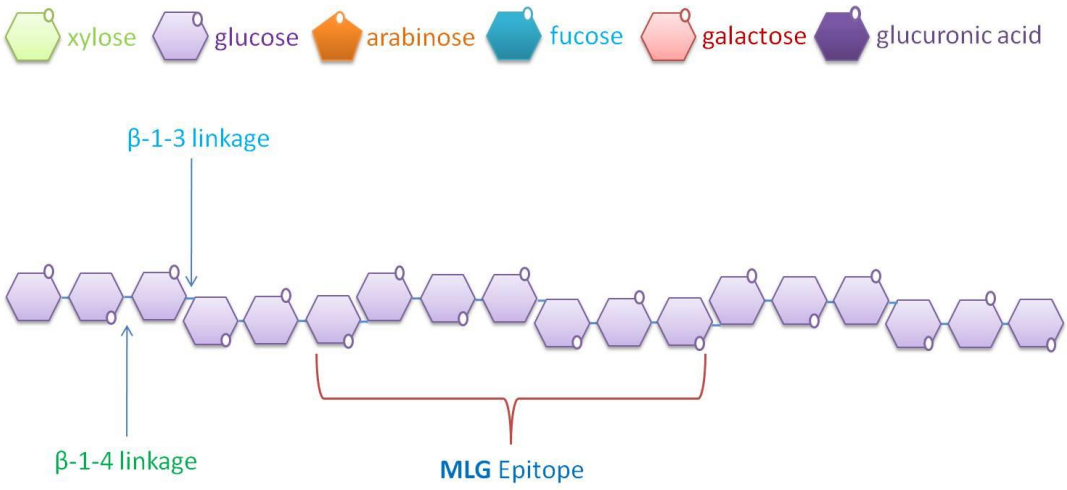

Figure 1.9: Schematic representation of the MLG polysaccharides structure showing the epitope of the monoclonal antibody BG1. The BG1 epitope is seven glucose residues with its β-1-3 and β-1-4 linkages.

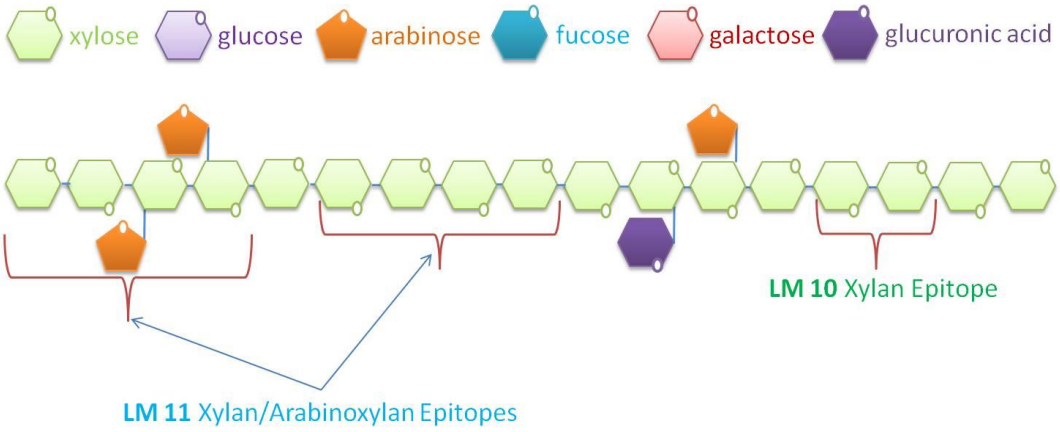

Figure 1.10: Schematic diagram of the xylan polysaccharides structure showing the epitopes of the monoclonal antibodies LM10 and LM11. The LM10 epitope is two xylose residues of the xylan backbone, while the LM11 epitope can be four xylose residues, and it can also be the four xylose residues with its side chains of the arabinose residues.

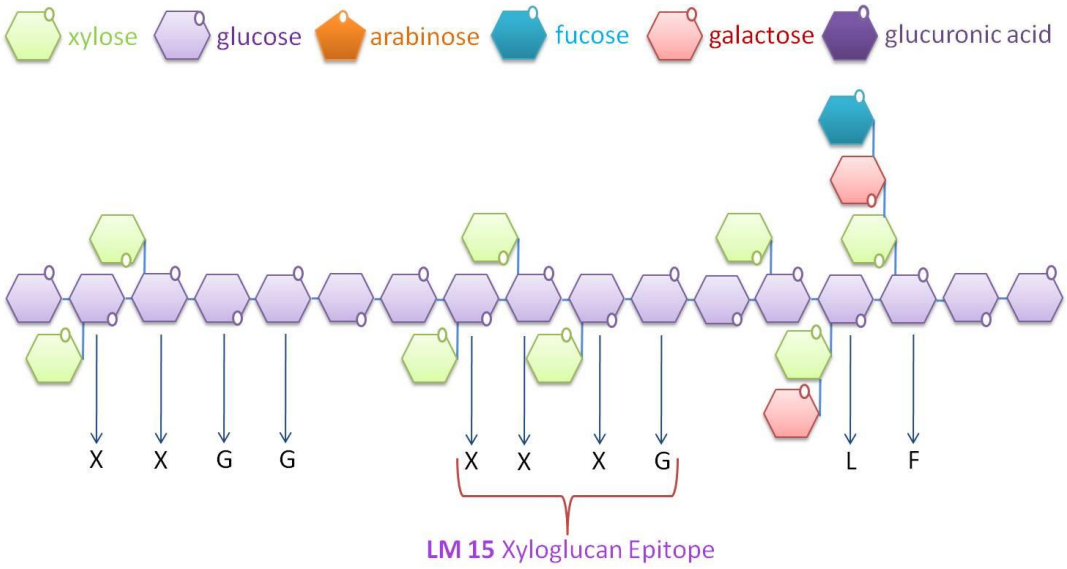

Figure 1.11: Schematic representation of the xyloglucan polysaccharides structure showing the epitope of the monoclonal antibody LM15. The LM15 epitope is four glucose residues with its three side chains of the xylose residues (XXXG motif).

1.10 Summary

The components of the grass cell walls are likely to play important roles in grass growth, development, grass yield and quality. Grasses are widely used as food and biofuels for human beings and livestock. Therefore, identifying the components of grass cell walls and their differences among different grass species will give us a clearer knowledge of the cell wall structure, which will contribute to improve our understanding of growth mechanisms and the use of biomass for energy and agriculture. However, *in situ* analysis of the stem cell wall polysaccharides of the three target grass species (*Miscanthus* species, wheat and *Brachypodium distachyon*) has not been reported, and that is what this project focuses on. This will be done by adopting an immunocytochemical approach using monoclonal antibodies and CBMs directed to celluloses and/or non-cellulosic polysaccharides to elucidate differences in cell wall structures among the grass species selected for study.

1.11 Aims and objectives

The objectives of the work carried out for this report were as follows:

- Investigate anatomical structures of stems of different *Miscanthus* species and lines: *Miscanthus* x *giganteus*, *Miscanthus sacchariflorus* and *Miscanthus sinensis*.
- Immunocytochemical characterisation of occurrence of polysaccharide epitopes in transverse sections of *Miscanthus* stems in different growth stages (both 50-day-old and 200-day-old stems), using the specific monoclonal antibodies and CBMs.
- Immunocytochemical characterisation of polysaccharide epitopes (both cellulose and non-cellulosic epitopes) in transverse sections of stems of wheat and *Brachypodium distachyon* in relation to growth and development.

- Study of the occurrence of polysaccharide masking in cell walls of the three *Miscanthus* species, wheat and *Brachypodium distachyon* stem materials using *in situ* enzyme deconstruction methods as well as specific monoclonal antibodies.
- Study of the major differences/similarities of the three *Miscanthus* species, wheat and *Brachypodium distachyon* stem materials to illustrate whether *Brachypodium distachyon* could be a good cell wall model plant for grasses.

Chapter 2

Materials and Methods

2.1 Plant materials

2.1.1 *Miscanthus* species

Miscanthus species were supplied by the Institute of Biological, Environmental and Rural Sciences-IBERS of Aberystwyth University (01/02/2011). The *Miscanthus* species used in this project were as follows: *Miscanthus* x *giganteus* (MB149 and MB312), *Miscanthus sacchariflorus* (MB177), and *Miscanthus sinensis* (MB183). All plants were grown in 5 L pots containing Osmocote exact patterned release fertilizer (standard 5-6 months) (Scotts, Australia), in the University of Leeds greenhouse with 16 h days and maintained at 20°C.

2.1.2 Wheat

Wheat (*Triticuma estivum* cv. Cadenza) grains were supplied by Rothamsted Research Institute. Plants were grown in 5 L pots containing Osmocote exact patterned release fertilizer, in the University of Leeds greenhouse with 16 h days and maintained at 20°C.

2.1.3 *Brachypodium distachyon*

Brachypodium distachyon (BD21-3) seeds were supplied by Professor W.G.T. Willats, University of Copenhagen. Plants were grown in 5 L pots containing Osmocote exact patterned release fertilizer, in the University of Leeds greenhouse with 16 h days and maintained at 20°C.

2.2 Molecular probes

2.2.1 Monoclonal Antibodies

Monoclonal antibodies used in this project are presented in Table 2.1 below.

Table 2.1: Monoclonal antibodies used in this study.

Anti-mannan	**Epitope**	**Reference**
LM21	Heteromannan	(Marcus et al. 2010)
LM22	Heteromannan	(Marcus et al. 2010)
Anti-xyloglucan		
LM15	XXXG motif of xyloglucan	(Marcus et al. 2008)
Anti-xylan		
LM10	(1-4)-β-D-xylan	(McCartney et al. 2005)
LM11	(1-4)-β-D-xylan/arabinoxylan	(McCartney et al. 2005)
LM12	Ferulated-heteroxylan	(Pedersen et al. 2012)
Anti-pectin		
Anti-HG		
LM18	Partially Me-HG/no ester	(Verhertbruggen et al. 2009a)
LM19	Low Me-HG/no ester	(Verhertbruggen et al. 2009a)
LM20	High Me-HG	(Verhertbruggen et al. 2009a)
LM7	Partially Me-HG/non-blockwise	(Clausen et al. 2003, Willats et al. 2001b)
Anti-RG-I		
LM5	(1-4)-β-D-galactan	(Jones et al. 1997)
LM6	(1-5)-α-L-arabinan	(Willats et al. 1998)
LM13	Linearised (1-5)-α-L-arabinan	(Moller et al. 2008, Verhertbruggen et al. 2009b)
Anti-AGP		
LM14	GlcA, AGP glycan	(Moller et al. 2008)
LM2	β-linked-GlcA in AGP glycan	(Smallwood et al. 1996, Yates et al. 1996)
JIM13-16	AGP glycan	(Knox et al. 1991, Yates et al. 1996)
MAC207	AGP glycan	(Pennell et al. 1989, Yates et al. 1996)
Other		
BG1	β-(1-3)(1-4)-glucan	(Meikle et al. 1994)

2.2.2 Carbohydrate-binding modules

Carbohydrate-binding modules directed to cell wall polymers that were used in this project are presented in Table 2.2 below.

Table 2.2: Carbohydrate-binding modules used as molecular probes of cell wall structures.

CBM	Ligand	Reference
CBM3a	Crystalline cellulose	(Blake et al. 2006)
CBM2b-12	Xylan	(Simpson et al. 2000)
CBM15	Xylan	(Pell et al. 2003)
CBM17	Amorphous cellulose	(Notenboom et al. 2001)
CBM35	Xylan, Δ4,5-GalA	(Montanier et al. 2009)

2.3 Microscopy and immunolabelling procedures

2.3.1 Preparation of plant materials for microscopy

After 50 or 200 days growth, stems of *Miscanthus*, wheat (50-day) and *Brachypodium distachyon* (50-day) were cut into 2 cm pieces, fixed in PEM buffer (50 mM piperazine-N,N'-bis[2-ethane-sulfonic acid] (PIPES), 5 mM methylene glycol bis(β-aminoethylether)-N,N,N',N'-tetraacetic acid (EGTA), 5 mM $MgSO_4$ (pH 6.9)) containing 4% paraformaldehyde and vacuum infiltrated using a strong vacuum pump for 60 - 90 min. All steps were carried out at room temperature. All samples were taken from the second internode of the stem, counting from the root to the shoot for all three species.

2.3.2 Steedman's wax-embedding of plant materials and sectioning for microscopy

The excised and fixed plant materials were washed with 1x PBS (phosphate buffered saline, 137 mM NaCl, 0.16 mM KCl, 8.0 mM Na_2HPO_4, 14.7 mM KH_2PO_4, pH 7.2) twice for 20 min each at room temperature, then dehydrated with a graded ethanol series (30%, 50%, 70%, 90%, and 100%) for 40 min each at 4°C. For the preparation of Steedman's wax, 900 g of polyethylene glycol 400 distearate (Sigma 30, 541-3) and 100 g 1-hexadecanol (Sigma C7882) were incubated at 65°C until melted. The wax was thoroughly mixed and poured into aluminium foil lined trays and allowed to cool. Samples were incubated in 1:1 Steedman's wax and 100% ethanol at 37°C overnight, followed by two changes of 100% wax for 1 - 2h at 37°C. The sections were placed into moulds, and molten wax poured over until a convex surface was visible. Moulds were left to set overnight at room temperature. The sections were cut to a thickness of 12 µm using a Microm HM-325 microtome, and placed onto glass slides coated with polysine (VWR International, Leuven, Belgium). Plant sections were de-waxed in a graded ethanol series (3x 97%, 90%, 50%, 2x water) 10 min each and allowed to dry before immunolabelling procedures.

2.3.3 Low temperature LR White resin-embedding and sectioning for microscopy

The excised and fixed plant materials were washed with 1x PBS twice for 15 min each at room temperature, dehydrated with a graded ethanol series (10%, 20%, 30%, 50%, 70%, 90%, 100%, and 100%) at -20°C for 15 min per stage. Samples were incubated in graded ethanol and LR White resin (Hard grade, London Resin Company) series (3:1, 2:1, 1:1, 1:2, 1:3, ethanol:resin) on a rotator, and then 100% LR White resin was infiltrated three times at room temperature for 24 h each time,

with the final infiltration left overnight in polymerisation capsule moulds (Agar Aids, UK). Polymerisation of the resin was completed at 60°C for 48 - 72h. Sections were cut with an Ultracut Microtome (Reighert-Jung, Australia) to a thickness of 1 µm using glass knives and placed on Vectabond coated multi-well microscope slides (ICN Biochemicals) before immunolabelling procedures.

2.3.4 Immunofluorescence labelling of sections using monoclonal antibodies

Plant sections were incubated for 30 min in 5% (w/v) milk protein/PBS to prevent non-specific binding, and then washed once for 5 min with 1x PBS. Primary monoclonal antibodies at 5-fold dilutions were incubated for at least 90 min at room temperature. Samples were washed three times with 1x PBS each for 5 min. The secondary antibody ((rabbit anti-rat IgG-fluorescein isothiocyanate (FITC) or anti-mouse IgG-FITC)) (Sigma, UK) was added at a 100-fold dilution in 5% milk protein/PBS and incubated for 90 min in dark. Samples were washed again with 1x PBS for three times each for 5 min. Calcofluor White (0.2 mg/mL in PBS, Fluorescent Brightner 28, Sigma, UK) was added for 5 min in the dark. This stains all β-glycans in the sections (Fischer et al. 1985, Harrington and Raper 1968, Hughes and McCully 1975). To diminish sample auto-fluorescence, 0.1% Toluidine Blue O (pH 5.5 in 0.2 M sodium phosphate buffer) was added for 5 min instead of Calcofluor White. Following Calcofluor White or Toluidine Blue O labelling, samples were washed twice with 1x PBS each for 5 min, then mounted in anti-fade reagent Citifluor AF1 (Agar Scientific, Cat.No.R1320) to reduce photobleaching. After adding the coverslip, slides were stored at 4°C in darkness. Sections were observed with an Olympus fluorescence microscope (Olympus BX61, Canada). Images were captured with a Hamamatsu ORCA285 camera (Hamamatsu City, Japan) and Volocity software (Perkin Elmer, UK). In some

cases, samples were pre-treated with cell wall polysaccharide degrading enzymes before immunofluorescence labelling.

2.3.5 Immunofluorescence labelling of plant sections using recombinant CBMs

Probing of sections with his-tagged CBMs was carried out using a three step protocol. Plant sections were incubated for 30 min in 5% (w/v) milk protein/PBS and then washed once with 1x PBS. Primary CBMs were added at a concentration of 10µg/ml and incubated for at least 90 min at room temperature. Samples were washed three times with 1x PBS each for 5 min. The secondary antibody (mouse anti-His IgG) (Sigma, UK) was added at a 1000-fold dilution in 5% milk protein/PBS and incubated for 90 min. Samples were washed again with 1x PBS for three times each for 5 min. The tertiary antibody (anti-mouse IgG-FITC) (Sigma, UK) was added at a 1 in 50 dilution in 5% milk protein/PBS and incubated for at least 90 min in the dark. Samples were washed three times with 1x PBS each for 5 min. Calcofluor White or Toluidine Blue O was added for 5 min in the dark, followed by 1x washing with PBS and the mounting slides with Citifluor and stored in the dark at 4°C as described above.

2.4 Enzymatic and chemical pretreatment of sections

2.4.1 Pectate lyase treatment to remove pectic homogalacturonan

In some cases, plant stem sections were pre-treated, prior to immunolabelling, with different enzymes to remove or modify specific cell wall polysaccharides. Removal of pectic HG was carried using pectate lyase (*Aspergillus* sp. Megazyme International, Bray, Ireland) at 25 ug/ml in 50 mM 3-(cylohexylamino)-1-propanesulfonic acid (CAPS), 2 mM $CaCl_2$ buffer, pH 10 for 2 h at room temperature. Samples were washed three times in 1x PBS each 5min

before immunofluorscence labelling. For microscopy and image capture, control sections not treated with enzymes were incubated for an equivalent time with the corresponding buffer alone.

2.4.2 Xylanase treatment to remove heteroxylans

Removal of heteroxylan was carried out using xylanase (*Cellvibrio japonicus*, a gift from Prof Harry Gilbert, Newcastle University) at 20 µg/ml in 25 mM Na-acetate buffer, pH 5.5 overnight at room temperature, followed by 1x PBS washing and immunofluorescence labelling.

2.4.3 Mannanase treatment to remove heteromannan

Removal of heteromannan was carried using mannanase (*Thermotoga maritime*, Megazyme International, Bray, Ireland) at 20 µg/ml in PBS overnight at room temperature, followed by 1x PBS washing and immunofluorescence labelling.

2.4.4 Lichenase treatment to remove MLG

Removal of MLG was carried using lichenase (*Bacillus subtilis*, Megazyme International, Bray, Ireland) at 20 µg/ml in 100 mM sodium acetate buffer at room temperature overnight (pH 5.0) before immunofluorescence labelling.

2.4.5 Xyloglucanase treatment to remove xyloglucan

Removal of xyloglucan was carried using xyloglucanase (*Paenibacillus* sp. Megazyme International, Bray, Ireland) at 20 µg/ml in 1x PBS buffer at room temperature overnight before immunofluorescence labelling.

2.4.6 KOH treatment

In some cases, samples were incubated with 4M KOH for 30min at room temperature before enzyme treatment, followed by 1x PBS washing and immunofluorescence labelling. This high pH treatment would result in de-acetylation of polysaccharides and also the de-esterification of methyl ester groups found on homogalacturonan (Brown et al. 2001).

2.5 Chemical extraction of *Miscanthus* cell wall polysaccharides

2.5.1 Preparation of alcohol-insoluble residue (AIR)

1.4g of fresh *Miscanthus* x *giganteus* (MB149) stem material (second internode of the 50-day old *Miscanthus* x *giganteus*) was frozen in liquid nitrogen in a pre-cooled mortar and ground to powder. These powders were added to 2ml Eppendorf tubes containing steel beads (1x 7mm, 2x 5mm, 10x 3mm beads) and placed in liquid nitrogen for 10 min. The Eppendorf tubes were placed in the chilled holders of a Tissue Lyser (QIAGEN Hilden, Germany) and crushed for 5min at 50 Hz. This was repeated at least three times to ensure the plant materials were ground into a fine powder. 80% ethanol was then added to the tubes, and removed along with the suspensions into clean tubes. The samples were incubated for 30 min at 4°C, and then centrifuged at 14,000 rpm for 12 min. The ethanol supernatant was discarded and the pellets washed twice in 80% ethanol. Then the pellets were incubated in 100% acetone at room temperature for 10min and then centrifuged at 14,000 rpm for 12 min. The acetone supernatant was discarded and the pellets were incubated in 100% methanol at room temperature for 10 min, and then centrifuged at 14,000 rpm for 12 min. The pellets were allowed to dry in a 65°C incubator, before being stored at 4°C.

2.5.2 Water extraction of AIR

0.3 g of homogenised *Miscanthus* AIR was added to a 2ml Eppendorf tube, incubated with 1ml dH_2O at room temperature for 25min using TissueLyser at 50 Hz, and then centrifuged at 14,000 rpm for 12 min. The dH_2O extracted supernatant was collected with a clean 1.5 ml tube, stored as frozen aliquots until needed. The pellet was allowed to dry.

2.5.3 CDTA-extraction

The pellet from the previous water extraction was resuspended in 1 ml of 0.1 M CDTA (1,2-cyclohexylene-dinitrilo-tetraaceticacid) at room temperature for 25 min using a TissueLyser at 50 Hz, and then centrifuged at 14,000 rpm for 12 min. The supernatant was collected and stored as frozen aliquots until needed. The pellet was allowed to dry.

2.5.4 Na_2CO_3 extraction

The pellet from the previous CDTA extraction was resuspended in 1 ml of 0.1 M Na_2CO_3 at room temperature for 25 min using the TissueLyser at 50 Hz, and then centrifuged at 14,000 rpm for 12 min. The supernatant was collected and stored as frozen aliquots until needed. The pellet was allowed to dry.

2.5.5 KOH extraction

The pellet from the previous Na_2CO_3 extraction was resuspended in 1 ml of 4 M KOH at room temperature for 25 min using a TissueLyser at 50 Hz, and then centrifuged at 14,000 rpm for 12 min. The supernatant was collected and stored as frozen aliquots until needed and the pellet was discarded.

2.6 Immuno-dot-assay (IDA)

1 µl aliquots of extraction supernatants were applied onto nitrocellulose paper and allowed to dry. They were then blocked with 5% milk protein powder in 1x PBS for 1 hour with shaking at 30 rpm before washing six times in tap water and then three times for 5 min each in 1x PBS. Primary antibody was added at a 1 in 5 dilution in 3% milk powder in 1x PBS for 1 hour at room temperature with shaking and then washed three times for 5 min each with tap water and 1x PBS. The secondary antibody (anti-rat IgG HRP (horse radish peroxidase), Sigma, UK) was added at a 1 in 1000 dilution in 3% milk powder in 1x PBS for 1 hour at room temperature with shaking before washing again three times for 5 min with 1x PBS. To detect antibody binding, samples were incubated with enzyme substrate (5 ml of chloronaphthol solution 5 mg/ml in ethanol) and 30 µl of 6% hydrogen peroxide made up to 25 ml with dH_2O. Positive dots were stained purple. The reaction was stopped by extensive washing in water (at least 3 min under the tap water).

2.7 Enzyme linked immunoabsorbent assay (ELISA)

100 µl per well of 5-50 µg/ml of appropriate samples solubilized in1x PBS were coated overnight at 4°C with 1x PBS onto 96 well Nunc-Immunomicrotitre plate with Maxisorp surface (Life Technologies, UK). Solutions were removed the following day and plates washed six times with tap water before being blocked with 200 µl per well 3% milk/PBS for 1h at room temperature. Plates were washed vigorously six times using tap water then shaken dry. The required primary antibody was added at a 1 in 10 dilution in 3% milk/PBS, 100 µl per well, and incubated for at least 1 h at room temperature. Plates were then washed extensively ten times in tap water then shaken dry. The secondary antibody of anti-rat IgG-HRP (Sigma, UK) was added at a concentration of 1 in 1000 in 3% milk/PBS 100 µl per well and plates incubated at room temperature for 1h before extensively washing ten times in tap water and shaken dry. Antibody binding was revealed by the

application of enzyme substrate. 150 µl of freshly prepared HRP substrate was added to each well which was made up of 18 ml water, 2 ml of 1 M sodium acetate buffer (pH 6.0), 200 µl of 3,3,5′5′-tetramethyl benzidine (Sigma T-2885) in10mg/ml in DMSO) and 20 µl 6% (v/v) hydrogen peroxide. A positive reaction produced a blue colour within 5 min and was stopped by the addition of 30 µl per well of 2.5 M sulphuric acid. The absorbance was determined at 450 nm on an ELX800 Thermo-Scientific MultiScan FC microplate reader (Bio-Tek instruments Inc., Winooski, USA). Omission of the primary antibody or sample provided negative controls.

2.8 Sodium dodecyl sulphate (SDS) polyacrylamide gel electrophoresis (PAGE) and Western blotting

2.8.1 Sample preparation

Samples of *Miscanthus* extracts (Section 2.5 or Section 2.10) were suspended in an equal volume of double strength SDS-PAGE sample buffer (25% v/v 0.5 M Tris-HCl pH 6.8, 20% v/v glycerol, 4% m/v SDS, 2.5 % v/v bromophenol blue, 10% v/v β-mercap to ethanol, 20% v/v dH_2O), vortexed and boiled for 5 min.

2.8.2 SDS-PAGE

The separation of *Miscanthus* extracted proteins was carried out by sodium dodecyl sulphate polyacrylamide gel electrophoresis (SDS-PAGE) (Laemmli 1970). Polyacrylamide resolving gels and stacking gels were used with a Mini-Protean II BioRadgel system according to manufacturers' instructions (Mini-Protean TGX Precast gel, BioRan, USA). Aliquots were loaded at 30 µl of each gel well, a 5 µl loading of pre-stained molecular weight standards (SDS-7B; Sigma, UK) was always co-electrophoresed with samples. Electrophoresis was carried out in a vertical tank (Bio-Rad, USA) in running buffer (0.025 M Tris-HCL, 0.1 M glycine,

0.05% (w/v) SDS) at 90V and 35mA per gel for 1h. Gels were then either used in Western blotting or stained with Coomassie blue protein dye or β-glucosyl Yariv reagent (βGlcY) (next section).

2.8.3 Coomassie brilliant blue protein gel staining

The SDS-PAGE gel was incubated in the staining Coomassie Brilliant Blue (0.25 % (w/v, Sigma, UK), 50% v/v methanol, 7.5% v/v glacial acetic acid) for 4 h and de-stained in several washes of de-stain solution (50% v/v methanol, 7.5% v/v glacial acetic acid). The stained gel was stored in de-stain solution at 4°C until electronically scanned.

2.8.4 Western blotting

Unstained SDS-PAGE gels were rinsed briefly in dH_2O and directly applied to nitrocellulose membranes, secured with 3MM filter paper (Whatman, Maidstone, Kent, UK) and nylon scour pads. The transfer of proteins to nitrocellulose membranes was carried out in a vertical tank using the Bio-Ran Mini Trans-Blot electrophoretic transfer cell (Bio-Rad, USA) in transfer buffer (14.4 g Tris-HCl, 3.6 g glycine, 250 ml methanol, 750 ml dH_2O) by running at 100 V and 250 mA for 1 h, at 4°C. After the protein transfer had been completed the nitrocellulose membranes were washed several times in tap water and 1x PBS before they were blocked in 3% milk/PBS and probed with monoclonal antibodies as described for the immuno-dot-assay (Section 2.6) or stained with βGlcY reagent (2 mg in 30 ml dH_2O containing 1% (w/v) NaCl, next section).

2.9 Preparation of AGP-binding β-glucosyl Yariv reagent

β-glucosyl Yariv reagent (βGlcY) was prepared according to published methods (Yariv et al. 1962).The phenyl glycoside ρ-aminophenyl-D-glucopyranoside (200mg) was dissolved in 6 ml of 0.5 M HCl in a conical flask on ice. An equal

volume of 0.3 mM aqueous $NaNO_2$ was added in 500 µl aliquots to the solution, mixing for 3-4 min. Phloroglucinol (12.3 ml of a 0.1 mM aqueous solution) was added and the pH increased to 9.0 by adding NaOH (0.5 M and then 0.1 M). The solution was stirred for 2 h with a magnetic stirrer to allow the pH to stabilise and the pH checked every 30 min. The total final volume was measured and to this an equal volume of 100% (v/v) methanol was added. The solution was centrifuged at 5111 x *g* for 12 min in a high-speed centrifuge (Beckman Coulter, Buckinghamshire, UK). The pellets were re-suspended in 20 ml of dH_2O, vortexed then dialysed for 3 h against 3 x 3 L of dH_2O. The βGlcY solution was divided into 1 ml aliquots and stored at -20°C until required.

2.10 Isolation of arabinogalactan-proteins by βGlcY precipitation

The method of the AGP precipitation with βGlcY was adapted from that of Schultz and colleagues (Schultz et al. 2000). 25g of fresh *Miscanthus* x *giganteus* (MB149) stem materials was frozen in liquid nitrogen in a pre-cooled large mortar and ground into a fine powder, then divided between four 35ml polypropylene tubes (Nalgene Centrifugeware, Nalgene Co., Sybron Corp., Rochester, NY, USA), approximately 0.5 g per tube. AGP extraction buffer (50 mM Tris-HCl, 10 mM EDTA (ethylene diaminetetraacetic acid), 1% (v/v) Triton-X-100, 0.1% (v/v) β-mercaptoethanol) was added at 10 ml per tube, the tubes were vortexed and stored at 4°C for 3 h with inversion every 30 min. Tubes were spun at 14,000 x *g* for 12 min in a high-speed centrifuge (Beckman Coulter, Buckinghamshire, UK) at 4°C. The supernatant was transferred to new 35 ml polypropylene tubes. 25 ml ethanol (100% (v/v) solution) was added and the solution left overnight at 4°C.

The following day, tubes were spun for 12 min at 14,000 x *g*, the supernatant discarded and the pellet dissolved in 4 ml of 50 mM Tris-HCl (pH 8.0), vortexing and mechanical disruption the pellet using a sterile disposable plastic pipette followed by centrifugation at 14,000 x *g* at 4°C, and the supernatant was transferred

to a new 35 ml tube. In total this pellet resuspension procedure was repeated 4 times. Samples were snap-frozen in liquid nitrogen and then freeze fried overnight till completely dry. The freeze-dried protein was dissolved in 1 ml 1% (w/v) NaCl then centrifuged at 14,000 x *g* for 12 min at 4°C. The supernatant was transferred to sterile 1.5 ml snap top tubes (ElKay, Galway, Ireland) as 0.5 ml aliquots per tube, followed by adding an equal volume βGlcY reagent (2 mg/ml in 1% (w/v) NaCl) each tube. Samples were stored at 4°C overnight to allow βGlcY-AGP complexes to precipitate.

The following day the tubes were spun at 14,000 x *g* for 1 h at 4°C in a micro-centrifuge (Eppendorf, Hamburg, Germany). The supernatant was discarded and the pellets washed in 1 ml NaCl (1% (w/v)). Samples were spun at 14,000 x *g* for 12 min at 4°C, the supernatant was discarded and the pellets washed in 1 ml NaCl (1% (w/v)) and this washing step was repeated at least 5 times. The pellet was then washed twice in 100% methanol (v/v) and dried in a Speedvac (Savant, NY, USA). In a fume hood, the pellet was dissolved in 400 µl DMSO (dimethyl sulphoxide), a spatula full (about 2 mm²) of solid sodium dithionite was added with an equal volume of dH_2O. Samples were vortexed well and allowed to stand for 5-10 min until the solution had changed to a yellow colour. Samples were spun for 2 min at 14,000 x *g* at 4°C, the supernatant was transferred to new 1.5 ml snap top tubes and the pellet washed with 500 µl of dH_2O. Samples were centrifuged for a further 2 min, the supernatant combined with the previous supernatants, and adjusted the total volume to 2 ml with dH_2O.

The samples were desalted on a PD10 column (Amersham Pharmacia Biotech, Inc, Piscataway, NJ, USA) as follows. The PD10 column was equilibrated with dH_2O (5 times column volume), then the dissolved βGlcY-AGP solution was added to the column, the snap top tube rinsed with 500 µl dH_2O and added to the column. After the flow had stopped, added 3.2 ml of dH_2O to the column and the fraction

containing AGPs was collected with a new tube. Samples were snap frozen in liquid nitrogen and freeze dried overnight, stored 4°C until use.

2.11 Lignin staining

De-waxed sections were incubated in a phloroglucinol lignin stain (100ml 95% ethanol, 16ml concentrated HCL, 0.1g phloroglucinol (Sigma, UK)) for 30-60 min (Jensen 1962). After covering the cover slip, samples were observed under visible light using an Olympus fluorescence microscope (Olympus BX61, Canada). Images were captured with a Hamamatsu ORCA285 camera (Hamamatsu City, Japan) and Volocity software (Perkin Elmer, UK). Lignin appears red-violet although the colour is not permanent and will disappear in an hour.

Chapter 3

Cell wall polysaccharides of *Miscanthus* species

3.1 Introduction

The three *Miscanthus* species that are *Miscanthus* x *giganteus* (*M.* x *giganteus*), *Miscanthus sacchariflorus* (*M. sacchariflorus*) and *Miscanthus sinensis* (*M. sinensis*) were grown in the University of Leeds greenhouse. In this chapter, initial experiments involved the polysaccharide analysis of the transverse sections of the second internode (Int2) of *M.* x *giganteus* at 50 days growth. After that, the polysaccharide analysis of the different internodes (internode 1 to internode 5), different positions of a internode (top, middle and base of a internode), and different growth development stages (50 days and 200 days growth) were explored in the transverse sections of *M.* x *giganteus* stem. Three major polysaccharide distributions (heteroxylan, MLG and pectic HG) were also observed in the second internode of the other two *Miscanthus* species - *M. sacchariflorus* and *M. sinensis* at both 50 days and 200 days growth. Photographs of the representative stems and leaves of *Miscanthus* samples taken from *M.* x *giganteus*, *M. sacchariflorus* and *M. sinensis* are are shown in Figure 3.1. At 50 days growth, *M.* x *giganteus* grows faster and taller than its parents - *M. sacchariflorus* and *M. sinensis* and usually has 6 stem internodes. At this time, *M. sinensis* grows the slowest and is also the shortest of the three species (4 stem internodes).

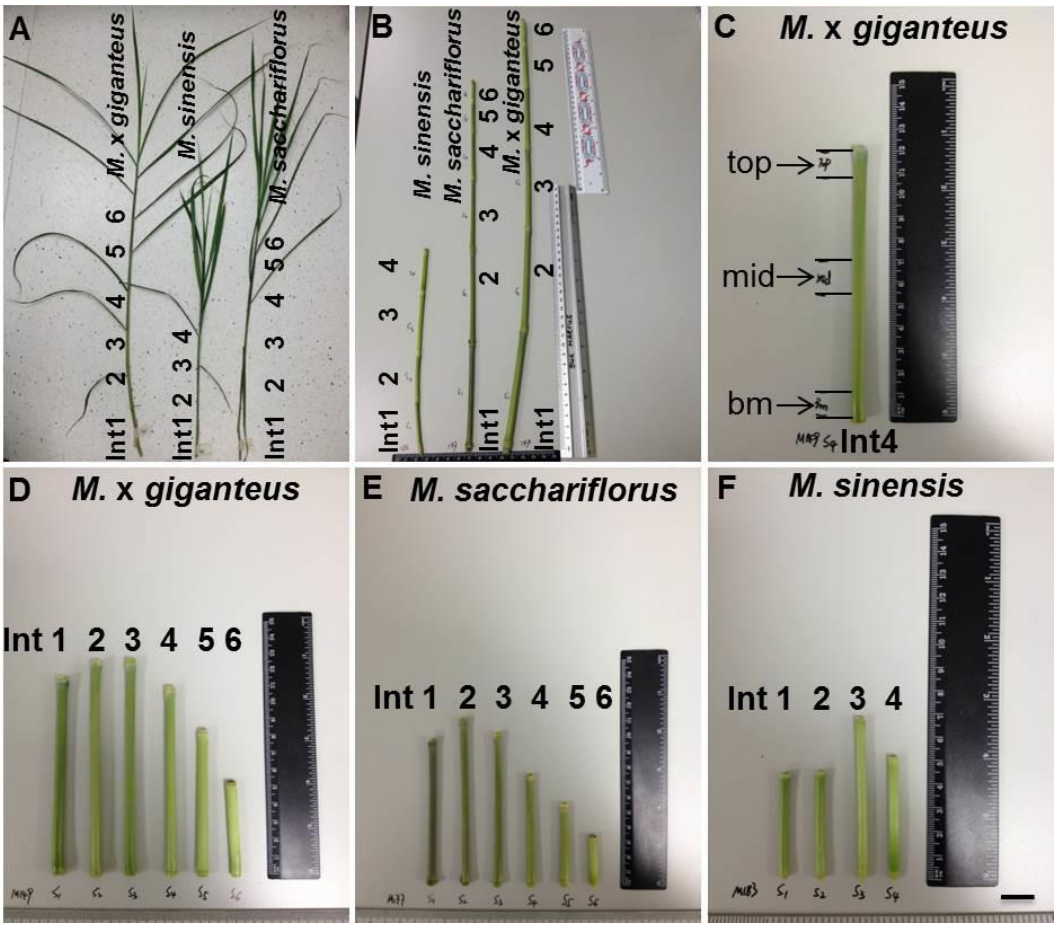

Figure 3.1: Photographs indicating sampling of stem materials from different internodes of *M.* x *giganteus*, *M. sacchariflorus* and *M. sinensis*. A: Representative stems and leaves of *Miscanthus* species at 50 days growth. B: Stems of *Miscanthus* species. C: The fourth internode (Int4) of *M.* x *giganteus* showing sampling positions of base (bm), middle (mid) and shoot (top). D: Internodes of a *M.* x *giganteus* stem. Int1 is the first internode of the stem (counting from the base), and Int6 is the youngest internode of a stem (near the shoot meristem). E and F: Internodes of stems of *M. sacchariflorus* and *M. sinensis.* Bar = 1 cm.

3.2 Anatomy of the stem of *Miscanthus* x *giganteus*

Labelling of transverse sections with Calcofluor White (Calc) which binds to all β-glucans including cellulose (Fischer et al. 1985, Harrington and Raper 1968, Hughes and McCully 1975) allowed the investigation of the anatomy of the second internode (Int2) of the 50-day-old stem of *M.* x *giganteus* (Figure 3.2). Figure 3.2A showing us the whole view image of the stem anatomy of Int2. The epidermis, parenchyma, vascular bundles, sheath of vascular bundles, phloem regions, xylem regions and pith parenchyma of the *M.* x *giganteus* stem can be clearly seen in Figure 3.2C. The binding of carbohydrate-binding module CBM3a (Blake et al. 2006) which binds to crystalline cellulose was detected uniformly in epidermis, parenchyma, vascular bundles, sheath of vascular bundles of Int2 of the *M.* x *giganteus* at 50 days growth (Figure 3.2). Omission of the primary antibodies provided a negative control (Figure 3.2D).

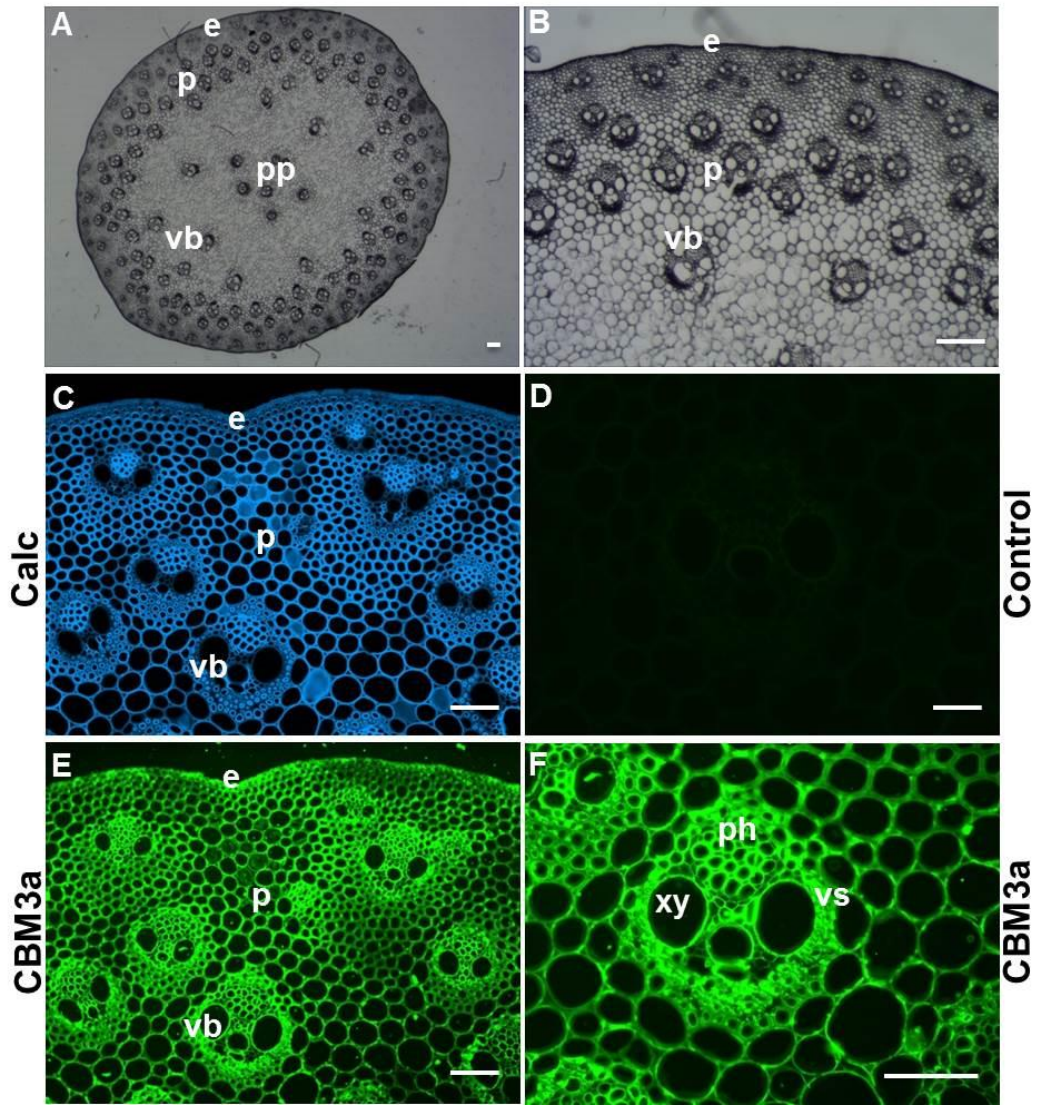

Figure 3.2: Anatomy and fluorescence imaging of cell walls in equivalent transverse sections of the second internode (Int2) of stem of *M.* x *giganteus* at 50 days growth. A: Bright field image showing stem anatomy of Int2. B: Higher magnification image of A showing cortical vascular bundles. C. Image generated with Calcofluor White (Calc, blue) and indirect immunofluorescence (green) with carbohydrate-binding module CBM3a to cellulose (E and F). D: Omission of the probe provided the negative control. F shows CBM3a binding to a vascular bundle (vb) at higher magnification. e = epidermis, p = interfascicular parenchyma, pp = pith parenchyma, vb = vascular bundle, vs = vascular bundle sheath, ph = phloem, xy = xylem. Bar = 100 µm.

3.3 Distribution of cell wall polysaccharides in transverse sections of 50-day *Miscanthus* x *giganteus* stem

3.3.1 Analysis of heteroxylan in transverse sections of *M.* x *giganteus* stem

Initial experiments included the detection of heteroxylan in transverse sections of Int2 of *M.* x *giganteus* stem at 50 days growth. Heteroxylans are known to be one of the most abundant non-cellulosic polysaccharides in grasses. Immunolabelling with anti-heteroxylan probes revealed that the LM10-unsubstituted xylan (McCartney et al. 2005), the LM11-xylan/arabinoxylan (McCartney et al. 2005) and the LM12-feruloylated xylan epitopes (Pedersen et al. 2012) were detectable in transverse sections of *M.* x *giganteus* stem (Figure 3.3). The LM12-feruloylated xylan epitope bound uniformly to parenchyma (Figure 3.3C), while the other two heteroxylan epitopes (LM10 and LM11) have a lower binding level in these corresponding parenchyma regions (Figure 3.3, (A) and (B)). Major differences of the LM10, LM11 and LM12 epitopes binding to the vascular bundle regions were shown in Figure 3.3, (D), (E) and (F). The LM10 xylan probe did not bind to the phloem cell walls (Figure 3.3D). The LM11 xylan/arabinoxylan and LM12-feruloylated xylan epitopes were detected in phloem regions (Figure 3.3, (E) and (F)). This indicates that phloem cell walls have distinct polysaccharide architecture that contains substituted xylan in *M.* x *giganteus*, which may link to their properties. Furthermore, the LM10-unsubstituted xylan probe bound much more strongly to vascular bundle sheath than the other two substituted xylan probes (Figure 3.3, (D), (E) and (F)).

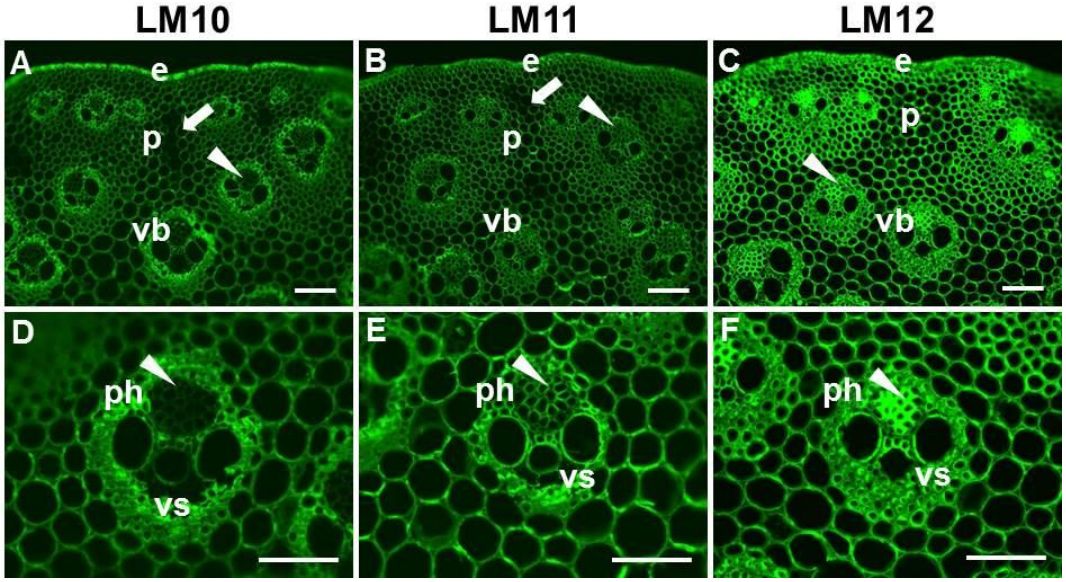

Figure 3.3: Fluorescence imaging of heteroxylan epitopes in equivalent transverse sections of Int2 of a *M.* x *giganteus* stem at 50 days growth. Images generated using indirect immunofluorescence with monoclonal antibodies LM10, LM11 and LM12 to heteroxylan. Arrowheads indicate phloem. Arrows indicate regions of interfascicular parenchyma that have relatively lower levels of heteroxylan detection. D - F show LM10, LM11 and LM12 labellings of vascular bundle (vb) at higher magnification. e = epidermis, p = parenchyma, ph = phloem, vb = vascular bundle, vs = vascular bundle sheath. Bar = 100 µm.

3.3.2 Analysis of MLG, XyG and mannan in transverse sections of *M.* x *giganteus* stem

The MLG polysaccharide is known to be one of the most abundant polysaccharide in grasses, whereas cell walls of grasses contain less mannan and XyG (Carpita 1996, Carpita and Gibeaut 1993, Vogel 2008). At 50 days growth, the MLG epitope (Meikle et al. 1994) was detected strongly in phloem, xylem and parenchyma cell walls of Int2 of *M.* x *giganteus*, and the MLG was particular abundant in the sub-epidermal parenchyma regions between the vascular bundles, and the MLG binding patterns in the sub-epidermal parenchyma regions were similar to that of the heteroxylan detections (Figure 3.3), however, this MLG probe

did not bind to the sheath of vascular bundles (the LM10-xylan bound strongly - Figure 3.3D) (Figure 3.4, (A) and (D)). The LM15 XyG epitope (Marcus et al. 2008) was restricted to phloem and xylem regions (Figure 3.4B). The LM21 mannan epitope (Marcus et al. 2010) was detected in phloem, xylem and sub-epidermal parenchyma cell walls of *M.* x *giganteus*, these LM21 binding patterns in the sub-epidermal parenchyma and vascular bundle regions were similar to that of the MLG detections, but it was not evenly detectable in these regions (Figure 3.4, (A) and (C)). These results indicate that phloem cell walls have distinct polysaccharide architecture that contains substituted xylan, XyG, MLG and heteromannan in *M.* x *giganteus*, and the sheath of vascular bundles contains heteroxylan in *M.* x *giganteus*. It is also interesting that the sub-epidermal parenchyma cell walls contain high level of MLG but less level of xylan.

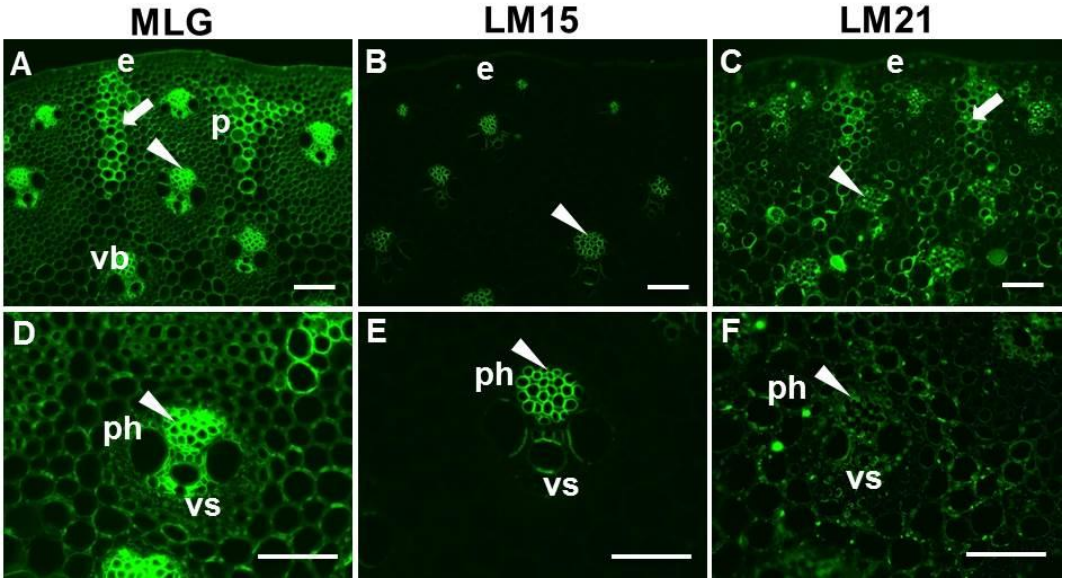

Figure 3.4: Fluorescence imaging of MLG, xyloglucan and heteromannan epitopes in equivalent transverse sections of Int2 of a *M.* x *giganteus* stem at 50 days growth. Immunofluorescence images generated with monoclonal antibodies to MLG, xyloglucan (LM15) and heteromannan (LM21). Arrowheads indicate phloem. Arrows indicate regions of interfascicular parenchyma that are labelled strongly by the probes. Bottom three micrographs show MLG, LM15 and LM21 labellings of vascular bundles (vb) at higher magnification. e = epidermis, p = parenchyma, ph = phloem, vb = vascular bundle, vs = vascular bundle sheath. Bar = 100 µm.

Therefore, the heteroxylan probes were most abundant in the vascular bundles and the sheaths of vascular bundles, the MLG was strongly detected in the phloem and specific regions of sub-epidermal parenchyma cell walls, the XyG was restricted to the phloem and xylem, and heteromannan was not evenly detected in parenchyma cell walls of Int2 of 50-day *M.* x *giganteus*.

3.3.3 Analysis of HG-related and RG-related pectin in transverse sections of *M.* x *giganteus* stem

Besides heteroxylan, XyG, MLG and heteromannan, grass cell walls also contain pectic polysaccharides, but these polysaccharides are less abundant polysaccharide in grasses (Carpita 1996, Carpita and Gibeaut 1993, Vogel 2008). Pectin is one of the most complex molecules which are thought to be responsible for plant growth. The most complex pectin molecules are HG and RG-I except RG-II. For Int2 of the 50 days *M.* x *giganteus*, all of the three HG-related pectin epitopes, that are the LM18 HG (low/no ester) epitope, the LM19 HG (no ester) epitope and the LM20 HG (ester) epitope (Verhertbruggen et al. 2009a), were abundant in phloem, xylem and parenchyma intercellular spaces of *M.* x *giganteus* (Figure 3.5, (A), (B) and (C)). At a lower magnification it was observed that the LM20 methylesterified-HG epitope was detected with more intensive fluorescence in pith parenchyma cell walls (Figure 3.5F), compared to LM18 and LM19 unesterified-HG epitopes (Figure 3.5, (D) and (E)). The LM5 RG-I related pectic galactan epitope (Jones et al. 1997) was detectable in phloem cell walls and weakly detected in part of the epidermal parenchyma cell walls, the LM6 RG-I related pectic arabinan epitope (Willats et al. 1998) bound uniformly to all types of cell walls. The LM6 pectic arabinan binding patterns in the sub-epidermal parenchyma and vascular bundle regions were similar to that of the MLG detections. The LM13 linearised-pectic arabinan epitope (Moller et al. 2008, Verhertbruggen et al. 2009b) did not bind to *M.* x *giganteus* except weakly bound to the epidermis (Figure 3.5, (G), (H) and (I)).

In summary, for all of these studied pectin epitopes, the LM6 RG-I related pectic arabinan was the most abundant in Int2 of 50-day *M.* x *giganteus*, the LM5 RG-I related pectic galactan was restricted to phloem and part of the parenchyma regions, the HG-related LM18, LM19 and LM20 epitopes were abundant in phloem, xylem and parenchyma intercellular spaces of *M.* x *giganteus*. These results indicate that

phloem cell walls have distinct pectic polysaccharide architecture that contains methylesterified-HG, unesterified-HG, pectic arabinan and galactan in *M.* x *giganteus*. Specially, it is intresting that the pith parenchyma cell walls showed intensive fluorescence of the high methylesterified-HG (LM20), and this may link to the parenchyma properties and may also related to the growth development of *M.* x *giganteus*. Summary of the distribution of cell wall epitopes addressed above in the Int2 of *M.* x *giganteus* at 50 days growth are presented in Table 3.1.

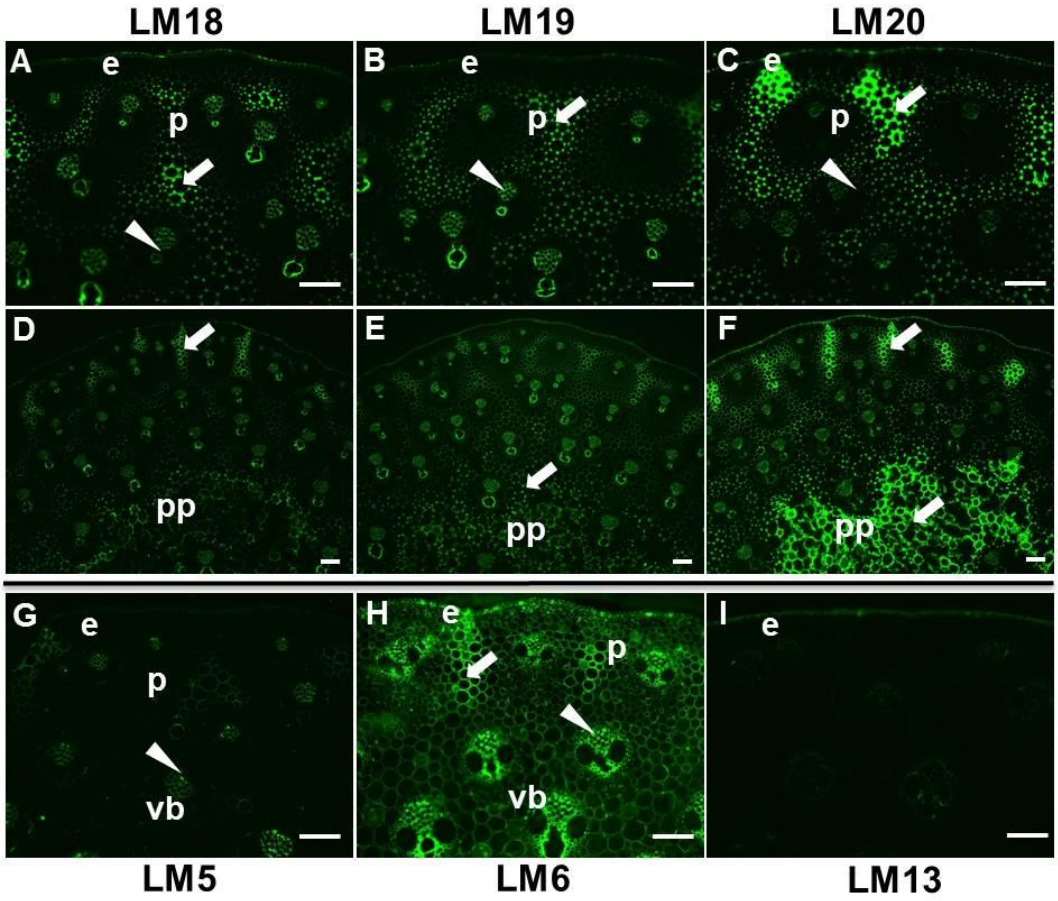

Figure 3.5: Fluorescence imaging of pectin epitopes in equivalent transverse sections of Int2 of a *M.* x *giganteus* stem at 50 days growth. Immunofluorescence images generated with monoclonal antibodies to pectic HG (LM18, LM19 and LM20), pectic galactan (LM5) and arabinan (LM6 and LM13). Arrowheads indicate phloem. Arrows indicate regions of interfascicular parenchyma that are labelled strongly by the probes. Middle three micrographs show LM18, LM19 and LM20 labelling at lower magnification to include central pith parenchyma (pp) of stems. e = epidermis, p = parenchyma, pp = pith parenchyma, vb = vascular bundle. Bars = 100 µm.

Table 3.1: Tissue-specific distribution of cell wall epitopes in the second internode (Int2) of *M.* x *giganteus* at 50 days growth.

	e	p	vb	vs	ph	xy	is
CBM3a	++	+	++	++	++	++	+
LM10	++	±	+	++	–	±	+
LM11	+	±	±	±	±	+	+
LM12	++	+	++	++	++	+	+
LM15	–	–	–	–	++	±	–
MLG	±	+	+	–	++	+	±
LM18	±	+	±	–	±	±	–
LM19	±	+	±	–	±	±	–
LM20	±	+/++	±	–	±	±	–
LM6	+	+	+	–	++	+	–
LM21	–	+	±	–	+	±	–

++ strong binding; + binding; ± weak binding; – no binding. e = epidermis, p = interfascicular parenchyma, vb = vascular bundle, vs = vascular bundle sheath, ph = phloem, xy = xylem, is = intercellular space. CBM3a = cellulose; LM10 = xylan; LM11 = xylan/arabinoxylan; LM12 = ferulated heteroxylan; LM15 = XyG; LM18/19/20 = pectic HG; LM6 = pectic arabinan; LM21 = heteromannan.

3.4 Analysis of major cell wall polysaccharides in different internodes of *Miscanthus* x *giganteus* stem

All of the above experiments were observed in the middle of the Int2 of 50-day-old *M*. x *giganteus*. The extent of the variation in detection of the heteroxylan, MLG and pectic HG epitopes in relation to growth stages in *M*. x *giganteus* stems was explored further. Analysis of the mid point of more distal, younger internodes (internode 5 - Int5 and internode 4 - Int4, counting from the base) at 50 days growth indicated a decreasing gradient in the detection of the heteroxylan epitopes (Figure 3.6), whereas this was not apparent for the MLG epitope (Figure 3.7). The LM10 unsubstituted xylan epitope was not detected in the youngest internode (Int5, fifth from the base) and the LM11/LM12 substituted arabinoxylan epitopes were only detected in association with the vascular bundles (Figure 3.6, (B), (C) and (D)). At this stage the sheath of fibre cells surrounding the vascular bundles are less developed (Figure 3.6, (B), (C) and (D)). Relative to the LM11 arabinoxylan epitope, the LM12 ferulated-arabinoxylan epitope was detected less in the peripheral vascular bundles but detected strongly in the phloem cell walls of the more distal vascular bundles (Figure 3.6 (C) and (D)). In contrast, the MLG epitope was abundant in the younger internodes (Int4 and Int5) (Figure 3.7) and particularly in the outer parenchyma cell walls of the youngest internode (Figure 3.7B). In the case of the pectic HG epitopes, the LM19 epitope of unesterified HG was less detectable in younger internodes (Int5 and Int4) (Figure 3.8, (A) and (C)), whereas the LM20 methyl-esterified HG epitope was abundantly detected in the parenchyma cell walls of all internodes (Figure 3.8), and this LM 20 epitope was detected with more intensive fluorescence in pith parenchyma cell walls of the older internodes (Int1 and Int2) (Figure 3.8 (H) and (j)).

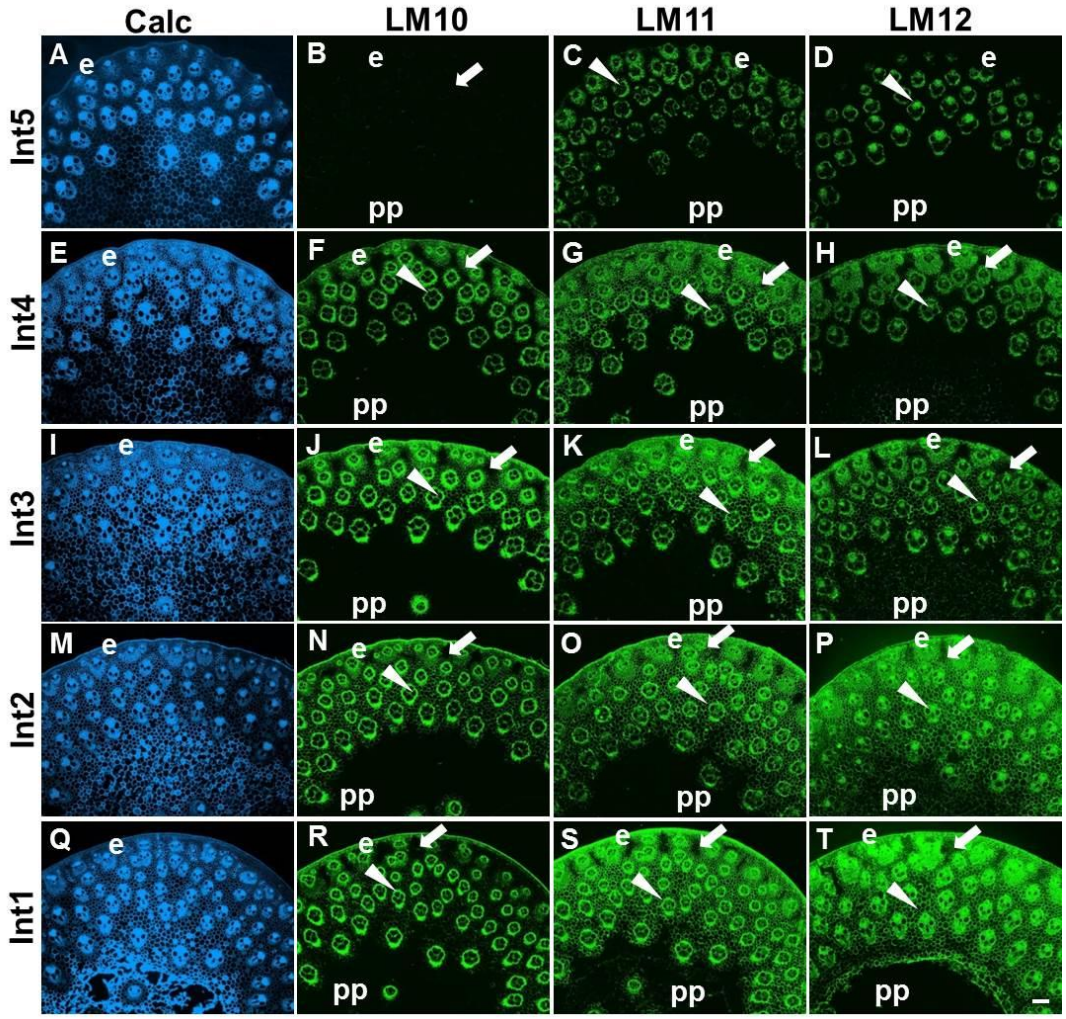

Figure 3.6: Fluorescence imaging of heteroxylan epitopes in transverse sections of the first (Int1, middle) to fifth (Int5, middle) internodes of a *M.* x *giganteus* stem at 50 days growth. Calc staining shown in blue. Immunofluorescence images generated with monoclonal antibodies to heteroxylan (LM10, LM11 and LM12). Arrows indicate regions of interfascicular parenchyma that have relatively lower levels of heteroxylan detection. Arrowheads indicate phloem. e = epidermis, pp = pith parenchyma. Bars = 100 µm.

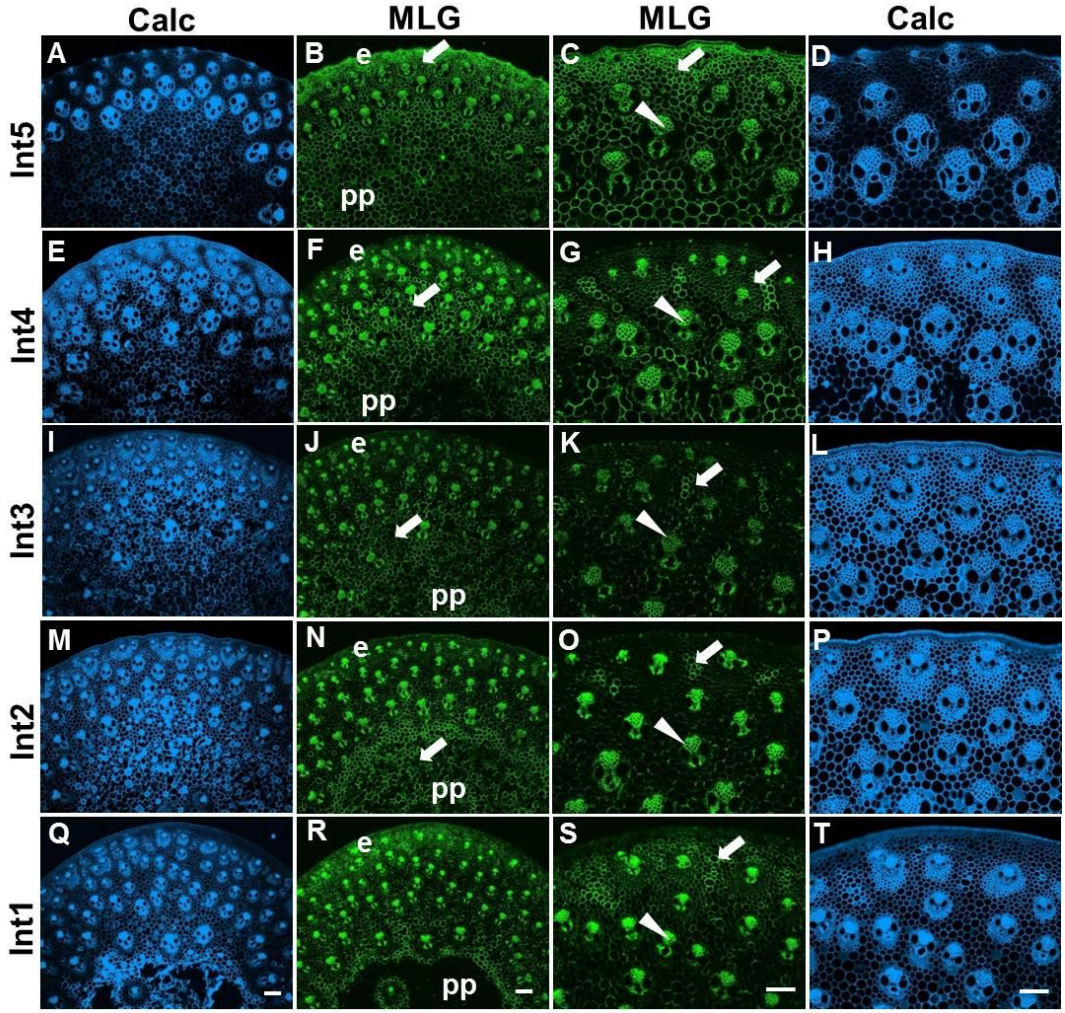

Figure 3.7: Fluorescence imaging of the MLG epitope in equivalent transverse sections of the first (Int1) to fifth (Int5) internodes of a *M.* x *giganteus* stem at 50 days growth. Calc staining shown in blue. Immunofluorescence images generated with monoclonal antibodies to MLG. Arrows indicate regions of interfascicular or pith parenchyma that are labelled strongly by the probes. Arrowheads indicate phloem. Right handside 10 micrographs show MLG and Calc labellings of epidermis, parenchyma and vascular bundles (vb) at higher magnification. e = epidermis, pp = pith parenchyma. Bars = 100 µm.

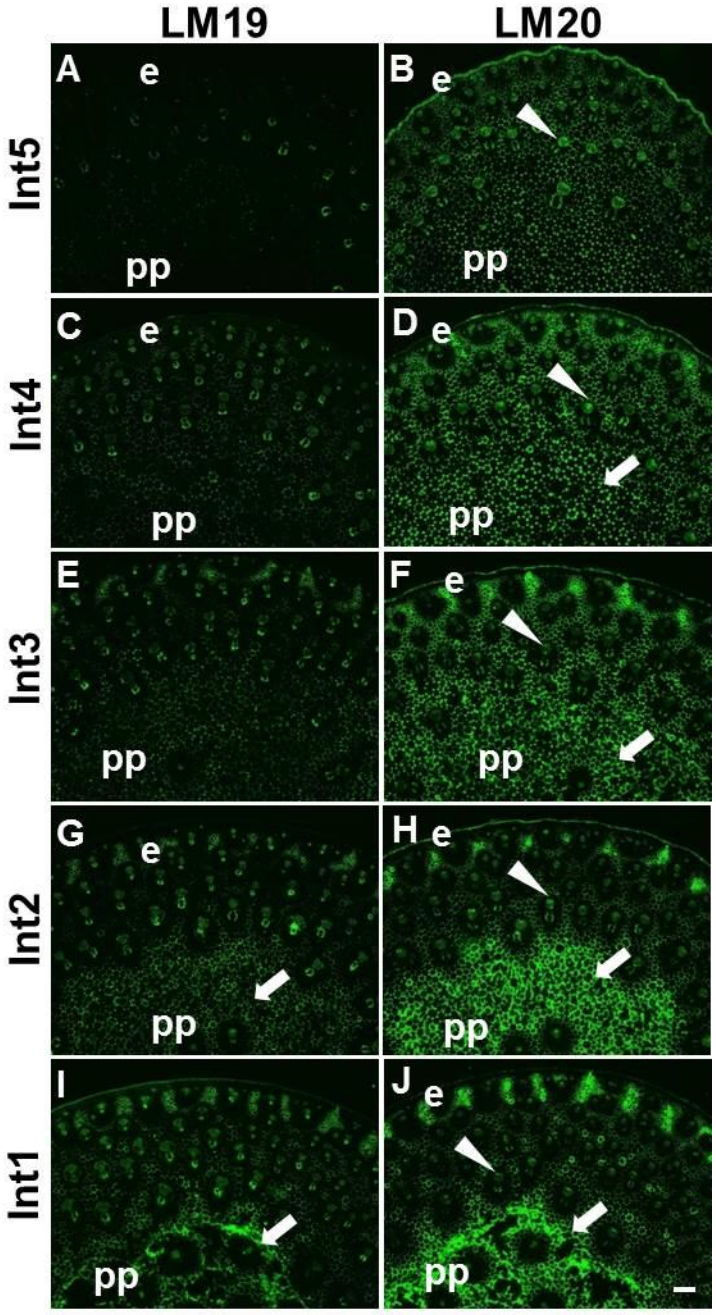

Figure 3.8: Fluorescence imaging of pectin epitopes of equivalent transverse sections of the first (Int1) to fifth (Int5) internodes of a *M.* x *giganteus* stem at 50 days growth. Immunofluorescence images generated with monoclonal antibodies to pectic HG (LM19, LM20). Arrows indicate regions of pith parenchyma that are labelled strongly by the probes. Arrowheads indicate phloem. e = epidermis, pp = pith parenchyma. Bars = 100 µm.

3.5 Major cell wall polysaccharides at different developmental stages of *Miscanthus* x *giganteus* stem

3.5.1 Analysis of heteroxylan/MLG/HG in second and fourth internodes of *M.* x *giganteus* stem

Grass internodes extend by intercalary growth by extension from the bottom of the internode, it occurred mainly around the vascular bundles at the base of the intercalary meristem and there is relatively more cell expansion at the bottom of the internodes (Cho and Kende 1997, Fisher and French 1976), therefore, to explore further the variation in polysaccharide epitope distribution, transverse cross sections were taken from the base, middle and the top of the second and fourth internodes of 50-day-old *M.* x *giganteus.* The analysis of the top, middle and base of Int2 of *M.* x *giganteus* stems at 50 days growth did not reveal any large differences in heteroxylan, MLG and pectic HG epitopes occurrence (Figure 3.9 and 3.10), except that the MLG was detected less in the sub-epidermal parenchyma cell walls of the base of Int2 (Figure 3.10D). At 50 days growth, the second internode was well developed, while the younger internodes such as the internode 4 and internode 5 were less developed. In the case of the younger fourth internode (Int4), the base of internodes indicated a decreasing gradient in the detection of the heteroxylan epitopes (Figure 3.11). The LM10 unsubstituted xylan was restricted to the phloem and xylem cell walls at the base of Int4, whereas it was abundant in the epidermis, vascular bundles, sheath of vascular bundles and outer parenchyma cell walls at the top of Int4 (Figure 3.11, (B), (F), (J) and (N)). The LM11/12 substituted xylan epitopes were detected uniformly in epidermis, vascular bundles and outer parenchyma cell walls of the top of Int4 (Figure 3.11, (C), (D), (K) and (L)). In the case of the base of Int4, the LM12 ferulated arabinoxylan epitope was restricted to the phloem and xylem cell walls (Figure 3.11, (H) and (P)), whereas the LM11 arabinoxylan epitope was abundant in epidermis, vascular bundles including the

sheath of fibre cells surrounding the vascular bundles (Figure 3.11G). In relation to the phloem regions, the LM10 unsubstituted xylan antibody did not bind to the top of Int4, whereas it bound to the base of Int4 (Figure 3.11, (J) and (N)). The LM11/12 substituted arabinoxylan bound to both the top and base of Int4 (Figure 3.11, (G), (H), (O) and (P)), which indicates the phloem in younger part of the internode (base of Int4) contains both xylan and substituted arabinoxylan, while in the better developed part of Int4 (top of Int4), the phloem only contain substituted arabinoxylan, and this also indicates that the level of unsubstituted xylan reduced as the internode developed. Furthermore, all of the three heteroxylan epitopes were not detected in the inner pith parenchyma cell walls at both top and base of Int4 (Figure 3.11).

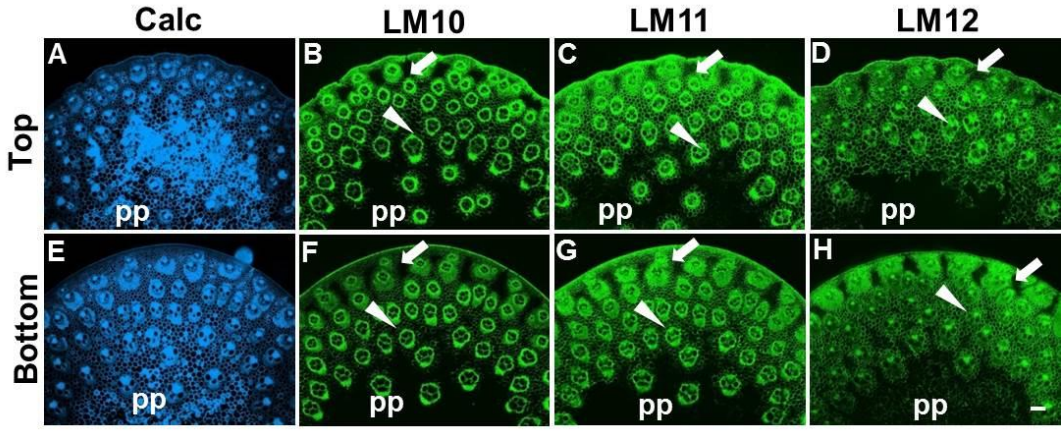

Figure 3.9: Fluorescence imaging of heteroxylan epitopes in transverse sections from top and bottom of Int2 (from base to shoot) of a *M.* x *giganteus* stem at 50 days growth. Calc staining shown in blue. Immunofluorescence images generated with monoclonal antibodies to heteroxylan (LM10, LM11 and LM12). Arrows indicate regions of interfascicular parenchyma that have relatively lower levels of heteroxylan detection. Arrowheads indicate phloem. e = epidermis, pp = pith parenchyma. Bars = 100 µm.

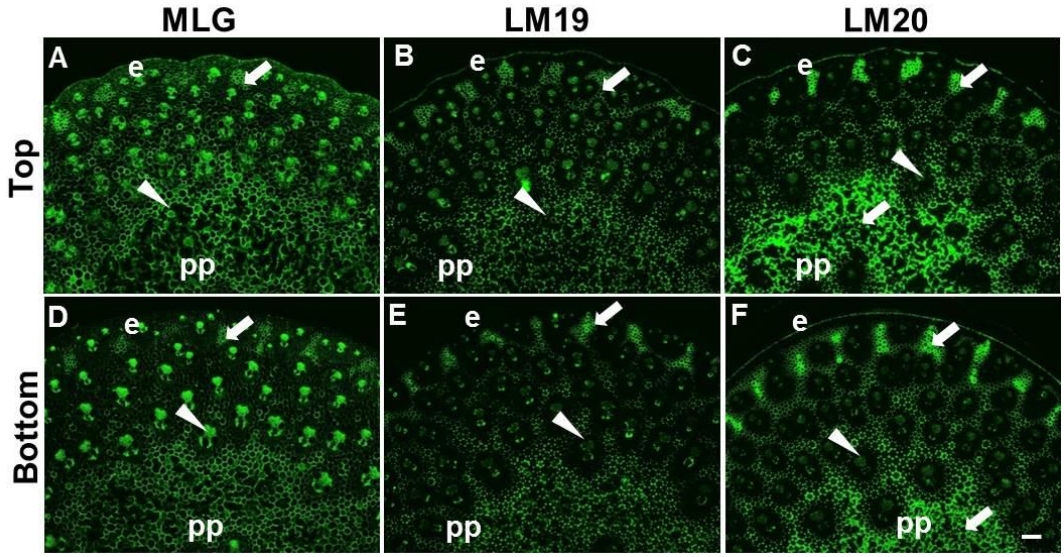

Figure 3.10: Fluorescence imaging of MLG and pectin epitopes in transverse sections from top and bottom of Int2 (from base to shoot) of a *M.* x *giganteus* stem at 50 days growth. Immunofluorescence images generated with monoclonal antibody to MLG and pectic HG (LM19, LM20). Arrowheads indicate phloem. Arrows indicate regions of interfascicular or pith parenchyma that are labelled strongly by the probes. pp = pith parenchyma, e = epidermis. Bars = 100 µm.

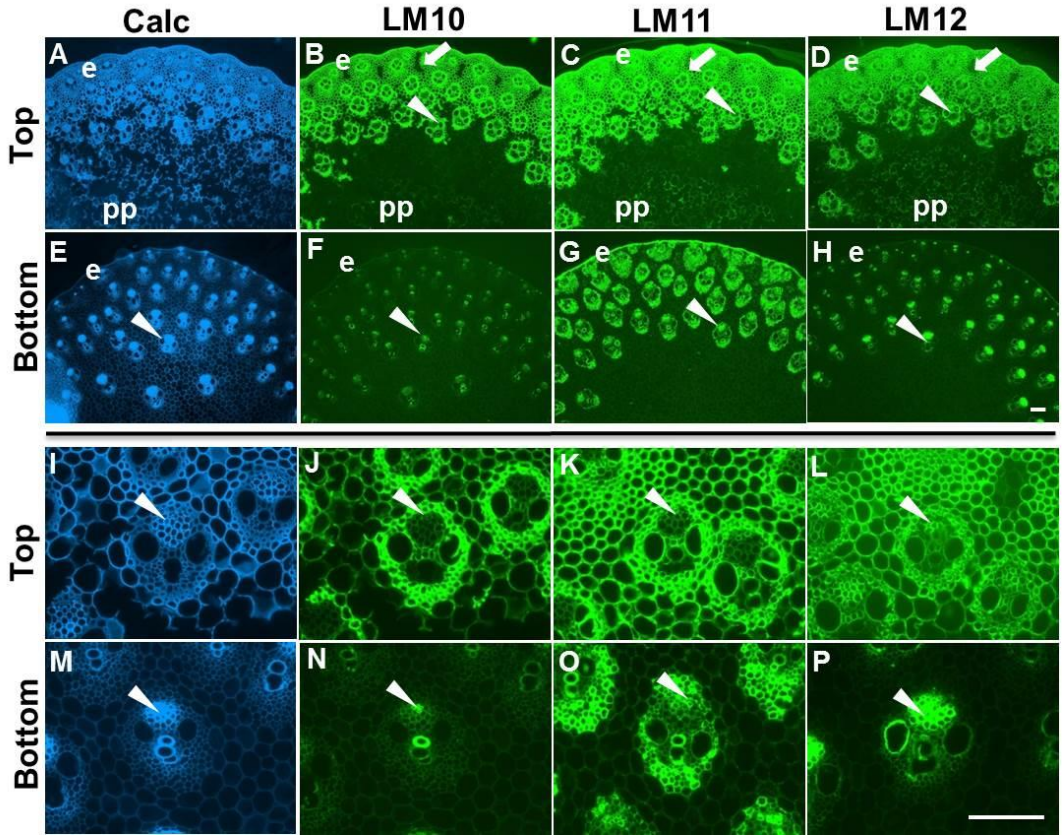

Figure 3.11: Fluorescence imaging of heteroxylan epitopes in transverse sections from top and bottom of Int4 (from base to shoot) of a *M.* x *giganteus* stem at 50 days growth. Calc staining shown in blue. Immunofluorescence images generated with monoclonal antibodies to heteroxylan (LM10, LM11 and LM12). Bottom eight micrographs show LM10, LM11 and LM12 labellings of vascular bundles (vb) at higher magnification. Arrows indicate regions of interfascicular parenchyma that have relatively lower levels of heteroxylan detection. Arrowheads indicate phloem. e = epidermis, pp = pith parenchyma. Bars = 100 µm.

Compared to the heteroxylan epitopes, the MLG epitope was detected uniformly to all types of cell walls at both top and base of Int4, and it was also abundant in pith parenchyma cell walls (no-heteroxylan binding regions) (Figure 3.12, (A) and (C)). However, the MLG was more abundant in parenchyma regions around the vascular bundles of base of Int4 but phloem of top of Int4 (Figure 3.12, (B) and (D)). In the case of the pectic HG epitopes, the LM19 epitope of unesterified HG was more detectable in the epidermal parenchyma cell walls of the top internodes (Figure 3.13, (A) and (B)), whereas the LM20 methylesterified HG epitope was much more abundantly detected in the epidermal parenchyma cell walls of the top (Figure 3.13, (H) and (G)) and phloem cell walls of the base of Int4 (Figure 3.13L), the LM19/20 pectic HG epitopes were abundant in pith parenchyma intercellular spaces of both top and base of Int4 (Figure 3.13, (A), (D), (G) and (J)).

In summary, the well-developed Int2 of 50-day-old *M.* x *giganteus* did not show big changes in the detection of heteroxylan, MLG and pectic-HG, whereas in the less developed Int4 striking changes were observed for heteroxylan detection, and it was uniformly detected in top of Int4 (the older part of Int4) but only restricted to the vascular bundles of base of Int4 (the younger part of Int4). The MLG was more abundant in vascular bundles of top internode, the LM19 unesterified HG was detected more in the sub-epidermal parenchyma of base of Int4, and the LM20 methylesterified HG epitope was more abundant in the epidermal parenchyma of top and phloem of base of Int4. Furthermore, the inner pith parenchyma regions that did not bind to heteroxylan were strongly bound by the MLG and HG antibodies.

Generally speaking, except slight differences of polysaccharide epitope binding patterns in different plant organs, these results of heteroxylan, MLG and pectic-HG observations in the top and base of Int4 were similar to those results of the different

internodes (Int1 to Int5) observations, that are the heteroxylan and pectic HG epitopes had increased bindings as the plant grown older (such as the Int1, top of Int4), while the MLG epitope was more abundant in the younger internodes (such as the Int5, base of Int4). In addition to these, the pith parenchyma regions that were not bind by the heteroxylan probes contain abundant amount of MLG and pectic HG.

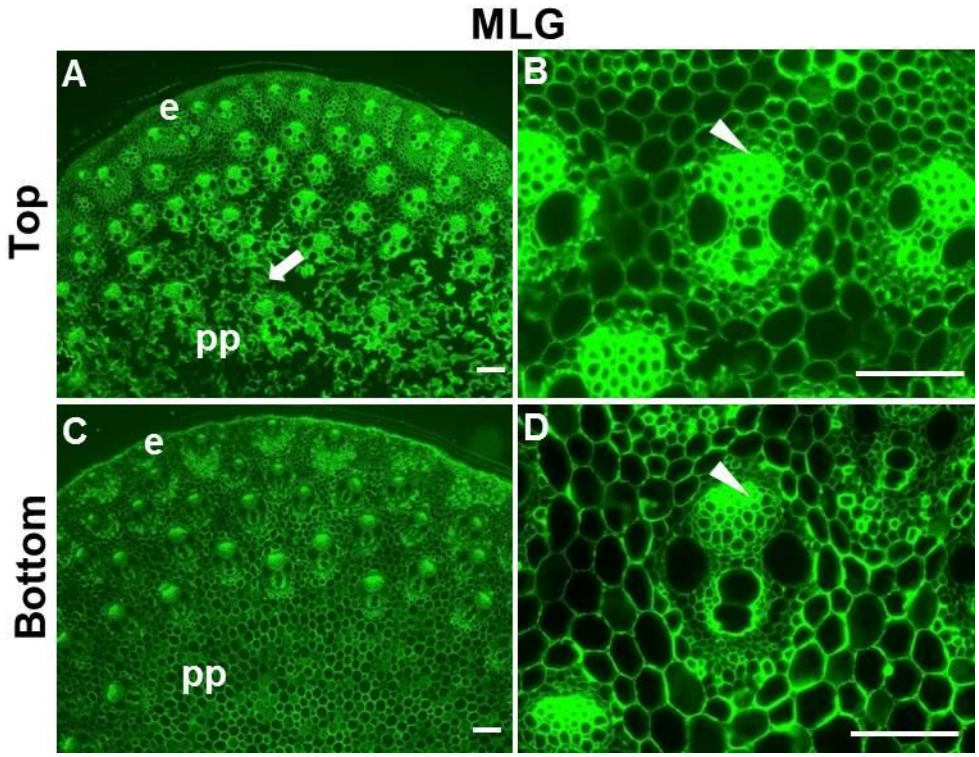

Figure 3.12: Fluorescence imaging of MLG epitopes in transverse sections from top and bottom of Int4 (from base to shoot) of a *M.* x *giganteus* stem at 50 days growth. Immunofluorescence images generated with monoclonal antibodies to MLG. B and D show MLG labellings of vascular bundles (vb) at higher magnification. Arrows indicate regions of interfascicular parenchyma that have relatively higher levels of MLG detection. Arrowheads indicate phloem. pp = pith parenchyma, e = epidermis. Bars = 100 µm.

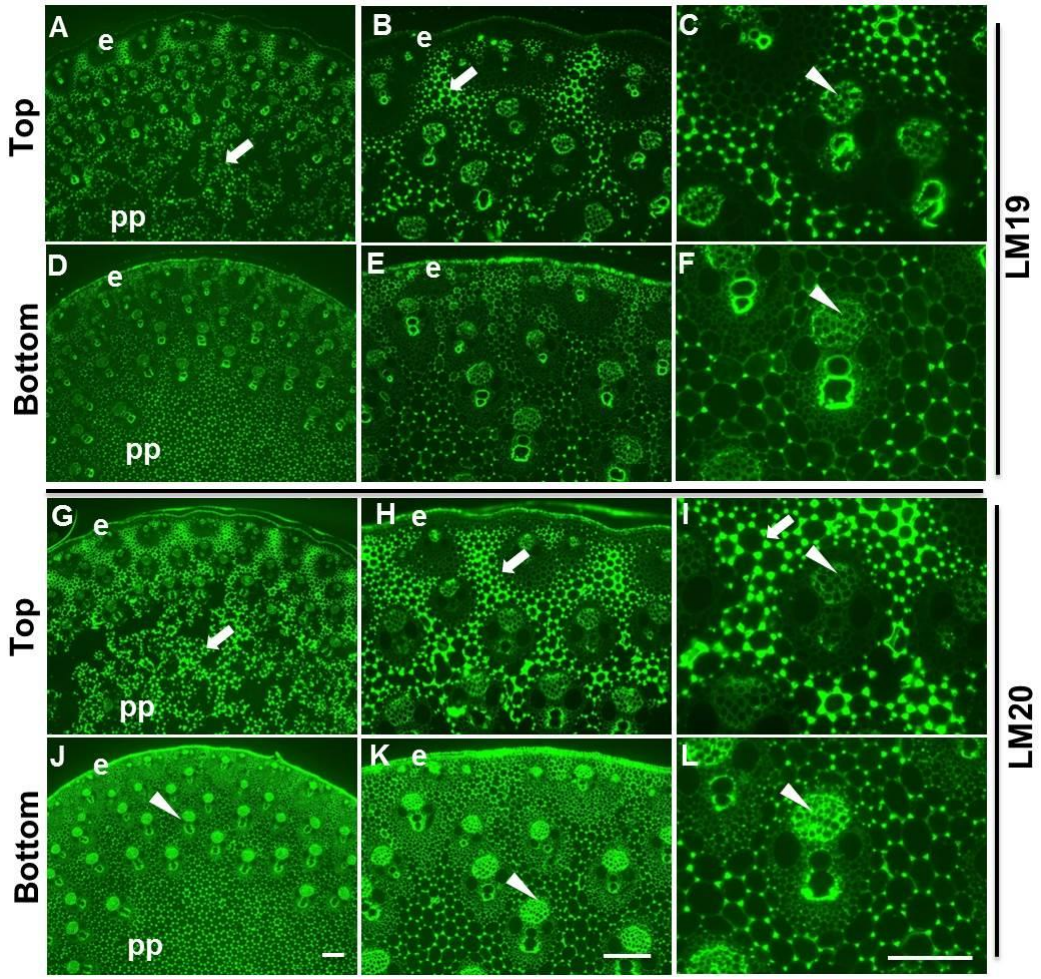

Figure 3.13: Fluorescence imaging of pectin epitopes in transverse sections from top and bottom of Int4 (from base to shoot) of a *M.* x *giganteus* stem at 50 days growth. Immunofluorescence images generated with monoclonal antibodies to pectic HG (LM19, LM20). C, F, I and L show LM19 and LM20 labellings of vascular bundles (vb) at higher magnification. Arrowheads indicate phloem. Arrows indicate regions of interfascicular parenchyma that are labelled strongly by the probes. pp = pith parenchyma, e = epidermis. Bars = 100 µm.

3.5.2 Analysis of lignin/heteroxylan/MLG/XyG/mannan/pectin in 50/200-day-old internodes of *M.* x *giganteus* stem

For the observations of *in situ* fluorescence imaging of polysaccharide epitopes at different developmental stages, this study observed these variations in several ways including the analysis of the middle of Int2 at 50 days, different internodes of 50-day-old plants, and the top and base of Int2 and Int4. An additional way to observe the developmental changes during time was by a study of looking at the Int2 after 200 days growth, compared to that of the 50 days *M.* x *giganteus*. Phloroglucinol staining (Clifford 1974) of lignin in transverse sections of the middle of Int2 of *M.* x *giganteus* at 50 and 200 days growth are shown in (Figure 3.14). The epidermis, epidermal parenchyma, vascular bundles and the vascular bundle sheaths are highly lignified in the more mature 200-day stems (Figure 3.14). The 200-day-old internodes indicated a decreasing gradient in the detection of the crystalline cellulose (Figure 3.15). Compared to the 50-day-old stems, the CBM3a crystalline cellulose was restricted to the vascular bundle sheath and weakly detected in the parenchyma cell walls of the 200-day-old internodes (Figure 3.15E), and it did not bind to the phloem regions (Figure 3.15F). The LM10/LM11 xylan/arabinoxylan epitopes did not reveal any large differences (Figure 3.16, (B), (C), (F) and (G)), whereas the LM12 ferulated arabinoxylan epitope was detected more abundantly in the pith parenchyma of the 200-day-old stems (Figure 3.16H). In contrast, the MLG epitope has a striking decreasing detections, it was less abundant and restricted to the phloem cell walls in the 200-day-old stems (Figure 3.17, (D), (E) and (F)).

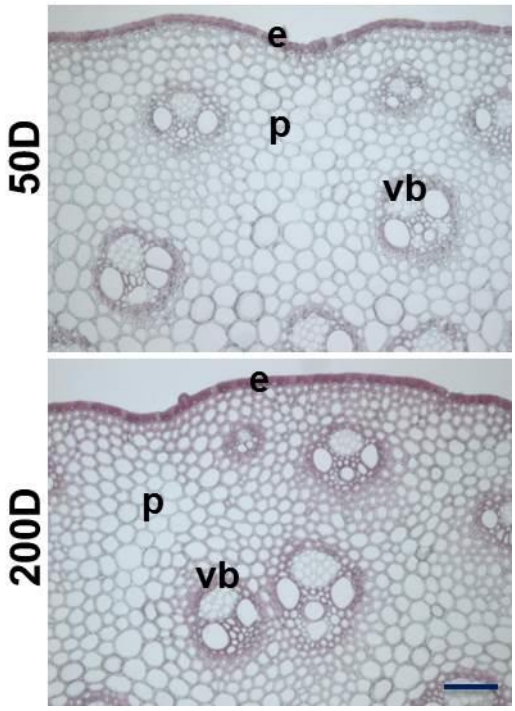

Figure 3.14: Phloroglucinol staining of lignin in transverse sections of Int2 of *M.* x *giganteus* stem at 50 and 200 days growth. e = epidermis, p = parenchyma, vb = vascular bundle. Bar = 100 µm.

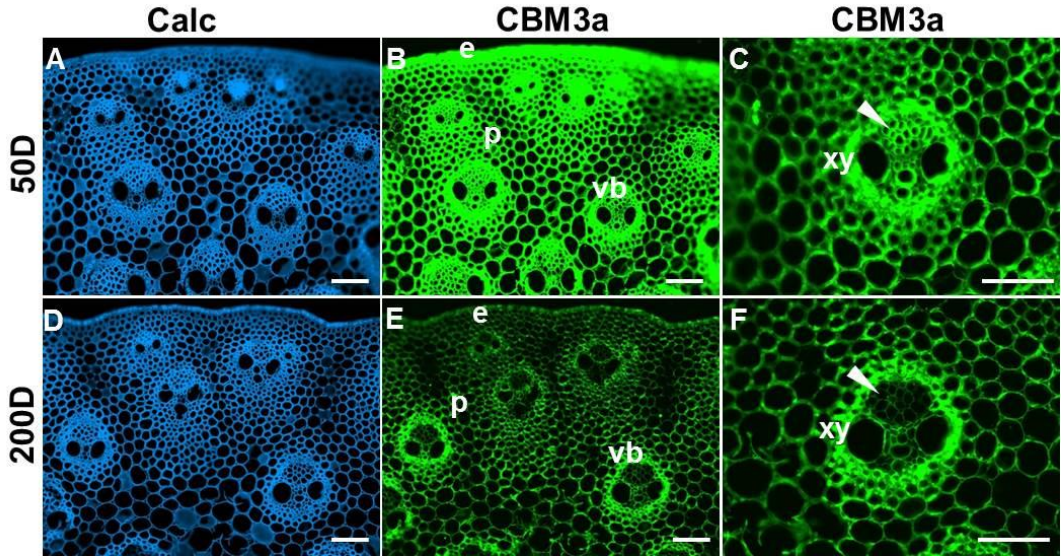

Figure 3.15: Fluorescence imaging of cellulose in transverse sections of Int2 of *M.* x *giganteus* stem at 50 and 200 days growth. Images generated with Calcofluor White (Calc, blue) and indirect immunofluorescence (green) with carbohydrate binding module CBM3a to crystalline cellulose. C and F show CBM3a labellings of vascular bundles (vb) at higher magnification. Arrowheads indicate phloem. e = epidermis, p = parenchyma, vb = vascular bundle, xy = xylem. Bar = 100 µm.

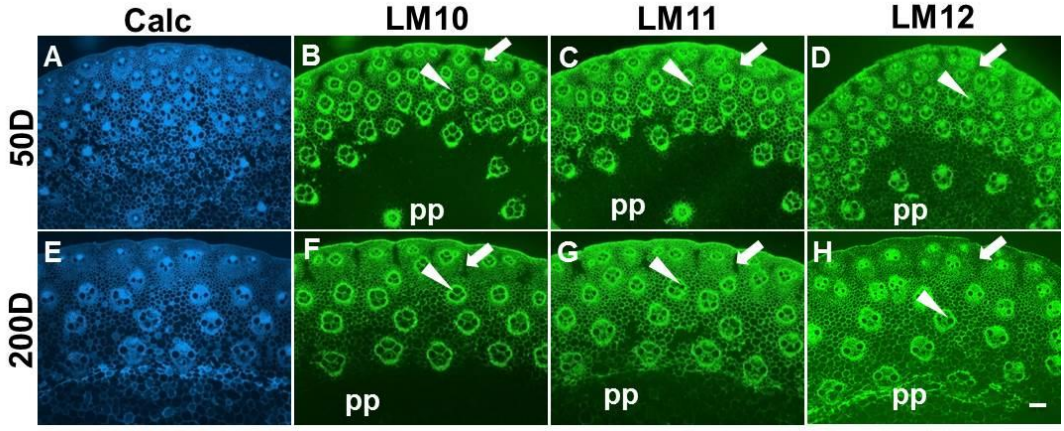

Figure 3.16: Fluorescence imaging of heteroxylan epitopes in transverse sections of Int2 of *M.* x *giganteus* stem at 50 and 200 days growth. Calc staining shown in blue. Immunofluorescence images generated with monoclonal antibodies to heteroxylan (LM10, LM11 and LM12). Arrows indicate regions of interfascicular parenchyma that have relatively lower levels of heteroxylan detection. Arrowheads indicate phloem. pp = pith parenchyma. Bars = 100 µm.

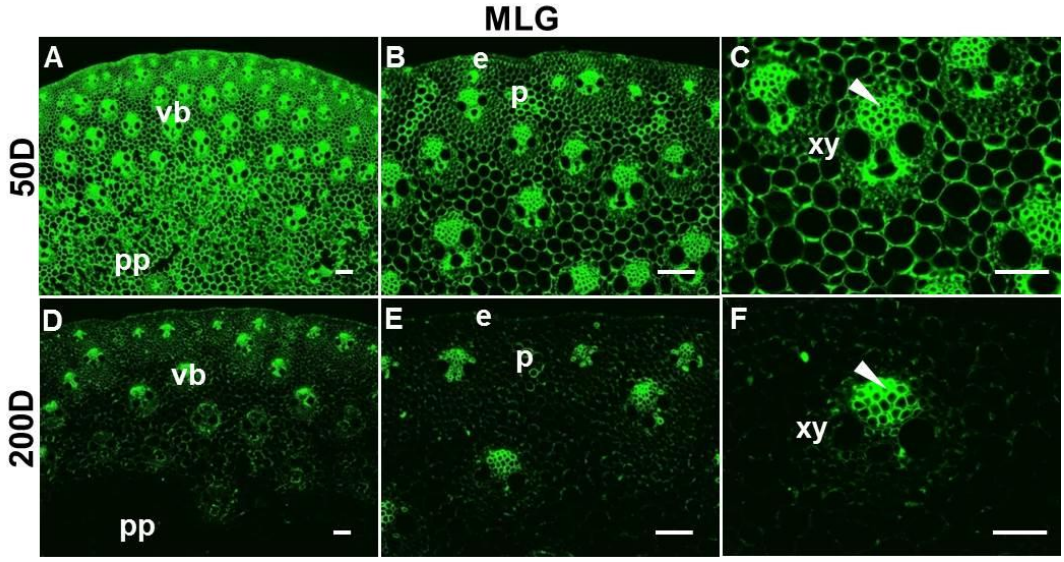

Figure 3.17: Fluorescence imaging of the MLG epitope in transverse sections of Int2 of *M.* x *giganteus* stem at 50 and 200 days growth. Immunofluorescence images generated with a monoclonal antibody to MLG. C and F show MLG labellings of vascular bundles (vb) at higher magnification. Arrowheads indicate phloem. e = epidermis, p = parenchyma, pp = pith parenchyma, vb = vascular bundle, xy = xylem. Bar = 100 µm.

In transverse sections of 200-day-old *M.* x *giganteus* stems for the vascular bundle regions, compared with the 50-day-old stems, the LM15 XyG did not bind to xylem cell walls (Figure 3.18, (B) and (F)), while the LM21 heteromannan epitope was more abundant in phloem, xylem and parenchyma regions around the vascular bundles (Figure 3.18, (C) and (G)). The LM5 pectic galactan epitope was detected in the sheath of the vascular bundles of the 200-day-old stems, whereas it was restricted to the phloem of the 50-day-old stems (Figure 3.18, (D) and (H)). In the case of the pectic HG epitopes, the LM19 unesterified epitope was more detectable in the phloem and xylem cell walls of 200-day-old stems (Figure 3.19E), whereas the LM20 methylesterified HG epitope was much more abundantly detected in the

epidermal parenchyma and pith parenchyma cell walls of 50-day-old stems (Figure 3.19, (C) and (I)).

In summary, the major differences between the 200-day-old and 50-day-old *M.* x *giganteus* stems were that the heteroxylan epitopes tended to display reduced detection and the MLG was abundant in the younger tissues, and the pectic HG was more abundant in the younger internodes. These trends of the three major non-cellulosic polysaccharide changes (xylans, MLG and pectic HG) during the *M.* x *giganteus* development were more or less similar to that of the results observed above (chapter 3.5.1). Summary of the distribution of heteroxylan (LM10/11/12), MLG and pectic HG (LM19/20) epitopes at different developmental stages of *M.* x *giganteus* stem at 50 days growth are presented in Table 3.2.

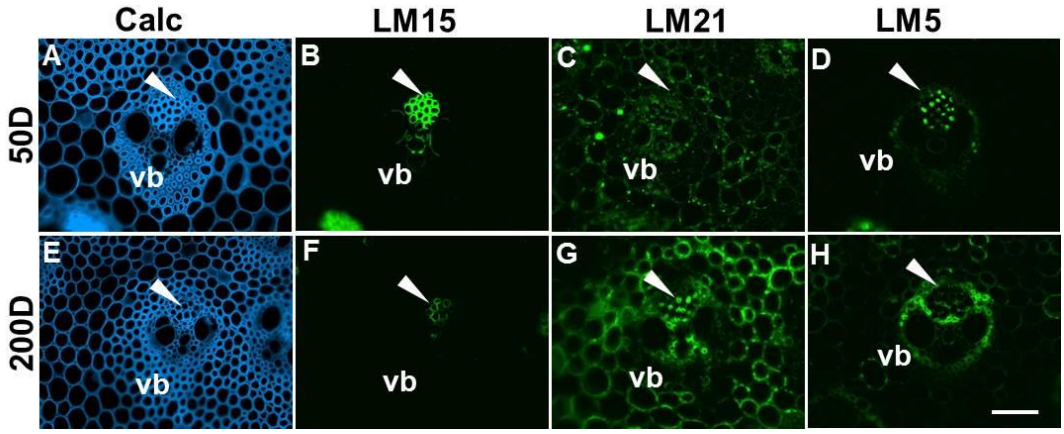

Figure 3.18: Fluorescence imaging of vascular bundles of Int2 of *M.* x *giganteus* stem at 50 and 200 days growth. Calc staining shown in blue. Immunofluorescence images generated with monoclonal antibodies to xyloglucan (LM15), heteromannan (LM21) and pectic galactan (LM5). Arrowheads indicate phloem. vb = vascular bundle. Bars = 100 µm.

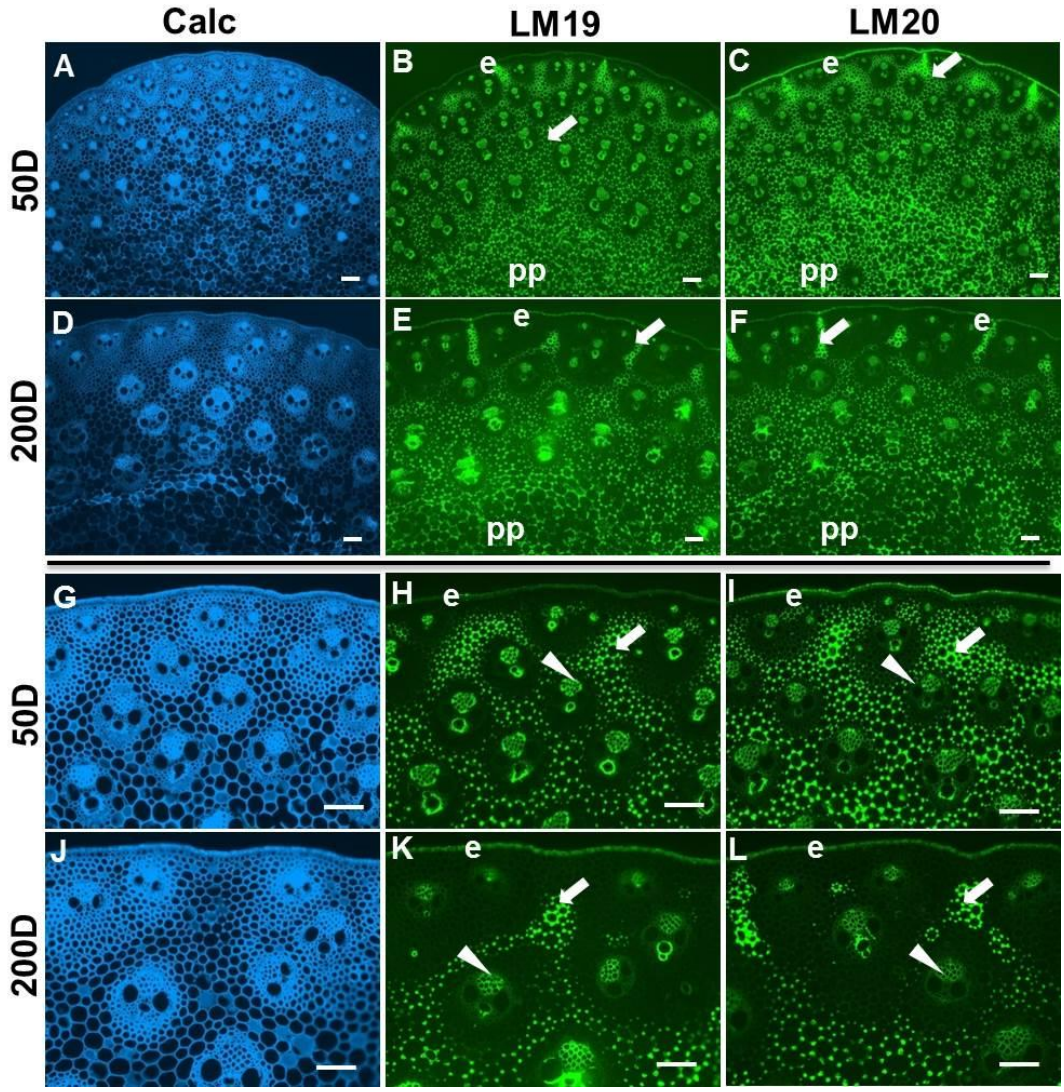

Figure 3.19: Fluorescence imaging of pectin epitopes in transverse sections of Int2 of *M.* x *giganteus* stem at 50 days and 200 days growth. Images generated with Calcofluor White (Calc, blue) and indirect immunofluorescence (green) with monoclonal antibodies to pectic HG (LM19, LM20). Arrowheads indicate phloem. Arrows indicate regions of interfascicular parenchyma that are labelled strongly by the probes. e = epidermis, pp = pith parenchyma. Bar = 100 µm.

Table 3.2: Tissue-specific distribution of heteroxylan (LM10/11/12), MLG and pectic HG (LM19/20) epitopes at different developmental stages of *M.* x *giganteus* stem.

	e	pp	vb	vs	ph	xy
50D Int5 mid	LM10 –	LM10 –	LM10 –	LM10 –	LM10 –	LM10 –
	LM11 –	LM11 –	LM11 ±	LM11 ±	LM11 ±	LM11 ±
	LM12 –	LM12 –	LM12 ±	LM12 ±	LM12 +	LM12 ±
	MLG ++	MLG ±	MLG +	MLG –	MLG ++	MLG +
	LM19 ±	LM19 –	LM19 –	LM19 –	LM19 ±	LM19 ±
	LM20 +	LM20 ±	LM20 ±	LM20 –	LM20 ±	LM20 ±
50D Int1 mid	LM10 ++	LM10 –	LM10 +	LM10 +	LM10 +	LM10 +
	LM11 ++	LM11 –	LM11 ++	LM11 +	LM11 ++	LM11 ++
	LM12 ++	LM12 –	LM12 ++	LM12 +	LM12 ++	LM12 ++
	MLG –	MLG –	MLG +	MLG –	MLG ++	MLG +
	LM19 –	LM19 +	LM19 +	LM19 –	LM19 ±	LM19 ±
	LM20 –	LM20 ++	LM20 –	LM20 –	LM20 ±	LM20 ±
50D Int2 mid	LM10 ++	LM10 –	LM10 +	LM10 +	LM10 –	LM10 +
	LM11 ++	LM11 –	LM11 +	LM11 +	LM11 ++	LM11 +
	LM12 ++	LM12 –	LM12 +	LM12 +	LM12 +	LM12 +
	MLG –	MLG –	MLG ++	MLG ±	MLG +	MLG +
	LM19 –	LM19 +	LM19 +	LM19 –	LM19 +	LM19 +
	LM20 +	LM20 ++	LM20 +	LM20 –	LM20 +	LM20 ±
200D Int2 mid	LM10 ++	LM10 –	LM10 +	LM10 +	LM10 –	LM10 +
	LM11 ++	LM11 –	LM11 +	LM11 +	LM11 +	LM11 +
	LM12 ±	LM12 +	LM12 +	LM12 +	LM12 +	LM12 +
	MLG ++	MLG ±	MLG ±/–	MLG –	MLG +	MLG –
	LM19 ±	LM19 –	LM19 +	LM19 –	LM19 +	LM19 +
	LM20 ±	LM20 +	LM20 +	LM20 –	LM20 +	LM20 ±

++ strong binding; + binding; ± weak binding; – no binding. e = epidermis, pp = pith parenchyma, vb = vascular bundle, vs = vascular bundle sheath, ph = phloem, xy = xylem, 50D = 50-day-old, 200D = 200-day-old. LM10 = xylan; LM11 = xylan/arabinoxylan; LM12 = ferulated heteroxylan; LM19/20 = pectic HG.

3.6 Comparison of distribution of cell wall polysaccharides in second internode of 50-day *Miscanthus* species: *Miscanthus* x *giganteus*, *Miscanthus sinensis* and *Miscanthus sacchariflorus* stems

3.6.1 Analysis of heteroxylan and cellulose in transverse sections of three *Miscanthus* species

After the initial analysis of polysaccharide epitopes in *M.* x *giganteus*, the polysaccharide investigation extended in the two parents species - *M. sacchariflorus* and *M. sinensis.* As shown before in this chapter, the major developmental difference among the three species was that the *M.* x *giganteus* grows faster and taller than its parents at 50 days. To further investigate the polysaccharide distribution differences, the transverse sections of the middles of Int2 of *M. sacchariflorus* and *M. sinensis* at 50 days were explored using different monoclonal antibodies.

The Calcofluor White (Calc) staining of the outer stem regions of the middle of Int2 from the base of 50-day-old stems of *M.* x *giganteus*, *M. sacchariflorus* and *M. sinensis* are shown in Figure 3.20. In all three *Miscanthus* species an anatomy of scattered vascular bundles within parenchyma regions was apparent (Figure 3.20, (A), (B) and (C)), and the vascular bundles nearest to the epidermis were generally smaller in diameter to those in more internal regions (Figure 3.20, (A), (B) and (C)). In all cases the vascular bundles consisted of a distal area of phloem cells (accounting for around a quarter of the vascular tissues) flanked by two large metaxylem vessels and a more central xylem cell in addition to surrounding sheaths of small fibre cells (Figure 3.20, (A), (B) and (C)). The most striking distinction seen in the Calc-stained sections was that in *M. sinensis* and *M.* x *giganteus* (Figure 3.20, (A) and (C)), Calc-staining was equivalent in cell walls whereas in *M.*

sacchariflorus the cell walls of the larger cells of the interfascicular parenchyma were not stained in the same way (Figure 3.20B), which indicates some difference to the structure of these sub-epidermal parenchyma cell walls.

The analysis of heteroxylan probes indicated that these xylan polymers were widely detected in *Miscanthus* stem cell walls (Figure 3.20). The analysis also indicated that non-Calc-staining cell walls in *M. sacchariflorus* had lower levels of detectable heteroxylan (Figure 3.20, (E) and (K)). This was particularly the case for the LM10 xylan epitope (unsubstituted xylan) and the LM12 feruloylated arabinoxylan epitope (Figure 3.20, (E) and (K)). Both of the two heteroxylan epitopes closely reflected the distribution of Calc-staining. In the case of *M.* x *giganteus*, some smaller regions of the interfascicular parenchyma were notable for reduced binding by the LM10 and LM11 probes (Figure 3.20, (D) and (G)). In the case of *M. sinensis*, such regions were most apparent as clusters of cells in sub-epidermal regions of parenchyma (Figure 3.20F). For all of the three *Miscanthus* species, the LM10 unsubstituted xylan did not bind to phloem, while the LM11 and the LM12 substituted xylan epitopes were detectable in phloem regions (Figure 3.20).

The analysis of the CBM3a cellulose revealed that the crystalline cellulose was widely detected in *Miscanthus* stem cell walls at 50 days (Figure 3.20, (M), (N) and (O)). The major difference in CBM3a binding was that in *M. sacchariflorus*, the cellulose analysis also indicated that non-Calc-staining cell walls in the sub-epidermal parenchyma regions had lower levels of cellulose detection (Figure 3.20N).

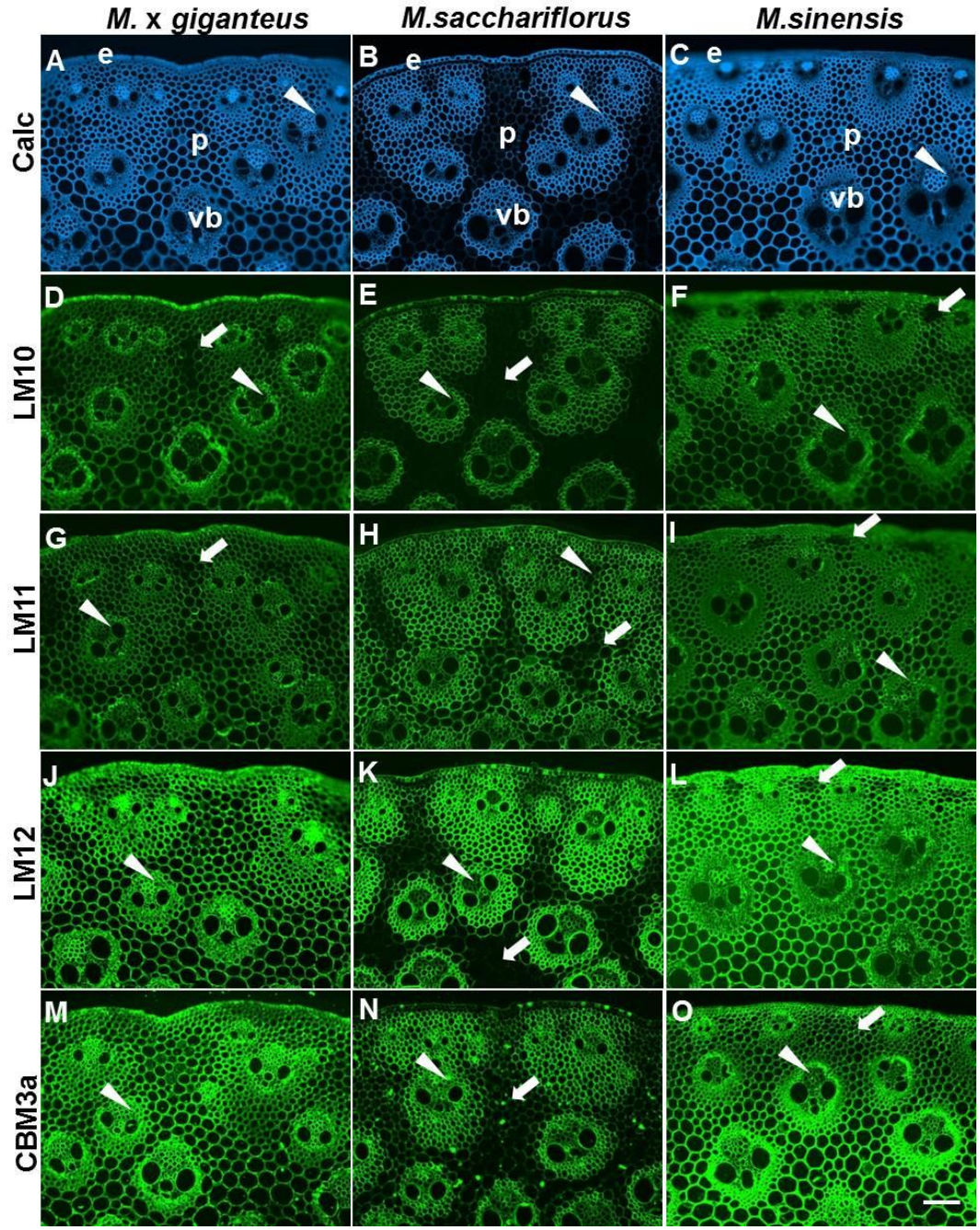

Figure 3.20: Fluorescence imaging of heteroxylan epitopes in transverse sections of Int2 of *M.* x *giganteus*, *M. sacchariflorus* and *M. sinensis* stems at 50 days growth. Images generated with Calcofluor White (Calc, blue) and indirect immunofluorescence (green) with monoclonal antibodies to epitopes of heteroxylan LM10, LM11 and LM12, and carbohydrate binding module CBM3a to cellulose. Arrowheads indicate phloem. Arrows indicate regions of interfascicular parenchyma that have relatively lower levels of heteroxylan and cellulose detection. e = epidermis, p = parenchyma, vb = vascular bundle. Bar = 100 µm.

3.6.2 Analysis of MLG, XyG and mannan in transverse sections of three *Miscanthus* species

At 50 days, in all three *Miscanthus* species, the MLG epitope was detected in all primary cell walls but with particular abundance in phloem cell walls, the central metaxylem cells and in specific regions of the interfascicular parenchyma (Figure 3.21, (A), (B) and (C)). Unlike the heteroxylan epitopes, the MLG epitope was not abundantly detected in the fibre cells surrounding the vascular bundles (sheath of vascular bundles) (Figure 3.21, (A), (B) and (C)). The specific patterns of abundant MLG epitope detection in interfascicular parenchyma varied between the three *Miscanthus* species, but were consistent for each species. In *M.* x *giganteus*, the MLG epitope was strongly detected in radially extended groups of cells in the stem periphery (Figure 3.21A). In *M. sinensis*, such groups of cells were smaller and were mostly sub-epidermal clusters of fewer than 10 cells (Figure 3.21C). In *M. sacchariflorus*, strong labelling was detected throughout the parenchyma regions (Figure 3.21B). For all three species these parenchyma regions were equivalent to those with reduced staining by the heteroxylan probes (Figure 3.20 and Figure 3.21).

The LM15 XyG epitope was restricted to phloem cell walls in all three species (Figure 3.21, (D), (E) and (F)). In *M.* x *giganteus* and *M.sinensis*, it was also detectable in metaxylem cells and that was consistent in both species (Figure 3.21). The LM21 heteromannan epitope was only weakly detected in scattered parenchyma cells in *M. sacchariflorus* and *M. sinensis* stem sections, reflecting the high MLG/low heteroxylan regions (Figure 3.21, (H) and (I)), and it was detected to some extent in phloem cell walls and more strongly to the MLG-rich parenchyma regions of *M.* x *giganteus* (Figure 3.21G).

Analysis of higher magnification micrographs of vascular bundles of the three *Miscanthus* species (Figure 3.22) indicated that the phloem cell walls have

abundant detectable LM11/12 substituted arabinoxylan epitopes, but not the LM10 unsubstituted-xylan epitope. This was consistent for all three species (Figure 3.22, (A) to (I)). The LM12 ferulated arabinoxylan epitope was notably highly detected in phloem cell walls and vascular bundle sheaths of *M.* x *giganteus* and *M. sacchariflorus* but less in equivalent cells in *M. sinensis* (Figure 3.22, (G), (H) and (I)), whereas the MLG and LM15 XyG epitopes were abundantly detected in phloem cell walls in all three species (Figure 3.22, (J) to (O)). In the xylem cells, however, the LM15 XyG was consistently detected in specific cell wall regions of the two large metaxylem cells (adjacent to the central metaxylem cell) and the cell wall of the central metaxylem cell in the vascular bundles in *M.* x *giganteus* and *M. sinensis* (Figure 3.22, (J) and (L)). This binding pattern was observed to some extent in *M. sinensis* xylem cell walls and only rarely in *M. sacchariflorus* cell walls (Figure 3.22K).

In summary, for all three *Miscanthus* species, cellulose was abundant. For the non-cellulosic polysaccharide detections, heteroxylan and MLGs were more abundant than XyG. For *M. sacchariflorus* and *M. sinensis*, the non-Calc staining parenchyma cells reflecting the high MLG/low heteroxylan parenchyma regions, and this indicates that these parenchyma cell walls have a distinct polysaccharide architecture which may relate to their functions. For all three species, the phloem cell walls contain abundant detection of cellulose, substituted arabinoxylan, XyG, MLG and less amount of heteromannan which may indicate their specific properties.

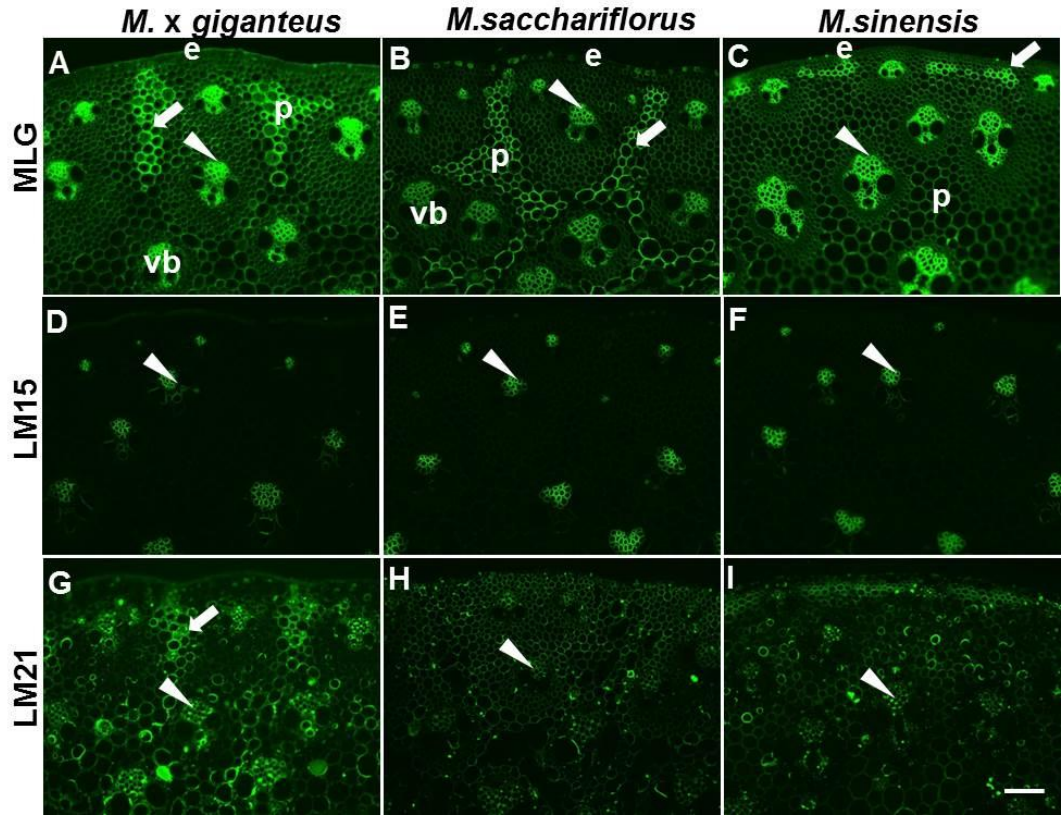

Figure 3.21: Fluorescence imaging of MLG, xyloglucan and heteromannan epitopes in transverse sections of Int2 of *M.* x *giganteus*, *M. sacchariflorus* and *M. sinensis* stems at 50 days growth. Immunofluorescence images generated with monoclonal antibodies to MLG, xyloglucan (LM15) and heteromannan (LM21). Arrowheads indicate phloem. Arrows indicate regions of interfascicular parenchyma that are labelled strongly by the probes. e = epidermis, p = parenchyma, vb = vascular bundle. Bar = 100 µm.

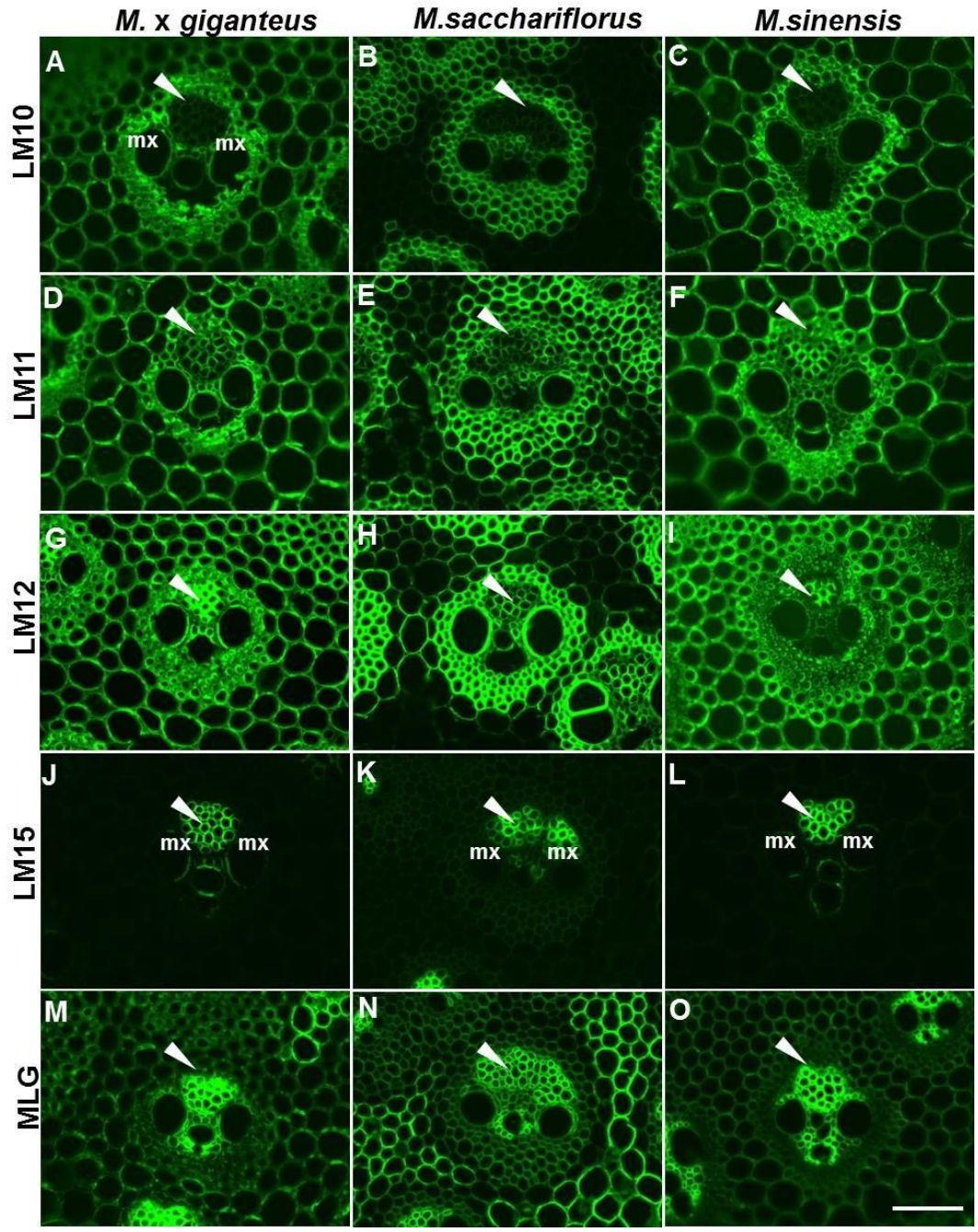

Figure 3.22: Fluorescence imaging of MLG, xyloglucan and heteromannan epitopes in transverse sections of Int2 of *M.* x *giganteus*, *M. sacchariflorus* and *M. sinensis* stems at 50 days growth. Immunofluorescence images generated with monoclonal antibodies to MLG, xyloglucan (LM15) and heteromannan (LM21). Arrowheads indicate phloem. Arrows indicate regions of interfascicular parenchyma that are labelled strongly by the probes. e = epidermis, p = parenchyma, vb = vascular bundle, mx = metaxylem. Bar = 100 µm.

3.6.3 Analysis of HG-related and RG-related pectin in transverse sections of three *Miscanthus* species

In addition to the analysis of cellulose and the major non-cellulosic polysaccharides, the pectic polysaccharides were also studied in all three *Miscanthus* species at 50 days. To some extent the abundance of these HG-related pectin epitopes (LM18/19/20) in parenchyma regions (Figure 3.23) reflected the occurrence of MLG epitope abundance shown in Figure 3.21 and Figure 3.22, as for example all of the four antibodies did not bind to sheaths of fibre cells surrounding the vascular bundles. This correlation was particularly the case for the LM20 methylesterified HG epitope in the radially extended groups of cells in *M.* x *giganteus* (Figure 3.23J) and sub-epidermal groups of cells in *M. sinensis* (Figure 3.23L). In these regions the HG epitopes were detected throughout cell walls and not just in regions lining intercellular parenchyma spaces (Figure 3.23, (J), (K) and (L)). In all three species, the HG epitopes were also detected in phloem cell walls. The LM20 methylesterified HG epitope was abundantly detected in pith parenchyma cell walls of *M.* x *giganteus* (Figure 3.23, (J) and (M)), whereas in the other two parents *Miscanthus* species - *M. sacchariflorus* and *M. sinensis* it was restricted to the intercellular spaces of these regions (Figure 3.23 (K), (L), (N) and (O)).

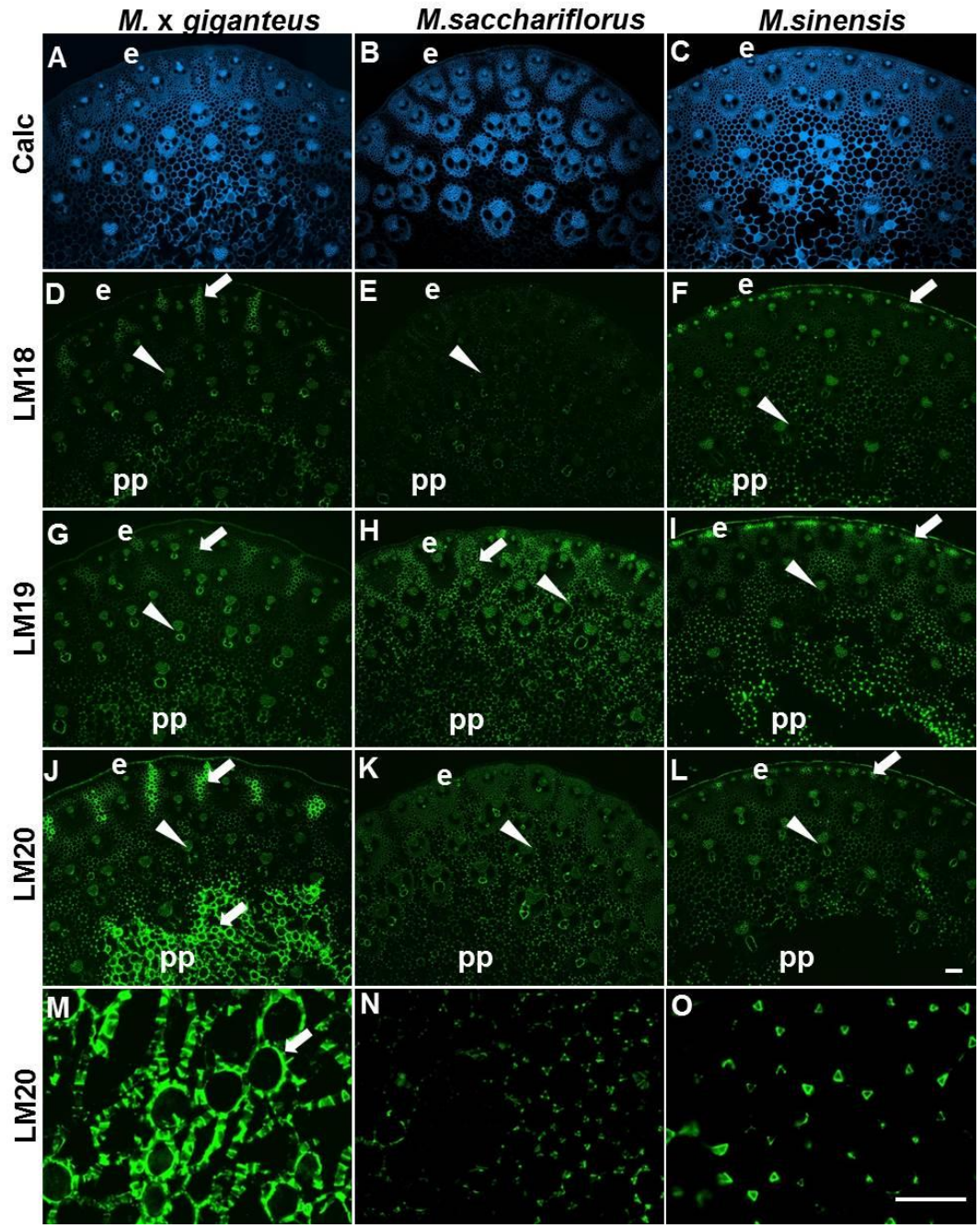

Figure 3.23: Fluorescence imaging of pectin epitopes of transverse sections of Int2 of *M.* x *giganteus*, *M. sacchariflorus* and *M. sinensis* stems at 50 days growth. Images generated with Calcofluor White (Calc, blue) and indirect immunofluorescence images generated with monoclonal antibodies to pectic HG (LM18, LM19, LM20). Arrowheads indicate phloem. Arrows indicate regions of interfascicular or pith parenchyma that are labelled strongly by the probes. Bottom three micrographs show LM20 labelling at higher magnification of central pith parenchyma (pp) of stems. e = epidermis. Bars = 100 µm.

Analysis of the RG-I related epitopes indicates that the LM5 pectic galactan epitope was only weakly detected in phloem cell walls of *M.* x *giganteus*, and in small amount of epidermal parenchyma cells of *M. sacchariflorus* and *M. sinensis* (Figure 3.24, (A), (B) and (C)). Strikingly, the LM6 arabinan epitope was more abundantly detected in the phloem, xylem and certain parenchyma regions in *M.* x *giganteus* and *M. sinensis* that had been identified previously by strong MLG and HG probe binding (Figure 3.24, (D) and (F)). In the case of *M. sacchariflorus*, the LM6 arabinan epitope was detected abundantly and evenly in all cell walls (Figure 3.24E).

In summary, for all three *Miscanthus* species, the HG-related pectin epitopes (LM18, LM19 and LM20) and RG-I related pectin epitopes (LM5 and LM6) in sub-epidermal parenchyma regions reflected the occurrence of MLG epitope abundance, and in these corresponding parenchyma regions, the heteroxylan epitopes (LM10, LM11 and LM12) were less abundant.

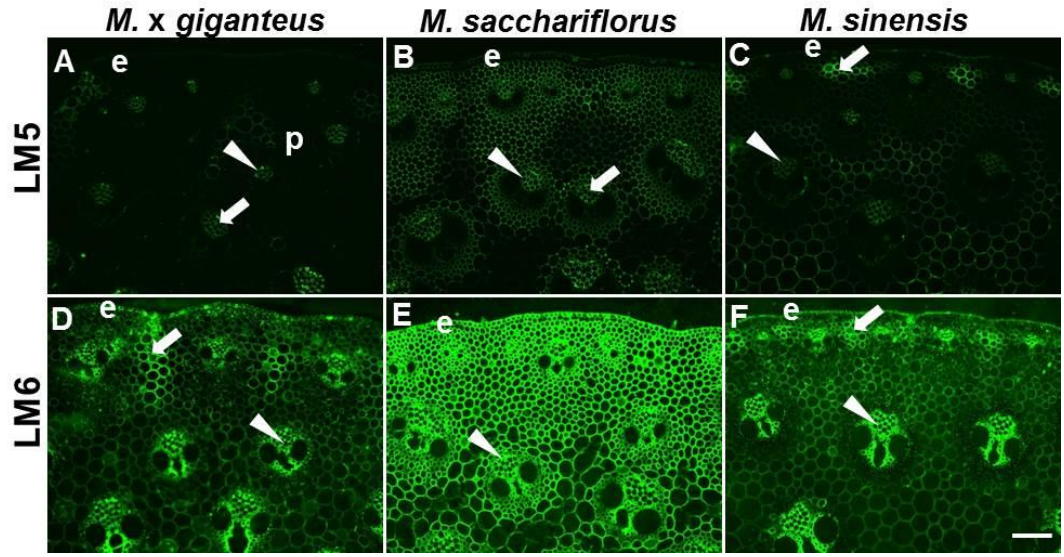

Figure 3.24: Fluorescence imaging of pectin epitopes in transverse sections of Int2 of *M.* x *giganteus*, *M. sacchariflorus* and *M. sinensis* stems at 50 days growth. Immunofluorescence images generated with monoclonal antibodies to pectic galactan (LM5) and arabinan (LM6). Arrowheads indicate phloem. Arrows indicate regions of interfascicular parenchyma that are labelled by the probes. e = epidermis. Bar = 100 µm.

3.7 Comparison of major cell wall polysaccharides distribution differences in different developmental stages of *Miscanthus* species: *Miscanthus* x *giganteus*, *Miscanthus sinensis* and *Miscanthus sacchariflorus* stems

To further explore the major developmental differences in the three *Miscanthus* species, transverse sections of middle of Int2 at 200 days were investigated. Detection of heteroxylan (LM10/11/12), MLG and pectic-HG epitopes (LM19/20) in transverse sections of Int2 of *Miscanthus* species at 50 and 200 days growth are shown in (Figure 3.16, 3.17, 3.19, 3.25-30). Generally speaking, *in situ* analysis of the 200-day-old *Miscanthus* internodes indicated an increasing gradient in the heteroxylan detection (Figure 3.16H, 3.25, 3.28), whereas a decreasing gradient in MLG (Figure 3.17, 3.26, 3.29) and HG detections (Figure3.27 and Figure 3.30) in

all of the three species (except for the HG detection in *M.* x *giganteus*, Figure 3.18), compared to the 50-day-old stems. The LM10/LM11 xylan/arabinoxylan epitopes did not reveal any large differences between 50-day-old and 200-day-old *M.* x *giganteus* (Figure 3.16), whereas they were more detectable in inner pith parenchyma cell walls of the other two parent species - *M. sinensis* and *M. sacchariflorus* at 200 days growth (Figure 3.25 and 3.28). The LM12 ferulated arabinoxylan epitope was detected more abundantly in the pith parenchyma of the 200-day-old stems of all three species (Figure 3.16, 3.25 and 3.28). In contrast, the level of MLG epitope detection decreased heavily in these corresponding pith parenchyma regions in the 200-day-old stems of all three species (Figure 3.17, 3.26 and 3.29). In the case of the pectic HG epitopes, the LM19 and LM20 epitopes were less abundantly detected in interfascicular parenchyma cell walls of 200-day-old stems in *M.sinensis* and *M. sacchariflorus* (Figure 3.27 and 3.30).

In summary, the major developmental differences between the three *Miscanthus* species were that compared to the younger 50-day-old *Miscanthus* stems, the older 200-day-old stems contain higher levels of heteroxylan, lower levels of MLG and HG in some particular parenchyma cells, which indicated the distinct polysaccharide architecture and function in these parenchyma regions (Table 3.3).

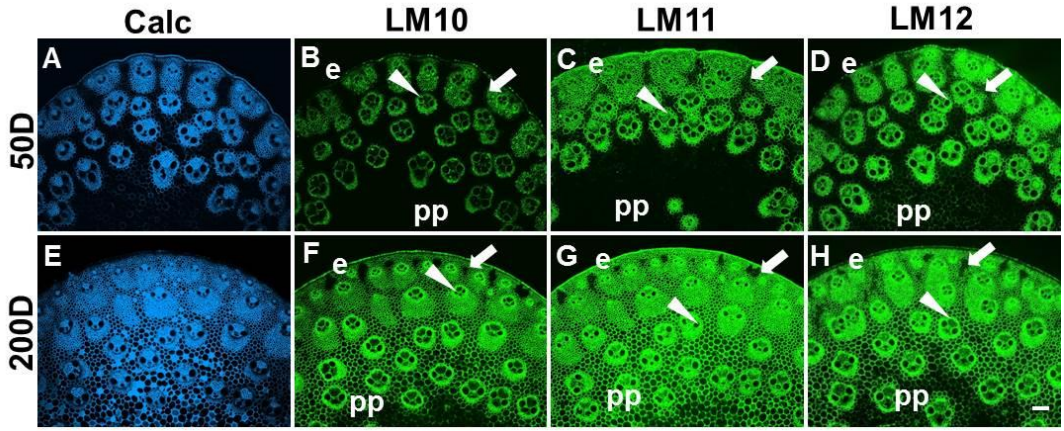

Figure 3.25: Fluorescence imaging of heteroxylan epitopes of transverse sections of Int2 of *M. sacchariflorus* stem at 50 and 200 days growth. Calc staining shown in blue. Immunofluorescence images generated with monoclonal antibodies to heteroxylan (LM10, LM11 and LM12). Arrows indicate regions of interfascicular parenchyma that have relatively lower levels of heteroxylan detection. Arrowheads indicate phloem. e = epidermis, pp = pith parenchyma. Bars = 100 µm

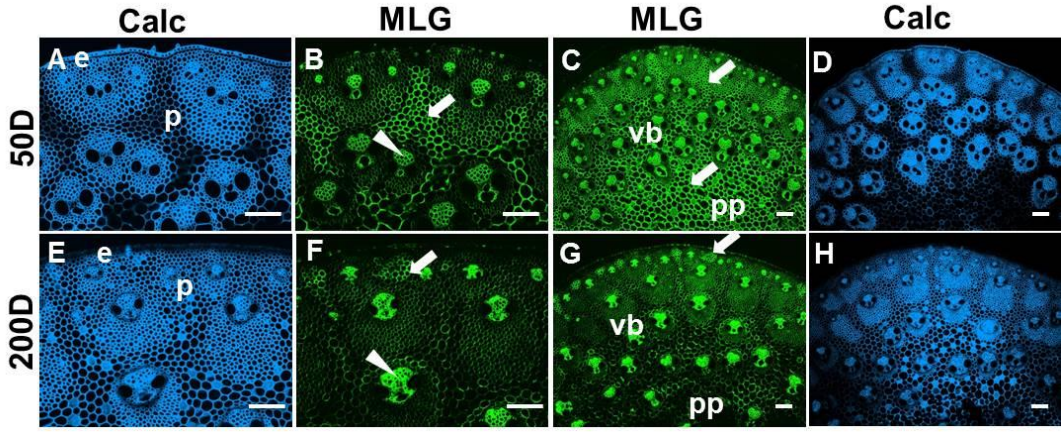

Figure 3.26: Fluorescence imaging of MLG epitopes of transverse sections of Int2 of *M. sacchariflorus* stem at 50 and 200 days growth. Calc staining shown in blue. Immunofluorescence images generated with monoclonal antibodies to MLG. Arrows indicate regions of interfascicular parenchyma that are labelled strongly by the probes. Arrowheads indicate phloem. e = epidermis, vb = vascular bundle, p = parenchyma, pp = pith parenchyma. Bars = 100 µm

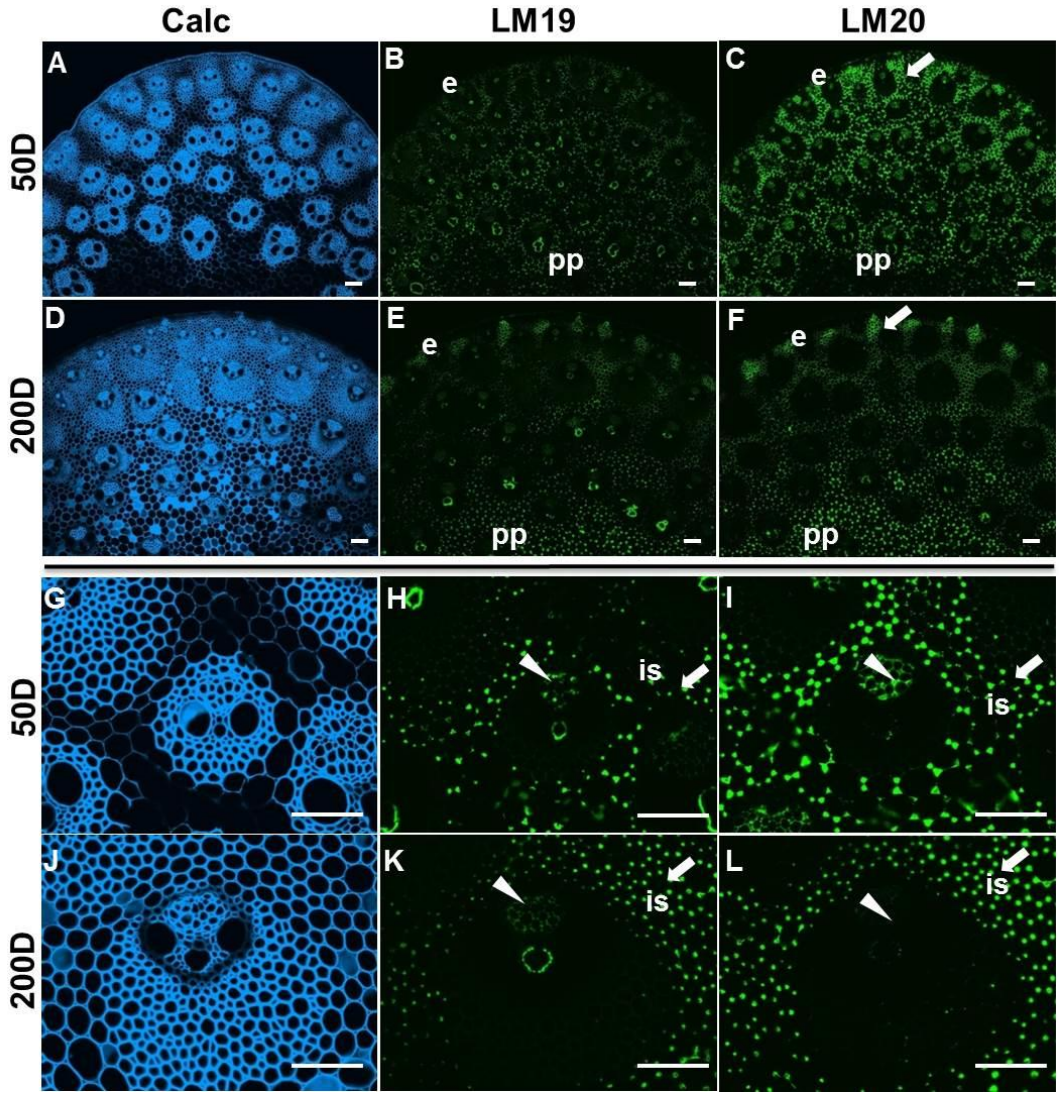

Figure 3.27: Fluorescence imaging of cell walls in transverse sections of Int2 of stems of *M. sacchariflorus* at 50 days and 200 days growth. Images generated with Calcofluor White (Calc, blue) and indirect immunofluorescence (green) with monoclonal antibodies to pectic HG (LM19, LM20). Arrowheads indicate phloem. Bottom six micrographs show LM19 and LM20 labellings of vascular bundles (vb) at higher magnification. Arrows indicate regions of interfascicular parenchyma that are labelled strongly by the probes. e = epidermis, is = intercellular space, pp = pith parenchyma. Bar = 100 µm.

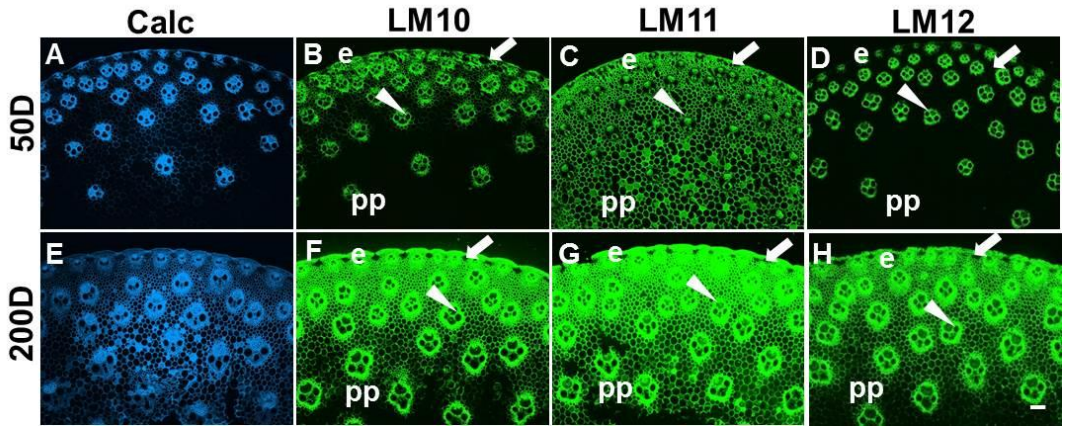

Figure 3.28: Fluorescence imaging of cell walls in transverse sections of Int2 of *M. sinensis* stems at 50 and 200 days growth. Calc staining shown in blue. Immunofluorescence images generated with monoclonal antibodies to heteroxylan (LM10, LM11 and LM12). Arrows indicate regions of interfascicular parenchyma that have relatively lower levels of heteroxylan detection. Arrowheads indicate phloem. e = epidermis, pp = pith parenchyma. Bars = 100 µm.

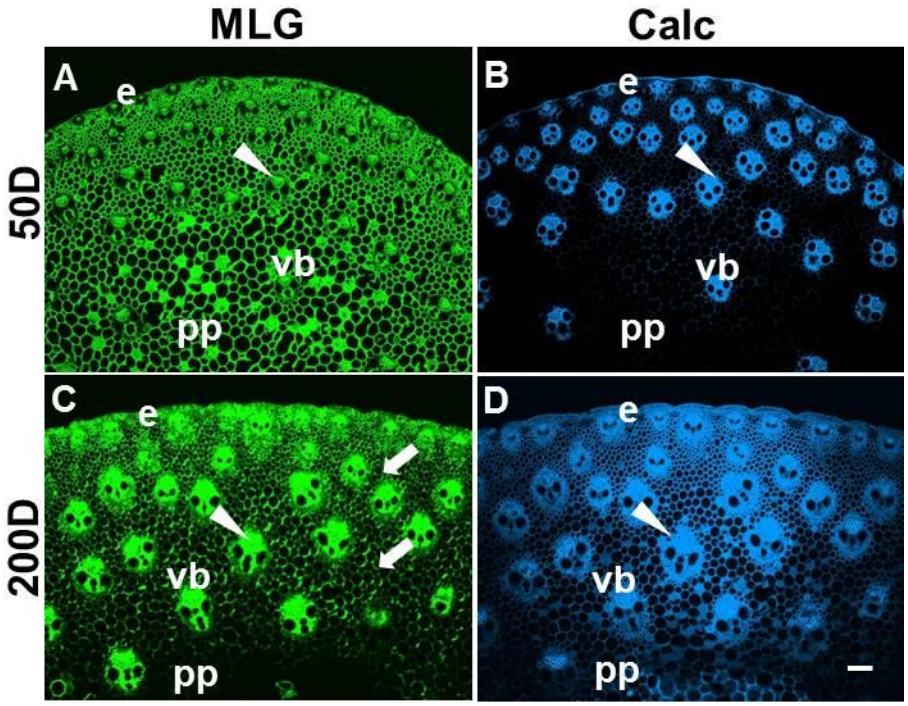

Figure 3.29: Fluorescence imaging of cell walls of transverse sections of Int2 of *M. sinensis* stems at 50 and 200 days growth. Calc staining shown in blue. Immunofluorescence images generated with monoclonal antibody to MLG. Arrows indicate regions of interfascicular parenchyma that have relatively lower levels of MLG detection. Arrowheads indicate phloem. e = epidermis, vb = vascular bundle, p = parenchyma, pp = pith parenchyma. Bars = 100 µm.

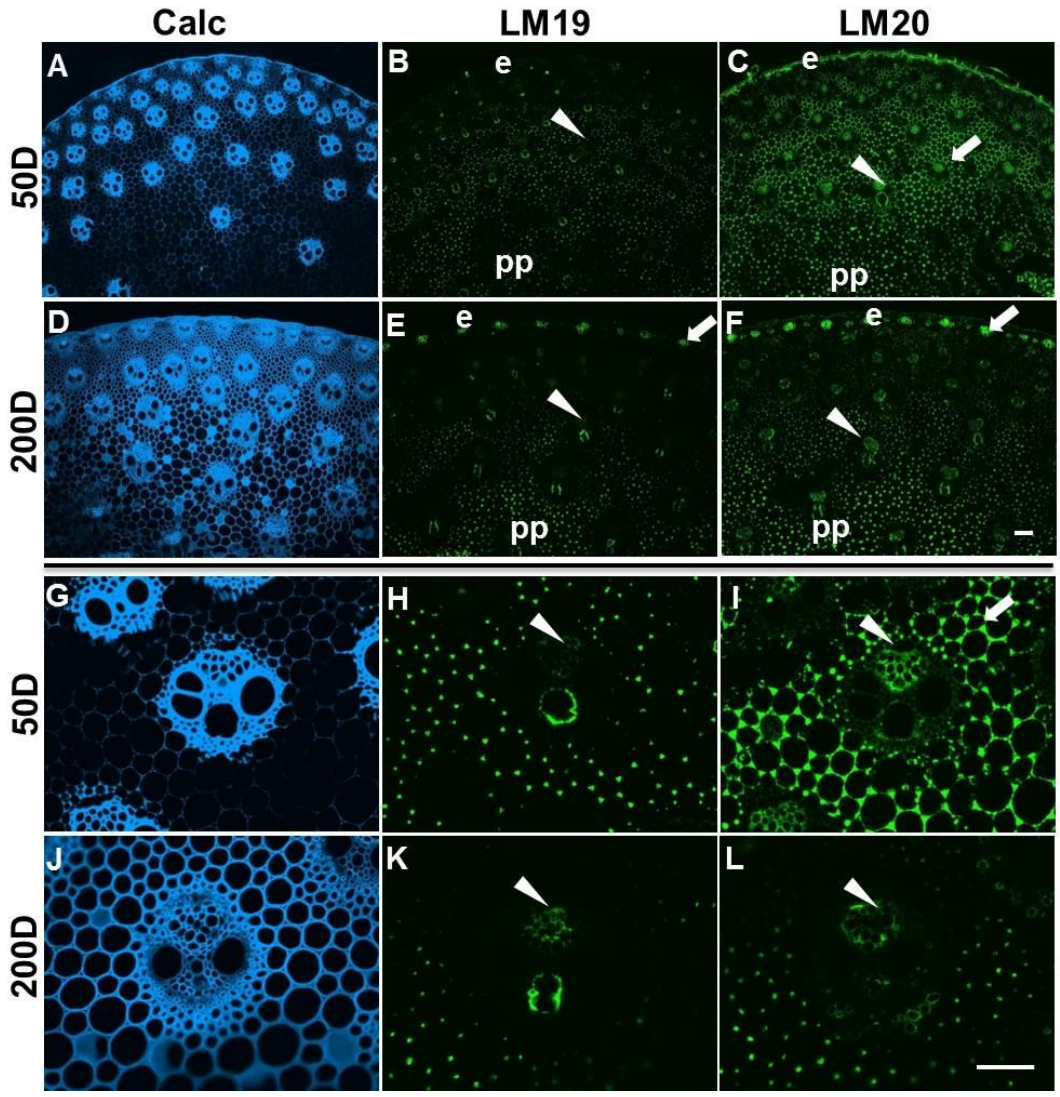

Figure 3.30: Fluorescence imaging of cell walls of transverse sections of Int2 of stems of *M. sinensis* at 50 days growth. Calc staining shown in blue. Immunofluorescence images generated with monoclonal antibodies to pectic HG (LM19, LM20). Bottom six micrographs show LM19 and LM20 labellings of vascular bundles (vb) at higher magnification. Arrowheads indicate phloem. Arrows indicate regions of interfascicular parenchyma that are labelled strongly by the probes. pp = pith parenchyma, e = epidermis. Bars = 100 µm.

Table 3.3: Distributions of heteroxylan (LM12), MLG and pectic HG (LM20) epitopes at different developmental stages of Int2 of *M.* x *giganteus*, *M. sacchariflorus* and *M. sinensis*.

	LM12	MLG	LM20
Younger tissue	*	***	***
Older tissue	***	*	*

*** more binding; * less binding. LM12 = ferulated heteroxylan; LM20 = pectic HG.

3.8 Discussion

This study demonstrates that extensive cell wall molecular heterogeneity occurs in the stems of *Miscanthus* species and specifically indicates that the non-cellulosic cell wall polymers of *Miscanthus* species are not evenly detected across the cell walls of stem tissues.

Immunocytochemical analysis of transverse sections of the three *Miscanthus* species revealed that the major anatomical difference of the stems is the vascular bundle. The phloem of the *M.* x *giganteus* stem, which has the function of transportation of photosynthesis products such as sugars from leaves to storage organs and growing parts of plant (Hendrix 1983), has a larger size than that of the *M. sacchariflorus* and *M. sinensis* species. The anatomical difference might be related to the differences in growth and/or development of these *Miscanthus* species. As shown earlier, *M.* x *giganteus* grows faster and taller than the other two species (Figure 3.1). However, knowledge concerning the importance of anatomy and functional cell wall composition of *Miscanthus* species is very scarce (Kaack et al. 2003).

Immunocytochemical analysis of heteroxylan epitopes in *Miscanthus* species revealed that xylans are present in the form of the substituted arabinoxylan and feruloylated arabinoxylan in phloem cell walls of *M.* x *giganteus* and *M. sinensis*. Xylans are present as arabinoxylan in these cell walls of *M. sacchariflorus*. This heteroxylan antibody binding profile (the LM11/12-substituted xylan epitopes were abundant in phloem cell walls whereas the LM10-unsubstituted xylan was not abundant in these cell walls of all three *Miscanthus* species) is different to what observed in the tobacco stems, that the LM10 and LM11 epitopes were abundant in cell walls of both phloem regions and xylem vessels (McCartney et al. 2005), but in accordance with the flax hypocotyls, where both antibodies bound to the secondary cell walls of xylem, but the LM11 epitope was also observed in

developing phloem regions, whereas the LM10 epitope was not detected in these regions (McCartney et al. 2005). Progress in the field of xylan biosynthesis revealed that at least five glycosyltransferases (GTs) activities may be involved in the biosynthetic process (Brown et al. 2007, Chiniquy et al. 2013, Faik 2010, Lee et al. 2007a, Peña et al. 2007, Wu et al. 2010a, Wu et al. 2009). Lygin et al suggested that further research should be studied on the xylan degradation in cell walls of grasses that used for bioethanol production (Lygin et al. 2011). In this study, distribution of xylans in cell walls of *Miscanthus* species was first analysed, this will be beneficial for the understanding of enzymatic deconstruction of xylans, and therefore make contribution to their use as biofuels.

However, for the phloem of *Miscanthus* species, the LM10 unsubstituted xylan epitope was not detected in the phloem cell walls of the three species, while the LM11/12 xylan/arabinoxylan epitope, the LM15 XyG epitope, the MLG epitope, the LM21 heteromannan epitope, the LM5 pectic galactan epitope, the LM6 pectic arabinan epitope and the LM18/19/20 HG epitopes were all detected in the phloem cell walls of the three *Miscanthus* species. These results suggest that the *Miscanthus* phloem cell walls have a distinct polysaccharide structure containing unsubstituted-arabinoxylan, MLG, XyG, mannan and pectins. The distinct cell wall polysaccharide architecture in phloem cell walls of the three *Miscanthus* species may be related to the distinct cell wall properties of the phloem regions, and might also be linked to their specific functions.

Interestingly, for the 50-day-old *M. sacchariflorus*, parts of the sub-epidermal parenchyma cell walls did not contain xylan and arabinoxylan epitopes recognised by the LM10 and the LM11 probes. Furthermore, Calcofluor White did not bind to these regions. As mentioned before, the Calcofluor White binds to all β-glucans including cellulose (Fischer et al. 1985, Harrington and Raper 1968, Hughes and McCully 1975). However, these equivalent cell wall regions were strongly labelled by the MLG and HG probes which is quite different form *M.* x *giganteus* and *M.*

sinensis, indicating that these cell walls have a unique architecture that were different from the other two *Miscanthus* species. This suggests that these parenchyma cell walls have unique polysaccharide architecture, which might be related to wall properties, and also may link to the genetic differences among the *Miscanshus* species and plant growth differences as the *M.* x *giganteus* grows faster and taller than its parents - *M. sacchariflorus* and *M. sinensis*. Specifically, a genomic *in situ* hybridisation study suggested that *M.* x *giganteus* and *M. sacchariflorus* shared a number of nucleotide substitutions and deletions, which could not be found in *M. sinensis* indicated that may be the most genetically distinct among the three species (Głowacka 2011, Hodkinson et al. 2002, Naidu et al. 2003). Here in this study, the MLG epitope was shown to have similar binding patterns in the parenchyma regions of *M.* x *giganteus* and *M. sacchariflorus*, but not in *M. sinensis*, whether the MLG distribution difference among the three species could be related to their genetic differences is not known. Previous studies revealed that MLG could be related to the cell growth development in cell walls of maize and barley (Carpita and McCann 2010, Wilson et al. 2006). The parenchyma of the stem could protect against the risk of collapse of stems (Ennos 1993, Kaack et al. 2003, Niklas 1991). Stem stability increases with the thickness of the parenchyma layer (Dunn and Briggs 1989, Ennos 1993, Kaack et al. 2003). Therefore, the distinct cell walls of parenchyma of *Miscanthus* stems might be related to its stem properties. It is very interesting that the higher MLG distribution in all the three *Miscanthus* species was correlated with lower level of xylan detection in some certain parenchyma regions. This result was in accordance with that of the *Equisetum ramosissimum* (Leroux et al. 2011). Although previous studies have shown that MLGs are unique to Poaceae and that they have distinct type II cell wall components (Carpita 1996, Carpita and Gibeaut 1993), later studies reported that MLGs were also abundant in green algae and *Equisetum* cell walls (Burton and Fincher 2009, Fry et al. 2008, Leroux et al. 2011, Sørensen et al. 2008). These

studies could deepen our understanding of the roles of cell walls and their exquisite molecular complexity (Knox 2008). Therefore, in addition to the type I and type II cell wall classification (Carpita 1996, Carpita and Gibeaut 1993), and probably type III cell wall classification (Leroux et al. 2013, Silva et al. 2011), there might be other cell wall classifications, and this needs further investigation with different plant species involved.

The heteromannan and pectic polysaccharide analysis revealed that the LM21 heteromannan epitope and the LM18/19/20 HG epitopes showed more abundant binding profiles in certain parenchyma regions in *M.* x *giganteus* than in *M. sacchariflorus* and *M. sinensis*. The glucomannan deposition in hardwood fibre cell walls is affected by tension stress (Kim and Daniel 2012). The arabinan is correlated with developmental events of plant cell walls (McCartney et al. 2000, Vicré et al. 1998, Willats et al. 1999). It has been reported that interactions between pectin and the cellulose-hemicellulose network give the plant cell wall strong but flexible properties (Burton et al. 2010, Cosgrove and Jarvis 2012, Willats et al. 2006, Willats et al. 2001a). These results indicate the distinct parenchyma cell wall architecture which may link to wall properties, and also the growth difference of the three *Miscanthus* species. In contrast, an analysis of the cell wall composition of senesced material has been reported that *M.* x *giganteus* was different from the other two species (Allison et al. 2011). The major differences between the three *Miscanthus* species used in this study in terms of cell wall stem molecular anatomies is that of the interfascicular parenchyma which is most distinctive in *M. sacchariflorus* and the high abundance of the LM20 pectic HG epitope in interfascicular and pith parenchyma of *M.* x *giganteus*. The interfascicular parenchyma cell walls of *M. sacchariflorus* are distinctive as they stain weakly with Calc, have reduced levels of heteroxylan epitopes, particularly those of LM10 unsubstituted xylan and LM12 ferulated ariabinoxylan and have relatively abundant levels of MLG and xylan-masked XyG - Chapter 5. The LM20

methylesterified HG antibody is the most specific probe for high ester HG yet isolated (Christiaens et al. 2011, Marcus et al. 2010) and its use indicates that the pectic HG is more methyl-esterified in the *M.* x *giganteus* in comparison to the two parent species. For 50-day-old *M.* x *giganteus*, the LM20 methylesterified HG was detected much more strongly in the pith parenchyma cell walls of Int1 and Int2 (older internodes of 50-day-old stems), while in the 200-day-old stems the LM20 was detected less than the 50-day-old stems in all three *Miscanthus* species, indicating that the LM20 methylesterified HG could be timely regulated during *Miscanthus* development. This is consistent with the studies that have reported that the HG of the cell wall could be temporally regulated during plant development (Ralet et al. 2008, Wolf et al. 2009). Methyl-ester HG is required for cell expansion (Derbyshire et al. 2007). The abundance of HG with a low level of esterification is increased in order to compensate for a lack of cellulose (Burton et al. 2000, Manfield et al. 2004). If this relates in any way to the faster growth rate of hybrid *M.* x *giganteus* than its parents - *M. sacchariflorus* and *M. sinensis* is a point for future analysis. There is also the potential issue of how pectic HG can influence cell expansion in this species if it is indeed restricted to cell walls lining intercellular spaces.

The detection of the other pectic related epitopes studied here, LM5 galactan and LM6 arabinan, which are presumed to occur within complex pectic RG-I polymers, suggest *Miscanthus* specific molecules - LM6 pectic-arabinan polymers may be more widely distributed throughout the cell walls. It is possible, however, that the abundant widespread detection of the LM6 arabinan epitope, for example in *M. sacchariflorus*, may indicate the distribution of arabinogalactan-proteins that can also carry this epitope (Lee et al. 2005a) (AGPs will be discussed later in Chapter 5 and Chapter 6). There is also considerable heterogeneity within the cell wall structures of the vascular tissues with patterns of heteroxylan, MLG, XyG and

pectin epitopes all indicating varied cell wall architectures of both phloem and xylem elements.

This work in this chapter therefore is a clear demonstration of cell wall heterogeneity relating to cell and tissue and organ development and also that cell wall biomass of *Miscanthus* is a highly heterogeneous material. How this heterogeneity changes in relation to other organs and through extended growth to harvested biomass awaits further study. The identified complementary anatomical patterning of detectable heteroxylan and MLG is also of interest in terms of the potential interactions of these glycans with cellulose microfibrils (a factor in biomass recalcitrance) as well as contributions to growth and stem properties.

Chapter 4

Cell wall polysaccharides of wheat and *Brachypodium distachyon*

4.1 Introduction

Miscanthus species, wheat and *Brachypodium distachyon* (*B. distachyon*) are all in the Poaceae family. To further explore *in situ* analysis of potential polysaccharide distribution similarities and/or differences among the three grass species, the wheat and *Brachypodium distachyon* were also grown in the University of Leeds greenhouse. In this chapter, initial experiments involved the anatomy analysis of the transverse sections of the second internode (Int2) of wheat and *B. distachyon* at 50 days growth. After that, the major non-cellulosic polysaccharide (heteroxylans, MLG and pectic HG) analysis of the different internodes (internode 1 to internode 4 for wheat, Int1, Int2 and Int5 for *B. distachyon*), different positions of a internode (top and base of Int3 for wheat, top and base of Int5 for *B. distachyon*) were explored in the transverse stem sections. Photographs of the representative stems of wheat and *B. distachyon* and sample taken places from different internodes are shown in Figure 4.1. At 50 days growth, a wheat stem usually has 4 internodes, while *B. distachyon* has 5 short internodes.

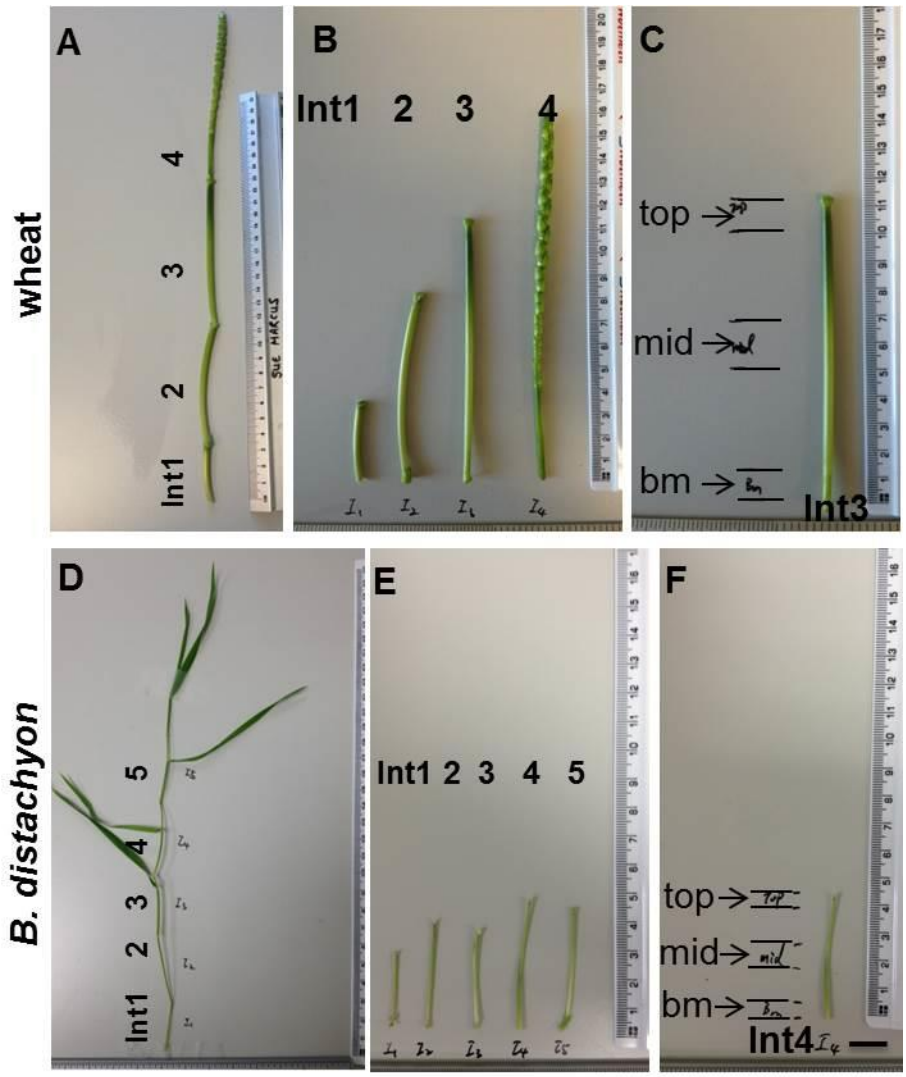

Figure 4.1: Photographs indicating sampling of stem materials from different internodes of wheat and *B. distachyon*. A and B: Representative stem internodes of wheat at 50 days growth. Int1 is the first internode of the stem (counting from the base), and Int4 is the youngest internode of a stem (near the shoot meristem). C: The third internode (Int3) of wheat showing sampling positions of base (bm), middle (mid) and top (top). D: Representative stems and leaves of *B. distachyon* at 50 days growth. E: Internodes of a *B. distachyon* stem. F: The fourth internode (Int4) of *B. distachyon*. Bar = 1 cm.

4.2 Cell wall polysaccharide distribution in different developmental stages of wheat stem

4.2.1 Anatomy of the wheat stem

Labelling of transverse sections with Calc allowed the investigation of the anatomy of the second internode (Int2) of the 50-day-old stem of wheat (Figure 4.2).The epidermis, vascular bundles, sheaths of vascular bundles, phloem, xylem and parenchyma can be clearly seen in Figure 4.2C, and 4.2D. Carbohydrate-binding module CBM3a bound evenly to all types of cell walls in Int2 of wheat stem at 50 days growth (Figure 4.2). Omission of the primary antibodies which were totally black provided negative control (data not shown).

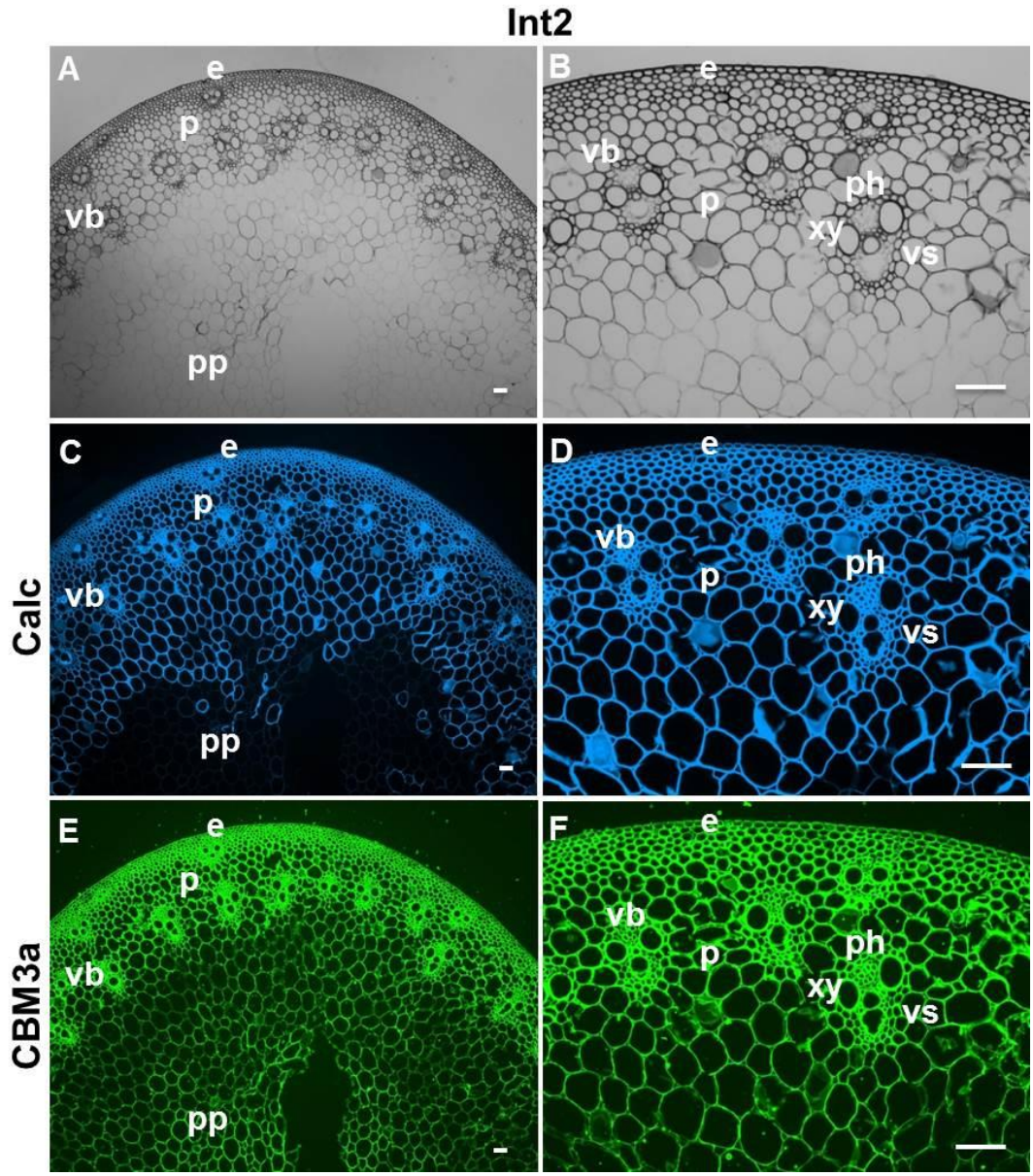

Figure 4.2: Anatomy and fluorescence imaging of cell walls in transverse sections of the second internode (Int2) of the stem of wheat at 50 days growth. A: Bright field image showing stem anatomy of Int2. B: Higher magnification image of A showing cortical vascular bundles. C and D: Image generated with Calcofluor White (Calc, blue) and indirect immunofluorescence (green) with carbohydrate-binding module CBM3a to cellulose (E and F). e = epidermis, p = interfascicular parenchyma, pp = pith parenchyma, vb = vascular bundle, vs = vascular bundle sheath, ph = phloem, xy = xylem. Bar = 100 µm.

4.2.2 Analysis of major non-cellulosic cell wall polysaccharides in different internodes of wheat stem

To explore the major non-cellulosic polysaccharides in relation to developmental differences, the LM10/11/12 heteroxylan, the MLG and the LM19/20 pectic HG monoclonal antibody probes were used in transverse sections of middle of different internodes of 50-day-old wheat stems. Analysis of the mid point of more distal, younger internodes (Int4) at 50 days growth indicated a decreasing gradient in the detection of the three LM10/11/12 heteroxylan epitopes (Figure 4.3), whereas it was an increasing gradient in the MLG detection (Figure 4.4, (D), (H), (L) and (P)). The LM10 unsubstituted xylan epitope was not detected in the youngest internode (Int4) (Figure 4.3B), and the LM11/LM12 substituted arabinoxylan epitopes were only detected in epidermis and vascular bundles of Int4 (Figure 4.3, (C) and (D)), these results are similar to what was observed of different internodes of the *Miscanthus* x *giganteus* at 50 days (Figure 3.6). In the case of the Int1, Int2 and Int3, the LM11/12 substituted arabinoxylan probe bound more in the pith parenchyma regions and phloem cell walls than the LM10 unsubstituted xylan probe (Figure 4.3, (F) to (P)). In the sub-epidermal stem regions, the LM10, LM11 and LM12 epitopes were detected uniformly in Int1, Int2 and Int3, except that the LM10 did not bind to the phloem cell walls (Figure 4.3).

In contrast, the MLG epitope was abundant in the younger internodes (Int4 and Int3) and particularly in the pith parenchyma of the younger internodes (Figure 4.4, (D) and (H)). The MLG was less abundant in the pith parenchyma cell walls in Int1 and Int2 (Figure 4.4, (L) and (P), while in these corresponding parenchyma regions of Int1 and Int2, the LM11 substituted arabinoxylan (Figure 4.3, (K) and (O)) and the LM19/20 pectic HG was much more abundant (Figure 4.4, (J), (K), (N) and (O)). In the case of the pectic HG epitopes, both of the LM19 and LM20 epitopes were detected in the intercellular parenchyma spaces of all internodes, and

the major difference was that the LM19 epitope of unesterified HG was less detectable in younger internodes (Int4) whereas the LM20 methylesterified HG epitope bound uniformly in these parenchyma cell walls of Int4 (Figure 4.4, (B) and (C)). Furthermore, the non-Calc-staining parenchyma cell walls of Int4 reflected the lower heteroxylan but higher MLG/HG detection regions which was similar to what was observed in *Miscanthus* species.

In summary, the binding changes in relation to developmental stages of wheat stems to some extent were consistent with that of the observations of the three *Miscanthus* species, such as the heteroxylan increased while the MLG decreased as the plants grew older. For the case of the wheat stem, for the younger internode (Int4), the sub-epidermal parenchyma regions with lower levels of heteroxylan detection bound strongly to MLG and pectic methylesterified HG, which was consistent with that of the *Miscanthus* species (Chapter 3). For the elder internode of wheat (Int1 and Int2), the inner pith parenchyma that did not bind to unsubstituted xylan or MLG bound strongly to substituted arabinoxylan and pectic HG.

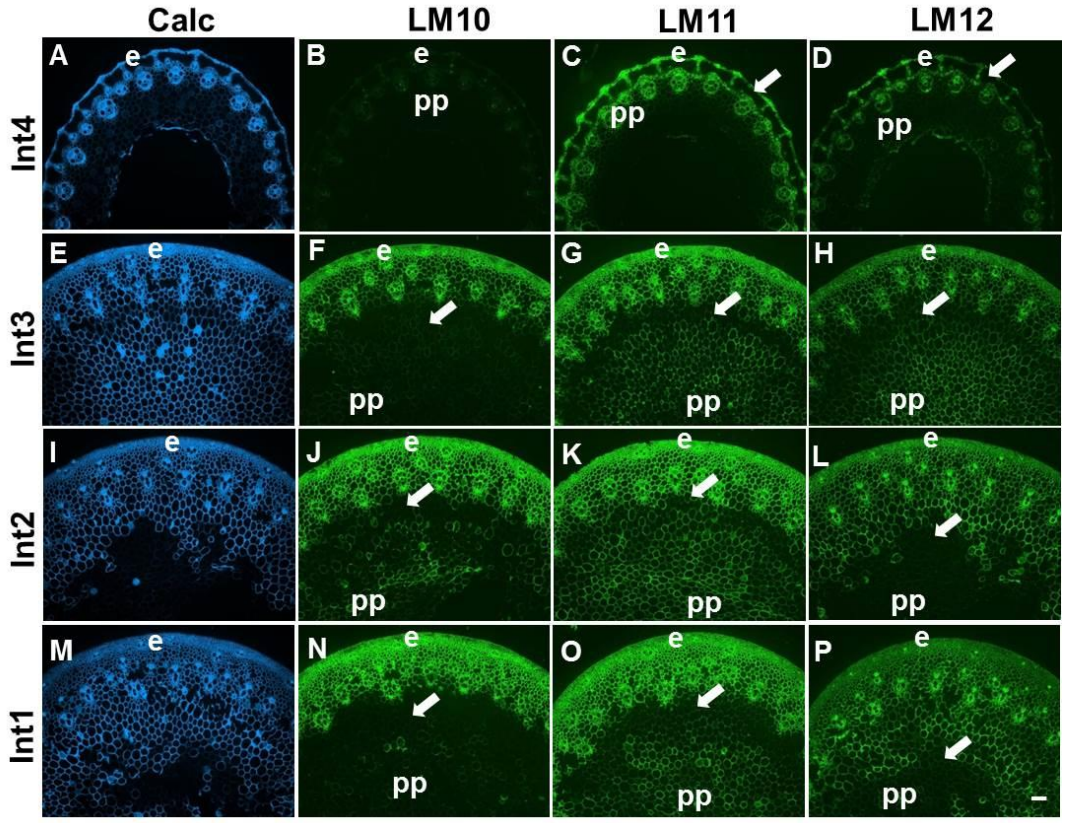

Figure 4.3: Fluorescence imaging of heteroxylan epitopes in transverse sections of the first (Int1, middle) to fourth (Int4, middle) internodes of a wheat stem at 50 days growth. Calc staining shown in blue. Immunofluorescence images generated with monoclonal antibodies to heteroxylan (LM10, LM11 and LM12). Arrows indicate regions of interfascicular parenchyma that have relatively lower levels of heteroxylan detection. e = epidermis, pp = pith parenchyma. Bars = 100 µm.

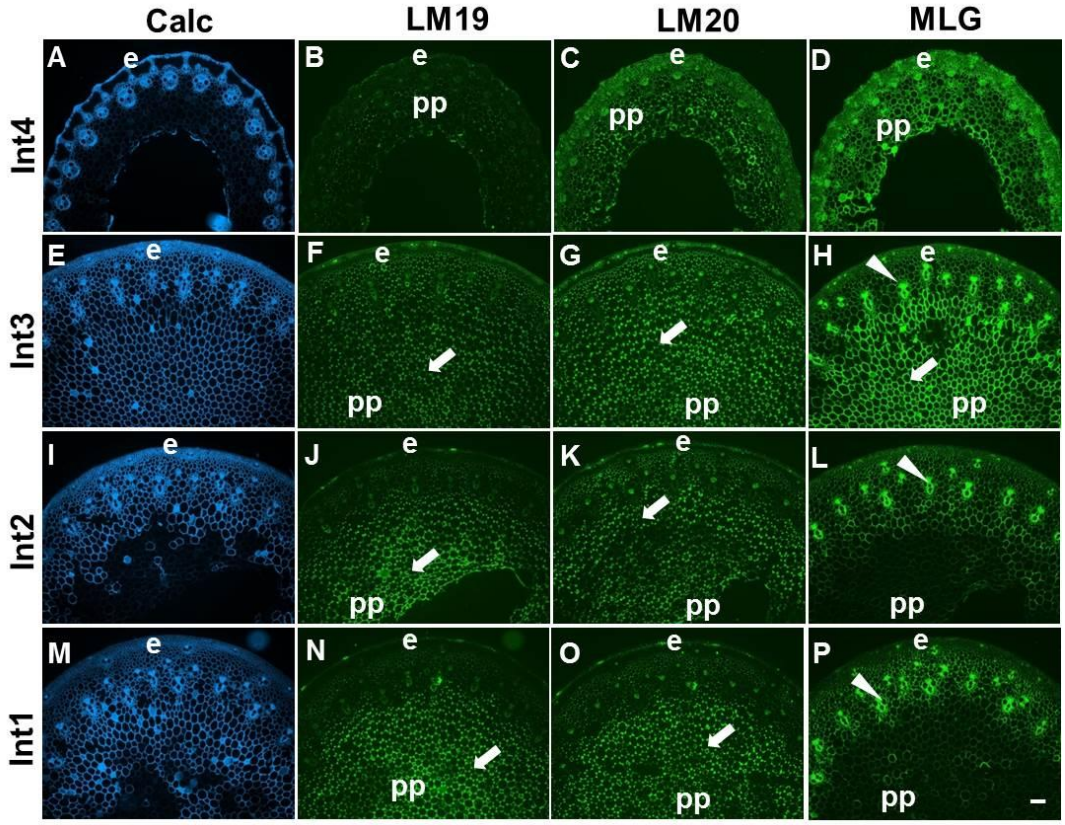

Figure 4.4: Fluorescence imaging of pectin and MLG epitopes in transverse sections of the first (Int1, middle) to fourth (Int4, middle) internodes of a wheat stem at 50 days growth. Immunofluorescence images generated with monoclonal antibody to pectic HG (LM19, LM20) and MLG. Arrowheads indicate phloem. Arrows indicate regions of interfascicular or pith parenchyma that are labelled strongly by the probes. pp = pith parenchyma, e = epidermis. Bars = 100 µm.

4.2.3 Analysis of major cell wall polysaccharides in top and base of the third internode of wheat stem

As shown above, the major non-cellulosic polysaccharide in different internodes of 50-day-old wheat stem were observed. To further explore the developmental differences, the base and top of Int3 of wheat stem were also investigated. Compared with the base of Int3, analysis of the top of Int3 of the 50-day-old wheat stems revealed that the heteroxylan (LM10/11/12) and MLG epitopes decreased in certain sub-epidermal parenchyma cell walls whereas the pectic HG (LM19/20) increased in these corresponding regions (Figure 4.5, (B), (C), (J) and (K), and Figure 4.6, (B), (C), (D), (J), (K) and (L)), and these results were consistent with what were observed in *Miscanthus* species (Chapter 3). In the case of both the top and base of Int3, the LM11/12 substituted arabinoxylan epitopes were detected more in the inner pith parenchyma cell walls, whereas the LM10 unsubstituted xylan was not detected in these regions (Figure 4.5, (A) to (H)). The MLG epitope was detected much more strongly abundant in the pith parenchyma cell walls in the younger base of Int3 (Figure 4.6, (D) and (H)), and the LM19/20 HG epitopes were abundant in intercellular spaces of these corresponding parenchyma regions (Figure 4.6, (B), (C), (F) and (G)). Summary of the distribution of heteroxylan (LM10), MLG and pectic HG (LM20) epitopes at different developmental stages of wheat stem at 50 days growth are presented in Table 4.1 below. These results of higher levels of heteroxylan detections and lower levels of MLG detections in older tissues were consistent with what were observed previously in different developmental stages of both wheat and *Miscanthus* species.

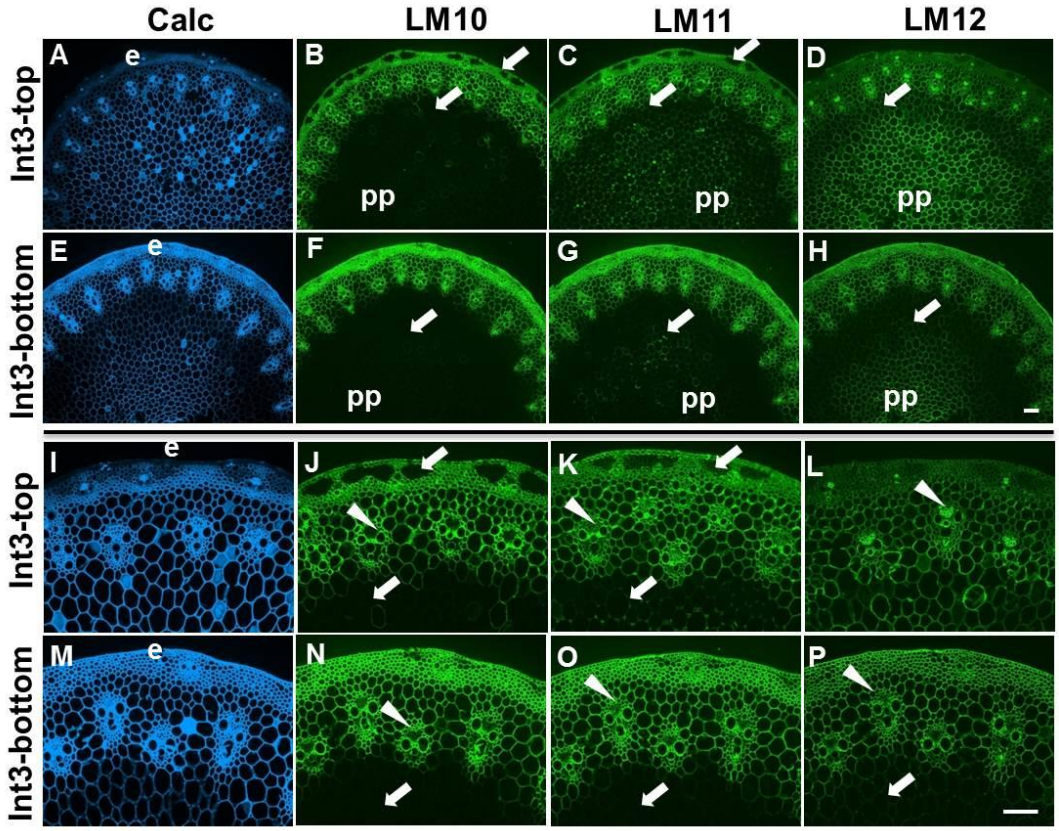

Figure 4.5: Fluorescence imaging of heteroxylan epitopes in transverse sections from top and bottom of Int3 (from base to shoot) of a wheat stem at 50 days growth. Calc staining shown in blue. Immunofluorescence images generated with monoclonal antibodies to heteroxylan (LM10, LM11 and LM12). Arrows indicate regions of interfascicular parenchyma that have relatively lower levels of heteroxylan detection. Arrowheads indicate phloem. e = epidermis, pp = pith parenchyma. Bars = 100 µm.

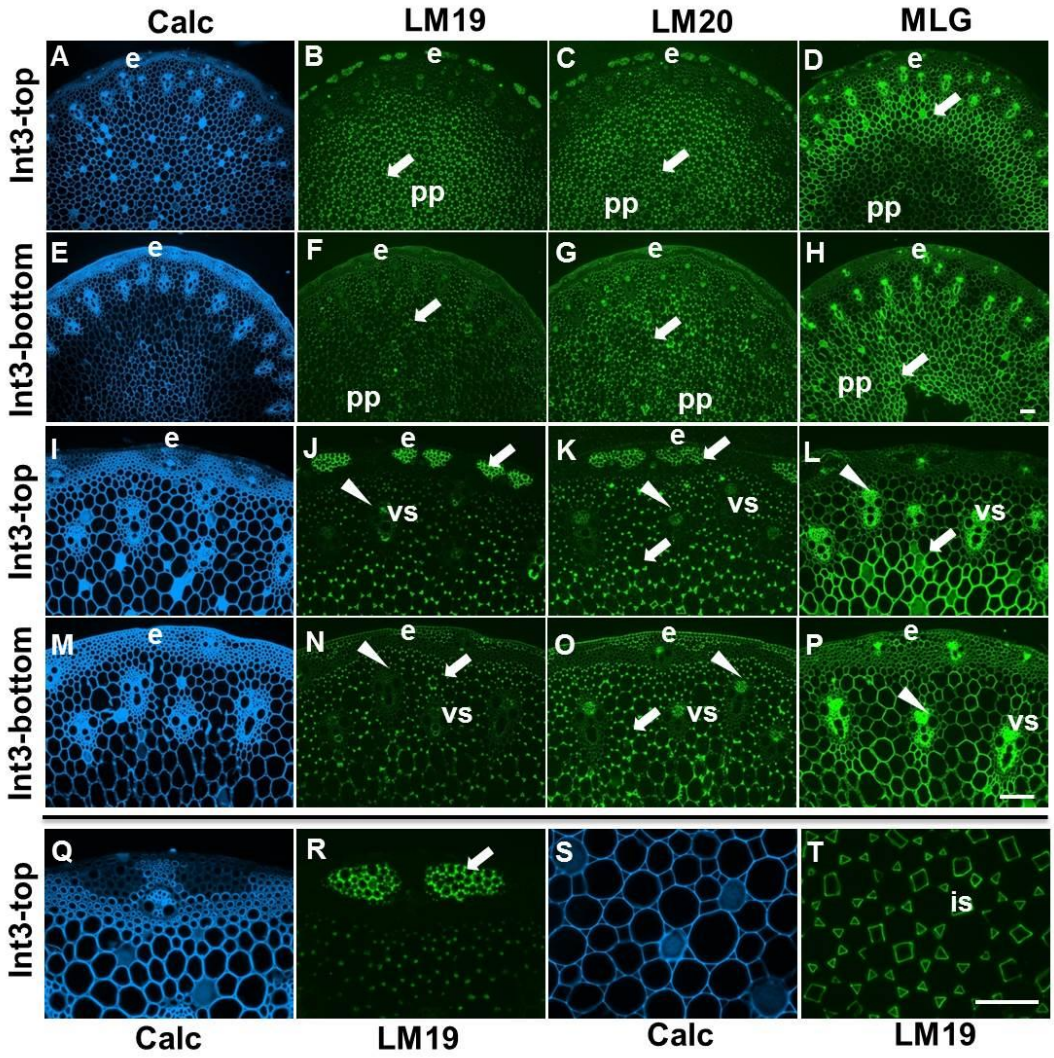

Figure 4.6: Fluorescence imaging of pectin and MLG epitopes in transverse sections sections from top and bottom of Int3 (from base to shoot) of a wheat stem at 50 days growth. Immunofluorescence images generated with monoclonal antibody to pectic HG (LM19, LM20) and MLG. Bottom four micrographs show LM19 and Calc labellings of epidermal parenchyma or intercellular spaces of pith parenchyma (pp) at higher magnification. Arrowheads indicate phloem. Arrows indicate regions of interfascicular or pith parenchyma that are labelled strongly by the probes. pp = pith parenchyma, is = intercellular spaces, vs = vascular bundle sheath, e = epidermis. Bars = 100 µm.

Table 4.1: Tissue-specific distribution of heteroxylan (LM10), MLG and pectic HG (LM20) epitopes at different developmental stages of wheat stem at 50 days growth.

	e	pp	vb	vs	ph	xy
Int4 mid	LM10 – MLG + LM20 ±	LM10 – MLG + LM20 +	LM10 – MLG + LM20 +	LM10 – MLG + LM20 +	LM10 – MLG + LM20 +	LM10 – MLG + LM20 +
Int1 mid	LM10 ++ MLG – LM20 –	LM10 – MLG – LM20 +	LM10 ++ MLG + LM20 +	LM10 ++ MLG + LM20 ±/–	LM10 + MLG + LM20 ±	LM10 ++ MLG + LM20 ±
Int3 top	LM10 – MLG ± LM20 ±	LM10 – MLG ± LM20 +	LM10 ± MLG + LM20 +	LM10 + MLG – LM20 –	LM10 – MLG ++ LM20 ±	LM10 ± MLG + LM20 ±
Int3 bm	LM10 ++ MLG ± LM20 +	LM10 – MLG ++ LM20 +	LM10 ++ MLG + LM20 +	LM10 ++ MLG – LM20 –	LM10 ± MLG ++ LM20 +	LM10 ± MLG + LM20 ±

++ strong binding; + binding; ± weak binding; – no binding. e = epidermis, pp = pith parenchyma, vb = vascular bundle, vs = vascular bundle sheath, ph = phloem, xy = xylem, mid = middle, bm = bottom. LM10 = xylan; LM20 = pectic HG.

4.3 Cell wall polysaccharide distribution in different developmental stages of *Brachypodium distachyon* stem

4.3.1 Anatomy of *Brachypodium distachyon* stem

As shown above, the major polysaccharide distributions in relation to growth and development were observed in *Miscanthus* species and wheat, further exploration

in grasses was carried out in different internodes of 50-day-old *B. distachyon* stems as *B. distachyon* has a small stature and genome size, a short life cycle and fast growth and has been used as a good model plant (Vogel and Bragg 2009, Vogel et al. 2006).

Labelling of transverse sections with Calc allowed the investigation of the anatomy of Int2 of the 50-day-old stem of *B.distachyon* (Figure 4.7). The epidermis, vascular bundles, sheaths of vascular bundles, phloem, xylem and parenchyma can be clearly seen in Figure 4.7B, and 4.7D. The CBM3a bound all types of cell walls (Figure 4.7, (E) and (F)). Omission of the primary antibodies which were totally black provided negative control (data not shown).

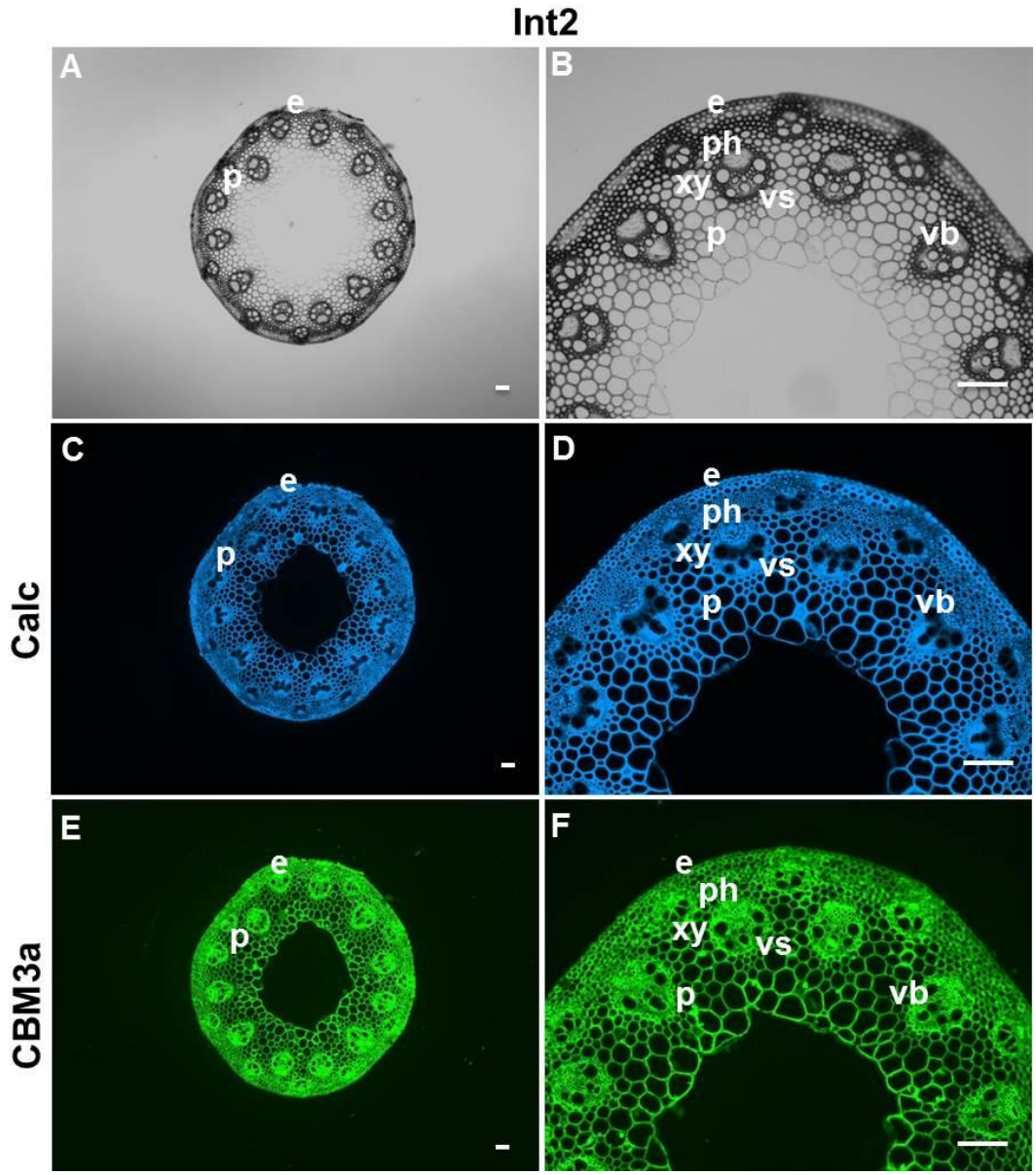

Figure 4.7: Anatomy and fluorescence imaging of cell walls in transverse sections of the second internode (Int2) of stem of *B. distachyon* at 50 days growth. A: Bright field image showing stem anatomy of Int2. B: Higher magnification image of A showing cortical vascular bundles. C and D: Image generated with Calcofluor White (Calc, blue) and indirect immunofluorescence (green) with carbohydrate-binding module CBM3a to cellulose (E and F). e = epidermis, p = interfascicular parenchyma, pp = pith parenchyma, vb = vascular bundle, vs = vascular bundle sheath, ph = phloem, xy = xylem. Bar = 100 µm.

4.3.2 Analysis of major non-cellulosic cell wall polysaccharides in different internodes of *Brachypodium distachyon* stem

Similar to what had been carried out in *Miscanthus* species and wheat stems, the major non-cellulosic polysaccharides - heteroxylan (LM10/11/12), the MLG and the pectic HG (LM19/20) epitopes in relation to growth and development were investigated in 50-day-old *B.distachyon* stems. The heteroxylan (LM10/11) and the MLG epitopes were detected uniformly in different internodes of *B. distachyon* stems (Figure 4.8 and Figure 4.9, (D), (H) and (L)), except that in some sub-epidermal parenchyma regions of Int5 heteroxylans (LM10/11) were less abundant (Figure 4.8, (B) and (C)), whereas the LM19 and LM20 pectic HG epitopes were restricted to these corresponding sub-epidermal parenchyma regions and also to the intercellular spaces of pith parenchyma and phloem cells (Figure 4.9, (B) and (C)). Among the three heteroxylan probes, the LM12 ferulated arabinoxylan was less abundant in all internodes, compared to the LM10 and LM11 epitopes (Figure 4.8, (D), (H) and (L)). The LM10 unsubstituted xylan epitope was not detectable in the phloem of the Int1, Int2 and Int5, while the LM11 arabinoxylan, the MLG and HG epitopes were abundant in these cell walls (Figure 4.8 and 4.9). The sub-epidermal parenchyma regions of the younger internode (Int5) indicated a decreasing gradient in the detection of the heteroxylan (LM10/11/12) and MLG epitopes (Figure 4.8B, Figure 4.8C, Figure 4.8D and Figure 4.9D), whereas in these corresponding parenchyma regions, the pectic HG detection (LM19/20) was increased (Figure 4.9, (B) and (C)). These results were consistent with the observations of *Miscanthus* (Chapter 3) and wheat (Chapter 4.2).

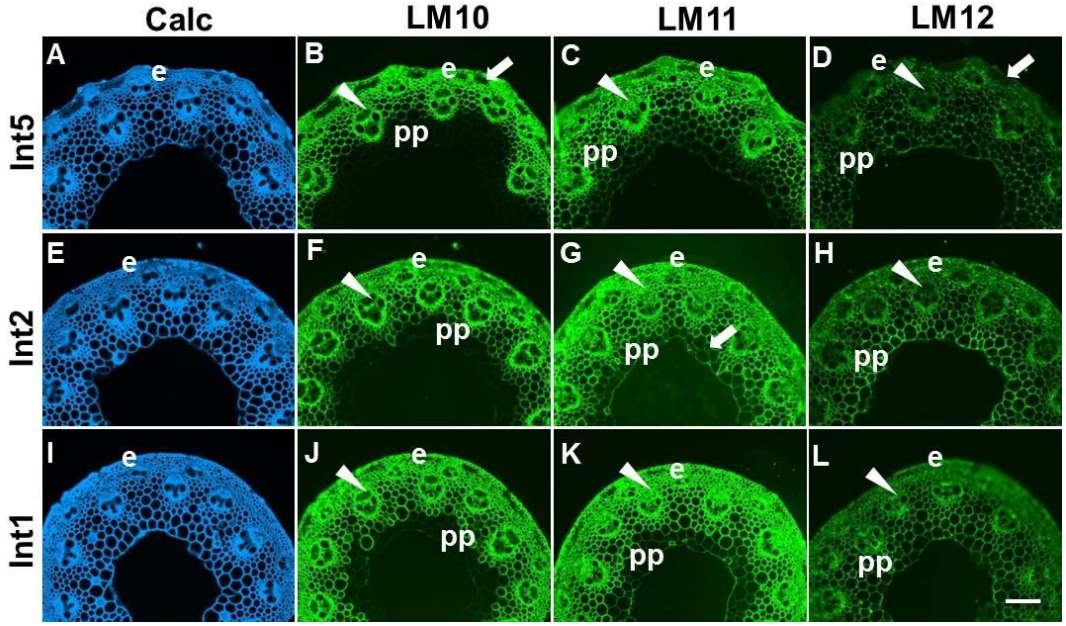

Figure 4.8: Fluorescence imaging of heteroxylan epitopes in transverse sections of the first (Int1, middle), second (Int2, middle) and fifth (Int5, middle) internodes of *B. distachyon* at 50 days growth. Calc staining shown in blue. Immunofluorescence images generated with monoclonal antibodies to heteroxylan (LM10, LM11 and LM12). Arrows indicate regions of interfascicular parenchyma that have relatively lower levels of heteroxylan detection. Arrowheads indicate phloem. e = epidermis, pp = pith parenchyma. Bars = 100 µm.

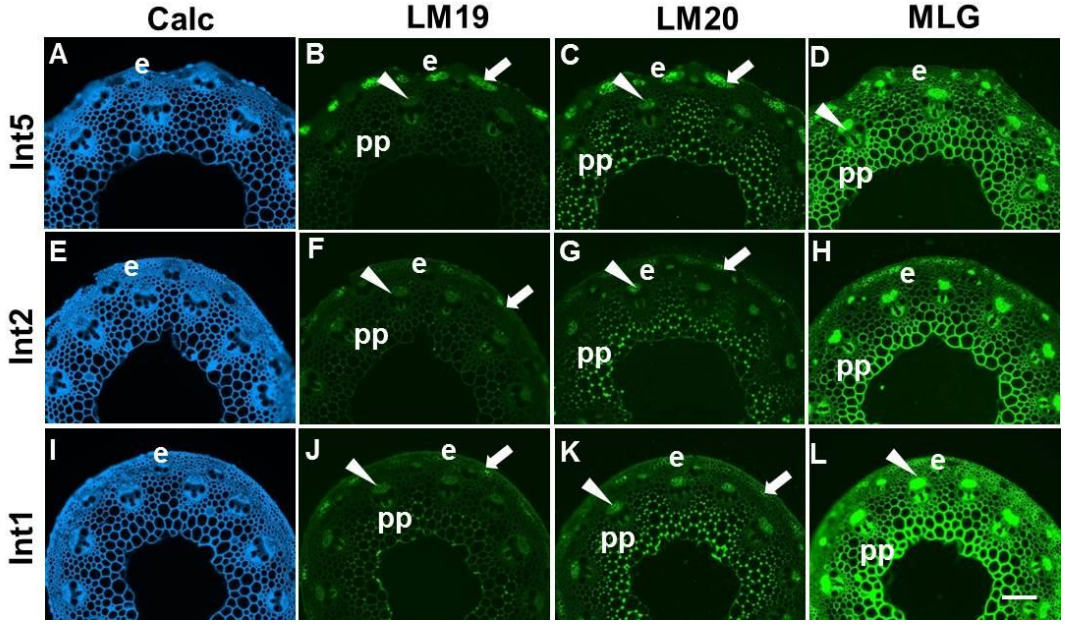

Figure 4.9: Fluorescence imaging of pectin and MLG epitopes in transverse sections of the first (Int1, middle), second (Int2, middle) and fifth (Int5, middle) internodes of *B. distachyon* at 50 days growth. Immunofluorescence images generated with monoclonal antibody to pectic HG (LM19, LM20) and MLG. Arrowheads indicate phloem. Arrows indicate regions of interfascicular or pith parenchyma that are labelled strongly by the probes. pp = pith parenchyma, e = epidermis. Bars = 100 µm.

4.3.3 Analysis of major cell wall polysaccharides in top and base of the fifth internode of *Brachypodium distachyon* stem

As shown above, the major non-cellulosic polysaccharide in different internodes of 50-day-old *B. distachyon* stem were observed. To further explore the developmental differences, the base and top of Int5 of *B. distachyon* stem was also investigated. In the Int5 of the 50-day-old *B. distachyon* stems, the LM10/11/12 heteroxylan and the MLG epitopes were detected less in some certain sub-epidermal parenchyma cell walls in top of the Int5 compared with the base of the fifth internodes (Figure 4.10, (J), (K) and (L), and Figure 4.11L), while in these regions the LM19/20 pectic HG were abundant (Figure 4.11, (J) and (K)). And these binding patterns were similar to those of the former observations of *Miscanthus* (Chapter 3) and wheat (Chapter 4.2). Among the three heteroxylan probes, the LM12 epitope was detected less abundant in parenchyma cells (Figure 4.10, (L) and (P)), while the LM11 bound strongly to all types cell walls (Figure 4.10, (K) and (O)). Furthermore, the LM10 unsubstituted xylan did not bind to phloem cell walls (Figure 4.10, (J) and (N)). The MLG epitope was much more strongly abundant in inner pith parenchyma cell walls in the younger base of Int5 (Figure 4.11, (P) and (L)). The LM19/20 pectic HG epitopes were more abundant in the sub-epidermal parenchyma regions of top of Int5 which containing lower levels of heteroxylan/MLG (Figure 4.11, (J) and (K)). And the LM20 methylesterified HG epitope was also more abundant in intercellular spaces of parenchyma regions (Figure 4.11 (B), (C), (F) and (G)). These results of higher levels of heteroxylan detections and lower levels of MLG detections in elder tissues of *B. distachyon* were consistent with what were observed previously in wheat and *Miscanthus* species.

In summary, in all of the three grasses analysed above (*Miscanthus* species, wheat and *B. distachyon*), during the plant development, the heteroxylan increased in

older tissues, while the MLG/HG was more abundant in the younger grass tissues (Table 4.2). In some certain parenchyma cell walls of the younger tissues, the non-Calc-staining regions reflected the lower heteroxylan but higher MLG/HG detections.

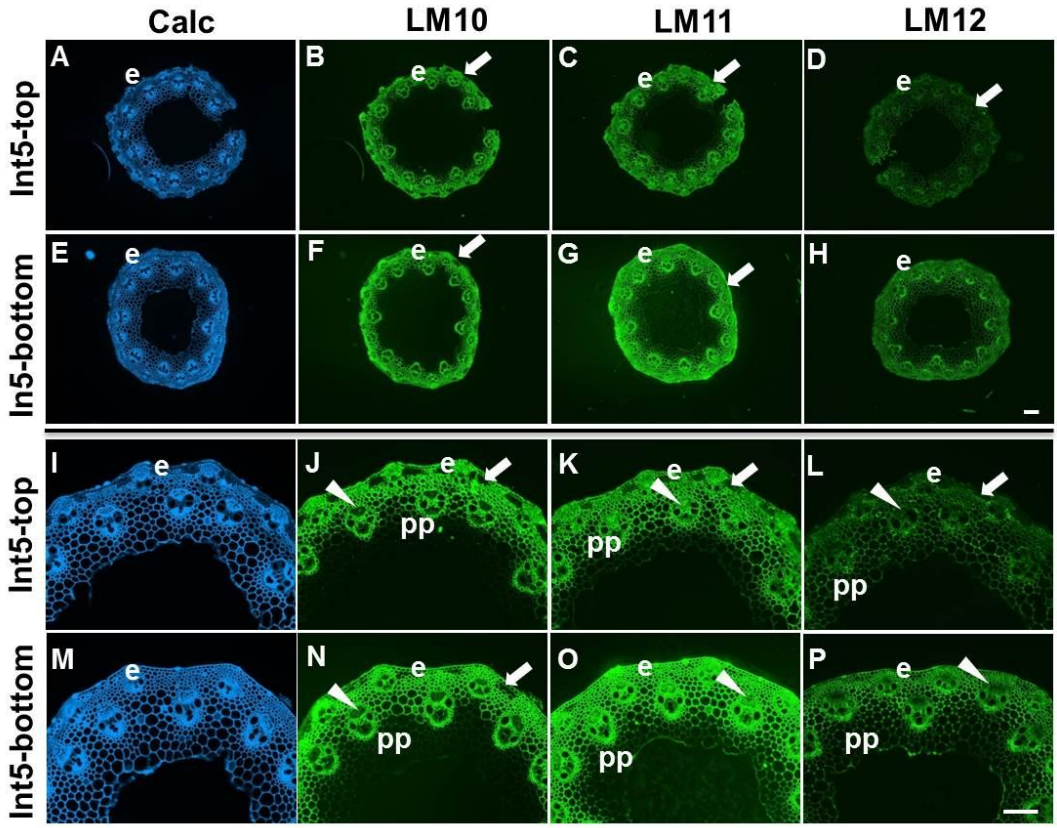

Figure 4.10: Fluorescence imaging of heteroxylan epitopes in transverse sections from top and bottom of Int5 (from base to shoot) of a *B. distachyon* stem at 50 days growth. Calc staining shown in blue. Immunofluorescence images generated with monoclonal antibodies to heteroxylan (LM10, LM11 and LM12). Bottom eight micrographs show LM10, LM11, and LM12 labellings of epidermal parenchyma and vascular bundles (vb) at higher magnification. Arrows indicate regions of interfascicular parenchyma that have relatively lower levels of heteroxylan detection. Arrowheads indicate phloem. e = epidermis, pp = pith parenchyma. Bars = 100 µm.

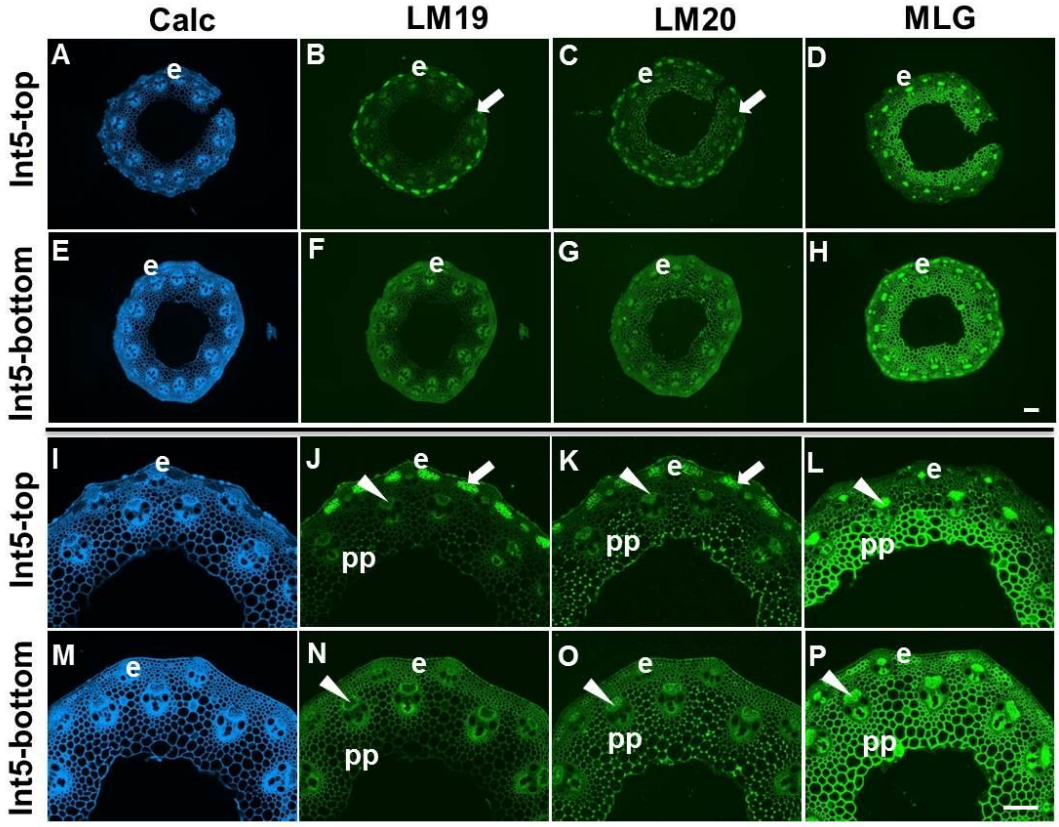

Figure 4.11: Fluorescence imaging of pectin and MLG epitopes in transverse sections sections from top and bottom of Int5 (from base to shoot) of a *B. distachyon* stem at 50 days growth. Immunofluorescence images generated with monoclonal antibody to pectic HG (LM19, LM20) and MLG. Bottom eight micrographs show LM19, LM20, and MLG labellings of epidermal parenchyma and vascular bundles (vb) at higher magnification. Arrowheads indicate phloem. Arrows indicate regions of interfascicular or pith parenchyma that are labelled strongly by the probes. pp = pith parenchyma, e = epidermis. Bars = 100 µm.

Table 4.2: Tissue-specific distribution of heteroxylan (LM10), MLG and pectic HG (LM20) epitopes at different developmental stages of *B. distachyon* stem at 50 days growth.

	e	ep	vb	vs	ph	xy
Int5 mid	LM10 + MLG ± LM20 –	LM10 +/– MLG ± LM20 +/–	LM10 + MLG + LM20 ±	LM10 ++ MLG – LM20 –	LM10 – MLG ++ LM20 ±	LM10 + MLG + LM20 –
Int1 mid	LM10 + MLG + LM20 ±	LM10 +/– MLG + LM20 ±	LM10 + MLG + LM20 ±	LM10 ++ MLG – LM20 –	LM10 – MLG ++ LM20 ±	LM10 + MLG ++ LM20 –
Int5 top	LM10 + MLG ± LM20 +/±	LM10 +/– MLG ± LM20 ±	LM10 + MLG + LM20 ±	LM10 ++ MLG – LM20 –	LM10 – MLG ++ LM20 ±	LM10 + MLG + LM20 ±
Int5 bm	LM10 + MLG ++ LM20 ±	LM10 +/– MLG + LM20 ±	LM10 + MLG + LM20 ±	LM10 ++ MLG – LM20 –	LM10 – MLG ++ LM20 ±	LM10 + MLG + LM20 ±

++ strong binding; + binding; ± weak binding; – no binding. e = epidermis, ep = epidermal parenchyma, vb = vascular bundle, vs = vascular bundle sheath, ph = phloem, xy = xylem, mid = middle, bm = bottom. LM10 = xylan; LM20 = pectic HG.

4.4 Discussion

Immunolocalisation of the major non-cellulosic polysaccharides in different internodes of wheat and *B. distachyon* stem sections using the LM10/11/12 heteroxylan, LM18/19/20 pectic HG and MLG probes revealed that the phloem cell walls of both wheat and *B. distachyon* contain substituted-arabinoxylan and MLG. During the growth of wheat and *B. distachyon*, the heteroxylan and HG increased in older tissues, whereas the MLG decreased during growth. As for the younger internodes, the sub-epidermal parenchyma regions that did not bind to Calc also had lower levels of heteroxylan/MLG, but higher detections of HG. In general, the heteroxylan, HG and MLG epitopes were detected evenly in both well-developed stems of wheat and *B. distachyon.* It has been reported that the grass cell wall composition including *B. distachyon* and maize changes with developmental maturity and different organ types (Abedon et al. 2006, MacAdam and Grabber 2002, MacAdam et al. 1996, Morrison et al. 1998, Rancour et al. 2012). These results are consistent with the observations of the three *Miscanthus* species, which indicates that wheat, *B. distachyon* and the *Miscanthus* species may have similar cell wall architecture. As *B. distachyon* has the simplest genome described in grasses to date, the self-fertile and short life cycle characteristics should make it amenable to genetics study (Christiansen et al. 2005, Draper et al. 2001, Hasterok et al. 2004, Shi et al. 1993, Vogel and Bragg 2009, Vogel et al. 2006), and it might also be a good model for *Miscanthus* species and wheat in the cell wall research area because of their similar cell wall polysaccharide architecture observed above in this study.

Chapter 5

Masking of cell wall polymers in three *Miscanthus* species, wheat and *Brachypodium distachyon*

5.1 Introduction

In some cases, the access to one cell wall polymer can be blocked by the other polymers which were known as masking has been reported in tobacco stems and seeds. To date it has only been reported in dicotyledon cell walls (Hervé et al. 2009, Lee et al. 2013, Marcus et al. 2008, Marcus et al. 2010). In order to explore polysaccharide blocking probe access to other polysaccharide polymers in grasses, in this chapter, a series of enzymatic deconstructions were carried out prior to the immunolabelling procedures. The monoclonal antibody probes used to generate the observations reported in chapter 3 and chapter 4 were applied after grass (three *Miscanthus* species, wheat and *B. distachyon*) transverse sections (50 days growth) had been separately pre-treated with a xylanase (to degrade xylan), a lichenase (to degrade MLG), a pectate lyase (PL, to degrade HG), a pectinex (Pec, to degrade HG) or a xyloglucanase (to degrade XyG).

5.2 Cell wall polymers masking in three *Miscanthus* species

To explore whether polysaccharide masking exists in *Miscanthus* species, the enzymes described above were used prior to the immunolabellings of the Int2 of all three *Miscanthus* species. After trying different combinations of specific enzymatic treatment with different monoclonal antibody probes, for the 50-day-old *Miscanthus* species, the only three detection of polysaccharide epitopes that were notably increased in abundance and/or altered after an enzyme treatment were the LM15 XyG epitope after pre-treatment with xylanase, the LM5 galactan epitope after pre-treatment with xylanase or with lichenase, and the LM2 AGP epitope after pre-treatment with PL or with Pec (Figure 5.1, 5.2 and 5.3). To investigate more polysaccharide masking in *Miscanthus* species, the same experiments were also carried out in the Int2 of the 200-day-old *Miscanthus* stems. However, for the 200-day-old *Miscanthus* species, no obvious changes were revealed for these

polysaccharide epitopes detection after the corresponding enzymatic pre-treatments (data not shown).

For the Int2 of 50-day-old *Miscanthus* species, after enzymatic removal of xylan, xylan detection with LM10 was totally abolished in all cell walls of the three *Miscanthus* species (data not shown). In the case of xylanase-treated *M.* x *giganteus* Int2 cell walls, the LM15 XyG epitope was revealed to be present in cell walls lining intercellular spaces of parenchyma regions (Figure 5.1 (D), (G) and (M)). In *M. sacchariflorus*, the unmasked XyG matched closely with parenchyma cell walls that did not stain with Calc (Figure 5.1, (B) and (E)), and it was also revealed in pith parenchyma regions after xylan removal using xylanase. As observed in previous chapter, in these corresponding non-Calc-staining/xylan-masking XyG parenchyma regions, the *M. sacchariflorus* has lower detections of heteroxylan but higher detectable level of MLG (Chapter 3 and 4). These results indicate the distinct cell wall polysaccharide architectures in these parenchyma regions which may link to their specific functions. Xylanase-unmasked LM15 XyG epitope was less abundant in *M. sinensis* stem sections although it was observed weakly in the sub-epidermal parenchyma regions that had been identified by abundant detection of both MLG and HG and low detection of heteroxylan (Figure 5.1, (F) and (I)), and this result was similar to that of *M. sacchariflorus*.

In the case of the LM5 pectic galactan epitope, after pre-treatment of xylanase or lichenase, the detection of this epitope increased in cell walls of the radially extended groups of parenchyma cells in the stem periphery, and also increased in the pith parenchyma and phloem cell walls of the three *Miscanthus* species (Figure 5.2, (G) to (L)). This increased detection of the LM5 galactan epitope after xylanase treatment was more abundant than after lichenase treatment (Figure 5.2, (G) to (L)).

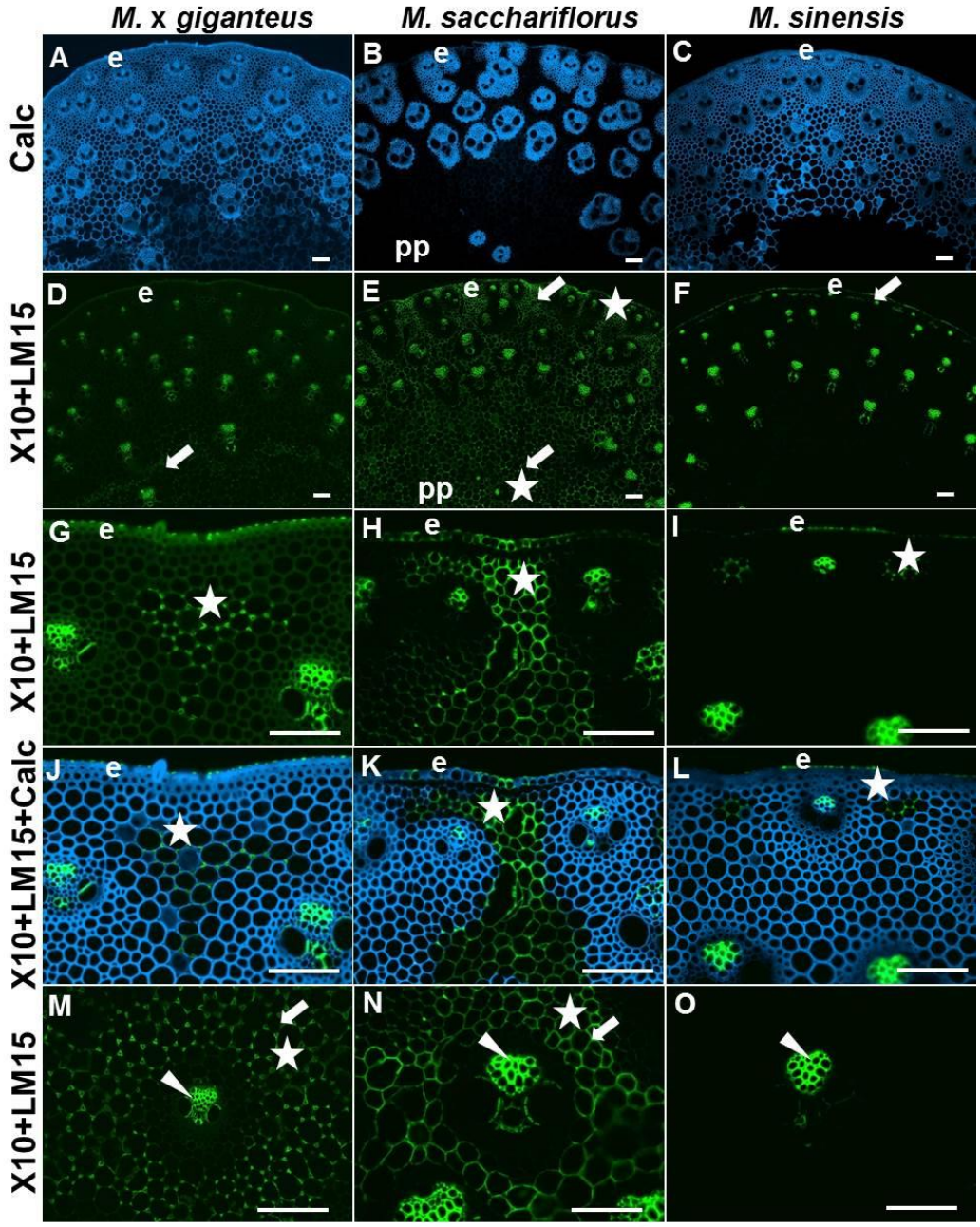

Figure 5.1: Fluorescence imaging of the LM15 xyloglucan epitope in xylanase-treated (X10) cell walls of transverse sections from Int2 of stems of *M.* x *giganteus, M. sacchariflorus* and *M. sinensis* at 50 days growth. Calc staining shown in blue. Immunofluorescence (FITC, green) images generated with monoclonal antibody to xyloglucan (LM15). Micrographs G-L and micrographs M-O show LM15 labellings after xylanase treatment at higher magnification of epidermal parenchyma and vascular bundles (vb) respectively. Arrowheads indicate phloem. Arrows indicate regions of interfascicular parenchyma that are labelled by LM15. Stars indicate regions of parenchyma that are unmasked by xylanase. e = epidermis, pp = pith parenchyma. Bars = 100 µm.

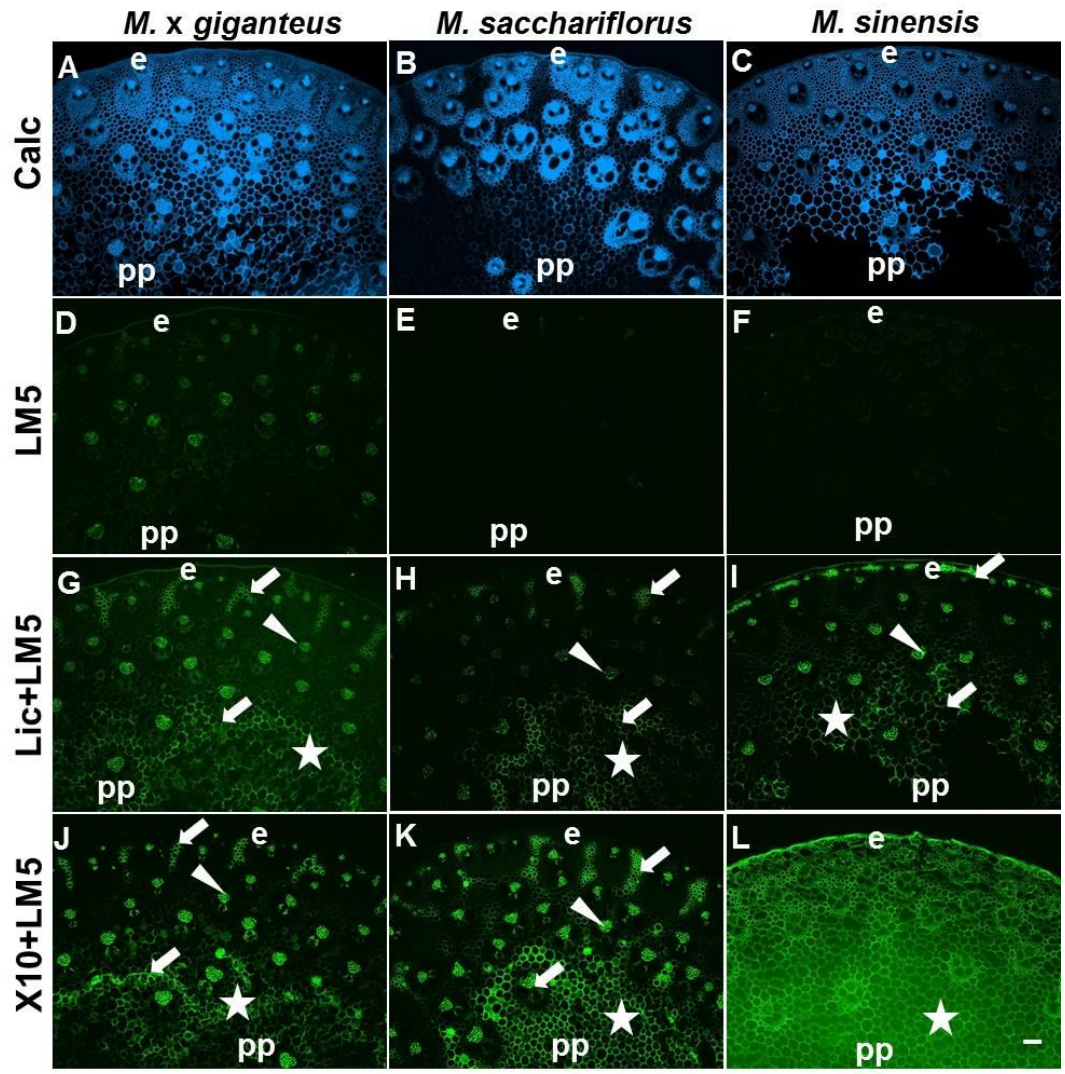

Figure 5.2: Fluorescence imaging of the LM5 galactan epitope in xylanase-(X10) and lichenase (Lic)-treated cell walls of transverse sections from Int2 of stems of *M.* x *giganteus, M. sacchariflorus* and *M. sinensis* at 50 days growth. Immunofluorescence (FITC, green) images generated with monoclonal antibody to pectic galactan (LM5). Arrowheads indicate phloem. Arrows indicate regions of interfascicular parenchyma that are labelled by LM5. Stars indicate regions of pith parenchyma that are unmasked. e = epidermis, pp = pith parenchyma. Bars = 100 µm.

For the LM2 AGP epitope, after the enzymatic removal of HG using PL or pec, the detection of the LM2 epitope increased strongly in cell walls of the epidermis (especially in *M. sacchariflorus*), phloem and sub-epidermal parenchyma regions of the Int2 of all three *Miscanthus* species but with different parenchyma binding patterns (Figure 5.3, (G), (H) and (I)). For *M. sacchariflorus*, this HG unmasked LM2 AGP matched closely with parenchyma cell walls that did not stain with Calc (Figure 5.3, (B) and (H)), and these parenchyma regions were also known to contain more MLG/HG, but less heteroxylan (Chapter 3).

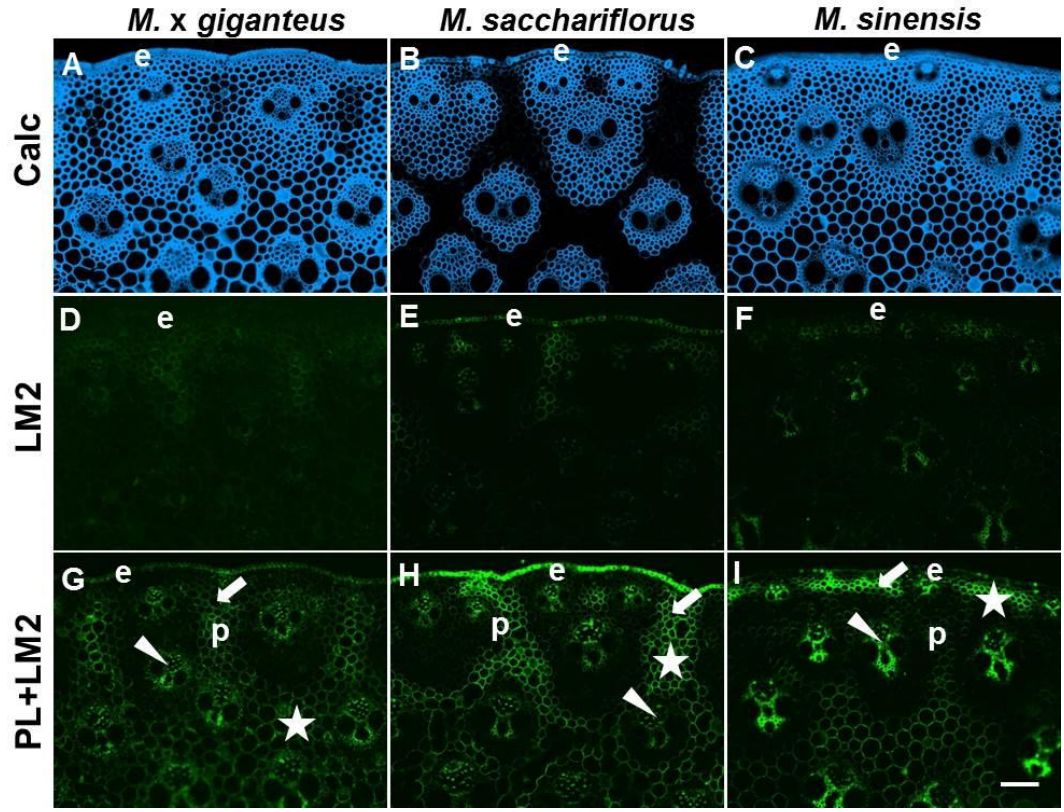

Figure 5.3: Fluorescence imaging of the LM2 AGP epitope in pectate lyase-(PL)-treated cell walls of transverse sections from Int2 of stems of *M.* x *giganteus, M. sacchariflorus* and *M. sinensis* at 50 days growth. Immunofluorescence (FITC, green) images generated with monoclonal antibody to arabinogalactan - protein (LM2). Arrowheads indicate phloem. Arrows indicate regions of interfascicular parenchyma that are labelled by LM2. Stars indicate regions of parenchyma that are unmasked. e = epidermis, p = parenchyma. Bars = 100 µm.

5.3 Masking of cell wall polymers in wheat

As shown previously, the polysaccharide masking was widely observed in *Miscanthus* species. To understand more about polysaccharide masking in grasses, similar experiments were carried out in different internodes (Int1 to Int4) and also the top and base of Int3 of 50-day-old wheat stems. After different combinations of enzymes and polysaccharide probes, similar polysaccharide masking results to *Miscanthus* species were observed in wheat. The LM15 XyG epitope was also masked by xylan in 50-day-old wheat stems (Figure 5.4). After xylanase treatment, the detection of LM15 XyG increased strongly in pith parenchyma regions of both elder and younger internodes (Int1 to Int4) (Figure 5.4), and increased much stronger in vascular bundle cell walls of the youngest internode Int4 (Figure 5.4C). And this is also the case for the analysis of the base and top of Int3, but with different binding patterns (Figure 5.5, (C) and (F)), the XyG increased more strongly in pith parenchyma regions in the elder top of Int3 (Figure 5.5C), and also the sub-epidermal parenchyma regions that detected previously with more MLG but less heteroyxlan (Chapter 4). While for the base of Int3, the XyG increased evenly in the outer parenchyma cell walls (Figure 5.5F).

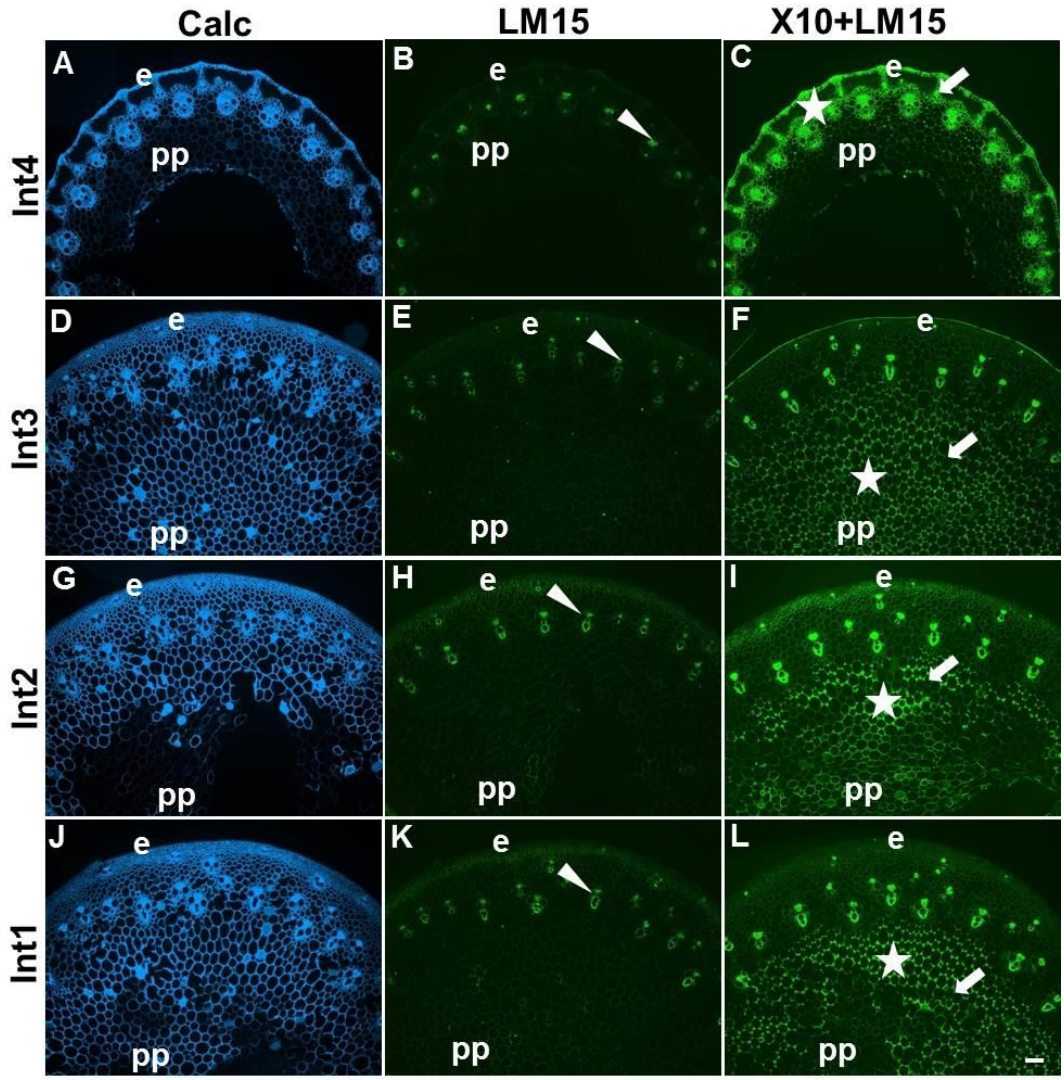

Figure 5.4: Fluorescence imaging of the LM15 xyloglucan epitope in xylanase-treated (X10) cell walls of transverse sections of the first (Int1, middle) to fourth (Int4, middle) internodes of a wheat stem at 50 days growth. Calc staining shown in blue. Immunofluorescence (FITC, green) images generated with monoclonal antibody to xyloglucan (LM15). Arrowheads indicate phloem. Arrows indicate regions of interfascicular parenchyma that are labelled by LM15. Stars indicate regions of parenchyma that are unmasked by xylanase. e = epidermis, pp = pith parenchyma. Bars = 100 µm.

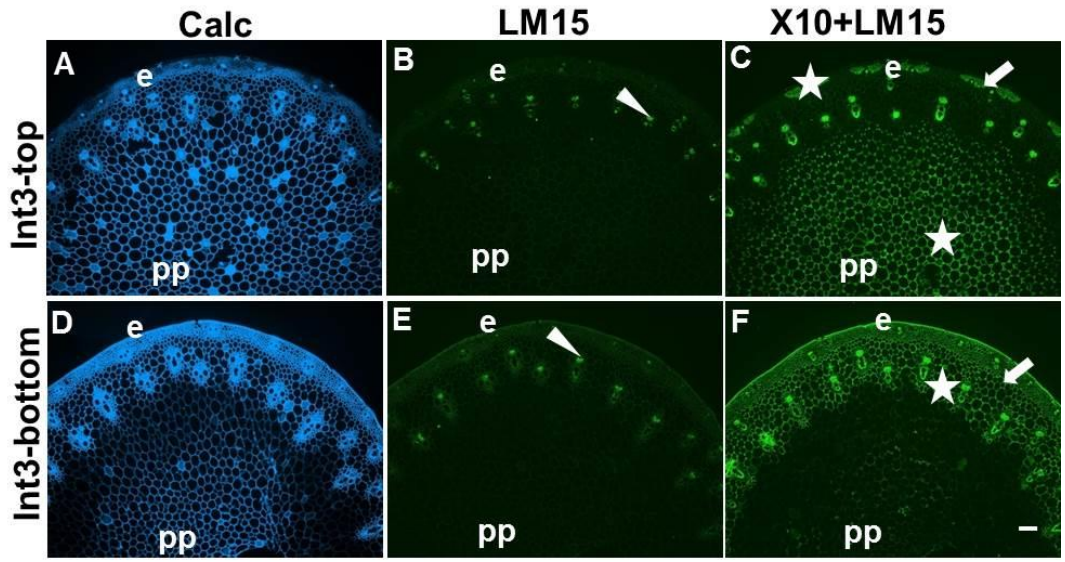

Figure 5.5: Fluorescence imaging of the LM15 xyloglucan epitope in xylanase-treated (X10) cell walls of transverse sections from top and bottom of Int3 (from base to shoot) of a wheat stem at 50 days growth. Calc staining shown in blue. Immunofluorescence (FITC, green) images generated with monoclonal antibody to xyloglucan (LM15). Arrowheads indicate phloem. Arrows indicate regions of interfascicular parenchyma that are labelled by LM15. Stars indicate regions of parenchyma that are unmasked by xylanase. e = epidermis, pp = pith parenchyma. Bars = 100 µm.

After pre-treatment of xylanase or lichenase, the detection of LM5 pectic galactan epitope increased in certain pith parenchyma cell walls, and also strongly increased in phloem and xylem cell walls of Int2 of wheat (Figure 5.6, (C) and (D)). This increased detection of the LM5 epitope after xylanase treatment was more abundant than after lichenase treatment (Figure 5.6, (C) and (D)), and this was consistent with that of the *Miscanthus* species (Figure 5.2).

In case of the LM2 AGP epitope, after the enzymatic removal of HG using PL or Pec, the detection of LM2 increased uniformly in parenchyma cell walls near the pith regions of Int2 of wheat (Figure 5.7, (C) and (D)). The LM2 AGP was also increased in the intercellular pith parenchyma spaces of wheat Int2 after pec pre-treatment (Figure 5.7D), and this was different from what was observed in *Miscanthus* species.

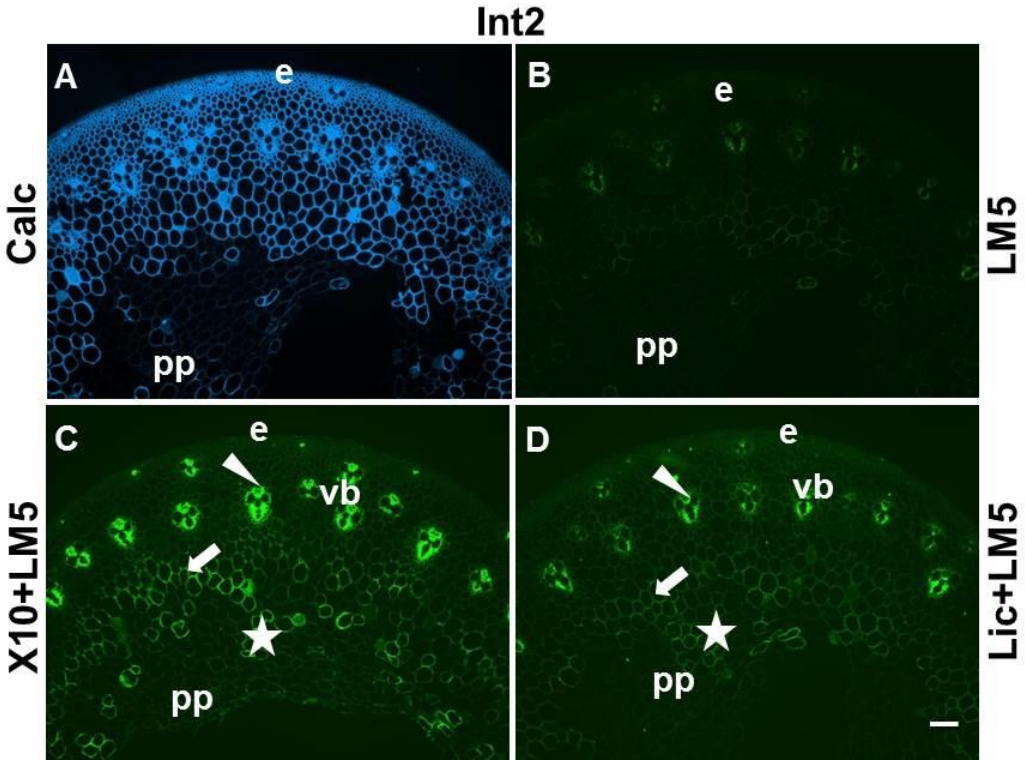

Figure 5.6: Fluorescence imaging of the LM5 galactan epitope in xylanase- (X10) and lichenase (Lic)-treated cell walls of transverse sections from Int2 of stems of wheat at 50 days growth. Immunofluorescence (FITC, green) images generated with monoclonal antibody to pectic galactan (LM5). Arrowheads indicate phloem. Arrows indicate regions of interfascicular parenchyma that are labelled by LM5. Stars indicate regions of pith parenchyma that are unmasked. e = epidermis, pp = pith parenchyma, vb = vascular bundle. Bars = 100 µm.

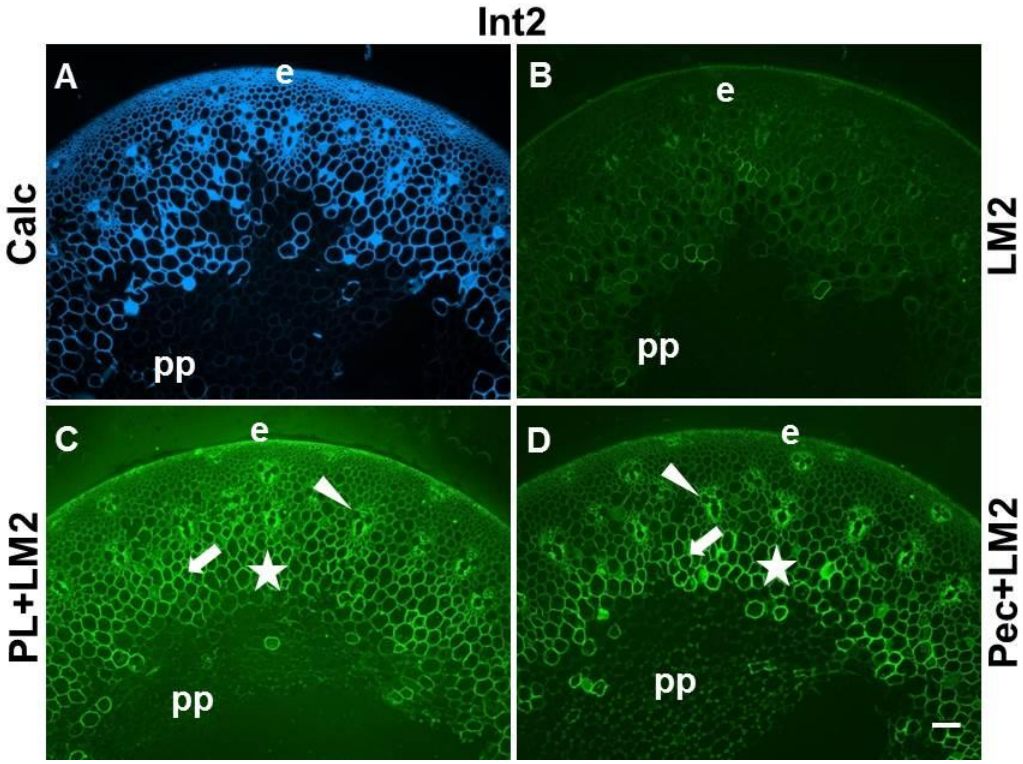

Figure 5.7: Fluorescence imaging of the LM2 AGP epitope in pectate lyase- (PL) or Pectinex (Pec)-treated cell walls of transverse sections from Int2 of stems of wheat at 50 days growth. Immunofluorescence (FITC, green) images generated with monoclonal antibody to arabinogalactan - protein (LM2). Arrowheads indicate phloem. Arrows indicate regions of interfascicular parenchyma that are labelled by LM2. Stars indicate regions of parenchyma that are unmasked. e = epidermis, p = parenchyma. Bars = 100 µm.

5.4 Cell wall polymers masking in *Brachypodium distachyon*

The LM15 XyG was masked by xylan, the LM5 galactan was masked by both xylan and MLG, and the LM2 AGP was masked by pectin in grasses - *Miscanthus* species and wheat stems, further polysaccharide masking observations were explored in Int2 (older internode) and Int5 (younger internode) of the 50-day-old *B. distachyon* stems. After specific enzymatic pre-treatment, for the 50-day-old *B. distachyon* stems, the detection of LM15 XyG epitope increased uniformly in all cell walls of Int2 (Figure 5.8, (H), (I), (K) and (L)), and increased much more strongly in the sub-epidermal parenchyma cell walls that had been identified by abundant detection of both MLG and HG and low levels of detection of heteroxylan (Chapter 4), and also abundant in intercellular pith parenchyma spaces of Int5 (Figure 5.8, (B), (C), (E) and (F)), and this was consistent with what was observed in *Miscanthus* and wheat stems.

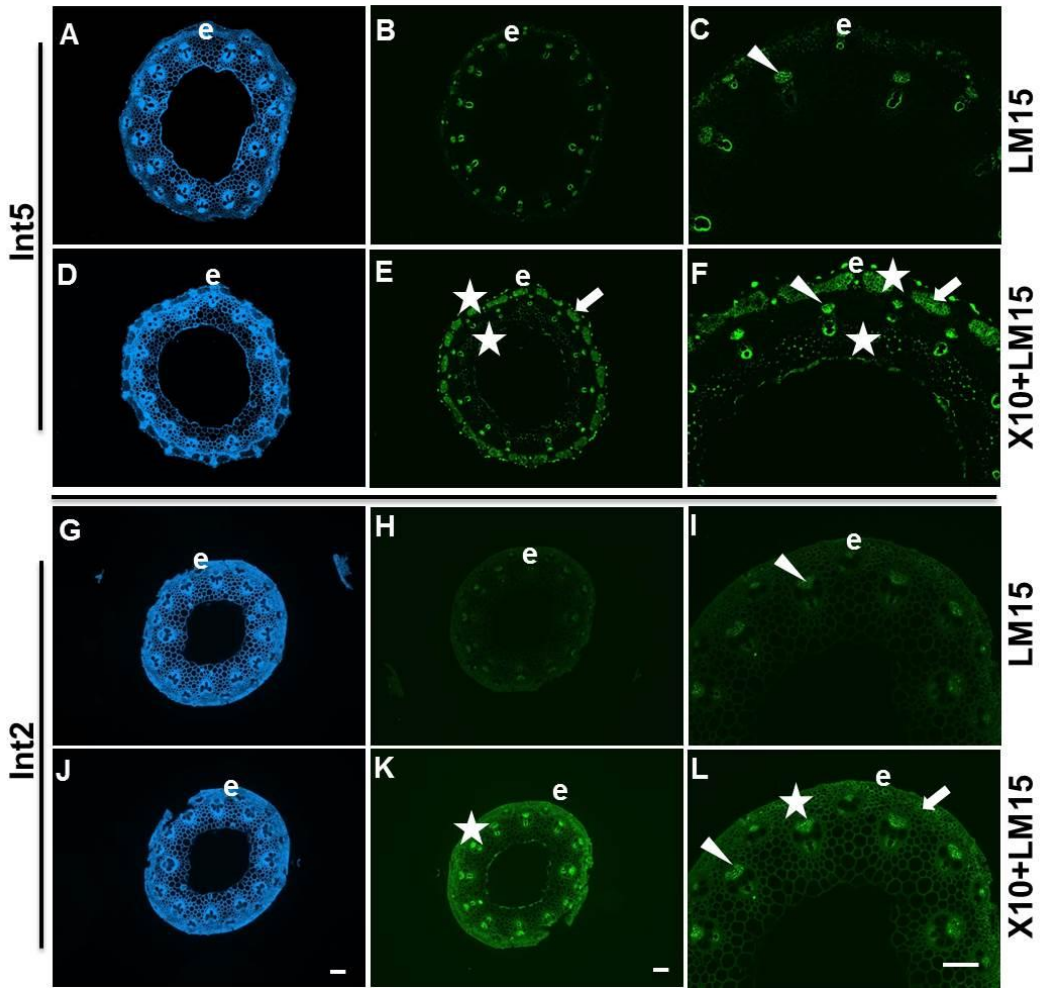

Figure 5.8: Fluorescence imaging of the LM15 xyloglucan epitope in xylanase-treated (X10) cell walls of transverse sections of the second (Int2, middle) and fifth (Int5, middle) internodes of *B. distachyon* at 50 days growth. Calc staining shown in blue. Immunofluorescence (FITC, green) images generated with monoclonal antibody to xyloglucan (LM15). C, F, I and L show LM15 labellings before and after xylanase treatment of epidermal parenchyma and vascular bundles (vb) at higher magnification. Arrowheads indicate phloem. Arrows indicate regions of interfascicular parenchyma that are labelled by LM15. Stars indicate regions of parenchyma that are unmasked by xylanase. e = epidermis, pp = pith parenchyma. Bars = 100 µm.

For the LM5 pectic galactan epitope, after pre-treatment of lichenase, the detection of LM5 increased strongly in phloem cell walls and in cell walls of the radially extended groups of parenchyma cells of both Int2 and Int5 (Figure 5.9, (F), (I), (O) and (R)). And again, similar to the *Miscanthus* and wheat, this increased detection of the LM5 epitope after xylanase treatment was more abundant than after lichenase treatment (Figure 5.9, Figure 5.2 and Figure 5.6). In the case of the LM2 AGP epitope, after the enzymatic removal of HG using PL, the detection of LM2 increased uniformly in all cell walls of the elder internode of *B. distachyon* - Int2 (Figure 5.10, (I) and (L)), but not in the younger internode - Int5 (Figure 5.10, (C) and (F)).

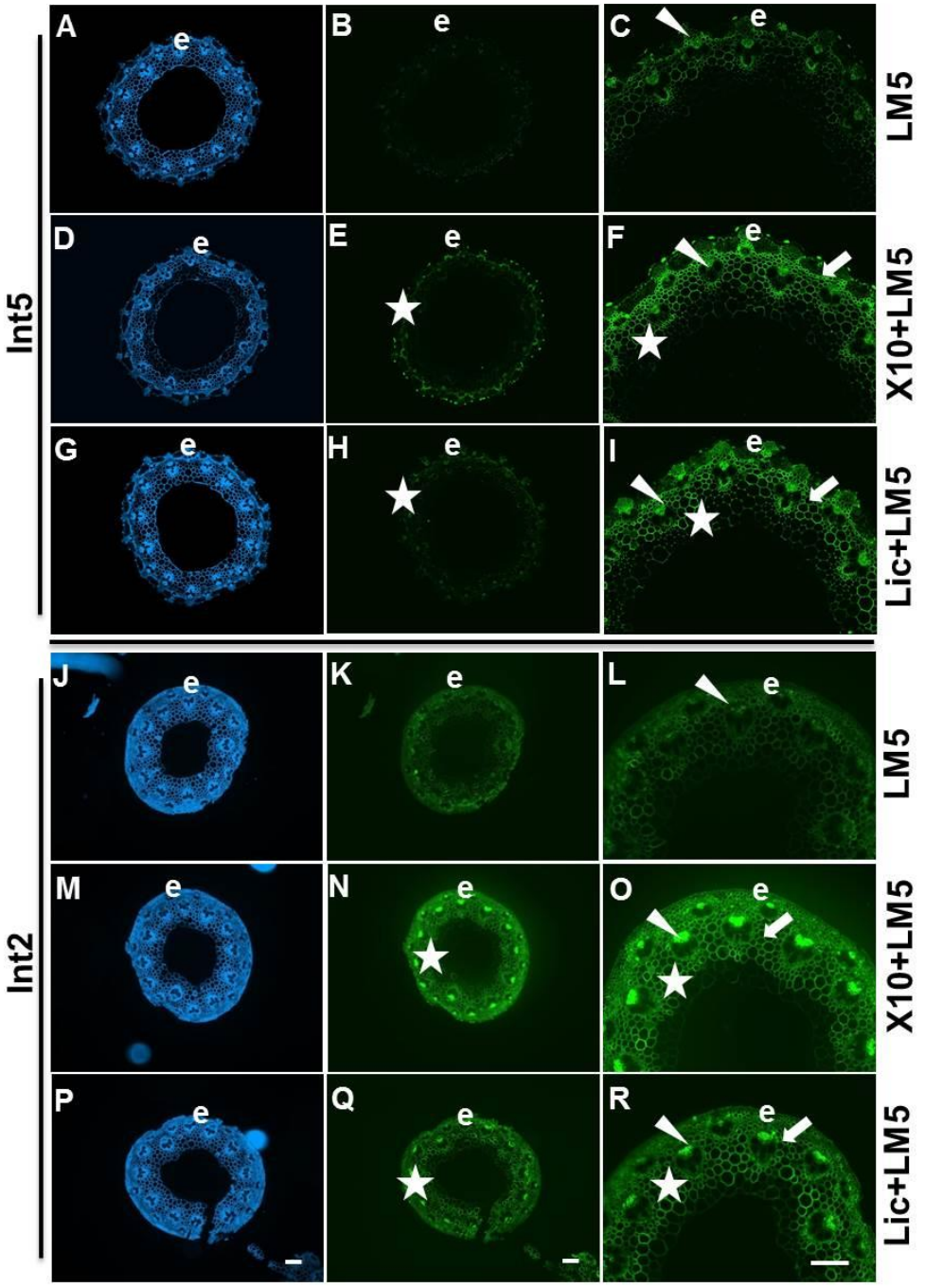

Figure 5.9: Fluorescence imaging of the LM5 galactan epitope in xylanase- (X10) and lichenase (Lic)-treated cell walls of transverse sections of the second (Int2, middle) and fifth (Int5, middle) internodes of *B. distachyon* at 50 days growth. Immunofluorescence (FITC, green) images generated with monoclonal antibody to pectic galactan (LM5). Right handside column micrographs show LM5 labellings before and after xylanase or lichenase treatment of epidermal parenchyma and vascular bundles (vb) at higher magnification. Arrowheads indicate phloem. Arrows indicate regions of interfascicular parenchyma that are labelled by LM5. Stars indicate regions of pith parenchyma that are unmasked. e = epidermis, pp = pith parenchyma. Bars = 100 µm.

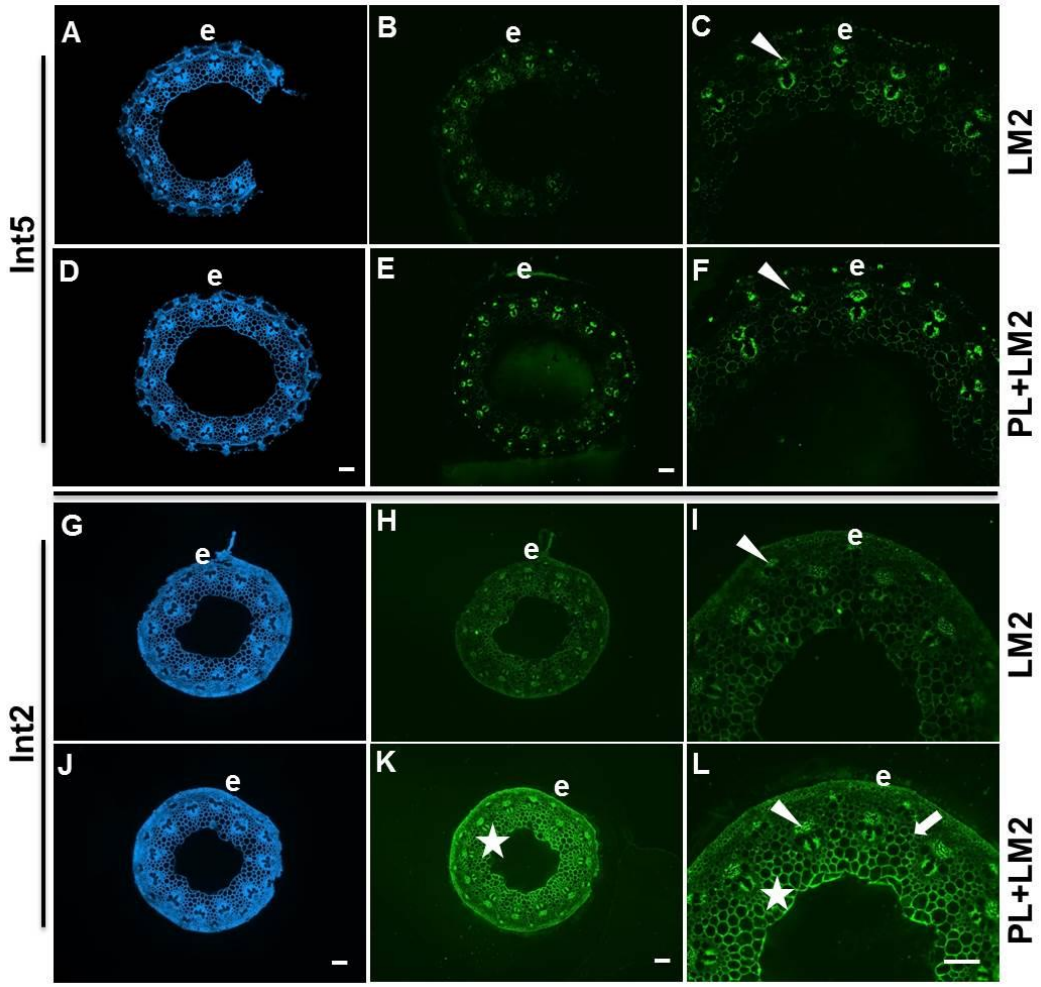

Figure 5.10: Fluorescence imaging of the LM2 AGP epitope in pectate lyase-(PL) -treated cell walls of transverse sections of the second (Int2, middle) and fifth (Int5, middle) internodes of *B. distachyon* at 50 days growth. Immunofluorescence (FITC, green) images generated with monoclonal antibody to arabinogalactan-protein (LM2). C, F, I and L show LM2 labellings before and after pectate lyase treatment of epidermal parenchyma and vascular bundles (vb) at higher magnification. Arrowheads indicate phloem. Arrows indicate regions of interfascicular parenchyma that are labelled by LM2. Stars indicate regions of parenchyma that are unmasked. e = epidermis, p = parenchyma. Bars = 100 µm.

Generally speaking, in the three grass species (*Miscanthus* species, wheat and *B. distachyon*), after enzymatic removal of xylan, the LM15 XyG detection was increased in certain parenchyma regions that had been identified by abundant detection of both MLG and HG and low levels of detection of heteroxylan, the LM5 galactan increased in pith parenchyma cell walls, the LM5 galactan was also increased in these regions after the enzymatic removal of MLG. The LM2 AGP was detected more in parenchyma cell walls after enzymatic removal of pectin in all three grass species (Table 5.1). All of these results indicate the polysaccharide masking is common in grasses, and also indicate the particular polysaccharide architecture and may also be related to the function of the unmasked-regions of grasses.

Table 5.1: Potential for polysaccharide masking in the second internode (Int2) of *M.* x *giganteus*, *M. sacchariflorus*, *M. sinensis*, wheat and *B. distachyon* at 50 days growth.

	Xylanase	Lichenase	Pectate lyase
LM10	–	no	no
MLG	no	–	no
LM5	yes	yes	–
LM15	yes	no	no
LM2	no	no	yes

yes/no = The polysaccharide epitope was/was not detectable after the enzymatic removal of specific cell wall polymers. LM10 = xylan; LM5 = pectic galactan; LM15 = XyG; LM2 = AGPs.

5.5 Discussion

The LM15 XyG epitope was detected in both the phloem and xylem regions of the two *Miscanthus* species - *M.* x *giganteus* and *M. sinensis*. By contrast, it was only detected in the phloem regions of *M. sacchariflorus*. This result is consistent with the finding that the LM15 monoclonal antibody bound to restricted regions of parenchyma cell walls of nasturtium seed which might be linked to the spatial regulation of XyG structure in cell walls (Marcus et al. 2008). However, after the enzymatic removal of xylan using xylanase, the XyG was detected more in certain parenchyma cell walls of all *Miscanthus* species. In wheat and *B. distachyon*, XyG is also masked by xylan in some certain parenchyma cell wall regions especially in the more MLG and HG and less heteroxylan regions. Pauly et al. reported that the structure of XyG changed in pea stems during cell elongation and proposed that the XyG plays an important role in cell wall growth and development (Pauly et al. 2001). Therefore, the XyG polysaccharide that was masked by xylan in the certain parenchyma cell walls indicated that these parenchyma regions may be related to the growth and/or development of the three grasss pecies. It is also of interest in this regards that the disposition of the regions of detected unmasked XyG is different in the three *Miscanthus* species - being in cell walls lining intercellular space regions in *M.* x *giganteus* and throughout parenchyma cell walls in *M. sacchariflorus* to some extent reflecting the low heteroxylans/high MLG regions, which may related to the different growth rate of *Miscanthus* species.

For *Miscanthus*, wheat and *B. distachyon*, the LM5 galactan epitope was detectable in certain parenchyma cell walls after enzymatic removal of xylan or MLG, which indicates that galactan is masked by both xylan and MLG. It is interesting that the XyG is masked just by xylan, while the galactan is masked by both xylan and MLG. After the enzymatic removal of pectin, the AGP epitope revealed more in stems of all three grass species. These results suggest the parenchyma regions have distinct cell wall architectures, and the XyG, xylan, galactan and AGP may have some

special cross-linkage in these cell wall regions, and this may also link to their functions. It has been reported that the xylan and mannan are masked by pectin in tobacco stems that contain more pectin and XyG but less xylan (Hervé et al. 2009, Marcus et al. 2010). This work was the first time that the xylan and MLG masking in grass cell walls which contain more xylan and MLG were explored. Deconstruction (enzymatic and chemical) of cell walls could further our understanding of cell wall structure heterogeneity, cell wall micro-environments, polysaccharides functions of and their specific corresponding enzymes (Marcus et al. 2010). To date, the work presented here is the first time to study the polysaccharide distribution, cell wall architecture and potential polysaccharide masking for *Miscanthus* species, as well as the wheat and *B. distachyon*. All these results indicate that the use of cell wall degrading enzymes has extended knowledge of grass cell wall architectures, and also shown us the heterogeneity of polysaccharide distribution and molecular architectures in grass species.

Chapter 6

Arabinogalactan-proteins (AGPs) of *Miscanthus* x *giganteus* stem

6.1 Introduction

As shown in chapters 3 and 5, the LM11 arabinoxylan epitope was detected uniformly to all cell walls in transverse sections of 50-day-old *M.* x *giganteus* stems (Figure 3.3). During the analysis of the cell walls and epitope detection, after the enzymatic removal of HG using pectate lyase (PL) or pectinex (Pec), it was discovered that the detection of the LM2 AGP epitope increased in cell walls of the epidermis, phloem and parenchyma regions of *M.* x *giganteus* (Figure 5.3), and these binding patterns were similar to that of the LM11 epitope (Figure 6.1). It has been reported that glucuronic acid is a component of the LM2 epitope (Smallwood et al. 1996). Glucuronic acid is also present as a substitution of xylan (Kabel et al. 2002). Furthermore, the LM2 AGP antibody was found to bind strongly to xylan preparations - purified oat xylan and birchwoodxylan as shown in Figure 6.1. The LM2 AGP epitope present in the oat xylan sample is almost similar to the level of the LM11 arabinoxylan epitope (Figure 6.1). To further explore the relationship between the heteroxylan and AGP, the cell wall polysaccharides of Int2 from 50-day-old *M.* x *giganteus* were extracted with water (H_2O), trans-1,2-cyclohexane diamine-N,N,N,N-tetra acetic acid (CDTA), sodium carbonate (Na_2CO_3) and potassium hydroxide (KOH). The presence of xylan and LM2 epitopes was then followed by ELISA, immunodot blot analysis (IDA), SDS-PAGE and Western blot analyses.

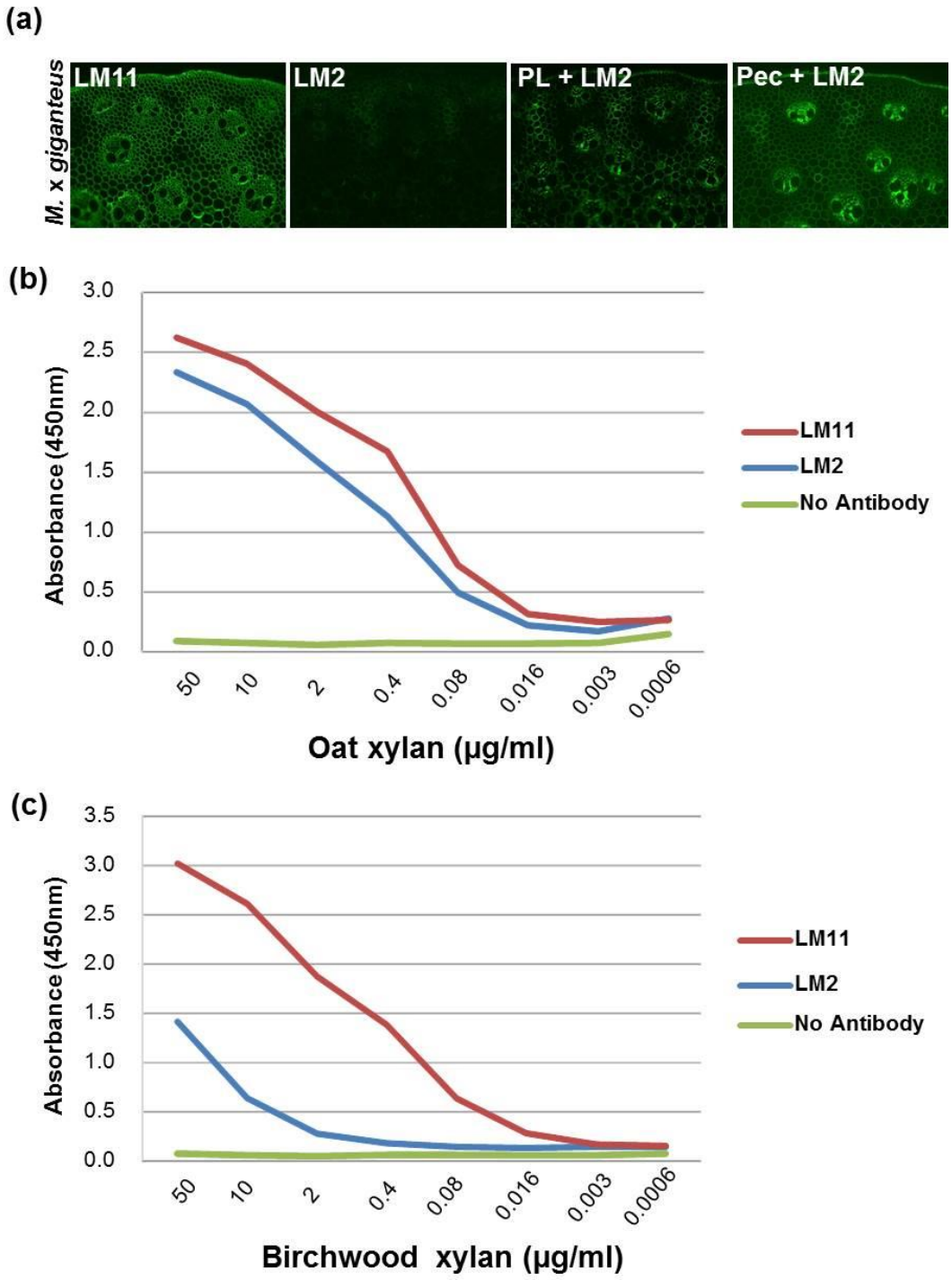

Figure 6.1: Fluorescence imaging of LM11 xylan and LM2 AGP epitopes in transverse sections (pectate lyase- (PL) or Pectinex (Pec)-treated) of Int2 of a *M.* x *giganteus* stem at 50 days growth (a) and ELISA analysis of the binding of LM11 xylan and LM2 AGP monoclonal antibodies to purified oat xylan and birchwood xylan (b) and (c). Monoclonal antibodies (LM2 and LM11) were used at a 5-fold dilution. Xylans were titrated in microtitre plate wells from 50 µg/ml at a 5-fold downwards.

6.2 Analysis of arabinogalactan-proteins (AGPs) in cell wall extractions of *Miscanthus* x *giganteus* stem

The ELISA binding analysis showed that the LM10/11 heteroxylans were abundantly detected in the KOH cell wall extracted 50-day *Miscanthus* x *giganteus* materials, with reduced levels of detection in the H_2O and Na_2CO_3 extracts (Figure 6.2). The LM2 and LM14 AGP epitopes (Moller et al. 2008) were abundantly detected in the CDTA and Na_2CO_3 extracted materials, followed by the H_2O extractions. However, for the H_2O extracted cell wall materials, the LM11 and LM2 probes bound quite equally (Figure 6.2), and the IDA analysis complemented these ELISA results for the LM2 and LM11 (Figure 6.3). These results indicate that the LM11 arabinoxylan and the LM2 AGP epitopes may be present on the same polysaccharide or polysaccharide complex in the H_2O soluble cell wall materials, or alternatively they are present on different polysaccharides that fractionate in the same way, but not in KOH/Na_2CO_3/CDTA extractions.

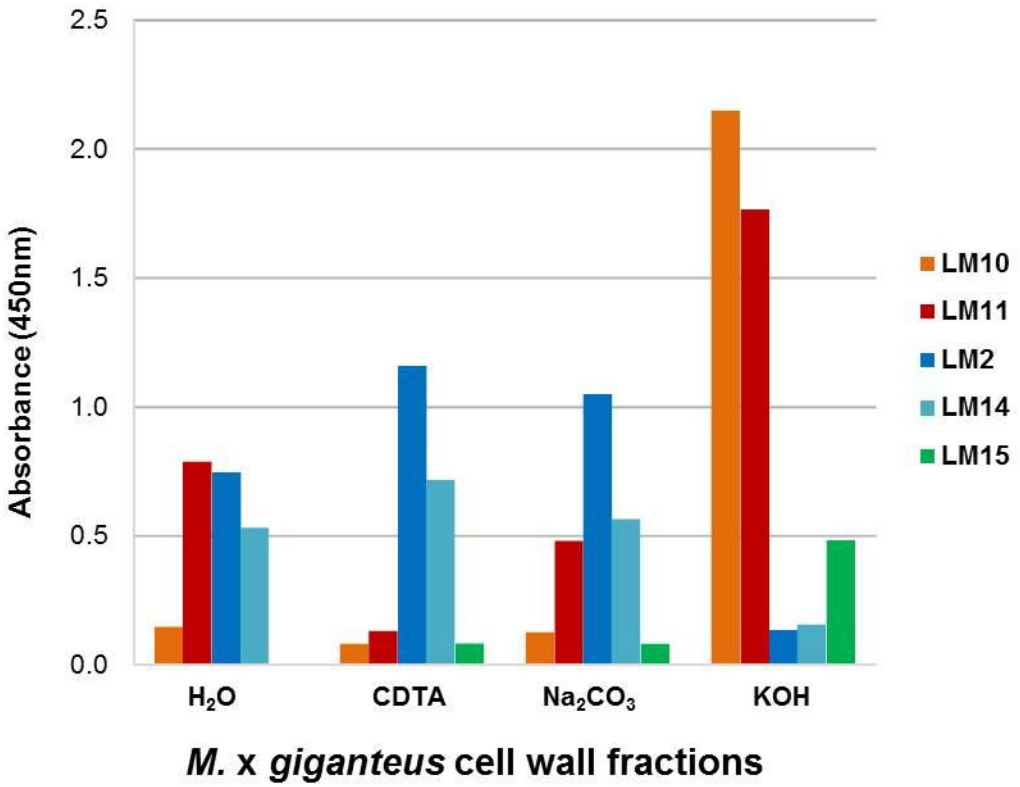

Figure 6.2: ELISA analysis of heteroxylan (LM10 - xylan, LM11 - xylan/arabinoxylan), AGP (LM2 and LM14) and xyloglucan (LM15 - xyloglucan) epitopes in H2O, CDTA, Na_2CO3, and KOH extracts of cell wall material from Int2 of stems of *M.* x *giganteus* at 50 days growth. 0.1 g of extracted cell wall material was used per 10 ml of buffer in each case. Monoclonal antibodies were used at a 5-fold dilution.

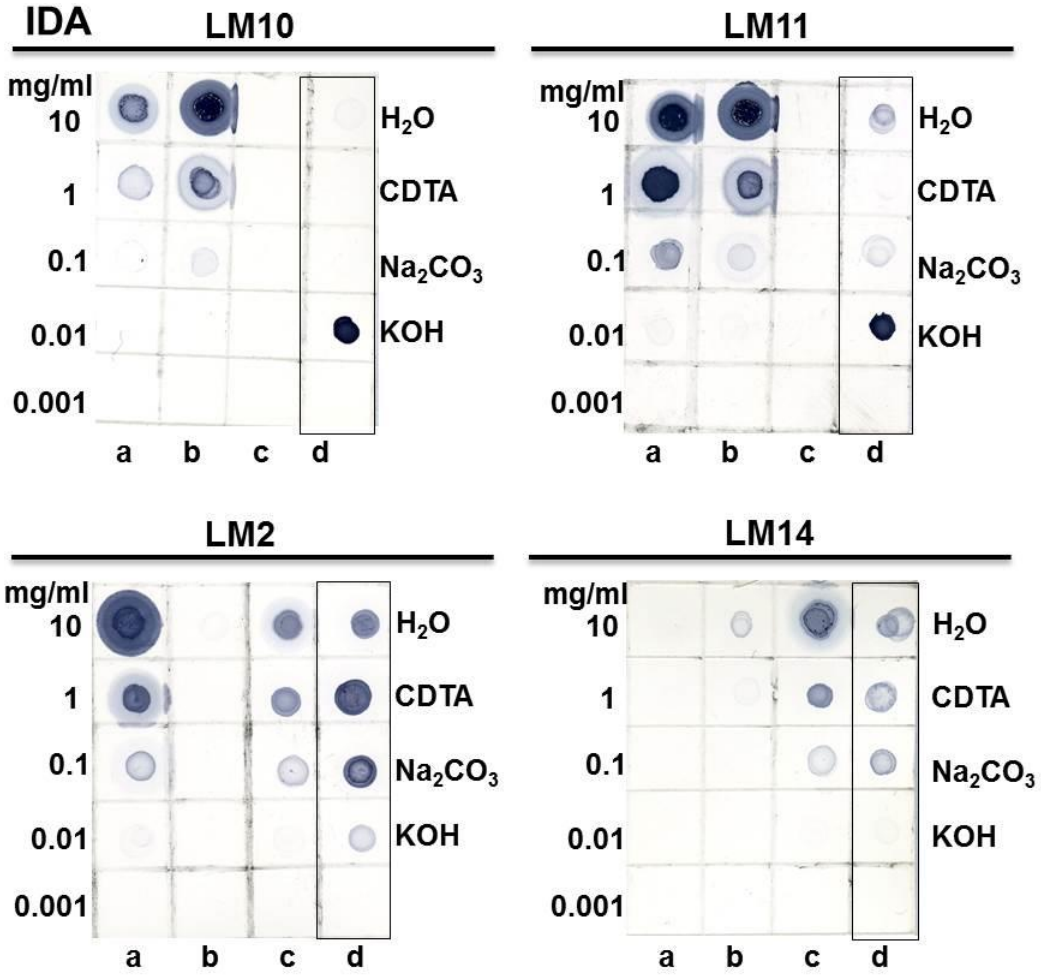

Figure 6.3: Immunodot assay detection of heteroxylan (LM10 and LM11) and AGP (LM2 and LM14) epitopes in different fractions of extracted cell wall material of Int2 of stems of *M.* x *giganteus* at 50 days growth, and in oat xylan, birchwood xylan and gum arabic. 1 µl loadings were applied to nitrocellulose. For each piece of nitrocellulose, lane a = oat xylan, lane b = birchwood xylan, lane c = gum arabic, lane d = *M.* x *giganteus* cell wall extractions. For lane a, b and c, from top to bottom, the loading concentration was 10, 1, 0.1, 0.01 and 0.001 mg/ml. For lane d, from top to bottom, the loading material was *M.* x *giganteus* cell wall material from H_2O, CDTA, Na_2CO_3, and KOH extractions.

As shown above in the H_2O soluble cell wall materials the LM11 epitope may be linked in the same polymer compelx as the LM2 epitope. To explore this further, these polysaccharides extracts from the four different solvents were analysed with SDS-PAGE and Western blot using the LM2 AGP and LM11 arabinoxylan probes (Figure 6.4). For the SDS-PAGE analysis, all of the four different cell wall extracts were not stained with Coomassie blue (Figure 6.4), and this may because of the low amount of the loading samples. The following western blotting analysis of these SDS gels showed that the LM11 arabinoxylan epitope was detected strongly in the KOH and H_2O extractions, and the LM2 AGP epitope was detected more in the H_2O, CDTA and Na_2CO_3 extractions (Figure 6.4). And these results again complemented the ELISA results above and indicate that in the KOH/CDTA/ Na_2CO_3 extractions, the LM11 epitope was not correlated with the LM2 epitope. However, in the H_2O soluble cell wall materials, it is possible that the LM11 arabinoxylan and the LM2 AGP epitopes may be present on the same polysaccharide or polysaccharide complex and this is consistent with the ELISA results observed above (Figure 6.2).

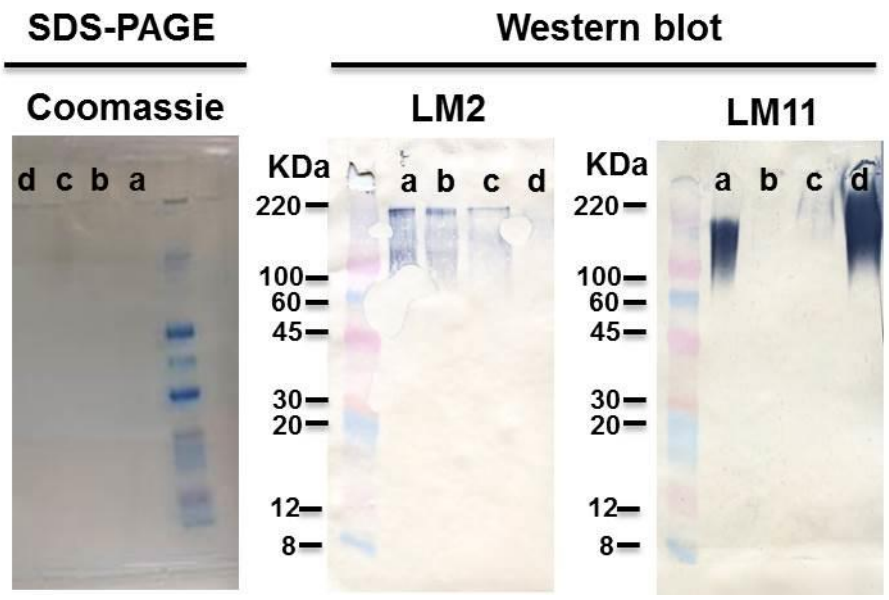

Figure 6.4: SDS-PAGE and Western blot of cell wall fractions of Int2 of stems of *M.* x *giganteus* at 50 days growth with LM2 AGP and LM11 heteroxylan antibodies. 20 µg carbohydrate loadings were applied to each gel lane. For each gel, lane a = H_2O-extracted material, lane b = CDTA-extracted material, lane c = Na_2CO_3-extracted material, lane d = KOH-extracted material.

To explore further whether the AGPs were attached to heteroxylan or the two epitopes shared the same polysaccharide or polysaccharide complex in 50-day-old *M.* x *giganteus*, the *M.* x *giganteus* AGPs were isolated using β-Glc-Yariv reagent (βGlcY) precipitation (Yariv et al. 1962, Yariv et al. 1967). The βGlcY-precipitated cell wall materials (βGlcY-precipitated AGPs) were extracted from the fresh Int2 of 50-day-old *M.* x *giganteus*, followed by the βGlcY binding assay. The IDA analysis of the βGlcY-precipitated cell wall materials showed the effectiveness of this AGP extraction using βGlcY precipitation (the yellow colour, Figure 6.5). The LM2 probe bound strongly to the βGlcY-precipitated cell wall materials (Figure 6.5). However, the LM11 arabinoxylan probe did not bind to these materials (Figure 6.5). Furthermore, the ELISA analysis of the LM2 and LM11 bindings to βGlcY-precipitated cell wall materials showed the similar results

(Figure 6.6). All of these results indicate that in *M.* x *giganteus* the βGlcY-precipitated AGPs had no detectable cross linkage to the LM11 arabinoxylan.

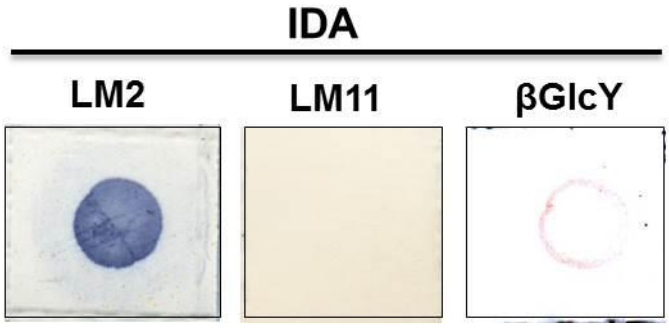

Figure 6.5: Immunodot assay detection of the LM2 AGP and LM11 heteroxylan epitopes and βGlcY binding assay of βGlcY-precipitated material (AGPs) from *M.* x *giganteus* stems (Int2 of stems of *M.* x *giganteus* at 50 days growth). Equivalent 1 µl loadings of purified AGPs were applied to the nitrocellulose in each case.

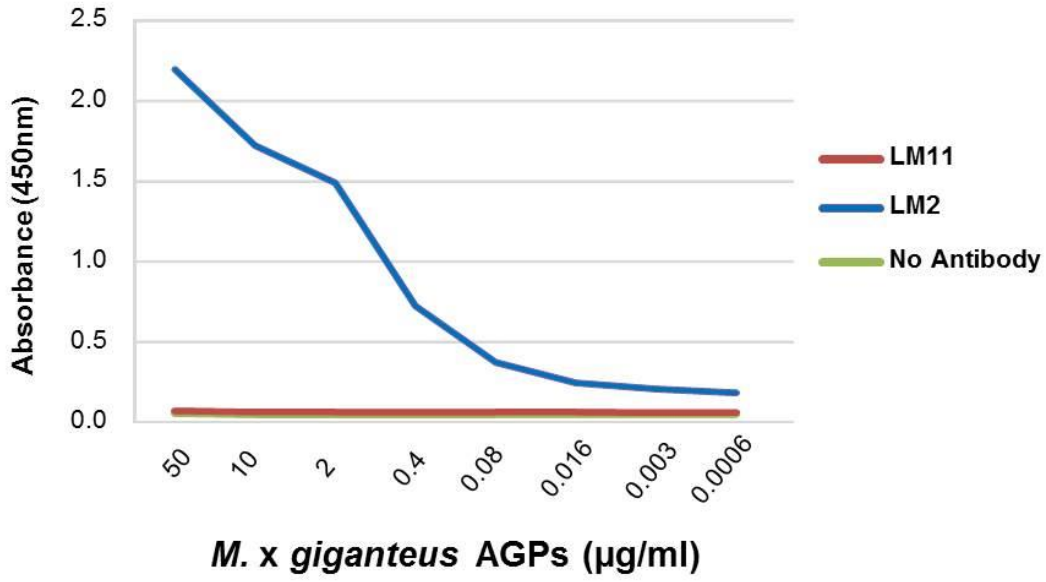

Figure 6.6: ELISA analysis of LM2 AGP and LM11 heteroxylan binding to βGlcY-precipitated material (AGPs) from *M.* x *giganteus* stems (Int2 of stems of *M.* x *giganteus* at 50 days growth). Monoclonal antibodies used at a 5-fold dilution.

6.3 Discussion

AGP glycan specific antibodies and β-Glc-Yariv reagent have been widely used to investigate AGP occurrence and activity within the plant kingdom (Ellis et al. 2010, Rafińska and Bednarska 2011, Seifert and Roberts 2007). The LM2 antibody has been selected to detect the AGPs in rice and carrot (Smallwood et al. 1996). In this study from the immunolabelling binding analysis of the LM2 AGP and the LM11 arabinoxylan epitope, and the presence of the LM2 epitope in xylan preparations of *M.* x *giganteus*, it was thought that these observations may indicate that the LM2 AGP epitope (that was unmasked by pectin-degradation) was binding to glucuronic acid in xylans, as glucuronic acid is an important sugar in the LM2 epitope in AGPs (Knox 1997, Yates et al. 1996). Blotting analysis from the water soluble *M.* x *giganteus* cell wall fractions indicated that the AGPs may be closely associated with xylans, and this may be the water soluble xylan.

As this is only a small proportion of the xylan, useful experiments with large amount of cell wall extractions of *Miscanthus* are suggested to be explored in future work. One possibility would be the blotting analysis of different chemical extracted *M.* x *giganteus* cell wall materials after pre-treatment of xylanase, to see whether the AGPs are more water soluble than xylans in these extracted cell wall fractions. Another possible experiment would be using affinity columns to separate *Miscanthus* arabinoxylan, and similar experiments carried out in this study are also suggested to be explored using the oat xylan samples.

It has been reported that AGPs may be involved in the cellulose deposition, and therefore contribute to plant stem strength and elasticity by cell wall integrity in *Arabidopsis thaliana* and *Eucalyptus* (MacMillan et al. 2010). Tan et al reported that the pectin and arabinoxylan are covalently linked to AGP at a very small polysaccharide molecule proportion in *Arabidopsis thaliana* cell walls (Tan et al. 2013). They suggested that AGPs may serve as a type of cross-linker in cell walls, that at least one AGP was connected with some of pectin and non-cellulosic polysaccharides (Tan et al. 2013), the xylan and pectin domains of the xylan/pectin-cross-linked AGPs (about 11-13 polysaccharide residues) are much shorter that those of the native xylans and pectins (hundreds polysaccharide residues) (Tan et al. 2013). However, after our following analysis of the βGlcY-precipitated cell wall materials (AGPs) in *M.* x *giganteus*, it seemed that the LM2 AGP epitope had no detectable cross-linkage with the LM11 arabinoxylan. The AGP fractions inter-linked with pectins have been widely reported form maize, grape, carrot, pea, flax and *Trifolium nigrescens* tissues (Immerzeel et al. 2006, Kato and Nevins 1984, Naran et al. 2008, Pellerin et al. 1995, Pilarska et al. 2013, Renard et al. 1997), and this covalent bonds could give the wall polymers a rigid structure and can withstand extreme pressure (Tan et al. 2013). Koniecznyet al reported that the polysaccharide epitope recognized by a single antibody may occur in different AGPs due to the different protein backbone and functions

(Konieczny et al. 2007) . Here in this study in *M.* x *giganteus*, there may be some association of AGP fractions and xylans together in the cell walls, but these may have been separated by the approaches/conditions we have applied. It is to be noted that the LM2 AGP epitope is abundant in the oat xylan sample.

In summary, the pectin-unmasked AGP binding patterns were similar to that of the heteroxylans in *M.* x *giganteus* stem sections and the LM2 AGP epitope was identified in commercial xylan samples. However, blotting analysis of extracted polymers indicate that βGlcY-precipitated cell wall materials (AGPs) and heteroxylans were not sharing the same polysaccharide or polysaccharide complex in 50-day-old *M.* x *giganteus* water soluble cell wall extractions. Further experiments as mentioned earlier are suggested to be explored in future.

Chapter 7

General Discussion

7.1 Similarity of grass cell wall polysaccharide composition in relation to plant development

This study demonstrates that grass cell walls contain high levels of MLG, heteroxylan, and also contain pectins, XyG and heteromannans as detected by *in situ* fluorescence imaging. Generally speaking, the epidermis of the well-developed Int2 of *Miscanthus* species contains cellulose, unsubstituted/substituted xylan, MLG, methylesterified HG and RG-I related arabinan; the phloem cell walls contain cellulose, substituted arabinoxylan, MLG, xyloglucan, unesterified/methylesterified HG, RG-I related arabinan/galactan and little amount of heteromannan; in addition to polysaccharides that phloem contains, xylem cell walls also consist of unsubstituted xylan. The sheaths of vascular bundles contain cellulose and unsubstituted/substituted xylans. The most complex polysaccharide architecture was detected in parenchyma cell walls. At the inner pith parenchyma regions, the cell walls contain cellulose, substituted xylan, MLG and a larger amount of methylesterified HG, while at the sub-epidermal parenchyma regions, cell walls are consist of lower amount of heteroxylan but higher levels of MLG and HG. During the growth, these cell wall polymers changed in different tissues. For example, the younger internodes and the younger tissues of the same internode (top and base of internode) had higher levels of MLG and HG, whereas the older internodes and the older tissues of the same internode had a larger amount of heteroxylan. For the other two grasses, wheat and *B. distachyon*, the major cell wall polysaccharide architecture are more or less similar to that of the *Miscanthus* species, but with very little differences and this will be discussed later in this chapter. All of these polysaccharide component similarities are consistent with what had been found in type II cell walls (Carpita 1996, Carpita and Gibeaut 1993).

7.2 Heterogeneity of grass cell walls

According to the anatomical analysis of transverse stem sections of the five grass species, *M.* x *giganteus* has the largest stem size whereas the *B. distachyon* has the smallest stem size of the grasses analysed in this study. The epidermis of the *Miscanthus* stem is thicker than that of the wheat and *B. distachyon*. During the growth, the *M.* x *giganteus* has more internodes and grows faster and taller than its parents and the other two grass species, therefore, the stem size and the internode number will be related entirely to growth stage. Grasses with many internodes may be less susceptible to lodging (Kaack et al. 2003, Niklas 1990). Previous study proposed that *M.* x *giganteus* was expected to have the highest lodging resistance due to its larger number or thickness of internodes among the *Miscanthus* species (Kaack et al. 2003), and this is not known at this stage.

Interestingly, this study also indicates that the non-cellulosic cell wall polymers of grass species are not evenly detected across the cell walls of stem tissues, that is different grass cell wall tissues and cell types contain specific polysaccharides. For example phloem cell walls of the three grass species containing substituted arabinoxylan, XyG, MLG and other polymers, this suggests that the cell walls of the phloem are distinct from the other wall tissues of the three grass species, especially the unsubstituted xylan, which has been found uniformly in other tissues. These results may be related to the phloem properties and xylan functions.

It has been reported that the mechanistic understanding of the contributions of diverse non-cellulosic polymers such as heteroxylan, XyG and MLG to cell wall properties and functions in growing organs is currently limited (Burton et al. 2010, Cosgrove and Jarvis 2012). Moreover, little is known of the distribution of non-cellulosic polysaccharides in the stem tissues of grasses. It has been reported that *in situ* labelling studies in maize stems that the unsubstituted xylans were more restricted to secondary cell walls (Suzuki et al. 2000). In rice stems, the LM10 -

unsubstituted xylan, LM11- xylan/arabinoxylan and LM12 -ferulated arabinoxylan epitopes have restricted occurrences relating to secondary cell walls (Zhang et al. 2012a). In this study in stems of *Miscanthus*, wheat and *B. distachyon*, the LM10/11/12 heteroxylan epitopes were widely detected in the epidermis, vascular bundles and parenchyma cell walls, with an increasing gradient in the older cell wall tissues, these are consistent with the former studies in maize and rice - heteroxylans present more in elder tissues. Among the three grass species, wheat stem cell walls contained the lowest detection levels of xylans as evidenced by the weak fluorescence intensity of LM10 and LM11 binding. Arabinoxylans represent the main xylan component of cereal grains (Ebringerova and Heinze 2000). Arabinoxylans cross-linked with other polysaccharides formed the skeletal framework of plant cell walls that gives tissue strength and integrity (Izydorczyk and Biliaderis 1995). Arabinoxylan accounts for about 20% of grass biomass, and some of the arabinose side chains may be ferulated therefore cross-linking with lignin and xylans (Kulkarni et al. 2012, Marcia 2009), and these complexes together with the other polysaccharide polymers and cellulose had been believed to be the important factors in the recalcitrance of biomass to release sugars (Himmel et al. 2007). Former studies on wheat straw suggested that the highest hydrolysis yields were obtained from the samples with lower xylan with di-ferulate content and high levels of cellulose (Holopainen-Mantila et al. 2013). Therefore, the xylan degradation in cell walls of grasses that used for bioethanol production should be further elucidated (Lygin et al. 2011). As the *B. distachyon* has a similar heteroxylan distribution to that of *Miscanthus* species and wheat, it is suggested in this study that *B. distachyon* could be a good model plant for the study of xylan degradation in grass cell walls in general. In summary in this project, the distribution of xylans in cell walls of the three grass species was uncovered, this will be beneficial for the enzymatic degradation of xylans, and therefore make contribution to their use as biofuels for industry. Specifically, for example, for the

purpose of generating xylan-related bioethnol from *M.* x *giganteus* stems, it is suggested by this study that older *M.* x *giganteus* tissues could require more specific enzymes to digest ferulated substitutions of heteroxylan.

It is now clear that MLG is widely present in the stems and other vegetative organs of grasses (Vega-Sánchez et al. 2013). Zhang et al suggested that in the organs that contain heteroxylans the MLG epitope is also widely distributed (Zhang et al. 2012a). In the three grass species, the MLG polysaccharide was detected more in sub-epidermal parenchyma regions (especially in *M.sacchariflorus*) as well as the younger cell wall tissues of the three grass species. Previous studies revealed that MLG appears transiently during cell elongation in growing tissues and accumulates in cell walls of the endosperm of certain grains such as maize and barley (Carpita and McCann 2010, Wilson et al. 2006). However, MLGs were abundant in both young and old regions of stems and more abundant in mature non-growing stem base regions of *Equisetum arvense*, a fern (Burton and Fincher 2009, Sørensen et al. 2008). Here in this study, the MLGs were abundant to the phloem and xylem regions in all five grass species, and also abundant in the parenchyma regions of *Miscanthus* species and *B. distachyon*, this might highlight the evolutionary diversity of MLGs between plant species. MLG is proposed to contribute to a higher extensibility in cell wall development of the early wheat grain development (Saulnier et al. 2012). In this study, it is observed that the MLGs decreased as the grasses (*Miscanthus*, wheat and *B. distachyon*) get older, and this result is also consistent with the former studies that MLGs are growth-stage dependent (Gibeaut et al. 2005, Wilson et al. 2006). These findings have important implications for our understanding of cell wall evolution, and also demonstrate that plant cell walls can be constructed in a way not previously envisaged (Sørensen et al. 2008).

For all of the five grass species, here we show that the major non-cellulosic and non-pectic polysaccharides, heteroxylans and MLG, contribute to a mosaic of occurrence in terms of stem anatomy with MLG being most abundantly detected in

regions of low heteroxylan detection. The complementary patterns of detection of heteroxylan and MLG are observed in terms of both stem anatomy and developmental stage with MLG being most readily detected (and heteroxylan less so) in regions of interfascicular parenchyma and in younger stem tissues. Furthermore, the LM18/19/20 pectic HG epitopes were broadly detected in the intercellular parenchyma spaces, and the LM20 methylesterified HG was also strongly bound to the pith parenchyma cell walls. It is of interest that pectic HG epitopes are also mostly detected in the MLG-rich interfascicular parenchyma regions and in this case the epitopes are often restricted to cell wall regions lining intercellular spaces. Pectic HG is known to occur at a low level in grasses and whether this is due to restriction to these cell wall regions or that pectic polymers occur in other cell wall regions and cannot be detected due to low abundance, structural differences or polymer masking is not yet known.

7.3 Cell wall polymer masking in grass type II cell walls

The work studied here indicates polymer masking is widely presented in cell walls of grass species. Xylanase removal of heteroxylan is effective in uncovering XyG, particularly in 50-day-old stems of *M.* x *giganteus, M. sacchariflorus,* wheat and *B. distachyon.* It is somewhat surprising to see this effect in the regions with low/absent LM10 xylan epitope detection - but this may indicate that only low levels of unsubstituted xylan are present in these locations and that these are effectively degraded to uncover the XyG. Grass heteroxylans/GAXs are complex polymers and all potential *Miscanthus,* wheat and *B. distachyon* GAX structural features, such as glucuronosyl substitutions, have not been assessed in this study due to a lack of a comprehensive set of probes. Recent work has, however, indicated that heteroxylan structure in *M.* x *giganteus* is comparable to that of other grasses (Kulkarni et al. 2012). It is of interest that for all of the three grass species, XyG is masked just by xylan (in regions where MLG is detected), whilst

pectic-galactan is observed to be masked, in similar regions, by both xylan and MLG. The current view of glycan masking is that it is indicative of microenvironments within cell wall architectures in which a possibly non-abundant glycan can be hidden from protein/enzyme access (Marcus et al. 2010). The differential enzymatic unmasking of XyG and galactan is likely to relate to aspects of cell wall architecture and the spatial connections between these sets of polymers and is therefore suggestive of a range of differing microenvironments within a cell wall. These unmasking experiments as well as the AGP polymer masking (pectin-unmasked AGPs, discussed in Chapter 6) were revealed after the enzymatic removal of polysaccharide could further indicate that the parenchyma regions with abundant MLG detection have highly distinctive cell wall architectures in which sets of polymers are specifically associated as aspects of wall architecture.

7.4 Summary

Heteroxylans and MLG are the most abundantly detected non-cellulosic polysaccharides in the five grass species studied above. Substituted arabinoxylans occur in the phloem cell walls of the three grass species. XyG showed subtle differences in occurrence in phloem and xylem regions among the three grass species, and XyG is masked by xylan in parenchyma cell walls. MLG was abundant in phloem, xylem and parenchyma regions of *Miscanthus* species and *B.distachyon*, it was more abundant in the sub-epidermal parenchyma cell walls of *M. sacchariflorus* which was correlated with low level of xylan detection, but with high level of HG detection, and this is consistent with the grass growth. Furthermore, in all the three grass species, pectic galactan is masked by both xylan and MLG, AGPs are masked by pectin in certain cell walls. As summarized above, the *B. distachyon* has a similar cell wall architecture to *Miscanthus* and wheat, and it is being considered as a good experimental model to observe the use of fast-growing biomass grasses in the context of biofuels and bioenergy (Gomez et al.

2008, Vogel 2008), and it could also be a useful model plant for the future understanding of grass cell wall modification. These polysaccharide distribution similarities and differences suggested that the different grass organs have distinct cell wall architecture that may relate to the cell wall properties and functions, and also genetic functions that have not yet been identified. This work is important for the understanding of grass cell wall diversity and properties and also to inform potential strategies for the efficient deconstruction of grass cell wall materials, which might also a contributor to the biofuel industry.

Chapter 8

References

Abedon BG, Hatfield RD, Tracy WF. 2006. Cell wall composition in juvenile and adult leaves of maize (*Zea mays* L.). Journal of Agricultural and Food Chemistry 54: 3896-3900.

Alejandro S, Lee Y, Tohge T, Sudre D, Osorio S, Park J, Bovet L, Lee Y, Geldner N, Fernie AR. 2012. AtABCG29 is a monolignol transporter involved in lignin biosynthesis. Current Biology 22: 1207-1212.

Allison GG, Morris C, Clifton-Brown J, Lister SJ, Donnison IS. 2011. Genotypic variation in cell wall composition in a diverse set of 244 accessions of *Miscanthus*. Biomass and Bioenergy 35: 4740-4747.

Amalraj VA, Balasundaram N. 2006. On the taxonomy of the members of 'Saccharum complex'. Genetic Resources and Crop Evolution 53: 35-41.

Anders N, Wilkinson MD, Lovegrove A, Freeman J, Tryfona T, Pellny TK, Weimar T, Mortimer JC, Stott K, Baker JM. 2012. Glycosyl transferases in family 61 mediate arabinofuranosyl transfer onto xylan in grasses. Proceedings of the National Academy of Sciences USA109: 989-993.

Anderson E, Arundale R, Maughan M, Oladeinde A, Wycislo A, Voigt T. 2011. Growth and agronomy of *Miscanthus* x *giganteus* for biomass production. Biofuels 2: 167-183.

Arsovski AA, Popma TM, Haughn GW, Carpita NC, McCann MC, Western TL. 2009. AtBXL1 encodes a bifunctional β-d-xylosidase/α-l-arabinofuranosidase required for pectic arabinan modification in *Arabidopsis* mucilage secretory cells. Plant Physiology 150: 1219-1234.

Atkinson RG, Schröder R, Hallett IC, Cohen D, MacRae EA. 2002. Overexpression of polygalacturonase in transgenic apple trees leads to a range of novel phenotypes involving changes in cell adhesion. Plant Physiology 129: 122-133.

Atmodjo MA, Hao Z, Mohnen D. 2013. Evolving views of pectin synthesis. Annual Review of Plant Biology 64: 747-779.

Atmodjo MA, Sakuragi Y, Zhu X, Burrell AJ, Mohanty SS, Atwood JA, Orlando R, Scheller HV, Mohnen D. 2011. Galacturonosyltransferase (GAUT) 1 and GAUT7 are the core of a plant cell wall pectin biosynthetic homogalacturonan: galacturonosyltransferase complex. Proceedings of the National Academy of Sciences USA 108: 20225-20230.

Bacic A, Stone B. 1981. Chemistry and organization of aleurone cell wall components from wheat and barley. Functional Plant Biology 8: 475-495.

Bacic A, Harris P, Stone BA. 1988. Structure and function of plant cell walls. The Biochemistry of Plants 14: 297-371.

Bar-Peled M, Urbanowicz BR, O'Neill MA. 2012. The synthesis and origin of the pectic polysaccharide rhamnogalacturonan II - insights from nucleotide sugar formation and diversity. Frontiers in Plant Science 3: 92.

Barkwoeth M, Anderton L, Capels K, Long S, Piep M. 2007. Manual of grasses for North America. HortScience 43: 968.

Baskin TI. 2001. On the alignment of cellulose microfibrils by cortical microtubules: a review and a model. Protoplasma 215: 150-171.

Baucher M, Monties B, Montagu MV, Boerjan W. 1998. Biosynthesis and genetic engineering of lignin. Critical Reviews in Plant Sciences 17: 125-197.

Baydoun E, Waldron KW, Brett CT. 1989. The interaction of xylosyltransferase and glucuronyltransferase involved in glucuronoxylan synthesis in pea (*Pisum sativum*) epicotyls. Biochemical Journal 257: 853.

Beeckman T, Przemeck GK, Stamatiou G, Lau R, Terryn N, De Rycke R, Inzé D, Berleth T. 2002. Genetic complexity of cellulose synthase A gene function in *Arabidopsis* embryogenesis. Plant Physiology 130: 1883-1893.

Beňová-Kákošová A, Digonnet C, Goubet F, Ranocha P, Jauneau A, Pesquet E, Barbier O, Zhang Z, Capek P, Dupree P. 2006. Galactoglucomannans increase cell population density and alter the protoxylem/metaxylem tracheary element ratio in xylogenic cultures of *Zinnia*. Plant Physiology 142: 696-709.

Berthet S, Demont-Caulet N, Pollet B, Bidzinski P, Cézard L, Le Bris P, Borrega N, Hervé J, Blondet E, Balzergue S. 2011. Disruption of LACCASE4 and 17 results in tissue-specific alterations to lignification of *Arabidopsis thaliana* stems. Plant Cell 23: 1124-1137.

Bevan MW, Garvin DF, Vogel JP. 2010. *Brachypodium distachyon* genomics for sustainable food and fuel production. Current Opinion in Biotechnology 21: 211-217.

Blake AW, McCartney L, Flint JE, Bolam DN, Boraston AB, Gilbert HJ, Knox JP. 2006. Understanding the biological rationale for the diversity of cellulose-directed carbohydrate-binding modules in prokaryotic enzymes. Journal of Biological Chemistry 281: 29321-29329.

Blevins DG, Lukaszewski KM. 1998. Boron in plant structure and function. Annual Review of Plant Biology 49: 481-500.

Boerjan W, Ralph J, Baucher M. 2003. Lignin biosynthesis. Annual Review of Plant Biology 54: 519-546.

Bolwell GP, Robbins MP, Dixon RA. 1985. Elicitor-induced prolyl hydroxylase from French bean (*Phaseolus vulgaris*). Localization, purification and properties. Biochemical Journal 229: 693.

Bonawitz ND, Chapple C. 2010. The genetics of lignin biosynthesis: connecting genotype to phenotype. Annual Review of Genetics 44: 337-363.

Boraston AB, Nurizzo D, Notenboom V, Ducros V, Rose DR, Kilburn DG, Davies GJ. 2002. Differential oligosaccharide recognition by evolutionarily-related β-1, 4 and β-1, 3 glucan-binding modules. Journal of Molecular Biology 319: 1143-1156.

Bouton S, Leboeuf E, Mouille G, Leydecker M-T, Talbotec J, Granier F, Lahaye M, Höfte H, Truong H-N. 2002. QUASIMODO1 encodes a putative membrane-bound glycosyltransferase required for normal pectin synthesis and cell adhesion in *Arabidopsis*. Plant Cell 14: 2577-2590.

Brennan CS, Cleary LJ. 2005. The potential use of cereal (1-3, 1-4)-β-D-glucans as functional food ingredients. Journal of Cereal Science 42: 1-13.

Brett CT. 2000. Cellulose microfibrils in plants: biosynthesis, deposition, and integration into the cell wall. International Review of Cytology 199: 161-199.

Brown D, Goubet F, Wong V, Goodacre R, Stephens E, Dupree P, Turner S. 2007. Comparison of five xylan synthesis mutants reveals new insight into the mechanisms of xylan synthesis. Plant Journal 52: 1154-1168.

Brown IE, Mallen MH, Charnock SJ, Davies GJ, Black GW. 2001. Pectate lyase 10A from *Pseudomonas cellulosa* is a modular enzyme containing a family 2a carbohydrate-binding module. Biochemical Journal 355: 155.

Brown RM. 2004. Cellulose structure and biosynthesis: what is in store for the 21st century? Journal of Polymer Science Part A: Polymer Chemistry 42: 487-495.

Buchanan BB, Gruissem W, Jones RL. 2000. Biochemistry & molecular biology of plants. New York, Wiley: 1367.

Buckeridge M, Pessoa dos Santos H, Tiné M. 2000. Mobilisation of storage cell wall polysaccharides in seeds. Plant Physiology and Biochemistry 38: 141-156.

Buckeridge MS. 2010. Seed cell wall storage polysaccharides: models to understand cell wall biosynthesis and degradation. Plant Physiology 154: 1017-1023.

Burton RA, Fincher GB. 2009. (1,3;1,4)-β-D-glucans in cell walls of the Poaceae, lower plants, and fungi: a tale of two linkages. Molecular Plant 2: 873-882.

Burton RA, Gidley MJ, Fincher GB. 2010. Heterogeneity in the chemistry, structure and function of plant cell walls. Nature Chemical Biology 6: 724-732.

Burton RA, Shirley NJ, King BJ, Harvey AJ, Fincher GB. 2004. The CesA gene family of barley. Quantitative analysis of transcripts reveals two groups of co-expressed genes. Plant Physiology 134: 224-236.

Burton RA, Jobling SA, Harvey AJ, Shirley NJ, Mather DE, Bacic A, Fincher GB. 2008. The genetics and transcriptional profiles of the cellulose synthase-like HvCslF gene family in barley. Plant Physiology 146: 1821-1833.

Burton RA, Gibeaut DM, Bacic A, Findlay K, Roberts K, Hamilton A, Baulcombe DC, Fincher GB. 2000. Virus-induced silencing of a plant cellulose synthase gene. Plant Cell 12: 691-705.

Burton RA, Collins HM, Kibble NAJ, Smith JA, Shirley NJ, Jobling SA, Henderson M, Singh RR, Pettolino F, Wilson SM. 2011. Over-expression of specific HvCslF cellulose synthase-like genes in transgenic barley increases

the levels of cell wall (1,3;1,4)-glucans and alters their fine structure. Plant Biotechnology Journal 9: 117-135.

Caffall KH, Mohnen D. 2009. The structure, function, and biosynthesis of plant cell wall pectic polysaccharides. Carbohydrate Research 344: 1879.

Cantarel BL, Coutinho PM, Rancurel C, Bernard T, Lombard V, Henrissat B. 2009. The carbohydrate-active enZymes database (CAZy): an expert resource for glycogenomics. Nucleic Acids Research 37: 233-238.

Capodicasa C, Vairo D, Zabotina O, McCartney L, Caprari C, Mattei B, Manfredini C, Aracri B, Benen J, Knox JP. 2004. Targeted modification of homogalacturonan by transgenic expression of a fungal polygalacturonase alters plant growth. Plant Physiology 135: 1294-1304.

Carpita NC. 1996. Structure and biogenesis of the cell walls of grasses. Annual Review of Plant Biology 47: 445-476.

Carpita NC, Whittern D. 1986. A highly substituted glucuronoarabinoxylan from developing maize coleoptiles. Carbohydrate Research 146: 129-140.

Carpita NC, Gibeaut D. 1993. Structural models of primary cell walls in flowering plants: consistency of molecular structure with the physical properties of the walls during growth. Plant Journal 3: 1-30.

Carpita NC, McCann MC. 2010. The maize mixed-linkage (1,3;1,4)-β-D-glucan polysaccharide is synthesized at the Golgi membrane. Plant Physiology 153: 1362-1371.

Carroll A, Somerville C. 2009. Cellulosic biofuels. Annual Review of Plant Biology 60: 165-182.

Cavalier DM, Keegstra K. 2006. Two xyloglucan xylosyltransferases catalyze the addition of multiple xylosyl residues to cellohexaose. Journal of Biological Chemistry 281: 34197-34207.

Cavalier DM, Lerouxel O, Neumetzler L, Yamauchi K, Reinecke A, Freshour G, Zabotina OA, Hahn MG, Burgert I, Pauly M. 2008. Disrupting two *Arabidopsis thaliana* xylosyltransferase genes results in plants deficient in xyloglucan, a major primary cell wall component. Plant Cell 20: 1519-1537.

Chabannes M, Ruel K, Yoshinaga A, Chabbert B, Jauneau A, Joseleau JP, Boudet AM. 2001. *In situ* analysis of lignins in transgenic tobacco reveals a differential impact of individual transformations on the spatial patterns of lignin deposition at the cellular and subcellular levels. Plant Journal 28: 271-282.

Chatterjee S, Mayor S. 2001. The GPI-anchor and protein sorting. Cellular and Molecular Life Sciences 58: 1969-1987.

Chiniquy D, Varanasi P, Oh T, Harholt J, Katnelson J, Singh S, Auer M, Simmons B, Adams PD, Scheller HV. 2013. Three novel rice genes closely related to the *Arabidopsis* IRX9, IRX9L, and IRX14 genes and their roles in xylan biosynthesis. Frontiers in Plant Science 4: 1-13.

Cho H-T, Kende H. 1997. Expansins and internodal growth of deepwater rice. Plant Physiology 113: 1145-1151.

Chrispeels MJ. 1984. Prolyl hydroxylase in plants. Methods in Enzymology 107: 361-369.

Christensen U, Alonso-Simon A, Scheller HV, Willats WG, Harholt J. 2010. Characterization of the primary cell walls of seedlings of *Brachypodium distachyon* - A potential model plant for temperate grasses. Phytochemistry 71: 62-69.

Christiaens S, Van Buggenhout S, Ngouémazong ED, Vandevenne E, Fraeye I, Duvetter T, Van Loey AM, Hendrickx ME. 2011. Anti-homogalacturonan antibodies: A way to explore the effect of processing on pectin in fruits and vegetables? Food Research International 44: 225-234.

Christiansen P, Andersen CH, Didion T, Folling M, Nielsen KK. 2005. A rapid and efficient transformation protocol for the grass *Brachypodium distachyon*. Plant Cell Reports 23: 751-758.

Chundawat SPS, Beckham GT, Himmel ME, Dale BE. 2011. Deconstruction of lignocellulosic biomass to fuels and chemicals. Annual Review of Chemical and Biomolecular Engineering 2: 121-145.

Clausen MH, Willats WG, Knox JP. 2003. Synthetic methyl hexagalacturonate hapten inhibitors of anti-homogalacturonan monoclonal antibodies LM7, JIM5 and JIM7. Carbohydrate Research 338: 1797-1800.

Clayton W, Renvoize S. 1986. Genera Graminum. Grasses of the world. (Kew, UK, Kew publishing).

Clifford MN. 1974. Specificity of acidic phloroglucinol reagents. Journal of Chromatography A 94: 321-324.

Clifton-Brown J, Lewandowski I. 2000. Overwintering problems of newly established *Miscanthus* plantations can be overcome by identifying genotypes with improved rhizome cold tolerance. New Phytologist 148: 287-294.

Clifton-Brown J, Chiang Y, Hodkinson T. 2008. *Miscanthus*: genetic resources and breeding potential to enhance bioenergy production. Genetic Improvement of Bioenergy Crops: 273-294.

Cocuron J-C, Lerouxel O, Drakakaki G, Alonso AP, Liepman AH, Keegstra K, Raikhel N, Wilkerson CG. 2007. A gene from the cellulose synthase-like C family encodes a β-1, 4 -glucan synthase. Proceedings of the National Academy of Sciences USA 104: 8550-8555.

Coimbra S, Costa M, Jones B, Mendes MA, Pereira LG. 2009. Pollen grain development is compromised in *Arabidopsis* agp6 agp11 null mutants. Journal of Experimental Botany 60: 3133-3142.

Cosgrove DJ. 2000. Loosening of plant cell walls by expansins. Nature 407: 321-326.

Cosgrove DJ. 2005. Growth of the plant cell wall. Nature Reviews Molecular Cell Biology 6: 850-861.

Cosgrove DJ, Jarvis MC. 2012. Comparative structure and biomechanics of plant primary and secondary cell walls. Frontiers in Plant Science 3: 204.

Coutinho PM, Deleury E, Davies GJ, Henrissat B. 2003. An evolving hierarchical family classification for glycosyltransferases. Journal of Molecular Biology 328: 307-317.

Dahlgren R. 1980. A revised system of classification of the angiosperms. Botanical Journal of the Linnean Society 80: 91-124.

Darvill A, McNeil M, Albersheim P, Delmer D. 1980a. The primary cell walls of flowering plants. Biochemistry of Plants 1: 91-162.

Darvill J, McNeil M, Darvill A, Albersheim P. 1980b. Structure of plant cell walls XI. Glucuronoarabinoxylan, a second hemicellulose in the primary cell walls of suspension-cultured sycamore cells. Plant Physiology 66: 1135-1139.

Davies LJ, Lilley CJ, Knox JP, Urwin P. 2012. Syncytia formed by adult female Heterodera schachtii in *Arabidopsis thaliana* roots have a distinct cell wall molecular architecture. New Phytologist 196: 238-246.

del Carmen Rodríguez-Gacio M, Iglesias-Fernández R, Carbonero P, Matilla ÁJ. 2012. Softening-up mannan-rich cell walls. Journal of Experimental Botany 63: 3976-3988.

Delmer DP, Amor Y. 1995. Cellulose biosynthesis. Plant Cell 7: 987.

Derbyshire P, McCann M, Roberts K. 2007. Restricted cell elongation in *Arabidopsis* hypocotyls is associated with a reduced average pectin esterification level. Plant Biology 7: 31.

Doblin MS, Pettolino FA, Wilson SM, Campbell R, Burton RA, Fincher GB, Newbigin E, Bacic A. 2009. A barley cellulose synthase-like CSLH gene mediates (1,3;1,4)-β-D-glucan synthesis in transgenic *Arabidopsis*. Proceedings of the National Academy of Sciences USA 106: 5996-6001.

Dohleman F, Long S. 2009. More productive than maize in the Midwest: how does *Miscanthus* do it? Plant Physiology 150: 2104-2115.

Dohleman F, Heaton E, Leakey A, Long S. 2009. Does greater leaf - level photosynthesis explain the larger solar energy conversion efficiency of *Miscanthus* relative to switchgrass? Plant, Cell & Environment 32: 1525-1537.

Donaldson LA. 2001. Lignification and lignin topochemistry - an ultrastructural view. Phytochemistry 57: 859-873.

Draper J, Mur LAJ, Jenkins G, Ghosh-Biswas GC, Bablak P, Hasterok R, Routledge APM. 2001. *Brachypodium distachyon*. A new model system for functional genomics in grasses. Plant Physiology 127: 1539.

Driouich A, Follet-Gueye M-L, Bernard S, Kousar S, Chevalier L, Vicré-Gibouin M, Lerouxel O. 2012. Golgi-mediated synthesis and secretion of matrix

polysaccharides of the primary cell wall of higher plants. Frontiers in Plant Science 3: 79.

Du H, Simpson RJ, Clarke AE, Bacic A. 1996. Molecular characterization of a stigma - specific gene encoding an arabinogalactan - protein (AGP) from *Nicotiana alata*. Plant Journal 9: 313-323.

Dunn G, Briggs K. 1989. Variation in culm anatomy among barley cultivars differing in lodging resistance. Canadian Journal of Botany 67: 1838-1843.

Ebringerova A, Heinze T. 2000. Xylan and xylan derivatives-biopolymers with valuable properties, 1. Naturally occurring xylans structures, isolation procedures and properties. Macromolecular Rapid Communications 21: 542-556.

Ebringerova A, Hromadkova Z, Heinze T. 2005. Hemicellulose. Advances in Polymer Science 186: 1-67.

Eda S, Kato K. 1980. Pectin isolated from the midrib of leaves of *Nicotiana tabacum*. Agricultural and Biological Chemistry 44: 2793-2801.

Edwards ME, Dickson CA, Chengappa S, Sidebottom C, Gidley MJ, Reid J. 1999. Molecular characterisation of a membrane - bound galactosyltransferase of plant cell wall matrix polysaccharide biosynthesis. Plant Journal 19: 691-697.

Egelund J, Damager I, Faber K, Olsen C-E, Ulvskov P, Petersen BL. 2008. Functional characterisation of a putative rhamnogalacturonan II specific xylosyltransferase. FEBS Letters 582: 3217-3222.

Egelund J, Petersen BL, Motawia MS, Damager I, Faik A, Olsen CE, Ishii T, Clausen H, Ulvskov P, Geshi N. 2006. *Arabidopsis thaliana* RGXT1 and RGXT2 encode Golgi-localized (1,3)-α-D-xylosyltransferases involved in the synthesis of pectic rhamnogalacturonan-II. Plant Cell 18: 2593-2607.

Ellis M, Egelund J, Schultz CJ, Bacic A. 2010. Arabinogalactan-Proteins: Key Regulators at the Cell Surface? Plant Physiology 153: 403-419.

Ennos A. 1993. The mechanics of the flower stem of the sedge Carex acutiformis. Annals of Botany 72: 123-127.

Ezaki N, Kido N, Takahashi K, Katou K. 2005. The role of wall Ca^{2+} in the regulation of wall extensibility during the acid-induced extension of soybean hypocotyl cell walls. Plant and Cell Physiology 46: 1831-1838.

Faik A. 2010. Xylan biosynthesis: news from the grass. Plant Physiology 153: 396-402.

Faik A, Abouzouhair J, Sarhan F. 2006. Putative fasciclin-like arabinogalactan-proteins (FLA) in wheat (*Triticum aestivum*) and rice (*Oryza sativa*): identification and bioinformatic analyses. Molecular Genetics and Genomics 276: 478-494.

Faik A, Price NJ, Raikhel NV, Keegstra K. 2002. An *Arabidopsis* gene encoding an α-xylosyltransferase involved in xyloglucan biosynthesis. Proceedings of the National Academy of Sciences USA 99: 7797-7802.

Fincher GB. 2009. Revolutionary times in our understanding of cell wall biosynthesis and remodeling in the grasses. Plant Physiology 149: 27-37.

Fincher GB, Stone B. 2004. Chemistry of nonstarch polysaccharides: In *Enchyclopedia* of Grain Science. Elsevier Academic Press.

Fincher GB, Stone BA, Clarke AE. 1983. Arabinogalactan-proteins: structure, biosynthesis, and function. Annual Review of Plant Physiology 34: 47-70.

Fischer JMC, Peterson CA, Bols N. 1985. A new fluorescent test for cell vitality using calcofluor white M2R. Biotechnic & Histochemistry 60: 69-79.

Fisher JB, French JC. 1976. The occurrence of intercalary and uninterrupted meristems in the internodes of tropical monocotyledons. American Journal of Botany 63: 510-525.

Franks PJ, Buckley TN, Shope JC, Mott KA. 2001. Guard cell volume and pressure measured concurrently by confocal microscopy and the cell pressure probe. Plant Physiology 125: 1577-1584.

Freshour G, Bonin CP, Reiter WD, Albersheim P, Darvill AG, Hahn MG. 2003. Distribution of fucose-containing xyloglucans in cell walls of the mur1 mutant of *Arabidopsis*. Plant Physiology 131: 1602-1612.

Fry SC, Nesselrode BH, Miller JG, Mewburn BR. 2008. Mixed-linkage-(1,3;1,4)-β-D-glucan is a major hemicellulose of *Equisetum* (horsetail) cell walls. New Phytologist 179: 104-115.

Gao M, Kieliszewski M, Lamport D, Showalter AM. 1999. Isolation, characterization and immunolocalization of a novel, modular tomato arabinogalactan-protein corresponding to the LeAGP-1 gene. Plant Journal 18: 43-55.

Gaspar YM, Nam J, Schultz CJ, Lee L-Y, Gilson PR, Gelvin SB, Bacic A. 2004. Characterization of the *Arabidopsis* lysine-rich arabinogalactan-protein AtAGP17 mutant (rat1) that results in a decreased efficiency of Agrobacterium transformation. Plant Physiology 135: 2162-2171.

Gibeaut DM, Pauly M, Bacic A, Fincher GB. 2005. Changes in cell wall polysaccharides in developing barley (*Hordeum vulgare*) coleoptiles. Planta 221: 729-738.

Gille S, de Souza A, Xiong G, Benz M, Cheng K, Schultink A, Reca I-B, Pauly M. 2011. *O*-acetylation of *Arabidopsis* hemicellulose xyloglucan requires AXY4 or AXY4L, proteins with a TBL and DUF231 domain. Plant Cell 23: 4041-4053.

Glinsky VV, Raz A. 2009. Modified citrus pectin anti-metastatic properties: one bullet, multiple targets. Carbohydrate Research 344: 1788-1791.

Głowacka K. 2011. A review of the genetic study of the energy crop *Miscanthus*. Biomass and Bioenergy 35: 2445-2454.

Goldberg RB. 1988. Plants: novel developmental processes. Science 240: 1460-1467.

Gomez LD, Bristow JK, Statham ER, McQueen-Mason SJ. 2008. Analysis of saccharification in *Brachypodium distachyon* stems under mild conditions of hydrolysis. Biotechnology for Biofuels 1: 1-12.

Gordon AH, Lomax JA, Dalgarno K, Chesson A. 1985. Preparation and composition of mesophyll, epidermis and fibre cell walls from leaves of perennial ryegrass (*Lolium perenne*) and Italian ryegrass (*Lolium multiflorum*). Journal of the Science of Food and Agriculture 36: 509-519.

Goubet F, Misrahi A, Park SK, Zhang Z, Twell D, Dupree P. 2003. AtCSLA7, a cellulose synthase-like putative glycosyltransferase, is important for pollen tube growth and embryogenesis in *Arabidopsis*. Plant Physiology 131: 547-557.

Goubet F, Barton CJ, Mortimer JC, Yu X, Zhang Z, Miles GP, Richens J, Liepman AH, Seffen K, Dupree P. 2009. Cell wall glucomannan in *Arabidopsis* is synthesised by CSLA glycosyltransferases, and influences the progression of embryogenesis. Plant Journal 60: 527-538.

Greef J, Deuter M. 1993. Syntaxonomy of *Miscanthus* x *giganteus* GREEF et DEU. Angewandte Botanik 67: 87-90.

Guillon F, Bouchet B, Jamme F, Robert P, Quéméner B, Barron C, Larré C, Dumas P, Saulnier L. 2011. *Brachypodium distachyon* grain: characterization of endosperm cell walls. Journal of Experimental Botany 62: 1001-1015.

Halpin C, Knight ME, Foxon GA, Campbell MM, Boudet AM, Boon JJ, Chabbert B, Tollier MT, Schuch W. 1994. Manipulation of lignin quality by downregulation of cinnamyl alcohol dehydrogenase. Plant Journal 6: 339-350.

Hamann T, Osborne E, Youngs HL, Misson J, Nussaume L, Somerville C. 2004. Global expression analysis of CESA and CSL genes in *Arabidopsis*. Cellulose 11: 279-286.

Hamman KD, Williamson RL, Steffler ED, Wright CT, Hess JR, Pryfogle PA. 2005. Structural analysis of wheat stems. Applied Biochemistry and Biotechnology 121: 71-80.

Han M, Kim Y, Koo B-c, Choi G-W. 2011. Bioethanol production by *Miscanthus* as a lignocellulosic biomass: Focus on high efficiency conversion to glucose and ethanol. BioResources 6: 1939-1953.

Handakumbura PP, Matos DA, Osmont KS, Harrington MJ, Heo K, Kafle K, Kim SH, Baskin TI, Hazen SP. 2013. Perturbation of *Brachypodium distachyon* CELLULOSE SYNTHASE A4 or 7 results in abnormal cell walls. Plant Biology 13: 131.

Handford MG, Baldwin TC, Goubet F, Prime TA, Miles J, Yu X, Dupree P. 2003. Localisation and characterisation of cell wall mannan polysaccharides in *Arabidopsis thaliana*. Planta 218: 27-36.

Harholt J, Suttangkakul A, Vibe Scheller H. 2010. Biosynthesis of pectin. Plant Physiology 153: 384-395.

Harholt J, Jensen JK, Sørensen SO, Orfila C, Pauly M, Scheller HV. 2006. ARABINAN DEFICIENT 1 is a putative arabinosyltransferase involved in biosynthesis of pectic arabinan in *Arabidopsis*. Plant Physiology 140: 49-58.

Harholt J, Jensen JK, Verhertbruggen Y, Søgaard C, Bernard S, Nafisi M, Poulsen CP, Geshi N, Sakuragi Y, Driouich A. 2012. ARAD proteins associated with pectic arabinan biosynthesis form complexes when transiently overexpressed in planta. Planta 236: 115-128.

Harpaz-Saad S, Western TL, Kieber JJ. 2012. The FEI2-SOS5 pathway and CELLULOSE SYNTHASE 5 are required for cellulose biosynthesis in the *Arabidopsis* seed coat and affect pectin mucilage structure. Plant Signaling & Behavior 7: 285-288.

Harrington BJ, Raper KB. 1968. Use of a fluorescent brightener to demonstrate cellulose in the cellular slime molds. Applied Microbiology 16: 106-113.

Harris PJ, Smith BG. 2006. Plant cell walls and cell wall polysaccharides: structures, properties and uses in food products. International Journal of Food Science & Technology 41: 129-143.

Harris PJ, Trethewey JA. 2010. The distribution of ester-linked ferulic acid in the cell walls of angiosperms. Phytochemistry Reviews 9: 19-33.

Harris PJ, Kelderman MR, Kendon MF, McKenzie RJ. 1997. Monosaccharide compositions of unlignified cell walls of monocotyledons in relation to the occurrence of wall-bound ferulic acid. Biochemical Systematics and Ecology 25: 167-179.

Hasterok R, Draper J, Jenkins G. 2004. Laying the cytotaxonomic foundations of a new model grass, *Brachypodium distachyon* (L.) Beauv. Chromosome Research 12: 397-403.

Hayashi T, Marsden MP, Delmer DP. 1987. Pea xyloglucan and cellulose VI. Xyloglucan-cellulose interactions in vitro and in vivo. Plant Physiology 83: 384-389.

Heaton EA, Dohleman F, Long S. 2008. Meeting US biofuel goals with less land: the potential of *Miscanthus*. Global Change Biology 14: 2000-2014.

Heaton EA, Long SP, Voigt TB, Jones MB, Clifton-Brown J. 2004. *Miscanthus* for renewable energy generation: European Union experience and projections for Illinois. Mitigation and Adaptation Strategies for Global Change 9: 433-451.

Hendrix J. 1983. Phloem function: an integrated view. What's New in Plant Physiology 14: 45-48.

Herrero J, Fernández-Pérez F, Yebra T, Novo-Uzal E, Pomar F, Pedreño MÁ, Cuello J, Guéra A, Esteban-Carrasco A, Zapata JM. 2013. Bioinformatic and functional characterization of the basic peroxidase 72 from *Arabidopsis thaliana* involved in lignin biosynthesis. Planta 237: 1599-1612.

Herth W. 1983. Arrays of plasma-membrane “rosettes” involved in cellulose microfibril formation of *Spirogyra*. Planta 159: 347-356.

Hervé C, Rogowski A, Gilbert HJ, Knox JP. 2009. Enzymatic treatments reveal differential capacities for xylan recognition and degradation in primary and secondary plant cell walls. Plant Journal 58: 413-422.

Hervé C, Rogowski A, Blake AW, Marcus SE, Gilbert HJ, Knox JP. 2010. Carbohydrate-binding modules promote the enzymatic deconstruction of intact plant cell walls by targeting and proximity effects. Proceedings of the National Academy of Sciences USA 107: 293-298.

Hieta R, Myllyharju J. 2002. Cloning and characterization of a low molecular weight prolyl 4-hydroxylase from *Arabidopsis thaliana* effective hydroxylation of proline-rich, collagen-like, and hypoxia-inducible transcription factor α-like peptides. Journal of Biological Chemistry 277: 23965-23971.

Himmel ME, Ding S-Y, Johnson DK, Adney WS, Nimlos MR, Brady JW, Foust TD. 2007. Biomass recalcitrance: engineering plants and enzymes for biofuels production. Science 315: 804-807.

Hodgson E, Lister S, Bridgwater A, Clifton-Brown J, Donnison I. 2010a. Genotypic and environmentally derived variation in the cell wall composition of *Miscanthus* in relation to its use as a biomass feedstock. Biomass and Bioenergy 34: 652-660.

Hodgson E, Nowakowski D, Shield I, Riche A, Bridgwater A, Clifton-Brown J, Donnisona I. 2011. Variation in *Miscanthus* chemical composition and implications for conversion by pyrolysis and thermo-chemical bio-refining for fuels and chemicals. Bioresource Technology 102: 3411-3418.

Hodgson E, Fahmi R, Yates N, Barraclough T, Shield I, Allison G, Bridgwater A, Donnison I. 2010b. *Miscanthus* as a feedstock for fast-pyrolysis: Does agronomic treatment affect quality? Bioresource Technology 101: 6185-6191.

Hodkinson TR, Chase MW, Takahashi C, Leitch IJ, Bennett MD, Renvoize SA. 2002. The use of DNA sequencing (ITS and trnL-F), AFLP, and fluorescent in situ hybridization to study allopolyploid *Miscanthus* (Poaceae). American Journal of Botany 89: 279-286.

Holland N, Holland D, Helentjaris T, Dhugga KS, Xoconostle-Cazares B, Delmer DP. 2000. A comparative analysis of the plant cellulose synthase (CesA) gene family. Plant Physiology 123: 1313-1324.

Holopainen-Mantila U, Marjamaa K, Merali Z, Käsper A, Bot Pd, Jääskeläinen A-S, Waldron K, Kruus K, Tamminen T. 2013. Impact of hydrothermal pre-treatment to chemical composition, enzymatic digestibility and spatial distribution of cell wall polymers. Bioresource Technology 138.

Hongo S, Sato K, Yokoyama R, Nishitani K. 2012. Demethylesterification of the primary wall by Pectin Methylesterase35 provides mechanical support to the *Arabidopsis* stem. Plant Cell 24: 2624-2634.

Hughes J, McCully ME. 1975. The use of an optical brightener in the study of plant structure. Biotechnic & Histochemistry 50: 319-329.

Imeson A. 1997. Thickening and gelling agents for food. Blackie Acabemic and Professional: 66.

Immerzeel P, Eppink MM, De Vries SC, Schols HA, Voragen AG. 2006. Carrot arabinogalactan proteins are interlinked with pectins. Physiologia Plantarum 128: 18-28.

Ishii T. 1997. Structure and functions of feruloylated polysaccharides. Plant Science 127: 111-127.

Ishii T, Matsunaga T. 2001. Pectic polysaccharide rhamnogalacturonan II is covalently linked to homogalacturonan. Phytochemistry 57: 969-974.

Ishii T, Ohnishi-Kameyama M, Ono H. 2004. Identification of elongating β-1, 4-galactosyltransferase activity in mung bean (*Vigna radiata*) hypocotyls using 2-aminobenzaminated 1, 4-linked β-D-galactooligosaccharides as acceptor substrates. Planta 219: 310-318.

Ishii T, Ono H, Ohnishi-Kameyama M, Maeda I. 2005a. Enzymic transfer of α-L-arabinopyranosyl residues to exogenous 1,4-linked β-D-galacto-oligosaccharides using solubilized mung bean (*Vigna radiata*) hypocotyl microsomes and UDP-β-L-arabinopyranose. Planta 221: 953-963.

Ishii T, Konishi T, Ito Y, Ono H, Ohnishi-Kameyama M, Maeda I. 2005b. A β-(1-3)-arabinopyranosyltransferase that transfers a single arabinopyranose onto arabino-oligosaccharides in mung bean (*Vigna radiate*) hypocotyls. Phytochemistry 66: 2418-2425.

Iwai H, Masaoka N, Ishii T, Satoh S. 2002. A pectin glucuronyltransferase gene is essential for intercellular attachment in the plant meristem. Proceedings of the National Academy of Sciences USA 99: 16319-16324.

Iwai H, Hokura A, Oishi M, Chida H, Ishii T, Sakai S, Satoh S. 2006. The gene responsible for borate cross-linking of pectin Rhamnogalacturonan-II is required for plant reproductive tissue development and fertilization. Proceedings of the National Academy of Sciences USA 103: 16592-16597.

Izydorczyk MS, Biliaderis CG. 1995. Cereal arabinoxylans: advances in structure and physicochemical properties. Carbohydrate Polymers 28: 33-48.

Jackson CL, Dreaden TM, Theobald LK, Tran NM, Beal TL, Eid M, Gao MY, Shirley RB, Stoffel MT, Kumar MV. 2007. Pectin induces apoptosis in human prostate cancer cells: correlation of apoptotic function with pectin structure. Glycobiology 17: 805-819.

Jarvis MC, Apperley DC. 1995. Chain conformation in concentrated pectic gels: evidence from ^{13}C NMR. Carbohydrate Research 275: 131-145.

Jensen JK, Sørensen SO, Harholt J, Geshi N, Sakuragi Y, Møller I, Zandleven J, Bernal AJ, Jensen NB, Sørensen C. 2008. Identification of a xylogalacturonan xylosyltransferase involved in pectin biosynthesis in *Arabidopsis*. Plant Cell 20: 1289-1302.

Jensen WA. 1962. Botanical histochemistry: Principles and Practices. W.H. Freeman & Co., San Francisco & London. pp 408.

Jones L, Seymour GB, Knox JP. 1997. Localization of pectic galactan in tomato cell walls using a monoclonal antibody specific to (1-4)-β-D-galactan. Plant Physiology 113: 1405-1412.

Jones L, Ennos AR, Turner SR. 2001. Cloning and characterization of irregular xylem4 (irx4): a severely lignin - deficient mutant of *Arabidopsis*. Plant Journal 26: 205-216.

Jordan DB, Bowman MJ, Braker JD, Dien BS, Hector RE, Lee CC, Mertens JA, Wagschal K. 2012. Plant cell walls to ethanol. Biochemical Journal 442: 241.

Jørgensen U. 1997. Genotypic variation in dry matter accumulation and content of N, K and Cl in *Miscanthus* in Denmark. Biomass and Bioenergy 12: 155-169.

Kaack K, Schwarz KU, Brander PE. 2003. Variation in morphology, anatomy and chemistry of stems of *Miscanthus* genotypes differing in mechanical properties. Industrial Crops and Products 17: 131-142.

Kabel M, Carvalheiro F, Garrote G, Avgerinos E, Koukios E, Parajó J, Gırio F, Schols H, Voragen A. 2002. Hydrothermally treated xylan rich by-products yield different classes of xylo-oligosaccharides. Carbohydrate Polymers 50: 47-56.

Kato Y, Nevins DJ. 1984. Structure of the arabinogalactan from *Zea* shoots. Plant Physiology 74: 562-568.

Keegstra K. 2010. Plant Cell Walls. Plant Physiology 154: 483-486.

Keegstra K, Talmadge KW, Bauer W, Albersheim P. 1973. The structure of plant cell walls III. A model of the walls of suspension-cultured sycamore cells based on the interconnections of the macromolecular components. Plant Physiology 51: 188-197.

Kelley JJ, Tsai AC. 1978. Effect of pectin, gum arabic and agar on cholesterol absorption, synthesis, and turnover in rats. The Journal of Nutrition 108: 630-639.

Kellogg EA. 2001. Evolutionary history of the grasses. Plant Physiology 125: 1198-1205.

Kiefer LL, York WS, Darvill AG, Albersheim P. 1989. Xyloglucan isolated from suspension-cultured sycamore cell walls is O-acetylated. Phytochemistry 28: 2105-2107.

Kim JS, Daniel G. 2012. Distribution of glucomannans and xylans in poplar xylem and their changes under tension stress. Planta 236: 35-50.

Kimura S, Laosinchai W, Itoh T, Cui X, Linder CR, Brown RM. 1999. Immunogold labeling of rosette terminal cellulose-synthesizing complexes in the vascular plant *Vigna angularis*. Plant Cell 11: 2075-2085.

Kitazawa K, Tryfona T, Yoshimi Y, Hayashi Y, Kawauchi S, Antonov L, Tanaka H, Takahashi T, Kaneko S, Dupree P. 2013. β-galactosyl Yariv reagent binds to

the β-1, 3-galactan of arabinogalactan proteins. Plant Physiology 161: 1117-1126.

Knox JP, Linstead P, Cooper JP, Roberts K. 1991. Developmentally regulated epitopes of cell surface arabinogalactan proteins and their relation to root tissue pattern formation. Plant Journal 1: 317-326.

Knox JP. 1997. The use of antibodies to study the architecture and developmental regulation of plant cell walls. International Review of Cytology 171: 79-120.

Knox JP. 2008. Mapping the walls of the kingdom: the view from the horsetails. New Phytologist 179: 1-3.

Kohorn BD, Johansen S, Shishido A, Todorova T, Martinez R, Defeo E, Obregon P. 2009. Pectin activation of MAP kinase and gene expression is WAK2 dependent. Plant Journal 60: 974-982.

Konieczny R, Świerczyńska J, Czaplicki AZ, Bohdanowicz J. 2007. Distribution of pectin and arabinogalactan protein epitopes during organogenesis from androgenic callus of wheat. Plant Cell Reports 26: 355-363.

Konishi T, Takeda T, Miyazaki Y, Ohnishi-Kameyama M, Hayashi T, O'Neill MA, Ishii T. 2007. A plant mutase that interconverts UDP-arabinofuranose and UDP-arabinopyranose. Glycobiology 17: 345-354.

Krupková E, Immerzeel P, Pauly M, Schmülling T. 2007. The TUMOROUS SHOOT DEVELOPMENT2 gene of *Arabidopsis* encoding a putative methyltransferase is required for cell adhesion and co-ordinated plant development. Plant Journal 50: 735-750.

Kulkarni AR, Pattathil S, Hahn MG, York WS, O'Neill MA. 2012. Comparison of arabinoxylan structure in bioenergy and model grasses. Industrial Biotechnology 8: 222-229.

Laemmli UK. 1970. Cleavage of structural proteins during the assembly of the head of bacteriophage T4. Nature 227: 680-685.

Lalanne E, Honys D, Johnson A, Borner GH, Lilley KS, Dupree P, Grossniklaus U, Twell D. 2004. SETH1 and SETH2, two components of the glycosylphosphatidylinositol anchor biosynthetic pathway, are required for pollen germination and tube growth in *Arabidopsis*. Plant Cell 16: 229-240.

Lamport DT, Kieliszewski MJ, Showalter AM. 2006. Salt stress upregulates periplasmic arabinogalactan proteins: using salt stress to analyse AGP function. New Phytologist 169: 479-492.

Le Ngoc Huyen T, Rémond C, Dheilly R, Chabbert B. 2010. Effect of harvesting date on the composition and saccharification of *Miscanthus* x *giganteus*. Bioresource Technology 101: 8224-8231.

Leboeuf E, Guillon F, Thoiron S, Lahaye M. 2005. Biochemical and immunohistochemical analysis of pectic polysaccharides in the cell walls of *Arabidopsis* mutant QUASIMODO 1 suspension-cultured cells: implications for cell adhesion. Journal of Experimental Botany 56: 3171-3182.

Lee C, O'Neill MA, Tsumuraya Y, Darvill AG, Ye Z-H. 2007a. The irregular xylem9 mutant is deficient in xylan xylosyltransferase activity. Plant and Cell Physiology 48: 1624-1634.

Lee C, Zhong R, Richardson EA, Himmelsbach DS, McPhail BT, Ye Z-H. 2007b. The PARVUS gene is expressed in cells undergoing secondary wall thickening and is essential for glucuronoxylan biosynthesis. Plant and Cell Physiology 48: 1659-1672.

Lee KJD, Sakata Y, Mau S-L, Pettolino F, Bacic A, Quatrano RS, Knight CD, Knox JP. 2005a. Arabinogalactan proteins are required for apical cell extension in the moss *Physcomitrella* patens. Plant Cell 17: 3051-3065.

Lee KJD, Cornuault V, Manfield I, Ralet M, Knox JP. 2013. Multiscale spatial heterogeneity of pectic rhamnogalacturonan-I (RG-I) structural features in tobacco seed endosperm cell walls. Plant Journal 75: 1018-1027.

Lee KJD, Sakata Y, Mau S-L, Pettolino F, Bacic A, Quatrano RS, Knight CD, Knox JP. 2005b. Arabinogalactan proteins are required for apical cell extension in the moss *Physcomitrella* patens. Plant Cell 17: 3051-3065.

Lee KJD, Dekkers BJ, Steinbrecher T, Walsh CT, Bacic A, Bentsink L, Leubner-Metzger G, Knox JP. 2012. Distinct cell wall architectures in seed endosperms in representatives of the Brassicaceae and Solanaceae. Plant Physiology 160: 1551-1566.

Leroux O, Knox JP, Masschaele B, Bagniewska-Zadworna A, Marcus SE, Claeys M, Van Hoorebeke L, Viane R. 2011. An extensin-rich matrix lines the carinal canals in *Equisetum ramosissimum*, which may function as water-conducting channels. Annals of Botany 108: 307-319.

Leroux O, Leroux F, Mastroberti AA, Santos-Silva F, Van Loo D, Bagniewska-Zadworna A, Van Hoorebeke L, Bals S, Popper ZA, de Araujo Mariath JE. 2013. Heterogeneity of silica and glycan-epitope distribution in epidermal idioblast cell walls in *Adiantum raddianum* laminae. Planta 237: 1453-1464.

Lerouxel O, Cavalier DM, Liepman AH, Keegstra K. 2006. Biosynthesis of plant cell wall polysaccharides - a complex process. Current Opinion in Plant Biology 9: 621-630.

Lewandowski I, Clifton-Brown J, Scurlock J, Huisman W. 2000. *Miscanthus*: European experience with a novel energy crop. Biomass and Bioenergy 19: 209-227.

Lewandowski I, Scurlock JMO, Lindvall E, Christou M. 2003. The development and current status of perennial rhizomatous grasses as energy crops in the US and Europe. Biomass and Bioenergy 25: 335-361.

Li X, Cordero I, Caplan J, Mølhøj M, Reiter W-D. 2004. Molecular analysis of 10 coding regions from *Arabidopsis* that are homologous to the MUR3 xyloglucan galactosyltransferase. Plant Physiology 134: 940-950.

Liepman AH, Wilkerson CG, Keegstra K. 2005. Expression of cellulose synthase-like (Csl) genes in insect cells reveals that CslA family members encode mannan synthases. Proceedings of the National Academy of Sciences USA 102: 2221-2226.

Liepman AH, Nairn CJ, Willats WG, Sørensen I, Roberts AW, Keegstra K. 2007. Functional genomic analysis supports conservation of function among cellulose synthase-like A gene family members and suggests diverse roles of mannans in plants. Plant Physiology 143: 1881-1893.

Liu XL, Liu L, Niu QK, Xia C, Yang KZ, Li R, Chen LQ, Zhang XQ, Zhou Y, Ye D. 2011. MALE GAMETOPHYTE DEFECTIVE 4 encodes a rhamnogalacturonan II xylosyltransferase and is important for growth of pollen tubes and roots in *Arabidopsis*. Plant Journal 65: 647-660.

Liwanag AJM, Ebert B, Verhertbruggen Y, Rennie EA, Rautengarten C, Oikawa A, Andersen MC, Clausen MH, Scheller HV. 2012. Pectin biosynthesis: GALS1 in *Arabidopsis thaliana* is a β-1,4-galactan β-1,4-galactosyltransferase. Plant Cell 24: 5024-5036.

Lygin AV, Upton J, Dohleman FG, Juvik J, Zabotina OA, Widholm JM, Lozovaya VV. 2011. Composition of cell wall phenolics and polysaccharides of the potential bioenergy crop - *Miscanthus*. Global Change Biology Bioenergy 3: 333-345.

MacAdam JW, Grabber JH. 2002. Relationship of growth cessation with the formation of diferulate cross-links and ρ-coumaroylated lignins in tall fescue leaf blades. Planta 215: 785-793.

MacAdam JW, Kerley MS, Sisson DW. 1996. Tiller development influences seasonal change in cell wall digestibility of big bluestem (*Andropogon gerardii*). Journal of the Science of Food and Agriculture 70: 79-88.

MacMillan CP, Mansfield SD, Stachurski ZH, Evans R, Southerton SG. 2010. Fasciclin-like arabinogalactan proteins: specialization for stem biomechanics and cell wall architecture in *Arabidopsis* and *Eucalyptus*. Plant Journal 62: 689-703.

Macquet A, Ralet M-C, Loudet O, Kronenberger J, Mouille G, Marion-Poll A, North HM. 2007. A naturally occurring mutation in an *Arabidopsis* accession affects a β-D-galactosidase that increases the hydrophilic potential of rhamnogalacturonan I in seed mucilage. Plant Cell 19: 3990-4006.

Madson M, Dunand C, Li X, Verma R, Vanzin GF, Caplan J, Shoue DA, Carpita NC, Reiter W-D. 2003. The MUR3 gene of *Arabidopsis* encodes a xyloglucan galactosyltransferase that is evolutionarily related to animal exostosins. Plant Cell 15: 1662-1670.

Maeda Y, Awano T, Takabe K, Fujita M. 2000. Immunolocalization of glucomannans in the cell wall of differentiating tracheids in *Chamaecyparis obtusa*. Protoplasma 213: 148-156.

Mahendran T, Williams P, Phillips G, Al-Assaf S, Baldwin T. 2008. New insights into the structural characteristics of the arabinogalactan - protein (AGP) fraction of gum arabic. Journal of Agricultural and Food Chemistry 56: 9269-9276.

Majewska-Sawka A, Nothnagel EA. 2000. The multiple roles of arabinogalactan proteins in plant development. Plant Physiology 122: 3-10.

Manfield IW, Orfila C, McCartney L, Harholt J, Bernal AJ, Scheller HV, Gilmartin PM, Mikkelsen JD, Knox JP, Willats WG. 2004. Novel cell wall architecture of isoxaben-habituated *Arabidopsis* suspension-cultured cells: global transcript profiling and cellular analysis. Plant Journal 40: 260-275.

Marcia MdO. 2009. Feruloylation in grasses: current and future perspectives. Molecular Plant 2: 861-872.

Marcus SE, Verhertbruggen Y, Hervé C, Ordaz-Ortiz JJ, Farkas V, Pedersen HL, Willats WGT, Knox JP. 2008. Pectic homogalacturonan masks abundant sets of xyloglucan epitopes in plant cell walls. BMC Plant Biology 8: 60.

Marcus SE, Blake AW, Benians TAS, Lee KJD, Poyser C, Donaldson L, Leroux O, Rogowski A, Petersen HL, Boraston A. 2010. Restricted access of proteins to mannan polysaccharides in intact plant cell walls. Plant Journal 64: 191-203.

Martel P, Gould JM. 1990. Cellulose stability and delignification after alkaline hydrogen peroxide treatment of straw. Journal of Applied Polymer Science 39: 707-714.

Matos DA. 2012. Rhythmic Growth and Vascular Development in *Brachypodium Distachyon.* University of Massachusetts.

Matsunaga T, Ishii T, Matsumoto S, Higuchi M, Darvill A, Albersheim P, O'Neill MA. 2004. Occurrence of the primary cell wall polysaccharide rhamnogalacturonan II in pteridophytes, lycophytes, and bryophytes. Implications for the evolution of vascular plants. Plant Physiology 134: 339-351.

Mau SL, Chen CG, Pu ZY, Moritz RL, Simpson RJ, Bacic A, Clarke AE. 1995. Molecular cloning of cDNAs encoding the protein backbones of arabinogalactan - proteins from the filtrate of suspension - cultured cells of *Pyrus communis* and *Nicotiana alata*. Plant Journal 8: 269-281.

McCartney L, Marcus S, Knox JP. 2005. Monoclonal antibodies to plant cell wall xylans and arabinoxylans. Journal of Histochemistry & Cytochemistry 53: 543.

McCartney L, Ormerod AP, Gidley MJ, Knox JP. 2000. Temporal and spatial regulation of pectic (1-4)-β-D-galactan in cell walls of developing pea cotyledons: implications for mechanical properties. Plant Journal 22: 105-113.

McCartney L, Blake AW, Flint J, Bolam DN, Boraston AB, Gilbert HJ, Knox JP. 2006. Differential recognition of plant cell walls by microbial xylan-specific

carbohydrate-binding modules. Proceedings of the National Academy of Sciences USA 103: 4765-4770.

McDougall GJ. 1988. Inhibition of auxin-stimulated growth of pea stem segments by a specific nonasaccharide of xyloglucan. Planta 175: 412-416.

McDougall GJ, Fry SC. 1989. Structure-activity relationships for xyloglucan oligosaccharides with antiauxin activity. Plant Physiology 89: 883-887.

McNeil M, Darvill AG, Fry SC, Albersheim P. 1984. Structure and function of the primary cell walls of plants. Annual Review of Biochemistry 53: 625-663.

Meikle PJ, Hoogenraad NJ, Bonig I, Clarke AE, Stone BA. 1994. A (1-3,1-4)-β-D-glucan specific monoclonal antibody and its use in the quantitation and immunocytochemical location of (1-3,1-4)-β-D-glucan. Plant Journal 5: 1-9.

Miao Y, Li H-Y, Shen J, Wang J, Jiang L. 2011. QUASIMODO 3 (QUA3) is a putative homogalacturonan methyltransferase regulating cell wall biosynthesis in *Arabidopsis* suspension-cultured cells. Journal of Experimental Botany 62: 5063-5078.

Miao YC, Liu CJ. 2010. ATP- binding cassette-like transporters are involved in the transport of lignin precursors across plasma and vacuolar membranes. Proceedings of the National Academy of Sciences USA 107: 22728-22733.

Mishra A, Malhotra AV. 2009. *Tamarind* xyloglucan: a polysaccharide with versatile application potential. Journal of Materials Chemistry 19: 8528-8536.

Mitchell RA, Dupree P, Shewry PR. 2007. A novel bioinformatics approach identifies candidate genes for the synthesis and feruloylation of arabinoxylan. Plant Physiology 144: 43-53.

Mohnen D. 2008. Pectin structure and biosynthesis. Current Opinion in Plant Biology 11: 266-277.

Molinari H, Pellny T, Freeman J, Shewry P, Mitchell R. 2013. Grass cell wall feruloylation: distribution of bound ferulate and candidate gene expression in *Brachypodium distachyon*. Frontiers in Plant Science 4: 50.

Moller I, Sørensen I, Bernal AJ, Blaukopf C, Lee K, Øbro J, Pettolino F, Roberts A, Mikkelsen JD, Knox JP. 2007. Hig-throughput mapping of cell wall polymers within and between plants using novel microarrays. Plant Journal 50: 1118-1128.

Moller I, Marcus SE, Haeger A, Verhertbruggen Y, Verhoef R, Schols H, Ulvskov P, Mikkelsen JD, Knox JP, Willats W. 2008. High-throughput screening of monoclonal antibodies against plant cell wall glycans by hierarchical clustering of their carbohydrate microarray binding profiles. Glycoconjugate Journal 25: 37-48.

Mollet J-C, Leroux C, Dardelle F, Lehner A. 2013. Cell wall composition, biosynthesis and remodeling during pollen tube growth. Plants 2: 107-147.

Montanier C, van Bueren AL, Dumon C, Flint JE, Correia MA, Prates JA, Firbank SJ, Lewis RJ, Grondin GG, Ghinet MG. 2009. Evidence that family 35 carbohydrate binding modules display conserved specificity but divergent function. Proceedings of the National Academy of Sciences USA 106: 3065-3070.

Morrison T, Jung H, Buxton D, Hatfield R. 1998. Cell-wall composition of maize internodes of varying maturity. Crop Science 38: 455-460.

Mouille G, Ralet MC, Cavelier C, Eland C, Effroy D, Hematy K, McCartney L, Truong HN, Gaudon V, Thibault JF. 2007. Homogalacturonan synthesis in *Arabidopsis thaliana* requires a Golgi - localized protein with a putative methyltransferase domain. Plant Journal 50: 605-614.

Murray AK, Nichols RL, Sassenrath-Cole GF. 2001. Cell wall biosynthesis: glycan containing oligomers in developing cotton fibers, cotton fabric, wood and paper. Phytochemistry 57: 975-986.

Naidu SL, Moose SP, Al-Shoaibi AK, Raines CA, Long SP. 2003. Cold tolerance of C4 photosynthesis in *Miscanthus* x *giganteus*: adaptation in amounts and sequence of C4 photosynthetic enzymes. Plant Physiology 132: 1688-1697.

Naran R, Chen G, Carpita NC. 2008. Novel rhamnogalacturonan I and arabinoxylan polysaccharides of flax seed mucilage. Plant Physiology 148: 132-141.

Nemeth C, Freeman J, Jones HD, Sparks C, Pellny TK, Wilkinson MD, Dunwell J, Andersson AA, Åman P, Guillon F. 2010. Down-regulation of the CSLF6 gene results in decreased (1,3;1,4)-β-D-glucan in endosperm of wheat. Plant Physiology 152: 1209-1218.

Nguyen QB, Itoh K, Van Vu B, Tosa Y, Nakayashiki H. 2011. Simultaneous silencing of endo-β-1,4 xylanase genes reveals their roles in the virulence of *Magnaporthe oryzae*. Molecular Microbiology 81: 1008-1019.

Niklas KJ. 1990. The mechanical significance of clasping leaf sheaths in grasses: evidence from two cultivars of Avena sativa. Annals of Botany 65: 505-512.

Niklas KJ. 1991. Bending stiffness of cylindrical plant organs with a 'core-rind' construction: evidence from Juncus effusus leaves. American Journal of Botany: 561-568.

Notenboom V, Boraston AB, Chiu P, Freelove AC, Kilburn DG, Rose DR. 2001. Recognition of cello-oligosaccharides by a family 17 carbohydrate-binding module: an X-ray crystallographic, thermodynamic and mutagenic study. Journal of Molecular Biology 314: 797-806.

Nothnagel EA. 1997. Proteoglycans and related components in plant cells. International Review of Cytology 174: 195-291.

Nunan KJ, Scheller HV. 2003. Solubilization of an arabinan arabinosyltransferase activity from mung bean hypocotyls. Plant Physiology 132: 331-342.

O'Neill MA, Ishii T, Albersheim P, Darvill AG. 2004. Rhamnogalacturonan II: structure and function of a borate cross-linked cell wall pectic polysaccharide. Annual Review of Plant Biology 55: 109-139.

O'Neill MA, Albersheim P, Darvill A. 1990. The pectic polysaccharides of primary cell walls. Methods in Plant Biochemistry 2: 415-441.

O'Sullivan. 1997. Cellulose: the structure slowly unravels. Cellulose 4: 173-207.

Øbro J, Harholt J, Scheller HV, Orfila C. 2004. Rhamnogalacturonan I in *Solanum tuberosum* tubers contains complex arabinogalactan structures. Phytochemistry 65: 1429-1438.

Ochoa-Villarreal M, Aispuro-Hernández E, Vargas-Arispuro I, Martínez-Téllez MÁ. 2012. Plant cell wall polymers: function, structure and biological activity of their derivatives. *In* Gomes, A.D.S., ed, Polymerization. InTech.

Odzuck W, Kauss H. 1972. Biosynthesis of pure araban and xylan. Phytochemistry 11: 2489-2494.

Ogawa M, Kay P, Wilson S, Swain SM. 2009. *Arabidopsis* dehiscence zone polygalacturonase1 (ADPG1), ADPG2, and QUARTET2 are polygalacturonases required for cell separation during reproductive development in *Arabidopsis*. Plant Cell: 216-233.

Oka T, Saito F, Shimma Y-i, Yoko-o T, Nomura Y, Matsuoka K, Jigami Y. 2010. Characterization of endoplasmic reticulum-localized UDP-D-galactose: hydroxyproline O-galactosyltransferase using synthetic peptide substrates in *Arabidopsis*. Plant Physiology 152: 332-340.

Olsen AN, Ernst HA, Leggio LL, Skriver K. 2005. NAC transcription factors: structurally distinct, functionally diverse. Trends in Plant Science 10: 79-87.

Opanowicz M, Hands P, Betts D, Parker ML, Toole GA, Mills EC, Doonan JH, Drea S. 2011. Endosperm development in *Brachypodium distachyon*. Journal of Experimental Botany 62: 735-748.

Orfila C, Knox JP. 2000. Spatial regulation of pectic polysaccharides in relation to pit fields in cell walls of tomato fruit pericarp. Plant Physiology 122: 775-782.

Orfila C, Seymour GB, Willats WG, Huxham IM, Jarvis MC, Dover CJ, Thompson AJ, Knox JP. 2001. Altered middle lamella homogalacturonan and disrupted deposition of (1-5)-α-l-arabinan in the pericarp of *Cnr*, a ripening mutant of tomato. Plant Physiology 126: 210-221.

Orfila C, Sørensen SO, Harholt J, Geshi N, Crombie H, Truong H-N, Reid JG, Knox JP, Scheller HV. 2005. QUASIMODO1 is expressed in vascular tissue of *Arabidopsis thaliana* inflorescence stems, and affects homogalacturonan and xylan biosynthesis. Planta 222: 613-622.

Paredez AR, Somerville CR, Ehrhardt DW. 2006. Visualization of cellulose synthase demonstrates functional association with microtubules. Science 312: 1491-1495.

Park MH, Suzuki Y, Chono M, Knox JP, Yamaguchi I. 2003. CsAGP1, a gibberellin-responsive gene from cucumber hypocotyls, encodes a classical arabinogalactan protein and is involved in stem elongation. Plant Physiology 131: 1450-1459.

Parker D, Beckmann M, Enot DP, Overy DP, Rios ZC, Gilbert M, Talbot N, Draper J. 2008. Rice blast infection of *Brachypodium distachyon* as a model system to study dynamic host/pathogen interactions. Nature Protocols 3: 435-445.

Pauly M, Porchia A, Olsen CE, Nunan KJ, Scheller HV. 2000. Enzymatic synthesis and purification of uridine diphospho-β-l-arabinopyranose, a substrate for the biosynthesis of plant polysaccharides. Analytical Biochemistry 278: 69-73.

Pauly M, Qin Q, Greene H, Albersheim P, Darvill A, York WS. 2001. Changes in the structure of xyloglucan during cell elongation. Planta 212: 842-850.

Pauly M, Gille S, Liu L, Mansoori N, de Souza A, Schultink A, Xiong G. 2013. Hemicellulose biosynthesis. Planta 238: 627-642.

Pedersen HL, Fangel JU, McCleary B, Ruzanski C, Rydahl MG, Ralet M-C, Farkas V, von Schantz L, Marcus SE, Andersen MC. 2012. Versatile high resolution oligosaccharide microarrays for plant glycobiology and cell wall research. Journal of Biological Chemistry 287: 39429-39438.

Pell G, Williamson MP, Walters C, Du H, Gilbert HJ, Bolam DN. 2003. Importance of hydrophobic and polar residues in ligand binding in the family 15 carbohydrate-binding module from *Cellvibrio japonicus* Xyn10C. Biochemistry 42: 9316-9323.

Pellerin P, Vidal S, Williams P, Brillouet J-M. 1995. Characterization of five type II arabinogalactan-protein fractions from red wine of increasing uronic acid content. Carbohydrate Research 277: 135-143.

Peña MJ, Darvill AG, Eberhard S, York WS, O'Neill MA. 2008. Moss and liverwort xyloglucans contain galacturonic acid and are structurally distinct from the xyloglucans synthesized by hornworts and vascular plants. Glycobiology 18: 891-904.

Peña MJ, Zhong R, Zhou G-K, Richardson EA, O'Neill MA, Darvill AG, York WS, Ye Z-H. 2007. *Arabidopsis* irregular xylem8 and irregular xylem9: implications for the complexity of glucuronoxylan biosynthesis. Plant Cell 19: 549-563.

Pennell RI, Knox JP, Scofield GN, Selvendran RR, Roberts K. 1989. A family of abundant plasma membrane-associated glycoproteins related to the arabinogalactan proteins is unique to flowering plants. Journal of Cell Biology 108: 1967-1977.

Perrin RM, DeRocher AE, Bar-Peled M, Zeng W, Norambuena L, Orellana A, Raikhel NV, Keegstra K. 1999. Xyloglucan fucosyltransferase, an enzyme involved in plant cell wall biosynthesis. Science 284: 1976-1979.

Persson S, Paredez A, Carroll A, Palsdottir H, Doblin M, Poindexter P, Khitrov N, Auer M, Somerville CR. 2007. Genetic evidence for three unique

components in primary cell-wall cellulose synthase complexes in *Arabidopsis*. Proceedings of the National Academy of Sciences USA 104: 15566-15571.

Petersen BL, Egelund J, Damager I, Faber K, Jensen JK, Yang Z, Bennett EP, Scheller HV, Ulvskov P. 2009. Assay and heterologous expression in *Pichia pastoris* of plant cell wall type-II membrane anchored glycosyltransferases. Glycoconjugate Journal 26: 1235-1246.

Pettolino F, Sasaki I, Turbic A, Wilson SM, Bacic A, Hrmova M, Fincher GB. 2009. Hyphal cell walls from the plant pathogen *Rhynchosporium secalis* contain (1,3;1,6)-β-D-glucans, galacto-and rhamno-mannans,(1,3;1,4)-β-D-glucans and chitin. FEBS Journal 276: 3698-3709.

Philippe S, Saulnier L, Guillon F. 2006. Arabinoxylan and (1,3;14)-β-glucan deposition in cell walls during wheat endosperm development. Planta 224: 449-461.

Pilarska M, Knox JP, Konieczny R. 2013. Arabinogalactan-protein and pectin epitopes in relation to an extracellular matrix surface network and somatic embryogenesis and callogenesis in *Trifolium nigrescens* Viv. Plant Cell, Tissue and Organ Culture 115: 35-44.

Piquemal J, Lapierre C, Myton K, O'connell A, Schuch W, Grima-pettenati J, Boudet AM. 1998. Down-regulation of cinnamoyl-CoA reductase induces significant changes of lignin profiles in transgenic tobacco plants. Plant Journal 13: 71-83.

Popper ZA, Fry SC. 2003. Primary cell wall composition of bryophytes and charophytes. Annals of Botany 91: 1-12.

Popper ZA. 2005. Widespread occurrence of a covalent linkage between xyloglucan and acidic polysaccharides in suspension-cultured angiosperm cells. Annals of Botany 96: 91-99.

Popper ZA. 2008. Xyloglucan - pectin linkages are formed intra-protoplasmically, contribute to wall-assembly, and remain stable in the cell wall. Planta 227: 781-794.

Popper ZA, Michel G, Hervé C, Domozych DS, Willats WG, Tuohy MG, Kloareg B, Stengel DB. 2011. Evolution and diversity of plant cell walls: from algae to flowering plants. Annual Review of Plant Biology 62: 567-590.

Porchia AC, Sørensen SO, Scheller HV. 2002. Arabinoxylan biosynthesis in wheat. Characterization of arabinosyltransferase activity in Golgi membranes. Plant Physiology 130: 432-441.

Purdy SJ, Maddison AL, Jones LE, Webster RJ, Andralojc J, Donnison I, Clifton-Brown J. 2013. Characterization of chilling-shock responses in four genotypes of *Miscanthus* reveals the superior tolerance of *M.*x *giganteus* compared with *M. sinensis* and *M. sacchariflorus*. Annals of Botany 111: 999-1013.

Qi W, Fong C, Lamport DT. 1991. Gum arabic glycoprotein is a twisted hairy rope: a new model based on *O*-Galactosylhydroxyproline as the polysaccharide attachment site. Plant Physiology 96: 848-855.

Rafińska K, Bednarska E. 2011. Localisation pattern of homogalacturonan and arabinogalactan proteins in developing ovules of the gymnosperm plant *Larix decidua Mill*. Sexual Plant Reproduction 24: 75-87.

Ragauskas AJ, Williams CK, Davison BH, Britovsek G, Cairney J, Eckert CA, Frederick WJ, Hallett JP, Leak DJ, Liotta CL. 2006. The path forward for biofuels and biomaterials. Science 311: 484-489.

Ralet M-C, André-Leroux G, Quéméner B, Thibault J-F. 2005. Sugar beet (*Beta vulgaris*) pectins are covalently cross-linked through diferulic bridges in the cell wall. Phytochemistry 66: 2800-2814.

Ralet M-C, Crépeau M-J, Lefèbvre J, Mouille G, Höfte H, Thibault J-F. 2008. Reduced number of homogalacturonan domains in pectins of an *Arabidopsis* mutant enhances the flexibility of the polymer. Biomacromolecules 9: 1454-1460.

Ralet M, Tranquet O, Poulain D, Moïse A, Guillon F. 2010. Monoclonal antibodies to rhamnogalacturonan I backbone. Planta 231: 1373-1383.

Ralph J, Grabber JH, Hatfield RD. 1995. Lignin-ferulate cross-links in grasses: active incorporation of ferulate polysaccharide esters into ryegrass lignins. Carbohydrate Research 275: 167-178.

Rancour DM, Marita JM, Hatfield RD. 2012. Cell wall composition throughout development for the model grass *Brachypodium distachyon*. Frontiers in Plant Science 3: 266.

Renard C, Weightman R, Thibault J-F. 1997. The xylose-rich pectins from pea hulls1. International Journal of Biological Macromolecules 21: 155-162.

Ridley BL, O'Neill MA, Mohnen D. 2001. Pectins: structure, biosynthesis, and oligogalacturonide-related signaling. Phytochemistry 57: 929-967.

Roach MJ, Mokshina NY, Badhan A, Snegireva AV, Hobson N, Deyholos MK, Gorshkova TA. 2011. Development of cellulosic secondary walls in flax fibers requires β-galactosidase. Plant Physiology 156: 1351-1363.

Robbins MP, Evans G, Valentine J, Donnison IS, Allison GG. 2012. New opportunities for the exploitation of energy crops by thermochemical conversion in Northern Europe and the UK. Progress in Energy and Combustion Science 38: 138-155.

Rolando M, Valente C. 2007. Establishing the tolerability and performance of *tamarind* seed polysaccharide (TSP) in treating dry eye syndrome: results of a clinical study. BMC Ophthalmology 7: 5.

Rolin C, De Vries J. 1990. Pectin. Food Gels: 401-434.

Rose JKC, Lee SJ. 2010. Straying off the highway: trafficking of secreted plant proteins and complexity in the plant cell wall proteome. Plant Physiology 153: 433-436.

Rubin EM. 2008. Genomics of cellulosic biofuels. Nature 454: 841-845.

Rudall P. 1992. Anatomy of flowering plants: an introduction to structure and development. Cambridge University Press, Cambridge.

Sanchez C, Schmitt C, Kolodziejczyk E, Lapp A, Gaillard C, Renard D. 2008. The acacia gum arabinogalactan fraction is a thin oblate ellipsoid: a new model based on small-angle neutron scattering and Ab initio calculation. Biophysical Journal 94: 629-639.

Sarkanen KV, Ludwig CH, ed. 1971. Lignins: occurrence, formation, structure and reactions. New York: Wiley, 916.

Sarossy Z, Blomfeldt TO, Hedenqvist MS, Koch CB, Ray SS, Plackett D. 2012. Composite films of arabinoxylan and fFibrous sepiolite: morphological, mechanical, and barrier properties. ACS Applied Materials & Interfaces 4: 3378-3386.

Saulnier L, Guillon F, Chateigner-Boutin A-L. 2012. Cell wall deposition and metabolism in wheat grain. Journal of Cereal Science 56: 91-108.

Savatin DV, Ferrari S, Sicilia F, De Lorenzo G. 2011. Oligogalacturonide-auxin antagonism does not require posttranscriptional gene silencing or stabilization of auxin response repressors in *Arabidopsis*. Plant Physiology 157: 1163-1174.

Saxena IM, Brown RM. 2005. Cellulose biosynthesis: current views and evolving concepts. Annals of Botany 96: 9-21.

Scally L, Hodkinson T, Jones M. 2001. Origins and taxonomy of *Miscanthus*. *Miscanthus* for Energy And Fibre. London: James & James: 1-9.

Scheller HV, Ulvskov P. 2010. Hemicelluloses. Annual Review of Plant Biology 61: 263-289.

Scheller HV, Doong RL, Ridley BL, Mohnen D. 1999. Pectin biosynthesis: a solubilized α1, 4-galacturonosyltransferase from tobacco catalyzes the transfer of galacturonic acid from UDP-galacturonic acid onto the non-reducing end of homogalacturonan. Planta 207: 512-517.

Schmidt L, Jøker D. 2001. Glossary of seed biology and technology. Danida Forest Seed Centre: 35.

Schultz CJ, Johnson KL, Currie G, Bacic A. 2000. The classical arabinogalactan protein gene family of Arabidopsis. Plant Cell 12: 1751-1767.

Schultz CJ, Rumsewicz MP, Johnson KL, Jones BJ, Gaspar YM, Bacic A. 2002. Using genomic resources to guide research directions. The arabinogalactan protein gene family as a test case. Plant Physiology 129: 1448-1463.

Seifert GJ, Roberts K. 2007. The biology of arabinogalactan proteins. Annual Review of Plant Biology 58: 137-161.

Shantz H. 1954. The place of grasslands in the Earth's cover. Ecology 35: 143-145.

Shi Y, Draper J, Stace C. 1993. Ribosomal DNA variation and its phylogenetic implication in the genus *Brachypodium* (Poaceae). Plant Systematics and Evolution 188: 125-138.

Showalter AM. 1993. Structure and function of plant cell wall proteins. Plant Cell 5: 9-23.

Showalter AM. 2001. Arabinogalactan-proteins: structure, expression and function. Cellular and Molecular Life Sciences 58: 1399-1417.

Siedlecka A, Wiklund S, Péronne M-A, Micheli F, Leśniewska J, Sethson I, Edlund U, Richard L, Sundberg B, Mellerowicz EJ. 2008. Pectin methyl esterase inhibits intrusive and symplastic cell growth in developing wood cells of *Populus*. Plant Physiology 146: 554-565.

Silva GB, Ionashiro M, Carrara TB, Crivellari AC, Tiné MA, Prado J, Carpita NC, Buckeridge MS. 2011. Cell wall polysaccharides from fern leaves: Evidence for a mannan-rich Type III cell wall in *Adiantum raddianum*. Phytochemistry 72: 2352-2360.

Simpson PJ, Xie H, Bolam DN, Gilbert HJ, Williamson MP. 2000. The structural basis for the ligand specificity of family 2 carbohydrate-binding modules. Journal of Biological Chemistry 275: 41137-41142.

Singh B, Avci U, Inwood SEE, Grimson MJ, Landgraf J, Mohnen D, Sørensen I, Wilkerson CG, Willats WG, Haigler CH. 2009. A specialized outer layer of the primary cell wall joins elongating cotton fibers into tissue-like bundles. Plant Physiology 150: 684-699.

Smallwood M, Yates EA, Willats WG, Martin H, Knox JP. 1996. Immunochemical comparison of membrane-associated and secreted arabinogalactan-proteins in rice and carrot. Planta 198: 452-459.

Smith BG, Harris PJ. 1999. The polysaccharide composition of Poales cell walls: Poaceae cell walls are not unique. Biochemical Systematics and Ecology 27: 33-53.

Smole MS, Kreže T, Strnad S, Kleinschek KS, Hribernik S. 2005. Characterisation of grass fibres. Journal of Materials Science 40: 5349-5353.

Somerville C. 2006. Cellulose synthesis in higher plants. Annual Review of Cell and Developmental Biology 22: 53.

Somerville C, Youngs H, Taylor C, Davis SC, Long SP. 2010. Feedstocks for lignocellulosic biofuels. Science 329: 790-792.

Somerville C, Bauer S, Brininstool G, Facette M, Hamann T, Milne J, Osborne E, Paredez A, Persson S, Raab T. 2004. Toward a systems approach to understanding plant cell walls. Science 306: 2206-2211.

Sørensen I, Pettolino FA, Wilson SM, Doblin MS, Johansen B, Bacic A, Willats WG. 2008. Mixed-linkage-(1-3),(1-4)-β-D-glucan is not unique to the Poales and is an abundant component of *Equisetum arvense* cell walls. Plant Journal 54: 510-521.

Sterling JD, Atmodjo MA, Inwood SE, Kolli VK, Quigley HF, Hahn MG, Mohnen D. 2006. Functional identification of an *Arabidopsis* pectin biosynthetic homogalacturonan galacturonosyltransferase. Proceedings of the National Academy of Sciences USA 103: 5236-5241.

Suliman M, Chateigner-Boutin A, Francin-Allami M, Partier A, Bouchet B, Salse J, Pont C, Marion J, Rogniaux H, Tessier D. 2012. Identification of glycosyltransferases involved in cell wall synthesis of wheat endosperm. Journal of Proteomics 78: 508-521.

Sumathi S, Ray AR. 2002. Release behaviour of drugs from *tamarind* seed polysaccharide tablets. Journal of Pharmacy & Pharmaceutical Sciences 5: 12-18.

Sun Y, Cheng J. 2002. Hydrolysis of lignocellulosic materials for ethanol production: a review. Bioresource Technology 83: 1-11.

Suzuki K, Kitamura S, Kato Y, Itoh T. 2000. Highly substituted glucuronoarabinoxylans (hsGAXs) and low-branched xylans show a distinct localization pattern in the tissues of *Zea mays* L. Plant and Cell Physiology 41: 948-959.

Suzuki S, Li L, Sun Y-H, Chiang VL. 2006. The cellulose synthase gene superfamily and biochemical functions of xylem-specific cellulose synthase-like genes in *Populus trichocarpa*. Plant Physiology 142: 1233-1245.

Taketa S, Yuo T, Tonooka T, Tsumuraya Y, Inagaki Y, Haruyama N, Larroque O, Jobling SA. 2012. Functional characterization of barley betaglucanless mutants demonstrates a unique role for CslF6 in (1,3;1,4)-β-D-glucan biosynthesis. Journal of Experimental Botany 63: 381-392.

Tan L, Showalter AM, Egelund J, Hernandez-Sanchez A, Doblin MS, Bacic A. 2012. Arabinogalactan-proteins and the research challenges for these enigmatic plant cell surface proteoglycans. Frontiers in Plant Science 3: 140.

Tan L, Eberhard S, Pattathil S, Warder C, Glushka J, Yuan C, Hao Z, Zhu X, Avci U, Miller JS. 2013. An *Arabidopsis* cell wall proteoglycan consists of pectin and arabinoxylan covalently linked to an arabinogalactan protein. Plant Cell 25: 270-287.

Tang H, Belton PS, Ng A, Ryden P. 1999. ^{13}C MAS NMR studies of the effects of hydration on the cell walls of potatoes and chinese water chestnuts. Journal of Agricultural and Food Chemistry 47: 510-517.

Taylor NG. 2008. Cellulose biosynthesis and deposition in higher plants. New Phytologist 178: 239-252.

Taylor NG, Laurie S, Turner SR. 2000. Multiple cellulose synthase catalytic subunits are required for cellulose synthesis in *Arabidopsis*. Plant Cell 12: 2529-2539.

Tiainen P, Myllyharju J, Koivunen P. 2005. Characterization of a second *Arabidopsis thaliana* prolyl 4-hydroxylase with distinct substrate specificity. Journal of Biological Chemistry 280: 1142-1148.

Topping D. 2007. Cereal complex carbohydrates and their contribution to human health. Journal of Cereal Science 46: 220-229.

Tsai C-J, Popko JL, Mielke MR, Hu W-J, Podila GK, Chiang VL. 1998. Suppression of O-methyltransferase gene by homologous sense transgene in quaking aspen causes red-brown wood phenotypes. Plant Physiology 117: 101-112.

Valdivia ER, Herrera MT, Gianzo C, Fidalgo J, Revilla G, Zarra I, Sampedro J. 2013. Regulation of secondary wall synthesis and cell death by NAC transcription factors in the monocot *Brachypodium distachyon*. Journal of Experimental Botany 64: 1333-1343.

Vanzin GF, Madson M, Carpita NC, Raikhel NV, Keegstra K, Reiter W-D. 2002. The mur2 mutant of *Arabidopsis thaliana* lacks fucosylated xyloglucan because of a lesion in fucosyltransferase AtFUT1. Proceedings of the National Academy of Sciences USA 99: 3340-3345.

Vega-Sánchez ME, Verhertbruggen Y, Scheller HV, Ronald P. 2013. Abundance of mixed linkage glucan in mature tissues and secondary cell walls of grasses. Plant Signaling & Behavior 8: e23143.

Vega-Sánchez ME, Verhertbruggen Y, Christensen U, Chen X, Sharma V, Varanasi P, Jobling SA, Talbot M, White RG, Joo M. 2012. Loss of Cellulose synthase-like F6 function affects mixed-linkage glucan deposition, cell wall mechanical properties, and defense responses in vegetative tissues of rice. Plant Physiology 159: 56-69.

Verhertbruggen Y, Marcus SE, Haeger A, Ordaz-Ortiz JJ, Knox JP. 2009a. An extended set of monoclonal antibodies to pectic homogalacturonan. Carbohydrate Research 344: 1858-1862.

Verhertbruggen Y, Marcus SE, Haeger A, Verhoef R, Schols HA, McCleary BV, McKee L, Gilbert HJ, Knox JP. 2009b. Developmental complexity of arabinan polysaccharides and their processing in plant cell walls. Plant Journal 59: 413-425.

Vicré M, Jauneau A, Knox JP, Driouich A. 1998. Immunolocalization of β-(1-4) and β-(1-6)-D-galactan epitopes in the cell wall and Golgi stacks of developing flax root tissues. Protoplasma 203: 26-34.

Vietor R, Kormelink F, Angelino S, Voragen A. 1994. Substitution patterns of water-unextractable arabinoxylans from barley and malt. Carbohydrate Polymers 24: 113-118.

Vincken J-P, York WS, Beldman G, Voragen A. 1997. Two general branching patterns of xyloglucan, XXXG and XXGG. Plant Physiology 114: 9-13.

Vinkx C, Delcour J. 1996. Rye (*Secale cereale*L.) Arabinoxylans: A Critical Review. Journal of Cereal Science 24: 1-14.

Vogel JP. 2008. Unique aspects of the grass cell wall. Current Opinion in Plant Biology 11: 301-307.

Vogel JP, Bragg J. 2009. *Brachypodium distachyon*, a new model for the Triticeae. Genetics and Genomics of the Triticeae: 427-449.

Vogel JP, Garvin D, Leong O, Hayden D. 2006a. Agrobacterium-mediated transformation and inbred line development in the model grass *Brachypodium distachyon*. Plant Cell, Tissue and Organ Culture 84: 199-211.

Vogel JP, Gu YQ, Twigg P, Lazo GR, Laudencia-Chingcuanco D, Hayden DM, Donze TJ, Vivian LA, Stamova B, Coleman-Derr D. 2006b. EST sequencing and phylogenetic analysis of the model grass *Brachypodium distachyon*. Theoretical and Applied Genetics 113: 186-195.

von Konrat MJ, Renner M, S derstr m L, Hagborg A, Mutke J. 2008. Early land plants today: liverwort species diversity and the relationship with higher taxonomy and higher plants. Fieldiana Botany 2: 87-102.

Vorwerk S, Somerville S, Somerville C. 2004. The role of plant cell wall polysaccharide composition in disease resistance. Trends in Plant Science 9: 203-209.

Wang D, Naidu S, Portis A, Moose S, Long S. 2008. Can the cold tolerance of C4 photosynthesis in *Miscanthus* x *giganteus* relative to *Zea mays* be explained by differences in activities and thermal properties of Rubisco? Journal of Experimental Botany 59: 1779-1787.

Wang J, Zhu J, Lin Q, Li X, Teng N, Li Z, Li B, Zhang A, Lin J. 2006. Effects of stem structure and cell wall components on bending strength in wheat. Chinese Science Bulletin 51: 815-823.

Wang Y, Mortimer JC, Davis J, Dupree P, Keegstra K. 2013. Identification of an additional protein involved in mannan biosynthesis. Plant Journal 73: 105-117.

Watson L, Dallwitz MJ. 1988. Grass genera of the world: illustrations of characters, descriptions, classification, interactive identification, information retrieval with microfiches, and floppy disks for MS-DOS microcomputers. Australian National University, Research School of Biological Sciences, Canberra.

Wende G, Fry SC. 1997. 2-O-β-d-xylopyranosyl-(5-O-feruloyl)-l-arabinose, a widespread component of grass cell walls. Phytochemistry 44: 1019-1030.

Wilder BM, Albersheim P. 1973. The structure of plant cell walls IV. A structural comparison of the wall hemicellulose of cell suspension cultures of sycamore (*Acer PseudoPlatAnus*) and of red kidney bean (*Phaseolus Vulgaris*). Plant Physiology 51: 889-893.

Willats WG, Marcus SE, Knox JP. 1998. Generation of a monoclonal antibody specific to (1-5)-α-L-arabinan. Carbohydrate Research 308: 149-152.

Willats WG, Knox JP, Mikkelsen JD. 2006. Pectin: new insights into an old polymer are starting to gel. Trends in Food Science & Technology 17: 97-104.

Willats WG, Steele-King CG, Marcus SE, Knox JP. 1999. Side chains of pectic polysaccharides are regulated in relation to cell proliferation and cell differentiation. Plant Journal 20: 619-628.

Willats WG, McCartney L, Mackie W, Knox JP. 2001a. Pectin: cell biology and prospects for functional analysis. Plant Molecular Biology 47: 9-27.

Willats WG, Orfila C, Limberg G, Buchholt HC, van Alebeek G-JW, Voragen AG, Marcus SE, Christensen TM, Mikkelsen JD, Murray BS. 2001b. Modulation of the degree and pattern of methyl-esterification of pectic homogalacturonan in plant cell walls implications for pectin methyl esterase action, matrix properties, and cell adhesion. Journal of Biological Chemistry 276: 19404-19413.

Willats WG, McCartney L, Steele-King CG, Marcus SE, Mort A, Huisman M, van Alebeek G-J, Schols HA, Voragen AG, Le Goff A. 2004. A xylogalacturonan epitope is specifically associated with plant cell detachment. Planta 218: 673-681.

Willför S, Sundberg K, Tenkanen M, Holmbom B. 2008. Spruce-derived mannans - A potential raw material for hydrocolloids and novel advanced natural materials. Carbohydrate Polymers 72: 197-210.

Wilson SM, Burton RA, Doblin MS, Stone BA, Newbigin EJ, Fincher GB, Bacic A. 2006. Temporal and spatial appearance of wall polysaccharides during cellularization of barley (*Hordeum vulgare*) endosperm. Planta 224: 655-667.

Wolf S, Mouille G, Pelloux J. 2009. Homogalacturonan methyl-esterification and plant development. Molecular Plant 2: 851-860.

Wu AM, Hörnblad E, Voxeur A, Gerber L, Rihouey C, Lerouge P, Marchant A. 2010a. Analysis of the *Arabidopsis* IRX9/IRX9-L and IRX14/IRX14-L pairs of glycosyltransferase genes reveals critical contributions to biosynthesis of the hemicellulose glucuronoxylan. Plant Physiology 153: 542-554.

Wu AM, Rihouey C, Seveno M, Hörnblad E, Singh S, Matsunaga T, Ishii T, Lerouge P, Marchant A. 2009. The *Arabidopsis* IRX10 and IRX10-LIKE glycosyltransferases are critical for glucuronoxylan biosynthesis during secondary cell wall formation. Plant Journal 57: 718-731.

Wu Y, Williams M, Bernard S, Driouich A, Showalter AM, Faik A. 2010b. Journal of Biological Chemistry 285: 13638-13645.

Yang J, Sardar HS, McGovern KR, Zhang Y, Showalter AM. 2007. A lysine - rich arabinogalactan protein in Arabidopsis is essential for plant growth and development, including cell division and expansion. Plant Journal 49: 629-640.

Yapo BM, Koffi KL. 2008. Dietary fiber components in yellow passion fruit rind: a potential fiber source. Journal of Agricultural and Food Chemistry 56: 5880-5883.

Yariv J, Rapport M, Graf L. 1962. The interaction of glycosides and saccharides with antibody to the corresponding phenylazo glycosides. Biochemical Journal 85: 383-388.

Yariv J, Lis H, Katchalski E. 1967. Precipitation of arabic acid and some seed polysaccharides by glycosylphenylazo dyes. Biochemical Journal 105: 1-2.

Yates EA, Valdor J-F, Haslam SM, Morris HR, Dell A, Mackie W, Knox JP. 1996. Characterization of carbohydrate structural features recognized by anti-arabinogalactan-protein monoclonal antibodies. Glycobiology 6: 131-139.

Ye Z-H. 2002. Vascular tissue differentiation and pattern formation in plants. Annual Review of Plant Biology 53: 183-202.

Yin L, Verhertbruggen Y, Oikawa A, Manisseri C, Knierim B, Prak L, Jensen JK, Knox JP, Auer M, Willats WG. 2011. The cooperative activities of CSLD2, CSLD3, and CSLD5 are required for normal *Arabidopsis* development. Molecular Plant 4: 1024-1037.

York WS, O'Neill MA. 2008. Biochemical control of xylan biosynthesis - which end is up? Current Opinion in Plant Biology 11: 258-265.

York WS, Darvill AG, Albersheim P. 1984. Inhibition of 2,4-dichlorophenoxyacetic acid-stimulated elongation of pea stem segments by a xyloglucan oligosaccharide. Plant Physiology 75: 295-297.

Yoshida M, Liu Y, Uchida S, Kawarada K, Ukagami Y, Ichinose H, Kaneko S, Fukuda K. 2008. Effects of cellulose crystallinity, hemicellulose, and lignin on the enzymatic hydrolysis of Miscanthus sinensis to monosaccharides. Bioscience, Biotechnology, and Biochemistry 72: 805-810.

Youl JJ, Bacic A, Oxley D. 1998. Arabinogalactan-proteins from *Nicotiana alata* and *Pyrus communis* contain glycosylphosphatidylinositol membrane anchors. Proceedings of the National Academy of Sciences USA 95: 7921-7926.

Young RE, McFarlane HE, Hahn MG, Western TL, Haughn GW, Samuels AL. 2008. Analysis of the Golgi apparatus in *Arabidopsis* seed coat cells during polarized secretion of pectin-rich mucilage. Plant Cell 20: 1623-1638.

Yu P, McKinnon J, Christensen D. 2005. Hydroxycinnamic acids and ferulic acid esterase in relation to biodegradation of complex plant cell walls. Canadian Journal of Animal Science 85: 255-267.

Yuasa K, Toyooka K, Fukuda H, Matsuoka K. 2005. Membrane - anchored prolyl hydroxylase with an export signal from the endoplasmic reticulum. Plant Journal 41: 81-94.

Zablackis E, Huang J, Muller B, Darvill AG, Albersheim P. 1995. Characterization of the cell-wall polysaccharides of *Arabidopsis thaliana* leaves. Plant Physiology 107: 1129-1138.

Zabotina OA. 2012. Xyloglucan and its biosynthesis. Frontiers in Plant Science 3: 134.

Zabotina OA, Van De Ven WT, Freshour G, Drakakaki G, Cavalier D, Mouille G, Hahn MG, Keegstra K, Raikhel NV. 2008. *Arabidopsis* XXT5 gene encodes

a putative α-1,6-xylosyltransferase that is involved in xyloglucan biosynthesis. Plant Journal 56: 101-115.

Zabotina OA, Avci U, Cavalier D, Pattathil S, Chou Y-H, Eberhard S, Danhof L, Keegstra K, Hahn MG. 2012. Mutations in multiple XXT genes of *Arabidopsis* reveal the complexity of xyloglucan biosynthesis. Plant Physiology 159: 1367-1384.

Zandleven J, Beldman G, Bosveld M, Schols H, Voragen A. 2006. Enzymatic degradation studies of xylogalacturonans from apple and potato, using xylogalacturonan hydrolase. Carbohydrate Polymers 65: 495-503.

Zandleven J, Sørensen SO, Harholt J, Beldman G, Schols HA, Scheller HV, Voragen AJ. 2007. Xylogalacturonan exists in cell walls from various tissues of *Arabidopsis thaliana*. Phytochemistry 68: 1219-1226.

Zeng W, Chatterjee M, Faik A. 2008. UDP-xylose-stimulated glucuronyltransferase activity in wheat microsomal membranes: characterization and role in glucurono (arabino) xylan biosynthesis. Plant Physiology 147: 78-91.

Zhang S, Song X, Yu B, Zhang B, Sun C, Knox JP, Zhou Y. 2012a. Identification of quantitative trait loci affecting hemicellulose characteristics based on cell wall composition in a wild and cultivated rice species. Molecular Plant 5: 162-175.

Zhang T, Wyman C, Jakob K, Yang B. 2012b. Rapid selection and identification of *Miscanthus* genotypes with enhanced glucan and xylan yields from hydrothermal pretreatment followed by enzymatic hydrolysis. Biotechnology for Biofuels 5: 1-14.